

# PROCEEDINGS OF THE FOURTH U.S. WATER JET CONFERENCE

held at

THE UNIVERSITY OF CALIFORNIA, BERKELEY  
AUGUST 26-28, 1987

sponsored by  
THE WATER JET TECHNOLOGY ASSOCIATION  
THE MINING AND EXCAVATION RESEARCH INSTITUTE

Conference Chairmen

MICHAEL HOOD      DAVID DORNFELD

published on behalf of the Conference by  
THE AMERICAN SOCIETY OF MECHANICAL ENGINEERS  
United Engineering Center • 345 East 47th Street • New York, N.Y. 10017

Library of Congress Catalog Number 87-71878

Permission to post to the WJTA web site granted to the WaterJet Technology Association  
by the publisher - The American Society of Mechanical Engineers.

**Please Note.** This text is a scanned in version of the original.

Statement from By-Laws: The Society shall not be responsible for statements or opinions advanced in papers . . . or printed in its publications (7.1.3)

Any paper from this volume may be reproduced without written permission as long as the authors and publisher are acknowledged.

Copyright © 1987 by  
THE AMERICAN SOCIETY OF MECHANICAL ENGINEERS  
All Rights Reserved  
Printed in USA

## **FOREWORD**

The U.S. Water Jet Conference, held every two years, provides a forum for research workers and 4 practitioners to exchange information and ideas on a variety of topics in this developing area of technology. This year, as in the past, the research work is well represented. Much of it has to do with the fast-growing field of water jets with entrained abrasives. At previous meetings practitioners have been largely representatives from the rock and concrete cutting, mining, and cleaning industries. While these industries are amply represented, this year, for the first time, emphasis also is being placed on the use of water jets in factories, reflecting the expanding applications for this technology to manufacturing industries.

The papers selected for presentation at the conference represent an excellent state-of-the-art review of the many different aspects of this important and growing field.

M. Hood  
D. Dornfeld

## CONTENTS

### FIELD APPLICATIONS—MANUFACTURING

Milling With Abrasive-Waterjets: A Preliminary Investigation

*M. Hashish*

The Use of High Pressure Waterjets in Cutting Foam

*S. Yazici and D. A. Summers*

### RESEARCH

Percussive Jets - State-of-the-Art

*E. B. Nebeker*

Theoretical Analysis and Experimental Study of The Self-Excited Oscillation Pulsed Jet Device

*Liao Zheng Fang and Tang Chuan Lin*

Dynamic Characteristics of Waterjets Generated From Oscillating Systems

*W. Z. "Ben" Wu, D. A. Summers, and M. J. Tzeng*

Flow Visualization of High-Speed Water Jets

*M. Szymczak, S. Tavoularis, A. Fahim, and M. M. Vijay*

Considerations in the Design of a Waterjet Device for Reclamation of Missile Casings

*D. A. Summers, L. J. Tyler, J. Blaine, R. D. Fossey, J. Short, and L. Craig*

### FIELD APPLICATIONS - CONSTRUCTION

Development of Cavitating Jet Equipment for Pavement Cutting

*A. F. Conn, M. T. Graced W. Rosenberg, and S. T. Gauthier*

Hydro Demolition—Technology for Productivity and Profits for America

*R. J. Nittinger*

Abrasive-Waterjet and Waterjet Techniques for Decontaminating and Decommissioning Nuclear Facilities

*D. C. Echert, M. Hashish, and M. Marvin*

### RESEARCH AND DEVELOPMENT MINING

Jet Kerfing Parameters for Confined Rock

*J.J. Kolle*

Conical Water Jet Drilling

*W. Dickinson, R. D. Wilkes, and R. W. Dickinson*

The Effect of Pre-Weakening a Rock Surface, by Waterjet Kerfing, on Cutting Tool Forces

*J. E. Geier and M. Hood*

### RESEARCH

Study of Particle Velocities in Water Driven Abrasive Jet Cutting

*R. K. Swanson, M. Kilman, S. Cerwin, and W. Carver*

Hydroabrasive Cutting Head—Energy Transfer Efficiency

*G. Galecki and M. Mazurkiewicz*

## **FIELD APPLICATIONS- MINING**

Water Jet Assisted Longwall Shearer: Development and Underground Test

*E. D. Thimons, K. F. Hauer, and K. Neinhaus*

Considerations in the Use of High Speed Water Jets for Deep Slotting of Granite

*M. M. Vijay, J. Remiss, B. Hawrylewicz, and R. J. Puchala*

An Abrasive Water Jet Rock Drill

*G. A. Savanick and W. G. Krawza*

## **FIELD APPLICATIONS—CLEANING**

A Relative Cleanability Factor

*A. F. Conn, M. T. Graced and W. Rosenberg*

The Development of a High Production Abrasive Water Jet Nozzle System

*M. J. Woodward and R. S. Judson*

Cleaning the Tube Side of Heat Exchangers

*R. Paseman and L. Griffith*

Rotary Waterblast Lancing Machines

*G. Zink and J. Wolgamott*

## **RESEARCH AND DEVELOPMENT—MANUFACTURING**

Material Dynamic Response During Hydroabrasive Jet Machining (HAJM)

*M. Mazurkiewicz and P. Karlic*

Surface Finish Characterization in Machining Advanced Ceramics by Abrasive Waterjet

*D. C. Hunt, C. D. Burnham, and T. J. Kim*

Abrasive Waterjet Cutting of Metal Matrix Composites

*K. F. Neusen, P. K. Rohatgi, C. Vaidyanathan, and D. Alberts*

# MILLING WITH ABRASIVE-WATERJETTS: A PRELIMINARY INVESTIGATION

M. Hashish, Senior Research Scientist  
Flow Research Company  
Kent, Washington

## ABSTRACT

The feasibility of milling with abrasive waterjets has been investigated in this research. Results of milling experiments indicate that abrasive waterjets have great potential to be used as a machining tool with advantages unmatched by existing techniques. Linear cutting experiments were first conducted on sample materials (aluminum, titanium and Inconel) to generate a data matrix. Cutting results indicate a similarity of trends among these materials. Also, data were correlated against a previously developed cutting model. Although there is a strong correlation between theory and experiments, accuracy of predictions must be improved for more precise machining prediction and planning. Single-pass milling tests were conducted to observe the geometry of produced slots and the nature of surface irregularity. Multi-pass milling tests were conducted on such materials as aluminum, glass, titanium and graphite composites. Surface topography was found to be a function of cutting and abrasive parameters, and surface finish was found to be strongly affected by abrasive particle size. A comparison with other machining techniques is presented in this paper. Abrasive-waterjet milling is among the most efficient methods of energy utilization for material removal.

## INTRODUCTION

The rapid growth of harder and difficult-to-machine materials over the past two decades necessitates the development of compatible machining techniques. Conventional edge tool machining may not be technically or economically adequate for the machining of such materials. New machining techniques have been correspondingly emerging to fill the gaps where conventional methods are inefficient. These new techniques employ different physical phenomena or energy utilization to remove material. For example, mechanical, thermal, chemical and radiation energy forms (Ref. 1 - 4) constitute over 15 different techniques of nontraditional machining methods. One of the most recent machining methods is the abrasive-waterjet (AWJ) technique.

Abrasive-waterjets are formed in a small abrasive-jet nozzle, as shown in Figure 1. Water is pressurized up to 400 MPa and expelled through a sapphire orifice to form a coherent, high-velocity waterjet (5). The waterjet and a stream of solid abrasives are introduced into a hard-material mixing and accelerating tube. Here, part of the waterjet's momentum is transferred to the abrasive particles, whose velocities rapidly increase. Typical particle velocities are 300-600 m/s with mass flow rates of about 10 g/s.

A focused, high-velocity abrasive-waterjet exits the accelerator nozzle and performs the cutting action. Cutting or controlled depth penetration (milling) of the target material occurs as a result of complex erosion phenomena.

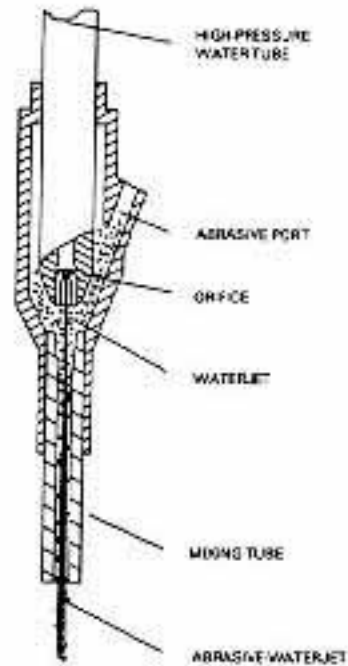


Figure 1. Abrasive-Waterjet Nozzle concept.

The cutting rate can be controlled by adjusting the abrasive-waterjet parameters, which include:

- Hydraulic parameters
  - Waterjet orifice diameter
  - Supply pressure
- Abrasive parameters
  - Material (density, hardness, shape)
  - Size
  - Flow rate
  - Feed method (force feed or suction)
  - Abrasive condition (dry or slurry)
- Mixing nozzle parameters
  - Mixing chamber dimensions
  - Nozzle material
- Cutting parameters
  - Traverse rate
  - Number of passes
  - Standoff distance
  - Angle of cutting

In this paper, a model of the AWJ cutting process is first employed to guide the milling experiments. Single-pass and multiple-pass milling experiments are then described. Finally, a comparison with another technique is presented.

## MODEL EMPLOYMENT

Three materials were used to conduct linear cutting tests: aluminum, titanium and Inconel. Hydraulic, abrasive, mixing and cutting parameters were varied to generate a data matrix on the effects of these materials on depth of cut. The main objectives of generating this data matrix are to:

- Use data to verify a prediction model.
- Use the prediction model, if adequate, to forecast a machining strategy.
- Observe the geometrical quality of cuts.
  - Roughness of produced surface
  - Variation of depth of cut along the direction of traverse

The following is a discussion of this effort:

### Review of Model

Cutting with abrasive-waterjets has been found to consist of two modes (6,7): the cutting wear mode occurs by the impact of particles at shallow angles (8), and the deformation wear mode occurs by impacts at large angles (9,10). The first mode results in a steady-state cutting interface, while the second is unsteady. The relative contribution of each mode to the total depth of cut depends on the traverse rate. Above a critical traverse rate, the cutting will be due only to the deformation wear mode. The total depth of cut ( $h$ ) can be expressed with a simplified model as

$$h = \sqrt{\frac{m_a v^2}{8 \sigma u}} + \frac{2m_a(1-c)v^2}{\pi u \varepsilon d_j} \quad (1)$$

where  $V$  is the jet velocity,  $\sigma$  is the flow stress,  $\varepsilon$  is the material specific energy,  $d_j$  is the abrasive-waterjet diameter and  $c$  is a constant. The term on the left is due to cutting wear, while that on the right is due to deformation wear. The critical traverse rate at which cutting wear terminates is (7)

$$u_c = \frac{m_a v^2}{20 \sigma d_j^2} \quad (2)$$

In the above equation, the effect of depth on particle velocity is neglected. When considering the decay of particle velocity with depth as a result of kerf wall interference, the following expression results (11) if the cutting wear mode is ignored (high traverse rates):

$$\frac{h}{d_j} = \frac{(1 - N_1)^2}{\left(\frac{N_2 N_3}{1 - c}\right) + C_f (1 - N_1)} \quad (3)$$

where

$$N_1 = \frac{V_c}{V}$$

$$N_2 = \frac{\pi}{2} \frac{\varepsilon d_j^2}{m_a v}$$

$$N_3 = \frac{u}{V}$$

$$N_4 = \frac{\varepsilon}{\sigma}$$

Setting  $V_c = 0$  and  $C_f = 0$  in Equation (3) will yield the second term in Equation (1) when  $c = 0.0$ . The first term in Equation (1), which is due to the cutting wear mode, can be combined with the deformation wear mode depth of cut given by Equation (3) to yield

$$\frac{h}{d_j} = c \sqrt{\frac{m_a v^2}{8 \sigma u d_j^2}} + \frac{(1 - N_1)^2}{\frac{N_2 N_3}{1 - c} + C_f (1 - N_1)} \quad (4)$$

If the ratio of the material specific energy ( ) to the flow stress ( ) is expressed as a nondimensional number ( $N_4 = \frac{\varepsilon}{\sigma}$ ), then Equation (4) can be rewritten as

$$\frac{h}{d_j} = 0.282c \sqrt{\frac{N_4}{N_2 N_3}} + \frac{(1 - N_1)^2}{\left(\frac{N_2 N_3}{1 - c}\right) + C_f (1 - N_1)} \quad (5)$$

### Comparison with Linear Cutting Results

Some problems are faced in using the prediction model given by Equation (5). These are:

- The knowledge of the dynamic material properties that are relevant to the cutting process. This has been a subject of extensive investigation in the field of erosion by solid particle impact (12,13). No conclusive results have yet been determined. However, for a given material, the two properties and can be approximated to best match experimental results. Keeping in mind that is a flow stress that is related to hardness and is a toughness property, a starting point can be identified.

- The knowledge of particle velocity. No efforts have yet been made to model the abrasive-waterjet mixing and acceleration processes. Previous efforts on modeling (14,15) have only restricted the jet - solid interaction process, assuming that the jet delivers particles with a velocity V. The simple prediction of the velocity of particles becomes inadequate if a wide range of mixing and hydraulic parameters is considered similar to the previously listed range of parameters.

The prediction model, Equation (5), was tested, however, to determine its feasibility for machining strategy forecasting and prediction. A simple particle velocity model (6) was used.

The results of correlating Equation (5) with the experimental results are given in Table 1. Figure 2 shows the experimental versus the predicted depths of cut.

Table 1. Correlation results of depth prediction.

Material	(MPa)	(MPa)	$V_c$ (m/s)	Correlation Coefficient
Aluminum	276	6900	30	0.9118
Titanium	883	11385	30	0.9144
Inconel	1035	21045	90	0.9472

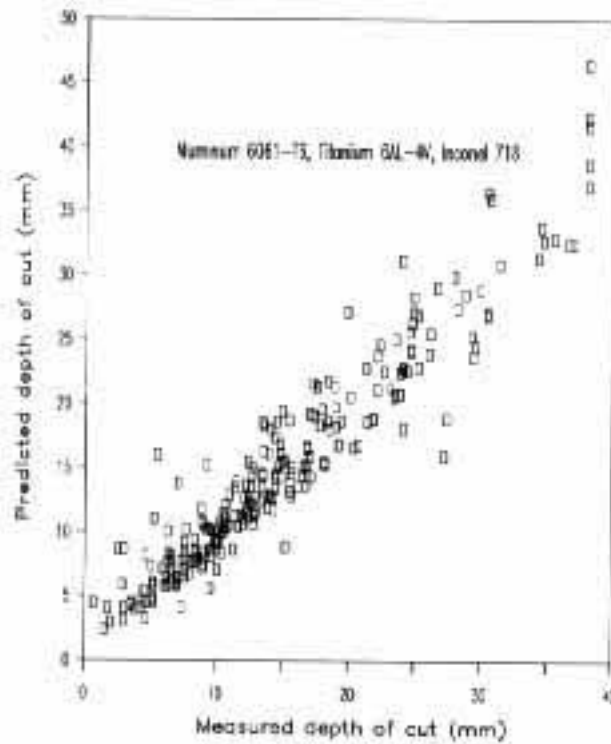


Figure 2. Measured versus predicted depth of cut.

The conclusions of this effort can be summarized as follows:

- Trends in the experimental data among the sample materials used are identical. This implies that a common strategy can be devised for machining. It also implies that one material can be used to simulate others for the investigation of machining feasibility.

- Although reasonable correlations are obtained between theory and experiment, the spread in the data is within a large band. This may be adequate for slotting but not for precise machining depth predictions.
- Inspection of data trends indicates that optimum parameters exist for maximizing performance. Examples include the rate of surface area generation, the specific energy consumption and the depth of cut, as will be shown in milling tests later.

### SINGLE-PASS MILLING TESTS

Non-through cutting is a milling process, though the required results are different. For cutting, the rate of kerf area generation is typically the parameter to be maximized. For milling, volume removal rates as well as surface topography parameters are of concern. Also, the process of milling will include multiple-pass application of the AWJ to produce the near-net shape. In order to understand how multiple passes will be applied, a first step is to recognize the features of single-pass cutting.

#### Observation of Produced Kerfs

The process of cutting deep slots with abrasive waterjets often results in an irregular slot depth as shown in Figure 3. The lateral profile of the slot produced is also non-uniform. The Irregularity and non-uniformity are most sensitive to traverse rate and standoff distance. The following is a discussion of these two variables.

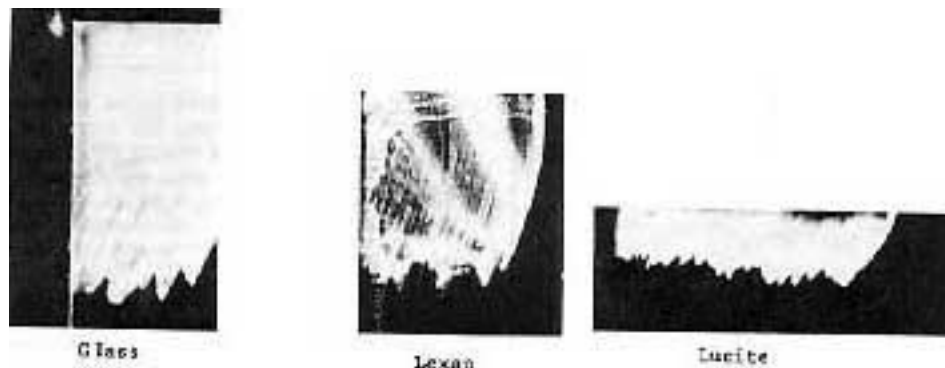


Figure 3. Irregular depth produced with AWJ

#### Effect of Standoff Distance

The effect of standoff distance is considered here to determine quantitatively optimum values for maximum rates of volume removal and to characterize qualitatively the cutting results with respect to surface roughness. Figure 4 shows the effect of standoff distance on volume removal for mild steel. A similar trend is shown in Figure 5 for aluminum. From these two figures it can be seen that there are optimum standoff distances for maximum volume removal rates. These standoff distances are typical of what is used in regular cutting of deep kerfs. An increased standoff distance, which results in the exposure of a larger portion of the surface to the jet, is associated with a decrease in volume removal. Increasing the abrasive flow rate, however, does not

significantly change the trend of the effect of standoff distance on volume removal, as shown in Figures 4 and 5.

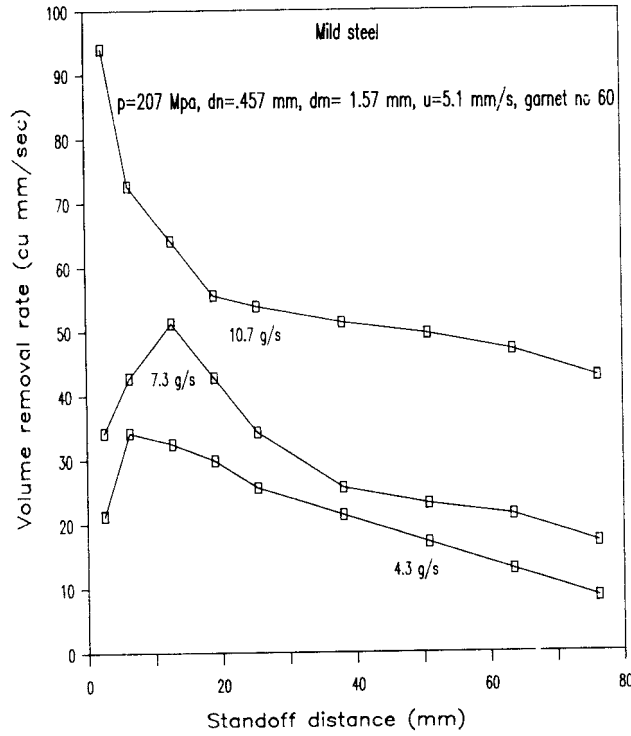


Figure 4. Effect of standoff distance on volume removal rate (mild steel).

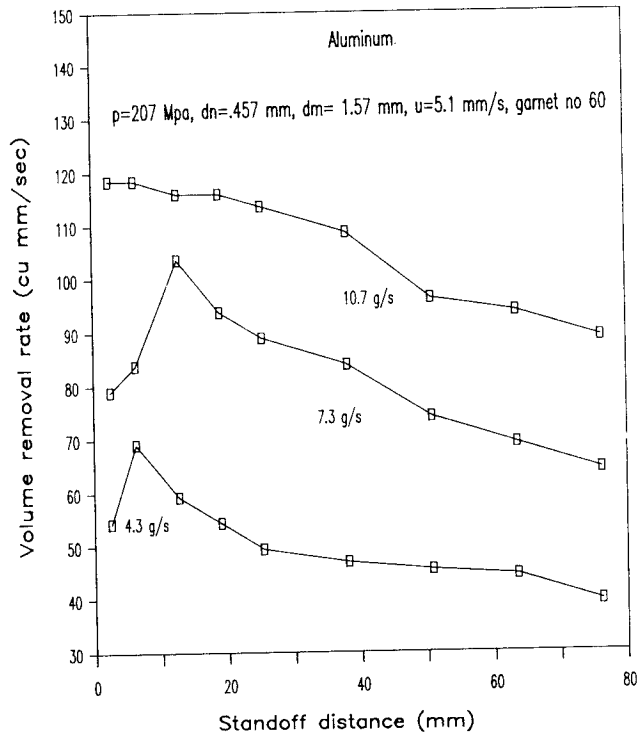


Figure 5. Effect of standoff distance on volume removal rate (Aluminum)

### Effect of Traverse Speed

Increasing the traverse rate will result in reduced volume removal and depth of cut, Figure 6. However, volume removal rates may increase with increasing traverse speed. The additional requirement for milling is that the surfaces produced be regular. This has been observed to be dramatically controlled by the traverse speed. Increasing the traverse speed continually improves the depth uniformity of the produced slot. Measurements of the depth of cut produced at locations along the cut were made to determine the ranges by which depths of cut vary as a function of the traverse rate. Figure 6 shows an example of that effect.

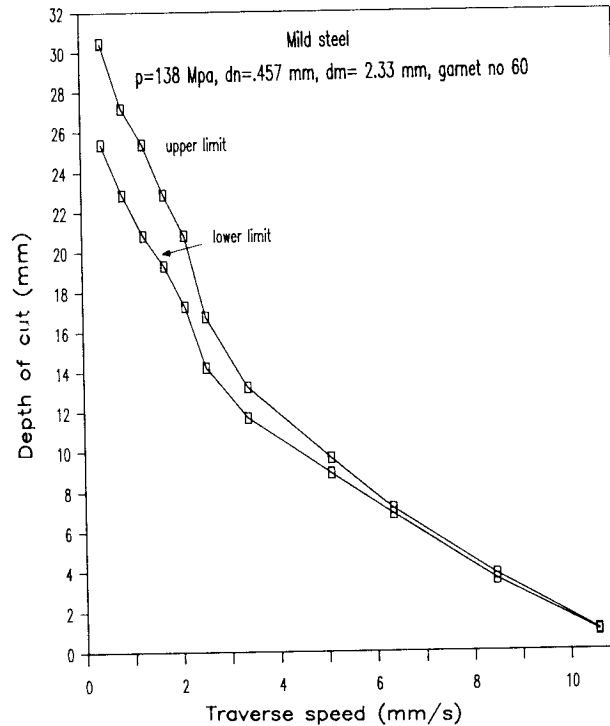


Figure 6. Effect of traverse rate on depth of cut and its uniformity.

Measurements of depth of cut variation with traverse rate in the range from 16 to 160 mm/s were made on aluminum and mild steel with a variation range of 10 to 250 micron. Table 2 shows additional data on volume removal rates and energy consumed in cutting. The shapes of the produced slots were also observed to vary with varying traverse rates. Figure 7. Shows a diagrammatic representation of both the effects standoff distance and of traverse rate in the slot geometry.

### Dual-Jet Milling Nozzle

Brief tests were conducted using a modified nozzle shape. This nozzle employs two parallel waterjets flowing into a single mixing chamber. The objective is to increase the effective width of the cutting jet. A total of 17 tests were conducted with this nozzle at different parameters as shown in Table 3. Comparison of results from Tables 2 and 3 shown that the dual-jet concept is inefficient in material removal. This is due to the inefficiency of the mixing process, which utilizes a relatively large mixing tube (10 mm

ID versus 1.19 mm ID for the single jet). Typically the shape of the cut produced is as shown diagrammatically in Figure 8.

Table 2. Material removal rate and specific energy obtained with a single jet AWJ nozzle in Aluminum 6061-T6

	Removal rate mm <sup>3</sup> /s	Effectiveness g/g	Sp. Energy J/mm <sup>3</sup>
Traverse Speed mm/s			
1.27	59.3	0.039	11.8
2.54	69.8	0.046	10.1
3.81	845.0	0.056	8.4
5.08	88.9	0.059	7.9
7.62	92.6	0.061	7.6
Abrasive Flow rate (g/s)	(		
1.3	29.0	0.060	24.2
1.7	40.1	0.062	17.5
2.4	52.5	0.059	13.4
4.1	72.8	0.048	9.6
4.7	84.6	0.048	8.1
7.3	100.6	0.037	7.0

Parameters other than listed are: Pressure = 207 MPa; Waterjet Orifice = 0.356 mm  
Abrasive flow rate = 4 g/s; traverse speed = 2.54 mm/s; garnet mesh = 80.

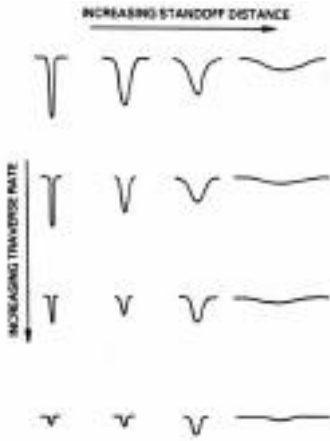


Figure 7. Geometry of cut shape variation with standoff distance and traverse rate.

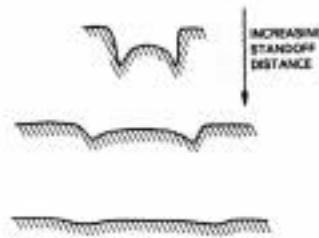


Figure 8. Geometry of slot produced with a dual-jet nozzle.

Table 3. Material removal rate and specific energy obtained with a dual jet AWJ nozzle in aluminum 6061-T6

	Removal rate mm <sup>3</sup> /s	Effectiveness g/g	Sp. Energy J/mm <sup>3</sup>
Abrasive mesh no.			
60	92.6	0.01	23.3
80	55.6	0.006	38.1
100	37.0	0.004	58.3
Abrasive Flow rate (g/s)			
11	18.5	0.005	116.7
26	55.6	0.006	38.1
34	74.1	0.006	29.2
No. of passes			
1	55.6	0.006	38.1
2	97.2	0.010	22.2
3	102.2	0.011	21.2
4	111.1	0.012	19.5
Standoff distance (mm)			
13	166.7	0.018	13.0
25	56.6	0.006	38.1
38	45.0	0.005	48.0
51	37.0	0.004	58.4
Traverse speed (mm/s)			
1.27	40.0	0.004	54.0
2.56	56.6	0.006	38.1
3.84	83.3	0.009	25.9

Parameters other than listed are; Pressure = 207 MPa; Water orifice 2 x 0.0457 mm  
 Abrasive flow rate = 26 g/s; traverse speed = 2.56 mm/s; garnet mesh = 80  
 Total jet power = 28 kW.

As a result of these tests with the dual-jet configuration, it was realized that only varying the parameters will not produce slots of a uniform depth. A nozzle modification is necessary to distribute the power equally across the cutting jet. This may require more waterjets with reduced spacing or a single "slit" orifice with a two-dimensional mixing chamber. This will require further research efforts.

#### Conclusions of Single-Pass Milling Tests

The following conclusions were arrived at as a result of the parametric tests:

- The standoff distance should be kept within 12 mm to achieve:
  - Increased volume removal rates
  - Reduced noise levels
  
- The traverse speed should exceed a critical value, which depends on a wide range of parameters. Speeds in excess of 16 mm/s should be used.
  
- The shape of the cut produced by a single jet traverse is significantly affected by standoff distance and traverse rate. More geometrical characterization requires further research.

## MULTIPLE-PASS MILLING TESTS

### Experimental Apparatus and Parameters

An in house six-axis robot was used to traverse an abrasive-waterjet nozzle. The use of this robot was limited in this phase to milling simple cavity shapes. Figure 9 shows the different components of the experimental setup. Samples to be milled were placed in the catcher tank. A rubber shield was fastened to the nozzle to control any splashing back of the jet.

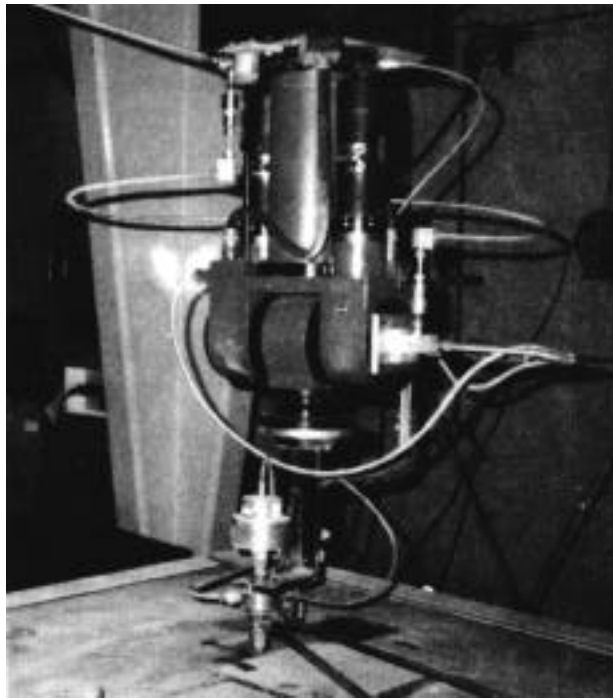


Figure 9. Test set-up for milling experiments

The parameters used for milling are:

Pressure	172 MPa
Waterjet diameter	0.356 mm
Type of abrasive	garnet, silica sand, glass beads
Size of abrasive particles	mesh Nos. 60, 80 150

Abrasive flow rate	7.5 g/s (maximum)
Traverse speed	420 mm/s
Standoff distance	12 mm

The lateral spacing of the jet was an additional parameter for the milling tests. A simple pattern was stored in the robot's controller to traverse simply in one direction, to shift the jet by a precise lateral increment, and then to traverse in the opposite direction. This scheme was used to simulate a continuous traverse as would be used in an actual milling process. To avoid excessive manipulator programming, masking plates were cut with the cavity shape to be milled. When the jet is traversed across such plates only, the cut shape will be milled in the masked material. Mild steel plates were used to mask aluminum, titanium, glass and graphite composite. The jet traverse can then overlap the cavity on the masking plate. Parameters were varied to determine their effect on the topography of the surfaces produced. The following is a discussion of the findings.

#### Effect of Abrasive Material

The strategy of milling with abrasive waterjets may include the use of different abrasive materials. The use of hard abrasives would be suitable for fast material removal rates. The use of soft frangible abrasives may be suitable for finishing. Two types of tests were conducted as discussed below. The first explored the use of alternating the abrasive materials for cutting and then finishing, and the second examined the effects of specific materials on surface topography.

#### Use of Alternative Abrasives for Finishing

Cavities were machined using typical garnet sand mesh No. 60 for fast material removal rates with side increments equal in size to one-half the jet diameter ( $d_j = 1.5$  mm). A total of 20 parallel cuts (a total width of, 15.24 mm) were made, and the whole sequence was repeated four times (passes) to produce a relatively deep cavity. The depth of the cavity varied within 2.5 mm. When silica sand was used to finish the cavity and improve the depth uniformity, no positive results were gained. On the contrary, the depth variation became 3 mm after two passes using a pattern traverse, although the traverse speed was kept the same at 34 mm/s. The use of glass beads gave similar results to those of silica sand.

It is concluded that depth uniformity control should be considered right at the beginning of the milling process. Irregularities produced by one pass or traverse are not corrected in the subsequent passes but rather exaggerated. A different pattern of traverse on every pass will complicate the milling process.

Single passes of 20 adjacent cuts, as discussed above, were made on aluminum samples using garnet, silica sand and glass beads of comparable size (mesh No. 80). Figure 10 shows magnified photographs of the surfaces produced with these different materials.



a) Garnet

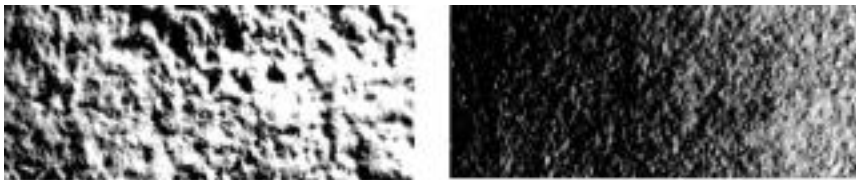
b) Silica sand

c) glass beads

Figure 10. Effect of abrasive material on surface topography (Aluminum)

### Effect of Particle Size

The effect of particle size is shown in Figure 11. It is a logical conclusion that finer particles produce finer surfaces. However, the use of finer particles may be associated with reduced volume removal rates.

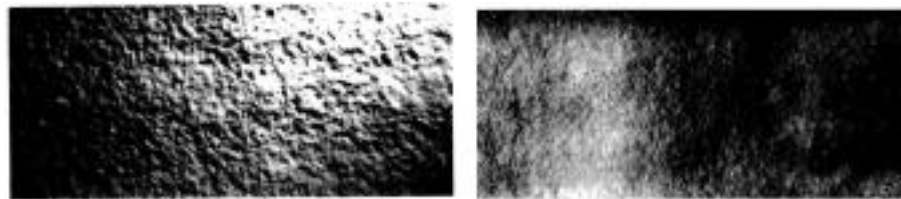


a) mesh no 80

b) mesh no 150

Figure 11. Effect of particle size on surface topography (Inconel)

Tests were conducted to machine initially a cavity with garnet sand (mesh No. 80) then finish it with garnet mesh No. 150. The cavity produced was compared to another produced by using only garnet mesh No. 150. The result is shown in Figure 12. The depth measurement showed a variation of about 0.51 mm when the two sizes were used (upper photo) and only 0.203 mm when only mesh No. 150 was used (lower photo).



a) one pass mesh no 80 + 1 pass mesh no 150

b) two passes mesh no 150.

Figure 12. Effect of abrasive size combination on surface topography (Inconel)

### Effect of Traverse Speed

The traverse speed was varied in the range of 42 to 420 mm/s during the milling tests. The lateral spacing was kept at 0.254 mm, and a total width of 7.62 mm was fixed. This implies the use of 30 side traverses. The time required to mill a slot of width  $b$  and length  $l$  will be

$$T = \frac{b}{\delta} \frac{l}{u} N_a$$

where  $u$  is the traverse rate in mm/sec. and  $N_a$  is the number of advances. For  $b = 25$  mm,  $w = 0.25$  mm and  $l = 25$  mm, the time  $T$  will then be

$$T = 2500 \frac{N_a}{u} \text{ sec} \quad (7)$$

The depth of the milled cavity versus the traverse speed is shown in Figure 13. This depth can be expressed as the specific volume removal, i.e., the volume removed per unit area. The volume removal rate can then be expressed as

$$V = h.u.w. \quad (8)$$

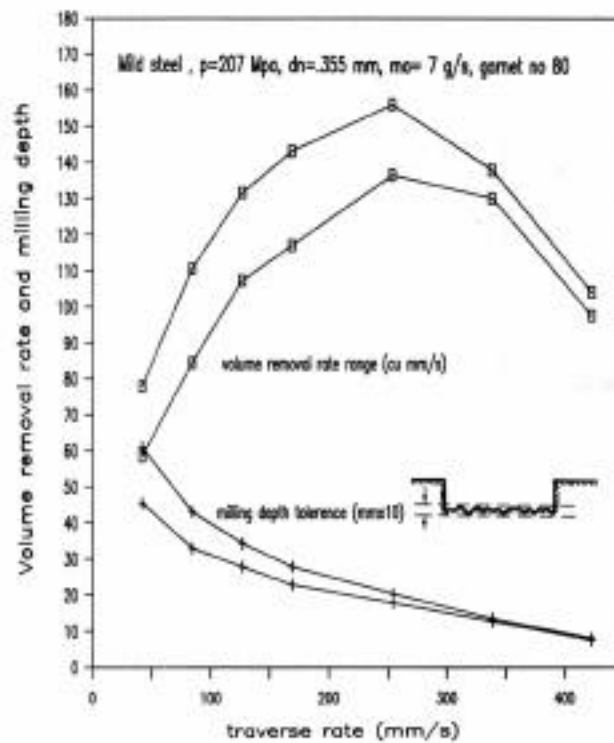


Figure 13 Effect of traverse rate on miling depth and volume removal rate.

The rate of volume removal is also shown in Figure 13. The volume removal rate peaks around 250 mm/s a depth non-uniformity of about 0.5 mm. At 420 mm/s, the depth non-uniformity is within 0.127 mm.

Additional tests were conducted to fix the total machining time when different traverse speeds are used. This also involved varying the number of passes. The speeds selected were 84 , 126, 168, 210 252, 336, and 420 mm/s, and the corresponding numbers of passes were 2, 3, 4, 5, 6, 8 and 10 passes. Results confirmed the previous conclusion that a 250 mm/s traverse rate yields the maximum volume removal, but a 420 mm/s traverse rate produces the smoothest cut.

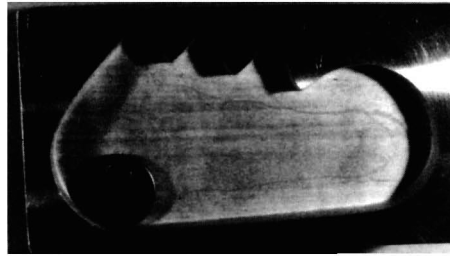
Demonstration Tests

Figure 14 shows examples of milled shapes in aluminum, titanium, and glass. The parameters used for milling these shapes are:

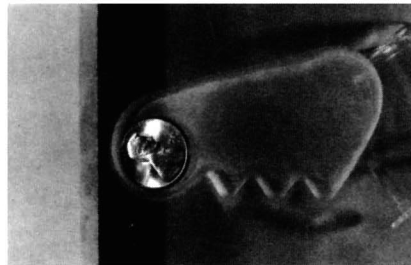
Pressure (P)	172 MPa
Waterjet diameter (dn)	0.356 mm
Type of abrasive	garnet sand
Size of abrasive particles	mesh No. 80
Abrasive flow rate ( $\dot{m}_a$ )	7 g/s
Traverse speed (u)	420 mm/s



a) Aluminum



b) Titanium



c) Glass

Figure 14. Examples of simple shapes milled with abrasive waterjets.

The measured volume removal rates were:

Titanium:	73 mm <sup>3</sup> /s
Aluminum:	123 mm <sup>3</sup> /s
Glass:	260 mm <sup>3</sup> /s

Table 4. Comparison of Material Removal Rate Ranges for Different Materials with a 9 kW Abrasive-Waterjet

Material	(mm <sup>3</sup> /s)
Aluminum	50- 300
Steel	40- 200
Cast Iron	50 - 250
Titanium	50- 250
Inconel	40- 200
Tungsten Carbide	0.1- 2
Alumina	0.2- 5
Silicon Carbide	0.2- 3
Graphite Epoxy	100 - 300

\*Depends on alloy type or grade and traverse rate. Garnet mesh No. 80 at 7 g/s and 207 MPa pressure.

Table 4 shows the results of additional milling tests conducted in different materials. The data show different ranges, which depend on the AWJ parameters and the specific grade of material. For example, an order of magnitude difference can be observed in the milling of tungsten carbide depending primarily on the binder content. The case is similar for alumina ceramics, which depend on the purity percentage.

#### COMPARISON WITH OTHER METHODS

No detailed efforts are conducted here to compare quantitatively the cost of abrasive-waterjet cutting to other techniques. Such a comparison should be carefully conducted and should include many factors other than the cutting operation itself. For example, the required finishing of cuts made using thermal cutting techniques is an additional process that may not be needed if an erosive cutting technique, such as abrasive-waterjet cutting, is employed. The cost of equipment, environmental considerations and versatility of use are, of course, other factors that couple with the technical performance for a full economic evaluation.

The data presented in this paper indicate the technical feasibility of abrasive-waterjet machining and how different parameters control the machining results. Specific advantages of abrasive-waterjets that may offset any economic disadvantages are as follows:

- Ability to machine very hard materials
- Ability to selectively machine multi-material composites
- Minimal deformation stresses
- Minimal thermal effects
- Reasonable material removal rates
- Omnidirectional machining
- No heavy clamping needed for workpieces
- No direct "hard" contact with workpiece
- Ideal for automation and remote control

Methods for three-dimensional metal shaping that may be replaced by abrasive-waterjet technology include the following:

- Electrical discharge machining (EDM)
- Electrochemical machining (ECM)
- Chemical machining (CHM)
- Ultrasonic machining (USM)
- Abrasive jet machining (AJM)
- Electron beam machining (EBM)
- Laser beam machining (IBM)
- Plasma arc machining (PAM)

For very specific applications, these technologies may have certain advantages over abrasive-waterjets. In general, the abrasive-waterjet technology appears to provide greater benefits.

A comparison of the various machining methods is made in Table 5. Data given for abrasive-waterjets were obtained from cutting tests and would be improved with optimization and further nozzle development.

Table 5. Typical volume removal rates and surface finish for different non-traditional machining techniques.

Method	Volume Removal Rate	Typical Power Requirements	Surface Roughness
EDM Electrical Dis-charge Machining	Material removal rate 7 mm <sup>3</sup> /s	Current of up to 20 amps and voltage of up to 400 volts are needed	3-12
ECM Electrochemical Machining	35 mm <sup>3</sup> /s per 1000 amps (typical for steel)	DC volts up to 30 is used; a 10,000-amp machine is typical	0.4-6.3
CHM Chemical Machining	0.3 mm <sup>3</sup> /s in steel; volume depends on area of blanking	Cost of blanking is 3 to 6 times that of mechanical blanking	
USM Ultrasonic Machining	4 to 60 mm <sup>3</sup> /s in tool steel glass		0.3-0.8
AJM Abrasive Jet Machining (air)	up to 1 mm <sup>3</sup> /s	Typical microblaster power requirement is 2-5 kW	
EBM Electron Beam Machining	up to 5 mm <sup>3</sup> /s	130 volts and 5000 microamps are needed	0.8-6.3
LBM Laser Beam Machining	Very inefficient in consumption; no date available	4000 volts and 3000-joule pulse for one millisecond are typical for operations	0.8-6.3
PAM Plasma Arc Machining	1000 mm <sup>3</sup> /s	200 kW is needed	
AWJ Abrasive-Waterjets	Volume removal rate of 50 to 200 mm <sup>3</sup> /s	Typical power of 10 to 50 kW	1-10

Electrical discharge machining, which is suitable only for electricity-conducting materials, uses a pulsating electrical discharge to melt the metal that is to be removed. Because of short tool life and high cost, ordinary EDM techniques are seldom competitive with other metal removal techniques. The EDM process increases the surface hardness and reduces the fatigue strength. Among the other disadvantages of EDM are the need to shape electrodes (tools) for every new machining task and the slow rate of metal removal.

Electrochemical machining is used for odd-shaped cavity machining or marking. Slow material removal rates and high cost of equipment are among the disadvantages of

this technique. The technique is also limited to materials that conduct electricity. Pilot testing is often required before the parameters are selected for cutting. ECM machines must also be rigid enough to withstand the pressures caused by the electrolyte.

Chemical machining utilizes chemical attack or etching to remove layers of metal. Nearly all metals can be chemically machined at very low rates of metal removal. Maximum blanking depth is about 1.5 mm. This process requires highly skilled operators.

Ultrasonic machining uses abrasive slurries in a gap between an oscillating tool and the workpiece to cause metal removal. It is used chiefly for hard and brittle materials that do not conduct electricity. It is suitable for producing relatively shallow irregular cavities. The main disadvantages of USM are the high cost and low rates of material removal.

Abrasive jet machining uses air to accelerate and entrain abrasives. Its primary use is in the cleaning and deburring of very hard, brittle materials. AJM is not really suitable for rapid machining operations because of the low power and low volume removal rates associated with this method. However, it does have the advantage of being able to cut hard, brittle materials without inducing thermal stresses.

Electron beam machining requires a vacuum chamber in which workpieces are placed. It is suited for drilling holes and making slots of a millimeter fractions in size. This process has the disadvantages of high cost, limited applicability (to a 6 mm depth), slow production rates and thermal distortions of produced surfaces.

Laser beam machining, while applicable to any known material, is not suitable for thin workpieces and the removal of small amounts of material. Precise alignment is required, which slows the production rate. Also, the resulting cuts are nonuniform and thermally damaged.

Plasma arcs are suitable for machining any metal. In spite of the high equipment and operating costs, rapid cutting rates make plasma cutting economical for straight cuts. Although the plasma cuts are smooth, the top surfaces are rounded. A second problem with this thermal cutting technique is the distortion of surface characteristics.

## CONCLUSIONS

As a result of this study, the feasibility of machining with abrasive-waterjets has been successfully demonstrated. Specific conclusions are listed below.

- Abrasive-waterjet nozzles typically used for slotting are adequate for machining operations such as milling.
- Reasonable rates of material removal can be obtained with the abrasive-waterjet technique with relatively low power levels.
- A full economic analysis and comparative studies with other techniques need to be conducted for a full economic assessment. The results of this preliminary testing, however, have been very encouraging.

- An optimum machining strategy will include parameter changes to maximize material removal rates and produce minimal surface irregularities.
- The prediction model for slotting needs refinement for its adequate use as an accurate machining prediction model. However, trends can be predicted very well with this model. The correlation between data and theory is over 90%.
- The surface finish of a produced surface is significantly affected by particle size and can accordingly be controlled. A model needs to be developed for surface quality parameters.
- Abrasive-waterjet machining is not limited to classes of materials and has great potential for difficult-to-machine materials, such as ceramics and composites.
- Machining with abrasive-waterjets is environmentally acceptable and safe, and it does not require extensive training. Automation will be preferred for the abrasive-waterjet technique.
  - o The accuracy of parameter settings and repeatability are important factors that affect the quality of produced surfaces.

#### ACKNOWLEDGEMENT

This work was supported by Grant No. MEA-8460065 from the National Science Foundation under the SBIR program. The author is grateful to this support and to the help of Mr. S. Craigen, Lab Technician.

#### REFERENCES

1. Machining Data Handbook, 3rd Edition, Vol. 2, Metcut Research Associates, 1980.
2. Nontraditional Machining, Conference Proceedings, Cincinnati, Ohio, ASM, 1985.
3. Pandey, P.C., and Shan, H. S., Modern Machining Processes McGraw Hill Book Company, 1980.
4. Advances in Nontraditional Machining, ASME Publication PED 22, 1986.
5. Hashish, M., et al., "Method and Apparatus for Forming High-Velocity Liquid Abrasive Jet," U.S. Patent 4,648,215.
6. Hashish, M., "A Modeling Study of Metal Cutting with Abrasive-Waterjets," ASME Transactions, Journal of Engineering Materials and Technology, Vol. 106, pp. 88-100, January 1984.
7. Hashish, M., "On the Modeling of Abrasive-Waterjet Cutting," Proceedings of the Seventh International Symposium on Jet Cutting Technology, BHRA, The Fluid Engineering Centre, Cranfield, Bedford, U.K., pp. 249-265, 1984.
8. Finnie, I., "The Mechanism of Erosion of Ductile Metals," Proceedings of the Third National Congress of Applied Mechanics, ASME, pp. 527-532, 1958.
9. Bitter, J. G. A., "A Study of Erosion Phenomena: Part I," Wear, Vol. 6, pp. 5-21, 1963.
10. Bitter, J. G. A., "A Study of Erosion Phenomena: Part II," Wear, Vol. 6, pp. 169-190, 1963.
11. Hashish, M., "Theoretical and Experimental Investigation of Abrasive-Waterjet Cutting," NSF Phase II Final Report for Grant No. MEA82-12878, 1985.

12. Preece, C., editor, "Treatise on Materials Science and Technology," Erosion, Vol. 16, Academic Press, New York, 1979.
13. Engel, P., Impact Wear of Materials, Elsevier Scientific Publishing Company, Amsterdam-Oxford, New York, 1976.
14. Hashish, M., "A Modeling Study of Abrasive Waterjet Metal Cutting," NSF Final Report for Grant No. ME&81-14500, 1982 (also published as Flow Industries Report No. 229).
15. Hashish, M., "Abrasive-Waterjet Cutting Studies," Computer-Based Factory Automation, Proceedings 11th Conference on Production Research and Technology, SME, Dearborn, Michigan, pp. 101-111, 1984.

# THE USE OF HIGH PRESSURE WATERJETS IN CUTTING FOAM

S. Yazici and D. A. Summers  
High Pressure Waterjet Laboratory  
Rock Mechanics Facility  
University of Missouri-Rolla  
Rolla, Missouri

## ABSTRACT

Expanded plastic foam is increasingly being used as a light, inexpensive yet effective method for providing object support in packaging. However, the most effective use of this support requires that the packaging material be carved to roughly conform to the shape of the packaged object. While this is a relatively easy accomplishment when the surrounding void is filled with small pieces of foam, it becomes more of a problem when the object contours must be generated in solid foam pieces. Solid foam, however, has the advantage of providing a more uniform loading of the object and holds it more rigidly in position. These requirements mandate that a simple but effective method be available for carving the foam to shape. The most prevalent of the current methods relies on either manual carving of the solid block, using heated scoops or wires, itself an expensive and relatively slow procedure, or that the foam support be composited by the glueing together of the different component parts, each of which has previously been manually carved to its required shape. Both of these processes can be relatively slow and therefore also expensive.

High Pressure waterjet cutting systems have been developed for use as industrial cutting tools, with significant market penetration having occurred within the last seven years. The majority of the applications for this novel tool have, however, been directed at cutting harder and more difficult materials, with the use of abrasive injection, or for the cutting of relatively soft materials. The range of foams which must be considered for the current operation lies over a range of densities which fits between these two extremes. The cutting of foam, in general, provides a material which it is extremely easy to cut at relatively rapid rates. This, in part, allows observation of cutting parameters at different ranges from those normally essayed. One requirement for the current program is, however, different to that sought for most industrial cutting where the cuts are made through relatively thin thicknesses of material. In contrast, in this operation, in order to cut the required contours of some of the objects to be packed, cutting depths on the order of one meter should be achievable.

## PROGRAM PLAN

As a means of assessing the parameters required to achieve the required cutting performance, a full factorial experiment was designed. The experiment utilized a pump (Ingersoll Rand<sup>1</sup>) which was capable of generating pressures of up to 400 MPa at flow rates of up to four liters/min. Nozzle diameters for the factorial experiment were chosen to insure that the full factorial could be completed within these limitations. The

---

<sup>1</sup> The use of trade names is for the purpose of identification only and should not be taken as an endorsement of any one particular product.

experiment was carried out to examine the effect of five factors on the depth of cut as the primary variable, but with cut quality being also considered. The five factors which were considered were the traverse speed of the nozzle over the target surface, the pressure of the waterjet, the diameter of the waterjet, the concentration of a polymer (Superwater) in the water, and the density of the foam being cut. The primary method for evaluating jet performance was by averaging the depth of cut achieved by the jet over a 5 cm. long traverse. It was also considered valuable to calculate the specific energy of the cutting operation. Analysis of the data from the experiment was carried out using a commercially available statistics program (Statview 512) on a desk-top computer (Macintosh Plus).

## EXPERIMENTAL SET-UP

A high pressure waterjet pump manufactured by the McCartney Division of Ingersoll Rand was used for this experiment. The high pressure cutting fluid utilized either plain water or water to which a small concentration of the polymer, Superwater, had been added prior to entry into the pump. Previous research had indicated that this polymer had the potential for generating superior results in this application. The fluid was fed, from the pump, to the cutting nozzle mounted above a light weight X - Y cutting table manufactured in the Research Center (Figure 1 ).

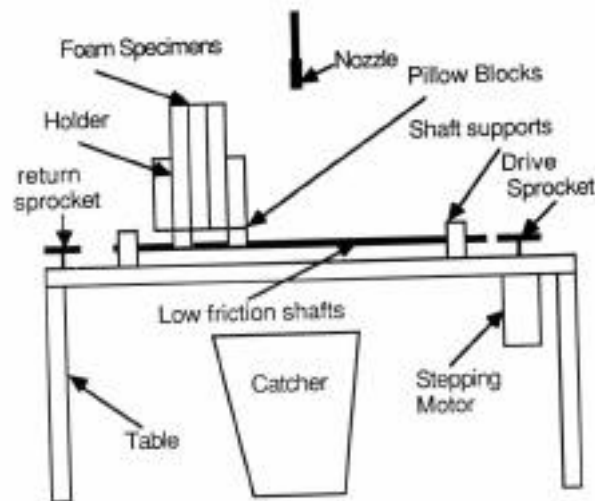


Figure 1. Side View of Traverse Table

For the purposes of this experiment only one direction of motion was utilized, although the table has since been configured to allow concurrent x and y motion to achieve the complex contour cutting required for the packaging operation. An initial estimate of the speed at which cutting might be achieved was set at 152 cm/second, although the configuration of the table did allow traverse speeds in excess of 254 cm/second with a table load of less than 4.5 kg. The cutting table was driven using a 25,000 step micro stepping motor from the Compumotor Corp., in turn controlled through a dedicated card and drive system from a program running on an IBM XT computer. It might be commented that the system obtained, which was considered close to the state of the art a year ago and which cost approximately \$6,500, is now sufficiently

out of date that it is no longer marketed and the new version of the system can be assembled for less than half this price.

The drive shaft from the stepping motor was connected to a drive chain through a suitably sized sprocket. The drive chain was connected through a shear pin to the underside of the light carriage (Figure 2) used to hold the foam package in place.

Light steel braces were used to support the upper 30 cm of the foam sample column, the remaining 70 cm of which were allowed to protrude below the table level. The table was guided along two precision shafts and held in place with linear bearings. The software program used to drive the table allowed definition of the acceleration and deceleration rates and distances. The precision of the table was checked using a Spin Physics 2000 high speed video camera, operated at 2000 frames /sec and was found to be accurate within the sensitivity of this instrument. Depending on the cutting speed and jet conditions, sample penetrations greater than 30 cm. could be anticipated (Figure 3). When this occurred the relatively narrow sample dimensions being used meant that there was insufficient rigidity in the lower section of the sample and it vibrated in the path of the jet. A light aluminum frame clamp was accordingly added to provide additional stiffness and to allow samples up to one meter deep to be tested.

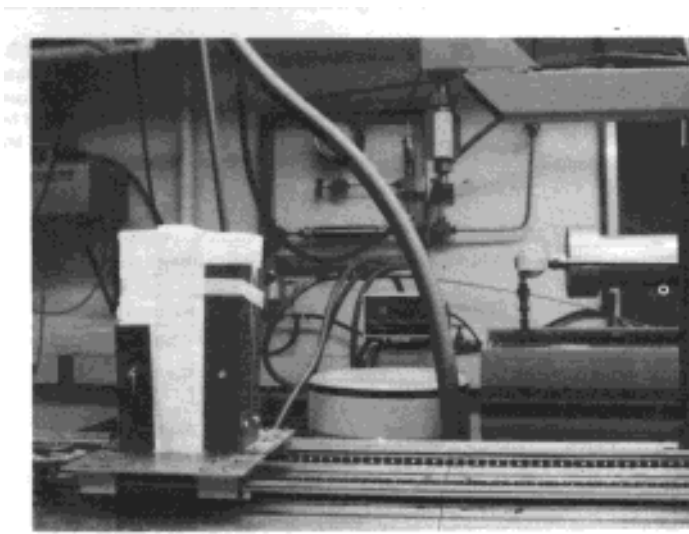


Figure 2. XY Table and Foam Specimens

For most tests samples of each of the three foam densities being evaluated were placed in the table at one time and a single common traverse made over all three sequentially. The samples were located so that the nozzle was some 1.25 cm. above the top surface of the samples. The foam samples were prepared by cutting pieces from larger sheets supplied either by the Navy (Foam #1) or from a local commercial source (Polystyrene--Foam #2, Soft Urethane foam--Foam #3).

The tests were carried out in two sequential factorial designs. The first evaluation was a 5 level factorial design examining, for three different densities of foam, the different effects

of changes in jet pressure, nozzle diameter and traverse speed on the depth of cut. Consequently an experiment was carried out using just one variety of foam to determine in a smaller factorial, what the effect of adding different levels of a long chain polymer would have on the cutting process. For this 3 levels of traverse speed, pressure and nozzle diameter were used while changing polymer concentration over 5 levels. The levels of these parameters are given in Table 1.

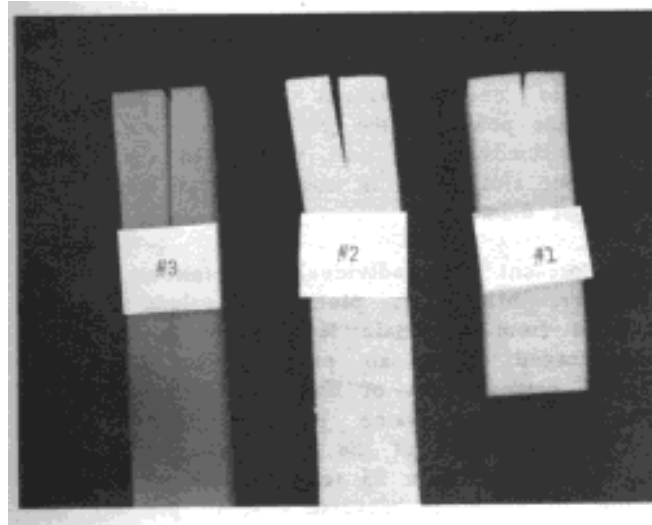


Figure 3. The Foam Specimens

Consequently a factorial of  $5 \times 5 \times 5 \times 3 = 375$  tests was made using water and one of  $5 \times 3 \times 3 \times 3 = 135$  tests with Foam #1 using polymer mixed water provided the data for the report (Table 2).

Table 1: Test Parameters for First Factorial

Stand-off distance (cm)	1.27				
Traverse speed (cm/sec)	2.54	12.7	25.4	50.8	127
Pressure (MPa)	52	69	138	207	276
Nozzle Diameter (mm)	0.13	0.18	0.26	0.31	0.36
Foam Types and Densities	#1, Navy Foam, $66 \text{ kg/m}^3$ #2, Polystyrene, $14.2 \text{ kg/m}^3$ , #3, Soft Urethane, $14 \text{ kg/m}^3$				

Table 2. The Levels of the Parameters for Polymer Mixed Water Experiments

Stand-off Distance (cm)	1.27		
Traverse Speed (cm/sec)	2.54	12.7	50.8
Pressure (MPa)	69	138	207
Nozzle Diameter (mm)	0.13	0.26	0.36
Foam Type	#1, Navy Foam		

After each sample had been cut to measure 5 x 7.5 cm it was placed in the holder, the sample length was adjusted to exceed only slightly the anticipated depth of cut, in order to provide maximum sample stability. A cutting run was made. The pump was raised to the required pressure prior to the test, and the traverse conditions were such that the samples had accelerated to the required velocity before they passed under the jet. Similarly deceleration did not occur until after the sample carriage had passed beyond the jet. After cutting, the depth of cut was determined by using a thin metal ruler. On every specimen between four and seven depth values were taken, the final result was then obtained by averaging the values measured for these depths.

Where polymer was added to the water, before test, the procedure was slightly different. The polymer was added to a container full of fresh filtered water. After adding the liquid polymer the solution was stirred vigorously by hand for between 15 and 20 minutes. The solution was then immediately used, any fluid remaining after the test was disposed after the experiment. Thus, for every test at a new polymer concentration, a fresh mixture was prepared.

## RESULTS

The results for the experiments were analyzed using the desk-top computer program Statview 512, available for the Macintosh computer. Several regression models were considered. Among these the best correlation coefficients were achieved when the exponential model was used. A general equation of the model can be expressed as below:

$$D = k P^y V^z \dots\dots\dots(1)$$

where

- D is the depth of cut (cm)
- P is the jet pressure (MPa)
- V is the traverse speed (cm/sec)
- k,y,z are the regression coefficients

For three different foam types and five different nozzle diameters, individual relations are given in the form above in table 3. A multiple regression on the 375 data points indicated that the equation correlating jet performance with parameters can be expressed by the equation

$$D = 16.305 f^{-0.97} P^{1.15} n^{1.44} V^{-0.3} \dots\dots\dots(2)$$

where

- f is the foam density in kg/m<sup>3</sup>
- n is the nozzle diameter measured in mm

The equation had an R-squared value of 0.945. A similar procedure was developed to analyze the results of Foam #1 when different concentrations of polymer were used in the feed water. Again a multiple regression equation was generated using 135 data points of the form:

$$D = 0.0911 P^{1.42} n^{1.37} V^{-0.39} (1 + c)^{0.71} \dots\dots\dots(3)$$

where  
 c is the concentration of polymer as a percentage.

The R-square value for this relationship is 0.98

Table 3. The coefficient of exponential relationship between traverse speed, pressure and depth of cut. Obtained from multiple regression analysis of 25 data points. (For the general form of the equations refer to the text).

Nozzle Dia (mm)	Regression Coefficients			Correlation Coefficient R-squared
	Constant	Tr. Speed	Pressure	
<b>Foam #1</b>				
0.13	0.0210	-0.37	1.43	0.988
0.18	0.0217	-0.37	1.37	0.990
0.26	0.0125	-0.39	1.44	0.974
0.31	0.0050	-0.40	1.53	0.982
0.36	0.0110	-0.41	1.29	0.960
<b>Foam #2</b>				
0.13	0.5983	-0.22	0.91	0.951
0.18	0.9379	-0.20	0.77	0.962
0.26	0.2604	-0.21	0.98	0.970
0.31	0.1120	-0.20	1.05	0.978
0.36	0.1273	-0.19	0.94	0.970
<b>Foam #3</b>				
0.13	1.5634	-0.26	0.79	0.933
0.18	0.9370	-0.24	0.86	0.941
0.26	0.2720	-0.29	1.08	0.953
0.31	0.0494	-0.33	1.34	0.953
0.36	0.0246	-0.40	1.42	0.918

Once the relative performance parameters for the jet cutting system had been established, it was also felt of interest to determine which set of jet cutting conditions provided the most efficient set of cutting parameters. For this reason a calculation of system specific energy was made (Ref. 1). This calculation was to determine the effect amount of energy required, under the different cutting conditions to generate unit volume of cut in the foam. The power of the jet can be given by the equation:

$$\text{Power(MJ/sec)} = \text{Pressure(MPa)} \times \text{FlowRate(m}^3\text{/sec)}$$

Specific energy values are determined by dividing the power of the jet by the volume of the material removed in unit time. In the volume calculation, slot width is considered as being equal to the jet diameter.

To present the individual correlations of the parameters briefly as plots, the values that are produced from a certain level of each parameter are averaged. As an example, to obtain the pressure versus depth of cut plot, all test values obtained at the same pressure levels were averaged, regardless of the other parameter levels. Thus an average from 25 tests is obtained for each relation to depth, in traverse speed, pressure and nozzle diameter in figures 4, 5 and 6. The same procedure was applied to specific energy. These relationships were plotted in figures 7, 8 and 9.

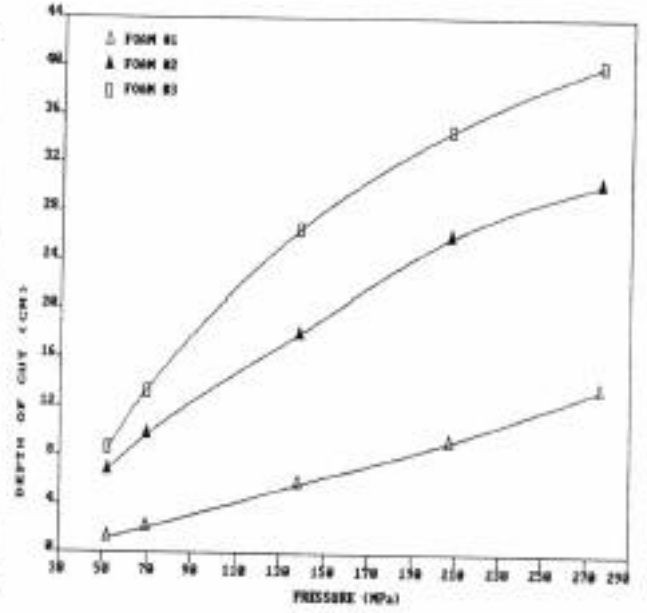
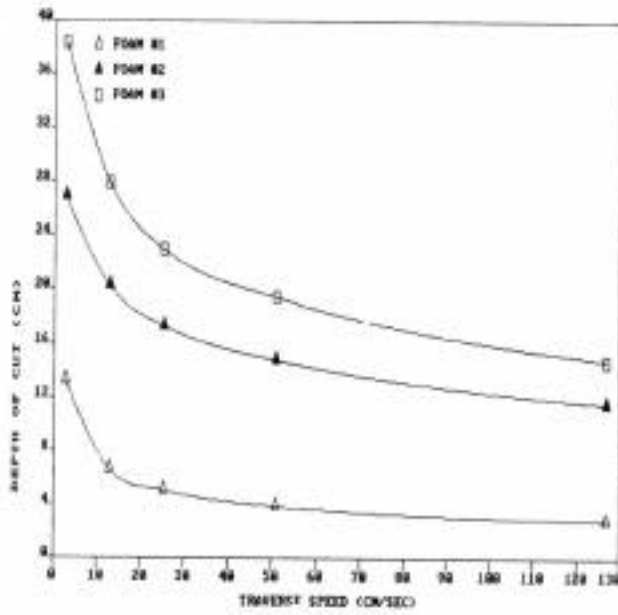


Figure 4. Average depth of cut versus traverse speed.

Figure 5. Average Depth of cut versus pressure.

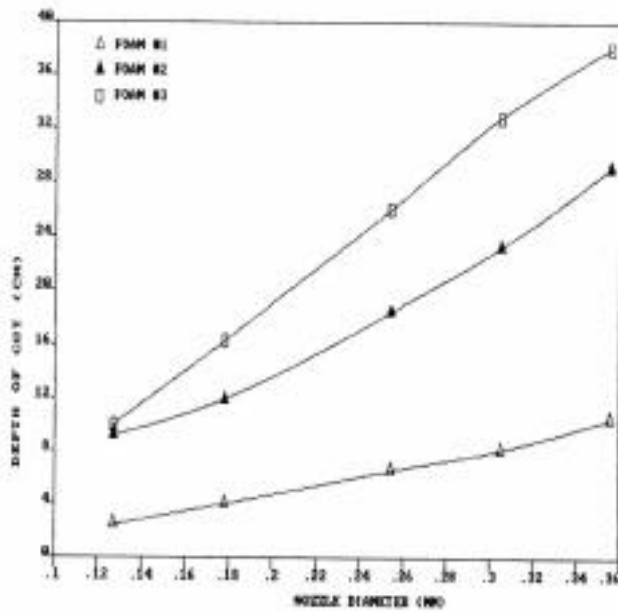


Figure 6. Average depth of cut versus nozzle diameter.

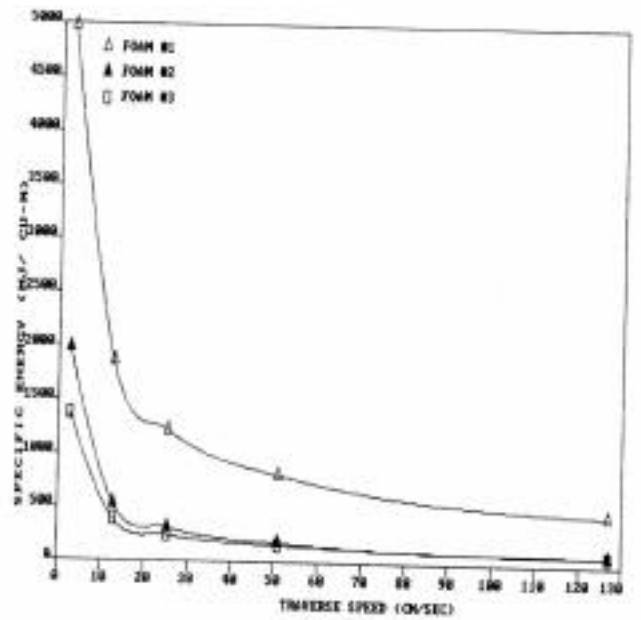


Figure 7. Average Specific Energy versus traverse speed.

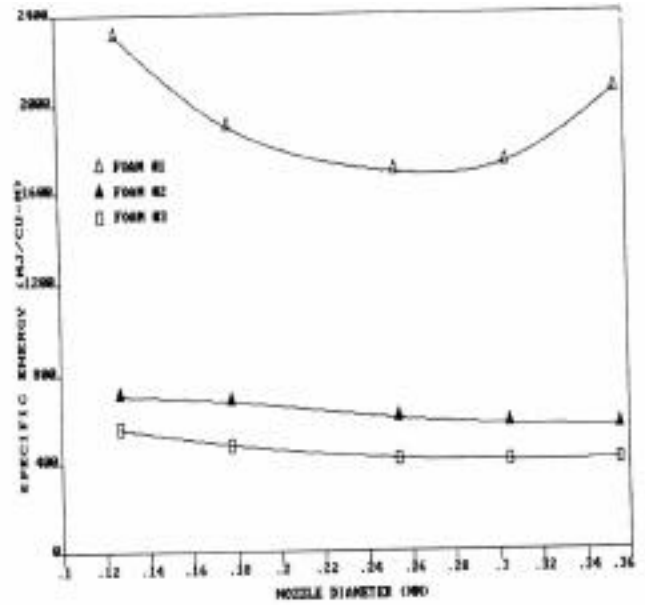
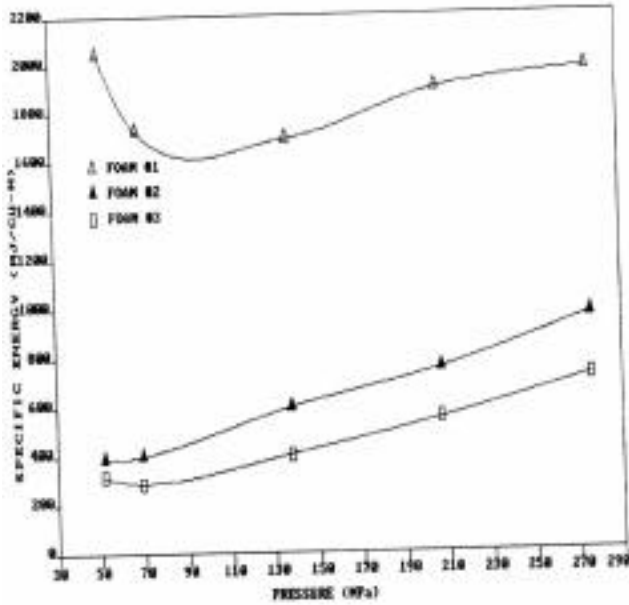


Figure 8. Average Specific Energy Versus Pressure      Figure 9. Average Specific Energy versus nozzle diameter.

The experiments which used the Superwater solution were performed under the range of test parameters shown in table 2. For ease in illustrating the effects of change in polymer concentration on depth of cut, individual depth values were normalized by dividing the depth achieved with particular polymer concentration by the equivalent depth of cut obtained with plain water. Then normalized depth values for every polymer concentration are averaged regardless of the other parameter levels. An average of 27 tests is obtained for each point plotted against polymer concentration (%) in figure 10.

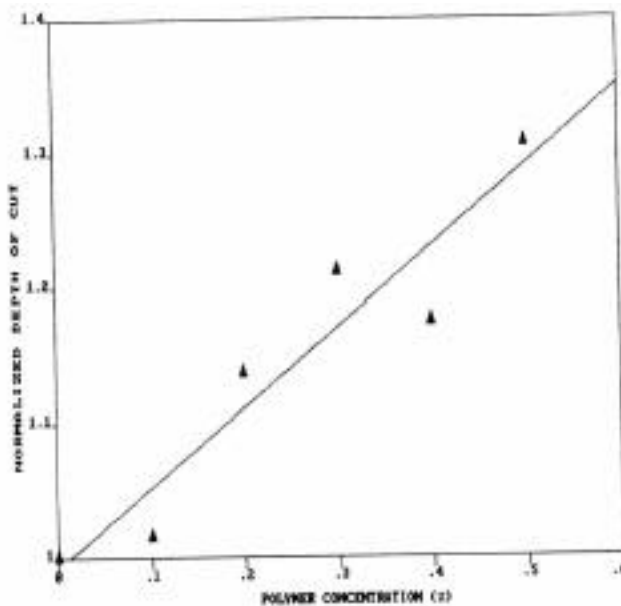


Figure 10. Average Normalized Depth of Cut Versus Polymer Concentration

## DISCUSSION OF RESULTS

Even though foam is a considerably softer material than normally tested in the Center, the results show close similarity to those relationships found when water jetting in geotechnical materials. The depth of cut achieved is sensibly linearly related to the jet pressure and is in a power relationship with nozzle diameter while it has a perfect inverse power relationship with traverse speed (Fig 4, 5, 6). The coefficient of parameters varies as a function of foam type, thus for traverse speed it ranges from -0.19 to -0.41 and pressure 0.79 to 1.54. These variations suggest that the physical properties of the target material will play a part in establishing those relationships. The range of materials tested in this program did not, however allow the exact determination of these relationships .

The depth of cut increases when the foam material gets softer. In order to represent foam type quantitatively a material property should be used. In this study, foam density was determined since it was the most easily measurable property

The relationship found between density of the foam and depth of cut found in this series of tests should not be used as more than a guide, because of the limitations in the range of foams tested. Determination of the exact relationship would require that more testing be carried out over a wider range of foam densities.

The effect of increasing the concentration of Superwater in the fluid showed that the depth of cut increased linearly with increase in polymer concentration (Fig 10). However the polymer concentration cannot be increased beyond 0.5% since the water becomes too viscous.

## SPECIFIC ENERGY

Although the major consideration in any cutting operation is likely to relate more to the speed at which the cut can be made, to the full depth of the specimen, and with an acceptable edge quality, the relative energy requirements do suggest which of the variety of options which might be available to the user would be most efficient. This is particularly true when the same effects can be achieved at different combination of jet parameters and cutting speeds. Specific energy was found to decrease with an increase in traverse speed (Fig. 7) in a similar manner to the depth of cut (Fig 4). Energy requirements decreased with increase in nozzle diameter (Fig. 9), for Foam #2 and 3 however the curve showed a minimum at 0.254 mm nozzle diameter for Foam #1, also there was a distinct minimum in the pressure:energy curve (Fig 8) between 70 and 140 MPa. at around 100 MPa. for Foam # 1. Foam #2 did not show such a minimum but the curve is nearly flat in the region below 70 MPa, while Foam #3 showed a minimum value at 70 MPa. This results suggest that water jets are most efficient in cutting foam at pressures below 100 MPa. A similar type of conclusion has previously been observed by Summers D.A. in rock and coal cutting (Ref 2 & 3).

As a consequence it is concluded that the most efficient combination for the cutting of foam lies in use of high traverse speeds, large and intermediate nozzle diameters and lower (<100 MPa) jet pressures with the specific choice of parameters varying slightly with changes in foam type. The energy required to cut foam increased

with the density of the material, or, more likely, because the hardness of the material is increased.

### QUALITY OF CUT

The quality of cut decreased as the slot depth increased. In the deepest part of the slot generally a fibrous structure was generated in the stronger foam, but was not as evident in the softer material. Long fibers and unclear cuts occurred at slow speeds, generally at less than 25 cm/sec, at pressures above than 200 MPa and at nozzle diameters above 0.25 mm. However the upper 30 cm. of a cut was usually smoother than the lower part in all cases. Higher speeds generally gave clear cuts. Consequently as the depth of cut was reduced smoother cuts should be expected.

### AN EXTRAPOLATION OF THE RESULTS

The ultimate requirements for the contract which funded this work are to cut the support foam which will underlay a variety of different geometries involved in shipping Navy stores around the world. Two configurations for the jet system can be envisioned as a result of this study. In the first . the shapes will be carved from the top, using a variation in the speed of the jet to achieve the necessary depths of cut at different points. Sequential adjacent passes would be required to fully cover the volume of the part to be supported. The alternate method is to contour the profile of the part and remove the isolated core of material, to leave the support foam. It is this last use which requires that the jet be capable of achieving deeper penetration levels. Incorporation of the nozzle as the cutting unit on an X-Y table has been found to provide the flexibility to follow the necessary contours of the cut.

To achieve the flexibility and required speed of motion a computer program is used, which drives two high precision stepping motors through cards and drives controlled by an IBM XT microcomputer. All motion commands for the necessary movement of the XY table are compiled and filed in the hard disk before the driving program loaded. This is necessary because of the relatively slow operating speed of the microprocessor using the Basic c language. Results from the experiments presented in this paper, were used to predict cutting conditions required to cut specially 56 cm thick billets of a different kind of foam ( $63.5 \text{ kg/m}^3$  density) for a specific purpose. When prediction equation 2 was used for this extrapolation, a 56 cm cut in this foam would require a pressure of 276 MPa, at a cutting traverse speed of 0.4 cm/ sec, with 0.36 mm nozzle diameter. 0.2 cm/sec traverse speed value and the values above were used in the experiment. The nozzle was moved on a circular path and cut through 56 cm of thickness. However only first 36 cm of the cut foam showed good surface quality while the surface roughness grew as the slot depth reached to 56 cm (figure 11).

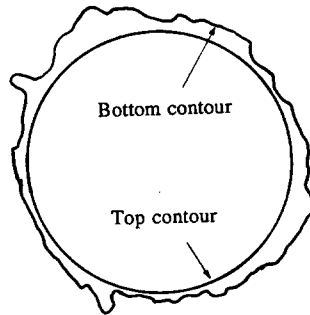


Figure 11. Edge quality and relative profiles of the top and bottom of a 56 cm cut.

#### REFERENCES

1. Teale R. The concept of specific energy in rock drilling. *Int J. Rock Mech and Min Sci*, Vol 2 No 1, March 1965, pp 57 - 74.
2. Summers, D.A. Water Jet Cutting Related to Jet and Rock Properties. *Proc. 14th Symp on Rock Mech.* June 11-14, 1972, pp. 569-588.
3. Summers, D.A. Water Jet Cutting of Sedimentary Rock. *Journal of Petroleum Technology*, July 1972, PP- 797-802.

#### ACKNOWLEDGEMENTS

This program was funded through the Naval Weapons Support Center, Crane, IN under contract N00164-86-M-5639, and we are grateful to Mr. Dennis Smith, Contracting Officer and Mr. Frank Niehaus, Technical Project Officer for their considerable help which they and their organization provided. This work was carried out with the help of Mr. J. Blaine, Mr. L. J. Tyler, Mr. R. Fossey, Mr. S. Gabel, all of the technical staff of the Rock Mechanics and Explosives Research Center, University of Missouri-Rolla. This paper was typed by Ms. J. Moutray. This help is gratefully acknowledged.

## PERCUSSIVE JETS—STATE-OF-THE-ART

E. B. Nebeker  
Scientific Associates, Inc.  
Santa Monica,  
California

### ABSTRACT

Percussive Jets are rapidly pulsing jets in which the frequency, amplitude, and waveform of the pulses are carefully controlled. Other investigators have attempted to create relatively high-frequency pulsing jets in a variety of ways which differ from Percussive Jets. Some of this work is reviewed. The importance of controlling frequency, amplitude, and waveform can be shown by examining the impact mechanisms of a pulsing jet. Impact mechanisms often attributed to Percussive Jets include a higher ratio of impact areas to water volume, initial impact effects such as water hammer and high lateral velocities, cyclical unloading of the target material to produce absolute tension, and fluid mechanics which allow these jets to resist aerodynamic disruption. Earlier work was done to demonstrate these mechanisms. Often, the results were dramatic. More recent work involves combining these effects in one jet in both a time-dependent and time-independent manner. Such an approach may involve complex waveforms but allows, for example, a jet to show good initial impact effects and also the ability to resist aerodynamic drag which gives great working or standoff distances. These effects as well as the jet interaction with target materials are briefly discussed.

### NOMENCLATURE

$c$  = speed of sound in water  
 $P$  = nozzle discharge pressure  
 $P_a$  = water hammer pressure  
 $P_s$  = stagnation pressure  
 $v$  = velocity  
 $\rho$  = density

### INTRODUCTION

Technically attractive and economically feasible applications for water jets are continually being found. However, at some point everyone becomes aware of the basic performance limitations of conventional water jets. In an effort to improve cutting performance, higher and higher pressures are used. As pressures are raised, more power is required and eventually equipment reliability becomes a problem. Abrasives are becoming increasingly popular but they add to the complexity of a water jet system and bring their own equipment concerns.

Many applications for water jet cutting would be more attractive if a water jet could cut at greater distances from the nozzle. Earlier attempts to improve cutting distance have consisted of improving nozzle design, conditioning the flow upstream of the nozzles, using polymer additives in the water, and employing air- or water-injected shrouds.

Our approach to improving the performance of conventional water jets is to fundamentally modify the physical fluid behavior of an ordinary, continuous water jet. We term these jets "Percussive Jets."

## PERCUSSIVE JETS

### General

The photograph in Figure 1 can be used to illustrate Percussive Jets in their simplest form. The special free-stream characteristics of Percussive Jets shown may be obtained by modulating the discharge of water through the jet nozzle, i.e., by cycling the discharge flow above and below its average value with some particular frequency, amplitude, and waveform. Details have been discussed in References (1), (2), and (3).



Figure 1. Example of Percussive Jets. A small cyclic variation or modulation impressed on a steady discharge of water causes the free jet to become bunched. Consequently the jet will strike a target in a sequence of sharp impacts rather than steadily.

In modulated free jet discharge, the slow and fast portions of each discharge cycle tend to flow together or bunch in the free stream. The stream thus becomes a train of bunches of water which eventually separate. Bunch diameter increases with downstream distance until the axial velocity becomes uniform within each bunch.

At any particular distance from the nozzle, the free flow produced by modulation is periodically thicker and thinner than the nozzle discharge. Maximum and minimum diameters depend on downstream distance according to modulation characteristics and to aerodynamic and surface tension effects. The diameter is a minimum of zero for part of the time if the stream bunches have separated.

When this varying free flow strikes a target, the momentum flux through the nozzle is not transmitted as a steady force, but as a possibly discontinuous sequence of force peaks or percussive impacts. The maximum stream impact area and force at any distance from the nozzle correspond to the maximum cross-sectional area produced by stream bunching up to that distance.

This process of discharge modulation which produces free stream bunching and Percussive Jets is very different from pulsed, intermittent, or off-and-on steady jet flow. Two distinguishing features are most important:

1. An intermittent steady jet would not produce enlargement of the stream and amplification of the impact force at a distance, i.e., force peaks. The intermittent jet would simply deliver segments of the steady-jet lowforce impact .
2. The Percussive Jet flow is produced in the free stream by the action of a relatively small modulation of the flow rate, e.g., a few percent modulation. In contrast to pulsed flow, the discharge system does not suffer water hammer and extreme variations in back thrust.

A variety of variables affect the Percussive Jet process and are discussed more thoroughly in Reference (4). Modulation frequency, amplitude, and waveform are the most important variables under the control of the user. However, other factors, such as aerodynamic forces, surface tension, fluid friction, turbulence, velocity profile, rotational flow components, etc. also may affect the process but are examined in Reference (3).

#### Frequency

The desired modulation frequency is determined by consideration of standoff distance, jet velocity, modulation amplitude, and objective in modulating the flow. As discussed in Reference (3), the growth of bunching, or Percussive Jet character, obtained at a particular distance from discharge depends on the discharge modulation amplitude and on the number of "bunching lengths" contained within the distance. The bunching length or the ratio jet velocity/ modulation frequency is simply the length of jet participating in such complete modulation cycle. Small modulation amplitude can yield considerable bunching after only a few bunching lengths of flight.

Small cutting jets typically operate at standoffs under 100 jet diameters because jet momentum decays rapidly beyond this distance, as shown in References (5) and (6). As an example, consider jets of discharge diameters of 0.060 - 0.080, which would presumably operate at standoffs of only a few inches. In order to produce Percussive Jets within such distance, the bunching length should be about an inch or less so that several bunches are included between discharge and target. Since the jet discharge velocity would normally be on the order of 1000 ft/sec, the modulation frequency would have to be at least 10,000 cycles/sec.

For operation of a jet at long standoff distances, other criteria should be applied. References (7) and (8) indicate the frequency should be determined by the effect of aerodynamic considerations.

Clearly, a useful modulator design would have to provide frequency control over a very broad range of experimental variables. In the past, the Percussive Jet has been operated from very low frequencies up to 50,000 cycles/sec. However, the most

commonly used range is between 100 and 15,000 cycles/sec. To be able to vary the frequency easily during a run over a considerable range of frequencies is most valuable.

### Amplitude

The modulator produces both a flow rate and pressure drop oscillation. The latter is always important so that, as a first approximation, the function of the modulator is to generate a varying pressure drop. In further approximation, pressure drop is proportional to the through flow area.

According to the discussion in Reference (3), if the acoustic pressure oscillation components were negligible, a reasonable pressure drop would yield about 10 percent peak-to-peak discharge modulation amplitude. Even with strong acoustic components, a few percent modulation would still be obtained and these are the magnitudes of interest.

### Waveform

Jet bunching behavior tends to be governed by the fundamental frequency component of the modulation. Hence, the precise pattern of area variation produced by the modulator is not of primary importance. However, although the precise determination of waveform may not be as important as frequency and amplitude, waveform must be controlled. Reference (4) shows the disastrous consequences of poor waveform.

## IMPACT CHARACTERISTICS

The percussive impact produced by jet flow modulation has various characteristics which promote better cutting efficiency. The most often discussed general features of Percussive Jet impact are as follows.

### Amplified Impact Area and Force

The bunching produced by discharge modulation enlarges the free stream cross-section as shown in Fig. 1 and hence the impact area and total force applied. The jet nozzle thus achieves the surface coverage of a larger nozzle but, since the bunching flow is discontinuous, a larger water volume is not actually discharged. This feature of Percussive Jets increases the area impacted per unit water volume, which, even without considering detailed mechanism, may be expected to improve cutting performance.

The underlying reason is probably that hydraulic pressure decays with depth within the cut being made by the jet, Ref. (9), so that, for cuts of equal volume, jet impact is more efficient for the shallower or wider surface area cuts. In addition, the discontinuous Percussive Jet flow implies greater residence time for spent water than does steady jet flow for the same cut. This property of the Percussive Jets would tend to improve on cutting inefficiency caused by interference between spent water and the incoming jet. Although the total force exerted is amplified in Percussive Jets, this amplification results from the enlarged impact area rather than representing increased stress, as is the case with the water hammer discussed below.

Figure 2 shows this effect on limestone. Notice that the Percussive Jet cuts are wider and deeper than a cut made by a conventional jet. This type of cutting improvement

has been demonstrated on all types of materials tested from very hard granite to soft brick and sandstone.

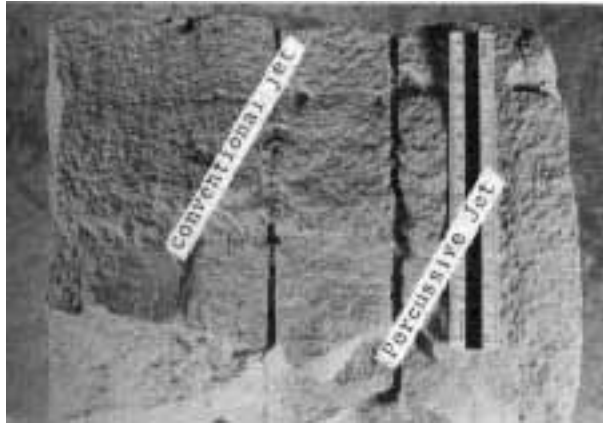


Figure 2. TRAVERSE CUTS ON LIMESTONE. Typical example of a Percussive Jet cutting wider and deeper than a conventional jet.

#### Initial Impact Effects

The initiation of each impact cycle of a Percussive Jet after arrival of each free stream bunch at the target is accompanied by two important effects.

1. Very large compressive stresses of very short duration are produced in the target material; these stresses correspond to "water hammer" pressure rise as each bunch is stopped by the target.
2. Very high lateral velocities with corresponding shear and impact develop in the initial spreading of each water bunch over the target-these velocities essentially derive from "shaped-charge" augmentation - water is squeezed out between the leading surface of each bunch and the target surface.

The magnitude, location, and duration of these initial impact effects depends on the shape and velocity of the water bunches plus the condition of the target surface. Both effects are considered instrumental in practical cases of damage by water drop impact, e.g., rain field erosion of aircraft surfaces, steam turbine blade erosion; the water hammer causes fracturing failure while the lateral outflow shears material from surface cracks and roughness, Ref. (10). Steady jets can have some initial impact effects owing to accidental discontinuities in the free stream. However, in the case of Percussive Jets, the repetitive initial impacts are deliberate and the entire stream participates coherently.

Water hammer is the more important effect; water hammer pressure can exceed the stagnation pressure of a water bunch or drop by an order of magnitude, Ref. (11). Hence, water hammer enables Percussive Jets to cut rocks which require cutting pressures much greater than the available hydraulic pressure. The initial high spreading velocities are also much larger than the impact velocity, Refs. (10) and (12). However, a water film over the target tends to cushion against scouring by the lateral outflow more

than against water hammer. Cushioning of the water hammer impact is not excessive if the bunch diameter is substantially greater than the film thickness, Ref. (12). Furthermore, the target is also attacked by cavitation produced at nuclei within the liquid film by the water hammer pressure wave, Ref. (13).

Since the pressure levels generated on a target surface can be expected to be a major factor in determining the effectiveness of the cutting operation, estimating these pressure levels is important. With a steady-state flow of water from a conventional steady-state jet impinging normally on a flat surface, the level of stress generated at the stagnation point is given by:

$$P_s = \frac{1}{2} \rho V^2$$

where:

$\rho$  is the water density  
 $V$  is the jet velocity.

However in applications using the Percussive Jet where the water jet tends to break up to form discrete liquid droplets or bunches, the impact stress can be order of magnitude higher  $P_s$ . Numerous studies have indicated that the transient stress between a liquid droplet and rigid plane surface can be given approximately by the simplified water hammer equation.

$$P_a = C \cdot V$$

where

$C$  is the acoustic wave speed.

Using the above equation the following table was constructed showing the manner in which the steady-state stagnation pressure,  $P_s$ , and intermittent “water hammer” pressure,  $P_a$ , vary with nozzle discharge pressure,  $P$ . The discharge velocity varies with nozzle characteristics but can be estimated from:

$$V = 12.0\sqrt{P}$$

$P$ (psig)	$V$ (ft/sec)	$P_s$ (psig)	$P_a$ (psig)
350	220	340	15,000
550	280	530	19,000
10,000	1,200	9,700	81,000
30,000	2,100	29,000	140,000

In considering the significance of this table, examine a 0.065-inch diameter nozzle firing 10 gallons of water per minute at a discharge pressure of 10,000 psig. The steady state stress on the target material will be 9,700 psig. However, for a Percussive jet, in which the bunches have completely separated the intermittent stress will be 81,000 psig. Incidentally, most rock materials have uniaxial tensile strengths that vary between

500 psig and 6,000 psig. Compressive strengths, however, range between 7,000 psig, and 70,000 psig.

This very approximate exercise is interesting because it indicates the possibility of modifying a conventional jet of only 10,000 psig discharge pressure into a Percussive Jet with impacts close to the compressive strength of granite.

Higher discharge pressures yield even higher impact stresses. For instance, if a Percussive Jet were operated in a way in which the bunches separated at 30,000 psig discharge pressure, the yield or proportional limit as well as the ultimate strength in tension and shear of steel would all be exceeded! Imagine what would happen if a material could be impacted over 10,000 times per second with impact stresses greater than the compressive strength of steel.

However, such a goal is not easy to obtain. The bunches that impact the target must be of proper size and shape. Again, the operator must have good control over frequency, amplitude and waveform. Condition of the target surface is important. Brief discussions in the literature have dealt with the size and shape of liquid droplet impact to obtain the best effect. We are trying to investigate this question at the present time.

Figure 3 may give an example of the effects of initial impacts on concrete block. The conventional jet could not effectively penetrate the aggregate. However, the Percussive Jet cut the aggregate as well as the softer matrix of the concrete block.

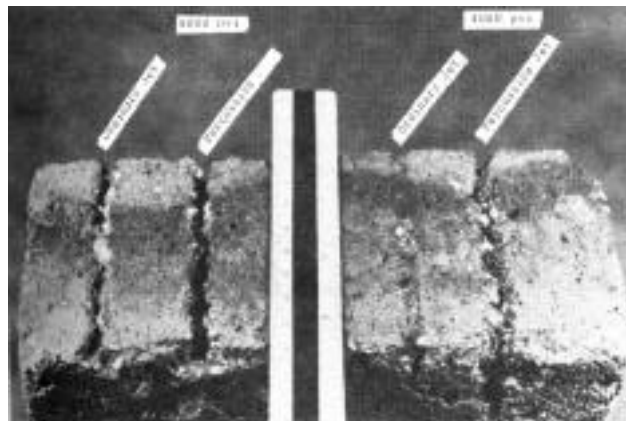


Figure 3. CONCRETE TRAVERSE CUTS. The conventional jet could not effectively penetrate the aggregate, whereas the Percussive Jet cut the aggregate as well as the softer matrix of the concrete block.

### Tensile Stresses

In a Percussive Jet, compression of the rock is periodically relieved at the termination of each water hammer pulse and of each bunch impact as a whole. This unloading is the necessary condition for obtaining absolute tension from stress pulses reflected at the free boundaries offered by natural or fracturing cracks, Ref. (14). Rock failure is very effectively induced by these tensile stresses as brittle fracture occurs more

readily in tension than in compression, Ref. (15). This consideration applies both to the water hammer and ordinary impact load, but, since water hammer stresses are the larger, their tension effects are correspondingly greater and can propagate farther within the target.

Figures 4, 5 & 6 give possible examples of this type of mechanism. The failures look as if the front face of the specimens were "pulled off." The traverses on granite shown in Figure 4 are extremely rough-looking. In Figure 5, the Percussive Jet has broken off a large piece from the face of the shale. All of the damage shown in these figures resembles brittle fracture as the material is removed in large pieces. The static impacts on brick shown in Figure 6 show the Percussive Jet induced failure within the front face of the brick.

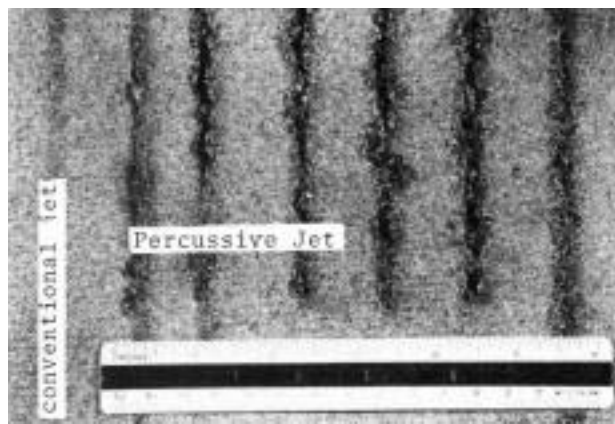


Figure 4. TRAVERSES ON GRANITE. Note rough-looking Percussive Jet cuts. At best, the conventional jet would only roughen the surface. Working pressure was 8000 psi.

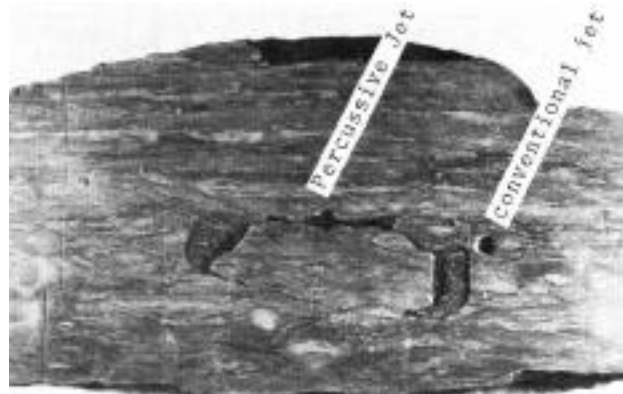


Figure 5. STATIC IMPACTS ON COALASSOCIATED SHALE. The Percussive Jet often induced massive failures as illustrated. The piece that was broken off has been replaced in this photograph. These impacts were about 2 seconds in duration at 4000 psi.

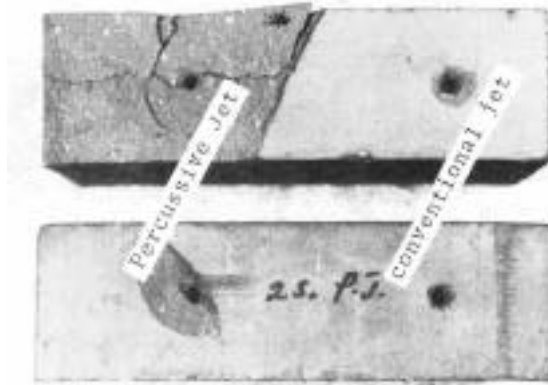


Figure 6. STATIC IMPACTS ON COMMERCIAL BRICK. These discharges were about 2 seconds in duration at 2300 psi pressure and illustrate massive-type failures induced by the Percussive Jet.

### Jet Persistence

Discharge modulation and stream bunching can act to reduce jet momentum decay at long standoff distances. At standoffs greater than 100 jet diameters or so, jet velocity decreases rapidly with distance by aerodynamic drag, Ref. (16). In this decay, distance scales directly to discharge diameter so that, if discharge velocity and other factors are equal, the thicker the jet, the greater the momentum retained at given distance. The free stream diameter in Percussive Jets becomes progressively less uniform with distance, i.e., the bunching process, so that the jet may be loosely regarded as an alternation of two other jets with bigger and smaller discharge diameter than the actual. By this transformation, the jet momentum passes progressively into the bigger jet component, where it is less subject to aerodynamic decay. Thus, the Percussive Jet should retain momentum better than the same discharge un-modulated. Of course, this viewpoint is highly simplified. References (7) and (8) discuss the phenomenon in more detail.

This jet persistence consideration is not as important for small cutting jets which are ordinarily used at standoffs under 100 diameters and suffer little velocity decay. In big jet applications, however, long range is highly desirable so that the jets are used up to distances involving severe velocity decay. Any of the favorable Percussive Jet impact characteristics discussed above can increase the effective range, but in the case of jet persistence, the range benefit is direct, i.e., velocity decay is deferred to greater distances. Furthermore, the velocity itself, or force exerted at impact, may not be the relevant parameter for jet performance, but rather some higher power of velocity, e.g., pressure against the target or hydraulic power per unit area. In the latter case, the benefits of improved jet persistence are correspondingly greater.

Figure 7 <sup>1</sup> shows examples of better jet persistence using Percussive Jets. Five-second duration firing of Percussive Jet and conventional jet were made side-by-side at 2000 psig discharge pressure. The block was 45 feet (1080 nozzle diameters) from the nozzle. The small hole in the upper left-hand side was made by a conventional jet and

<sup>1</sup> EDITORIAL NOTE – THIS FIGURE WAS NOT SUPPLIED WITH THE MANUSCRIPT.

was 3/4-inch deep by 6 inches in diameter. The large hole was produced by a Percussive Jet under identical conditions and is 6 inches deep and about 9 inches in diameter. This large crater has a deep central hole only about 2 inches in diameter.

We generally feel that if the Percussive Jet is operated properly, the distance to which the Jet fails to cut is about twice as far from the nozzle as that distance at which a conventional jet can no longer cut. This applies to most cutting and mining situations.

#### OTHER INVESTIGATION

Conventional water jets have proven to be very useful in many applications. However, if conventional jets can be made to "pulse," performance is further improved under certain conditions. The literature review shown here illustrates that a variety of approaches have been used to make jets pulse rapidly.

References (17), (18), (19), and (20). Mechanically interrupted a water jet downstream of the nozzle with a rotating device and reported improved cutting performance. Reference (21) discussed the possibility of interrupting a small water jet with a laser. These techniques can improve performance but waste a considerable portion of the material and momentum of the jet during the mechanical interruption.

Reference (22) discusses the possibility of using an ultrasonic transformer to induce vibrations upstream of the nozzle. Reference (23) indicates the basics leading to electric discharge in water upstream of the nozzle to produce pulsing. Neither reference shows equipment or experimental cutting results.

Reference (24) oscillates a jet nozzle in the axial direction of the jet but found no improvement in performance. They felt the velocity of oscillation was too small in relation to the velocity of the jet to show an appreciable effect.

Reference (25) used an acoustic generator to induce surface tension or Rayleigh instability leading to drop formation. Owing to surface energy changes, cylindrical liquid surfaces are unstable against sinusoidal surface disturbances having wavelengths which exceed the cylinder circumference. Reference (6) allowed a conventional water jet to proceed far enough downstream of the nozzle so that the natural processes of aerodynamic disruption and Rayleigh instability disrupted the jet into droplets. As a rule of thumb, this process begins approximately 300 nozzle diameters from the nozzle. Both investigations relying on Rayleigh instability obtained improvements in performance. Unfortunately, these processes occur sufficiently downstream of the nozzle that a considerable amount of the energy of the jet dissipated.

Reference (26) discussed the possibility of using the elastic properties of the piping system upstream of the nozzle to produce pressure oscillations at the nozzle. A pulsing jet would then issue from the nozzle. Reference (2) used the natural frequency of oscillation of a volume upstream of the nozzle to produce pressure pulsation. This was done with and without an imposed modulated signal further upstream. This approach was

not pursued because frequency, amplitude and waveform of the resulting signal were fundamentally too difficult to vary and control.

Reference (27) uses a self-excited oscillation upstream of the nozzle to interrupt a water jet. They report that by varying the dimensions of the system and operating pressure, three separate mode resonances (frequencies) can be selected. Test results indicated that although the depth of the cut was not improved over a conventional jet, the cut width was increased appreciably.

Reference (28) reports some preliminary results of a jet driven Helmholtz oscillator to produce pressure oscillations upstream of a nozzle. No cutting or performance data is given.

Reference (29) presents a theoretical analysis and concludes a self-excited oscillation upstream of the nozzle can be used to create pulsed jets.

## COMBINING EFFECTS

### General

Hence, many investigators have used a variety of approaches to produce rapidly pulsing jets. Almost all who have gotten to the experimental stage report increased effectiveness in many cleaning and cutting situations.

In spite of these favorable results, our preference for creating pulsed jets is to use a variable flow resistance upstream of the nozzle. Our work over the last 15 years has resulted in a patented device and method which creates Percussive Jets. The proven models are rugged, reliable, and have thousands of running hours without any signs of wear.

A variety of reasons for this preference in producing Percussive Jets exists, which include:

1. ability to control frequency, amplitude and waveform. Reference (4) gives examples of the disastrous effects of poor control. As a result of good control, the bunch which strikes a target can be shaped to increase the likelihood of a particular effect. Figures 8 and 9<sup>2</sup> give examples of "water hammer" and "shaped charge" tailoring of the leading edge of the bunch.

2. ability to easily change frequency, amplitude and waveform. Frequency and amplitude can be continuously changed or "dialed-in."

### Time-Dependent Combinations

Recent experimental results have indicated the feasibility of combining several "pulses" which are repeated in a time dependent manner. The waveform and resulting jet

---

<sup>2</sup> EDITORIAL NOTE – THESE FIGURES WERE NOT SUPPLIED WITH THE MANUSCRIPT

appear considerably different than the sample jet shown in Figure 1. In this way, a variety of pulses can be included in one jet. For example, one pulse may create "water hammer" on the target surface, another may clear out residual water and material with a "shaped change" leading edge and another protect the entire stream from aerodynamic disruption.

#### Time-Independent Combinations

Experimental evidence shows the benefits of being able to "dial-in" jet performance features to create maximum target damage. The parameters can be searched by the operator at will, independent of any time frame. The range of Percussive Jet variables can be much greater than in the time-dependent combinations. This approach to jet cutting is especially beneficial when working with inhomogeneous materials.

#### SUMMARY

1. Being able to control frequency, amplitude and waveform in pulsed jets is not only important but essential if the full potential of pulsed jets is to be realized.
2. A variety of different pulses can be incorporated in a single jet in a time dependent or time-independent manner.

#### REFERENCES

1. Nebeker, E.B. and Rodriguez, S.E., "Percussive Water Jets for Rock Cutting," Proc. Third International Symposium on Jet Cutting Technology, BHRA Fluid Engineering, 1976, Paper BI, 9 pp.
2. Nebeker, E.B. and Rodriguez, S.E., "Percussive Water Jets for Rapid Excavation," 1973, Scientific Associates, Inc.
3. Nebeker, E.B. and Rodriguez, S.E., "Development of Percussive Water Jets," 1979, Scientific Associates, Inc.
4. Nebeker, E.B. and Rodriguez, S.E., "Pulsing Water Jets," Proc. Seventh International Symposium on Jet Cutting Technology, BHRA Fluid Engineering, 1984.
5. Donnelly, R.J. and Glaberson, W., "Experiments on the Capillary Instability of a Liquid Jet," Proc. Roy. Soc. London, 1966, A290.
6. Houlston, R. and Vickers, G W., "Surface Cleaning Using Water-Jet Cavitation and Droplet Erosion," Proc. Fourth International Symposium on Jet Cutting Technology, BHRA Fluid Engineering, ~ 1978, Paper H1, 18 pp.
7. Nebeker, E.B., "Standoff Distance Improvement Using Percussive Jets," Proc Second U.S Water Jet Conference, 1983, 10 pp
8. F. Nebeker, E.B., "Development and Test of Large Diameter Percussive Jets," 1982, Scientific Associates, Inc.
9. Leach, S.J. and Walker, G.L., "Some Aspects of Rock Cutting by High Speed Water Jets," Phil. Trans. Roy. Soc. London, 1966,
10. Brunton, J.H., "Deformation of Solids by Impact of Liquids at High Speeds," Erosion and Cavitation, Amer. Soc. Testing Mats., ASTM STP 307, 1962.
11. Cooley, I.C., "Rock Breakage by Pulsed High Pressure Water Jets," Proc. First International Symposium on Jet Cutting Technology, BHRA Fluid Engineering, 1972, Paper B7.

12. Ponchot, W.D., "Hydrodynamic Model of Correlation of Metal Removal Rates from Repetitive Drop Impact," Erosion and Cavitation, Amer. Soc. Testing Mats., ASTM STP 474, 1970.
13. Eisenberg, P., "Cavitation and Impact Erosion," Characterization and Determination of Erosion Resistance, Amer. Soc. Testing Mats., ASTM STP 474, 1970.
14. Jaeger, J.C. and Cook, N.G.X., "Fundamentals of Rock Mechanics." Chapman and Hall Ltd. and Science Paperbacks, 1971
15. Bieniawski, Z.T., "Mechanism of Brittle Fracture of Rock," MEG 580, 1967, Council for Scientific and Industrial Research, Pretoria, South Africa.
16. Yanaida, K., "Flow Characteristics of Water Jets," Proc. Second International Symposium on Jet Cutting~Technology, BHRA Fluid Engineering, 1974, Paper A2, 14 pp.
17. Brook, N. and Summers, D.A., "The Penetration of Rock by High-Speed Water Jets," Int. Journal of Rock Mechanics & Mining Science, Vol. 6, 1969, pp. 249-259.
18. Lichtarowicz, A. and Nwachukwu, G., Proc. Fourth International Symposium on Jet Cutting Technology, BHRA Fluid Engineering, 1978, Paper B2, 6 pp.
19. Erdmann-Jesnitzer, F. and Schikorr, H. Louis a.W., "Cleaning, Drilling and Cutting by Interrupted Jets," Proc. Fifth International Symposium on Jet Cutting Technology, BHRA Fluid Engineering, 1980, Paper B1, 11 pp.
20. Kiyohaski, H., Kyo, M, and Tanaka, S., "Hot Dry Rock Drilling by Interrupted Water Jets," Proc. Seventh International SvmDosium on Jet Cutting~Technology, BHRA Fluid Engineering, 1984.
21. Mazurkiewicz, M., "The Analysis of the Possibility of Bunching with a High Pressure Water Jet," Proc. Second U. S. Water Jet Conference, 1983, 8 pp.
22. Puchala, R.J. and Vijay, M.M., "Study of an Ultrasonically Generated Cavitating or Interrupted Jet: Aspects of Design," Proc. Seventh International Symposium on Jet Cutting Technology, BHRA Fluid Engineering, 1984.
23. Hawrylewicz, B.M., Purkala, R.J., and Vijay, M.M., "Generation of Pulsed or Cavitating' Jets by Electric Discharge in High Speed Continuous Water Jets," Proc. Eighth International Symposium on Jet Cutting Technology, BHRA Fluid Engineering, 1986.
24. Erdmann-Jesnitzer, F., Hassan, A.M., and Louis, H., "A Study of the Oscillation's Effects on the Cleaning and Cutting Efficiency of High Speed Water Jet," Proc. Third International Symposium on Jet Cutting Technology, BHRA Fluid Engineering, 1976, Paper C3, 15 pp.
25. Danel, F. and Guilloud, J.C., "A High Speed Concentrated Drop Stream Generator," Proc. Second International Symposium on Jet Cutting-Technology, BHRA Fluid Engineering, 1974, Paper A3, 6 pp.
26. Wylie, E.B., "Pipeline Dynamics and the Pulsed Jet," Proc. First International Symposium on Jet Cutting Technolozy, BHRA Fluid Engineering, 1972, Paper A5, 12 pp.
27. Chahine, G.L., Conn, A.F., Johnson, V.E., and Frederick, G.S., "Cleaning and Cutting with Self-Resonating Pulsed Water Jets," Proc. Second U. S. Water Jet Conference, 1983, 12 pp.

28. Sami, S. and Anderson, C., "Helmholtz Oscillator for the Self-Modulation of a Jet," Proc. Seventh International Symposium on Jet Cutting Technology, BHRA Fluid Engineering,
29. Liao, Z.F. and Huang, D.S., "Nozzle Device for the Self-Excited Oscillation of a Jet," Proc. Eighth International Symposium on Jet Cutting Technology, BHRA Fluid Engineering, 1986.

# THEORETICAL ANALYSIS AND EXPERIMENTAL STUDY OF THE SELF-EXCITED OSCILLATION PULSED JET DEVICE

Liao Zheng Fang and Tang Chuan Lin  
Chongqing University  
China

## ABSTRACT

This paper explores the self-excited oscillation mechanism of jet-impinging edge-cavity system; amplification condition of shear layer instability and feedback condition of fluid-dynamic excited. A mathematical model is developed for vortex-impinging edge interaction. Experimentally it has been found that the shape of cylindrical cavity impinging edge and diameters of nozzle play an important role in disturbances feedback and have a strong effect on the production of discrete vortex ring.

## NOMENCLATURE

D: diameter of cavity

$D_1$ : diameter of the interior nozzle

$D_2$ : diameter of the external nozzle

H: the cavity height

h: the height of strain wave

I:  $I = \sqrt{-1}$

k:  $k = r/U_m h$

L: the cavity length

M: number of equality

N: harmonic wave number

P: pressure in the cavity

$P_{rms}$ : root-mean-square value of pressure

s: shear layer thickness

T: pulsed period

t: time

U: dimensionless velocity in stream direction

$U_m$ : velocity at jet axle center

u: jet velocity

$u_1$ :  $u_1 = u/U_m$

V: dimensionless velocity in y direction

w: wave number

x: distance from interior nozzle

$x_0, y_0$ : the position of point unit vortex in physical plane

Z: physical plane

$Z_0$ : time-dependent position of vortex in physical plane

$\lambda_0$ : time-dependent position of point unit vortex

$\bar{\lambda}_0$ : conjugate point of  $\lambda_0$

$\partial_i$ : the phase difference of the ith harmonic wave

r: strength of point unit vortex

$\theta$ : dimensionless unsteady potential function

## Subscripts

i: the number of the harmonic wave

j: the foot-note of variable h

## INTRODUCTION

It is known that the cleaning and breaking effects of pulsed water jets are superior to a continuous water jet. The device of self-excited oscillation pulsed jet among pulsed jet devices is considered a jet device having a potential for future development because of its simple structure and small volume as well as requiring no external excitation source or moving seals.

According to the inducement cause of self-excited oscillation, Rockwell and E. Naudscher have categorized the self-excited oscillation into three groups (4):

- (1) Fluid-dynamic excited. Where oscillation arises from inherent instability of the shear layer, amplifies in the shear layer and intensifies through disturbance feedback.
- (2) Fluid-resonant excited. Where oscillation is influenced by resonant wave effects. The disturbances are amplified when standing waves form in the proper flow-type.
- (3) Fluid-elastic oscillation. Where oscillation arises from the motion of solid boundary periodically.

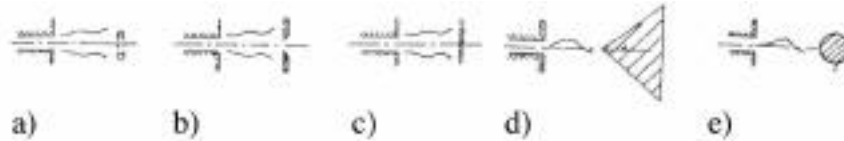


Fig.1 Basic flow-types to produce self-excited oscillation  
a) Jet-ring b) Jet-hole c) Jet-plate d) Jet-edge e) Jet-cylinder

Several flow-types which give rise to self-excited oscillation are shown in figure 1. The mechanism of the self-excited oscillation is generalized for these flow-types and described as following: Unsteady disturbances waves (vorticity fluctuations) through shear layer in cavity can be amplified for the instability of shear layer. When the disturbances travel to the downstream edge and impinge on the impinging edge, pulsed pressure disturbances are induced in the vicinity of downstream edge. The induced disturbances propagate upstream to the sensitive region of shear layer near separation. The feedback of disturbances induce new perturbation waves at separation and it is followed by amplification of the disturbances in the streamwise direction. The events above are repeated lead to large amplitude self-excited oscillation. Therefore, in the course of production of the self-excited oscillation, the structural parameters and shape of cavity and fluid-dynamic, fluid-resonant and fluid-elastic effects have influence on self-excited oscillation. To utilize effectively self-excited oscillation of fluid to produce pulsed or unsteady jet and enhance peak of jet, this paper explores the relationships between structural parameter of the device of self-excited oscillation jet and its amplitude, frequency as well as effect of feedback. Especially considered are the shape of the impinging edge and the diameter of the nozzle. According to the investigation of

D.Rockwell, E.Naudascher, Thomas and V.Sarohia et al (3,4,5),we conceive to add a axis-cylindrical cavity on the jet impinging edge (different shapes) system in fig 1.They evolve into the device below in fig 2. This is physical model which we studied.

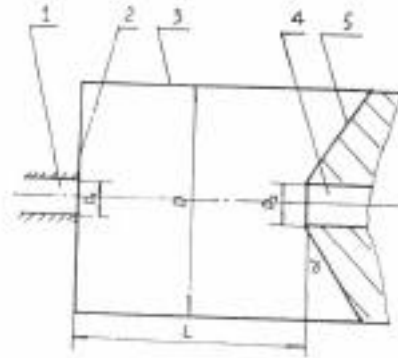


Fig.2 The physical model of self-excited oscillation pulsed jet device  
 1 Interior nozzle    2 upstream edge    3 cylindrical cavity    4 external nozzle  
 5 impinging edge

### THE MATHEMATICAL MODEL FOR VORTEX-IMPINGING EDGE INTERACTION

To research the interaction of a vortex-impinging edge, a simple two-dimensional vortex model is developed. Four different shapes of impinging edge are discussed. For the sake of simplicity, the size of the vortex ring is ignored. It is assumed that the physical place  $z$  is transformed to plane  $\lambda$  by a non-formal mapping method. In the transformed plane ,the complex velocity potential  $F(\lambda)$  at point  $y$  is given by:

$$F(\lambda) = u\lambda + I \frac{r}{\partial\pi} \ln \frac{\lambda - \lambda_0}{\lambda - \bar{\lambda}_0} \quad (1)$$

Where:

- $r$ : strength of point unit vortex
- $\lambda_0$ : time-dependent position of the vortex
- $u$ : jet velocity

To obtain velocity field of physical plane  $z$ ,it is necessary to know the relationship between variable  $z$  in the physical plane and variable  $\lambda$  in the transformed plane.

Let

$$Z = f(\lambda) \quad (2)$$

Hence,the velocity field of physical plane can be shown by:

$$U - IV = \frac{dF(\lambda)}{d\lambda} \frac{1}{f'(\lambda)} = [U_1 + I \frac{K}{2\pi} \frac{1}{\lambda - \lambda_0} - \frac{1}{\lambda - \bar{\lambda}_0}] \frac{1}{f'(\lambda)} \quad (3)$$

Where:

- $U, V$  and  $U_1$  are non-dimensional velocities
- $U_m$ ,axis velocity of jet

H:cavity height

Variable  $\lambda$  has been non-dimensionalized on height H. Equation (3) becomes non-dimensional velocity field equation. It is obvious that equation (3) isn't valid at  $\lambda_0$  point. For getting velocity field of vortex, Routh's rule must be used.

$$F_{z_0}(Z) + \frac{Ir}{\partial\pi} \ln(Z - Z_0) = F_{\lambda_0}(\lambda) + \frac{ir}{\partial\pi} \ln(\lambda - \lambda_0) \quad (4)$$

Where

$F_{z_0}(Z), F_{\lambda_0}(\lambda)$  are velocity field of Z and  $\lambda$  respectively.

$$F_{z_0}(Z) = F_{\lambda_0}(\lambda) + \frac{Ir}{2\pi} \ln \frac{\lambda - \lambda_0}{z - z_0} \quad (5)$$

According to Taylor's series:

$$Z = f(Z) = f(\lambda_0) + (\lambda - \lambda_0)f'(\lambda_0) + \frac{1}{2}(\lambda - \lambda_0)^2 f''(\lambda_0) + 0(\lambda - \lambda_0)^3 \quad (6)$$

$$Z - Z_0 = (\lambda - \lambda_0)f'(\lambda_0) + \frac{1}{2}(\lambda - \lambda_0)^2 f''(\lambda_0) + 0(\lambda - \lambda_0)^3$$

Equation (5) becomes:

$$F_{z_0}(z) = F_{\lambda_0}(\lambda) - \frac{Ir}{2\pi} \ln \left[ f'(\lambda_0) + \frac{1}{2}(\lambda - \lambda_0)f''(\lambda_0) + 0(\lambda - \lambda_0)^2 \right]$$

$$U - IV = \frac{dF_{\lambda_0}}{d\lambda} \frac{d\lambda}{dz} - \frac{IK}{2\pi} \frac{\frac{1}{2}f''(\lambda_0) + 0(\lambda - \lambda_0)}{f'(\lambda_0) + 0(\lambda - \lambda_0)} \frac{d\lambda}{dz} \quad (7)$$

Equation (7) is transformed into the equation of vortex velocity field when Z approaches  $Z_0$  and  $\lambda$  approaches  $\lambda_0$ .

$$U_0 - IV_0 = \left[ U_1 - I \frac{K}{2\pi(\lambda - \lambda_0)} \right] \frac{1}{f'(\lambda_0)} - \frac{IK}{4\pi} \frac{f''(\lambda_0)}{[f'(\lambda_0)]^2} \quad (8)$$

It is seen from the above that we can calculate the position of the vortex with  $U_0, V_0$  in equation (8) Because:

$$\frac{dx_0}{dt} = U_0(x_0, y_0)$$

$$\frac{dy_0}{dt} = V_0(x_0, y_0) \quad (9)$$

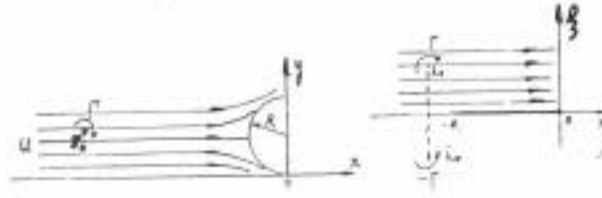


Fig. 3 Flow model

Hence we can compute time-dependent position of vortex by numerical integration for equation (9). But the velocity components in equation (8) is given by variable  $Z$ , the calculation above must use the velocity components which is given by variable  $Z$ . It is necessary to use function  $Z=f(A)$  to transform.

To estimate the pressure pulse induced on the impinging edge during its movement along its streamline and consider vortex effect on pressure pulse, an appropriate pressure coefficient that contains only the effect of the vortex and not of jet itself is following:

$$C_p = \frac{P_x - P_o}{P_o} = U^2 - V^2 - (U_k^2 - V_k^2) - \frac{\partial \phi}{\partial t} \quad (10)$$

Equation (3) is used for the calculation of the velocity components  $U, V$  assuming that there is no vortex in jet ( $k=0$ ), while the components  $U_k, V_k$  include the vortex term ( $k \neq 0$ ).

Where

$\frac{\partial \phi}{\partial t}$ : non-dimensional unsteady potential

The non-dimensional unsteady potential function of the physical model which we studied is the real part of (1):

$$\phi = \text{Re}(u\lambda) + \frac{K}{2\pi} [\text{avg}(\lambda - \bar{\lambda}_o) - \text{avg}(\lambda - \lambda_o)] \quad (11)$$

Non-dimensional unsteady potential  $S$  is estimated numerically by using the difference scheme:

$$\frac{\partial \phi}{\partial t} = \frac{1}{t} (\phi_{m+1} - \phi_m) \quad (12)$$

Where

$M$  stand for position  $M$ .

It follows from this that we can get transformed relationship  $Z=f(x)$  with Nonformal mapping method transforming different shapes of impinging edge into plate surface and calculate pressure coefficient by numerical calculation and demonstrate quantitatively effects of vortex for oscillating pressure.

## THE EFFECTS OF NOZZLE DIMENSION AND IMPINGING EDGE

We have operated experiment with the device which have different nozzle diameter ratios ( $D_2/D_1=0.8-1.5$ ) and four shapes of impinging edge (taper surface,convex spherical surface, concave spherical and plate surface).It is shown in figure 4,5,6 and 7 for shapes of impinging edge.

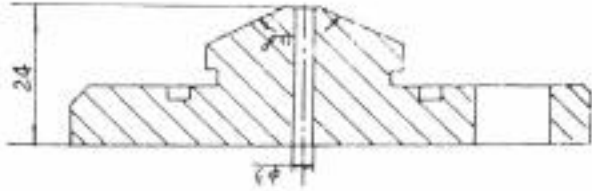


Fig.4 Taper surface

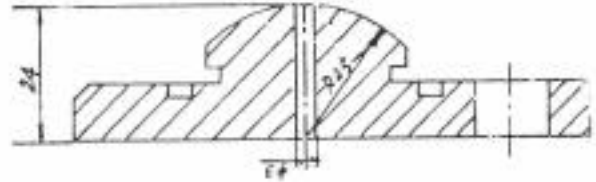


Fig.5 Convex spherical surface

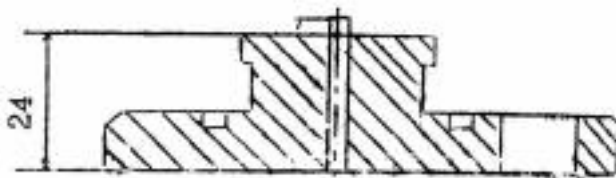


Fig.6 Plate surface

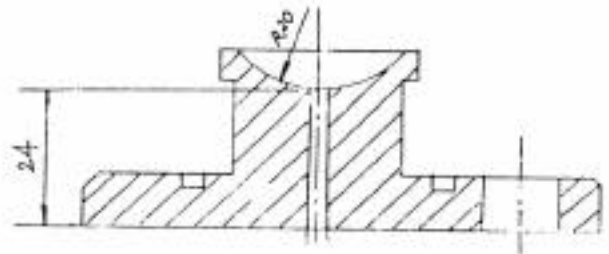


Fig.7 Concave spherical surface

### 1) The Effects of nozzle diameter

Maintaining the structural parameters of the device and system pressure or discharge to be constant, we studied the effects of different nozzle diameter for self-excited oscillation.

When  $D_2/D_1 < 1$ , the oscillating amplitude of jet spurting from external nozzle is very small, we didn't clarify whether it is self-excited oscillation or turbulence oscillation of jet.

When  $D_2/D_1 > 1$  - the device can produce strongly oscillation and the pulse amplitude is very large. It is researched that the nozzle diameter ratio is equal to 1.2 for the self-excited oscillation is optimal. Therefore, for studying different shape effects on self-excited oscillation, we made use of the nozzle diameter ratio 1.2.

### 2) The Effects of The Shapes of Impinging Edge

#### A Taper Surface

(1) Effects of Cavity Length Changing With Maintaining System Pressure To Be Constant When cavity length is increased step by step the jet will be changed from steady into unsteady. Initially the pulsed frequency is very high and pulsed amplitude is very small. When cavity length is equal to 1.6, the pulsed amplitude increases abruptly and the cavity length arrives 2.4, the oscillating amplitude is up to maximum. The pulsed

amplitude decreases suddenly when cavity length increases continuously at the moment to  $L/D_1=4.8$ , and produces sound. When the cavity length is increased further, pressure water begin to flow from the air hole and induced oscillations die away completely. On the position where pulsed amplitude is very large, the oscillation appears periodicity and includes more frequency components. But in other position, the oscillation is unregularly. The amplitude of one frequency component arrives at a maximum and decreases lately sometimes. Before it didn't vanish completely, another one peak appears again. At the moment, the summits of the two frequency components may co-exist, and one is vanishing another is increasing. The record curves of test is shown in figure 8.

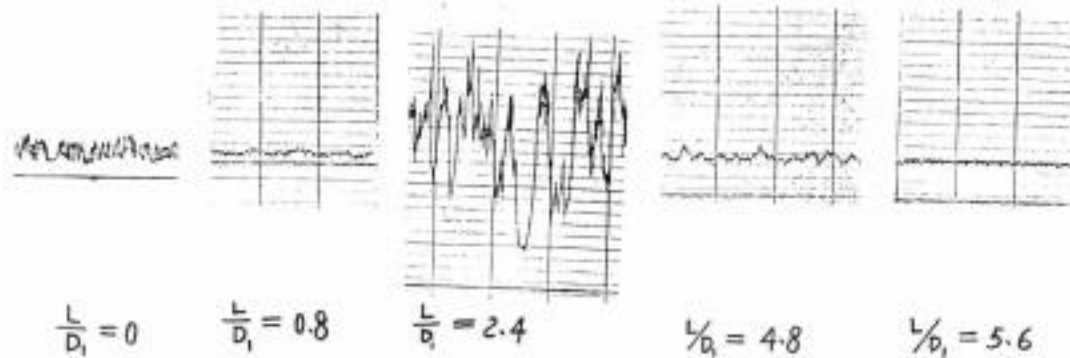


Fig.8 Record curves of test for taper surface when cavity length is changed and system pressure is constant

(2) The Position Where The Induced Oscillation Was Largest Was Unchanged, We Studied Effects of The System Pressure For Self-excited Oscillation We modulated system pressure with overflow valve. When pressure is up to 1.2MPa, the induced oscillation begins to appear. Induced oscillation is more strong and oscillation crest increases with system pressure rises lately. A record of the curves of the test are shown in fig. 9.

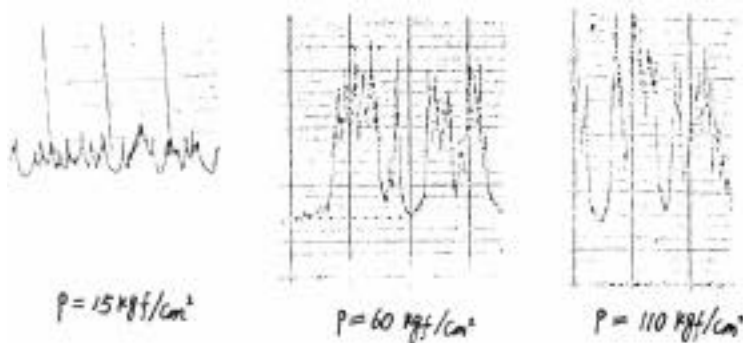


Fig.9 Record curves of test for taper surface for pressure is changed

### B Convex Spherical Surface

The phenomenon observed in the experiment is similar to a taper surface. But the positions where the oscillating crest were maximum, produced sound and the cavity

length that oscillation vanished are different. Of course, the amplitude and frequency differ from taper surface. A record of the curves of test is shown in fig.10.

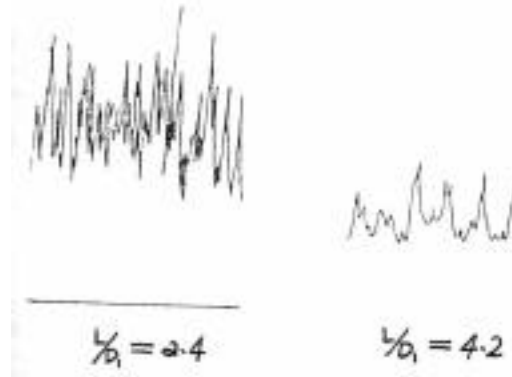


Fig.10 Record curves of test for convex spherical surface when cavity length is changed and system pressure is constant

### C Plate Surface

When impinging edge is plate surface, its experimental phenomenon is similar to above two impinging edge. But its oscillating amplitude is very small. Record curves of test is shown in fig. 11.

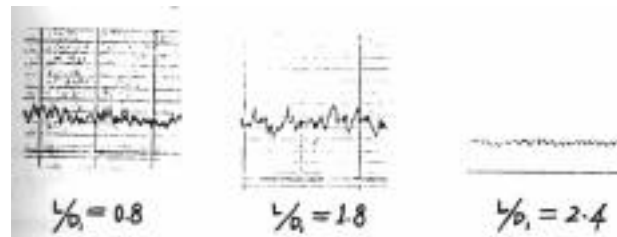


Fig.11 Record curves of test for plate surface when cavity length is changed and system pressure is constant

### D Concave Spherical Surface

Whether we change cavity length or system pressure, its oscillating amplitude is rather small. We didn't clarify which is self-excited oscillation or system itself oscillation.

### 3) Experimental Data Treatment

It is necessary to make harmonic analysis for the strain wave survey which consists of a lot of frequency components. The curves were recorded by light oscilloscope.

According to Fourier series theory, periodical function can substitute with infinite trigonometric series. Let  $g(t)$  be given by:

$$g(t) = \frac{a_0}{2} + \sum_{i=1}^n \left( a_i \cos \frac{2\pi}{T} it + b_i \sin \frac{2\pi}{T} it \right) \quad (13)$$

Where

T: wave function period

If we replace the wave function  $h(t)$  with  $g(t)$ , it can exist error  $h(t)$

$$h(t) = h(t) - g(t) \quad (14)$$

If t axis is divided by M at (0,T), there exists error  $h(j)$  at every  $t_j(j=1,2,\dots,M)$ .

According to the method of the least square principle, trigonometric polynomial exactly approximate to wave function  $h(t)$  when its error root-square-value is minimum. Hence it can determine coefficient  $a_0/2, a_i, b_i$ ,

$$\begin{aligned} \frac{a_0}{2} &= \frac{1}{m} \sum_{\delta=1}^m h(t_\delta) \\ a_i &= \begin{cases} \frac{2}{m} \sum_{\delta=1}^m h(t_\delta) \cos i(\delta \frac{2\pi}{m}) & \text{when } i = \frac{m}{2} \\ \frac{1}{m} \sum_{\delta=1}^m h(t_\delta) \cos \delta\pi & \text{when } i = \frac{m}{2} \end{cases} \quad (15) \\ b_i &= \frac{2}{m} \sum_{\delta=1}^m h(t_\delta) \sin i(\delta \frac{2\pi}{m}) \end{aligned}$$

Where

$j=1,2,\dots,M$ . M is equality number

$i=1,2,\dots,N$ . N is the Nth harmonic wave. It must satisfy  $N \leq (m-1)/2$ .

If let  $a_i = A_i \sin \delta_i$ ,  $b_i = A_i \cos \delta_i$ ; then  $g(t)$  can be expressed by

$$g(t) = A_0 + \sum_{i=1}^n A_i \sin(\frac{2\pi}{T}it + \delta_i) \quad (16)$$

Where

$$A_0 = a_0/2, A_i = \sqrt{a_i^2 + b_i^2}, \delta_i = \text{tg}^{-1} \frac{a_i}{b_i} \quad (17)$$

According to the fomula given above, we can compile program to set about harmonic analysis with computer. Under the condition of  $L/D_1=2.4$  and system pressure  $P=10.5\text{MPa}$ , we finished harmonic analysis for self-excited oscillation, computing a result which is shown in fig. 12.

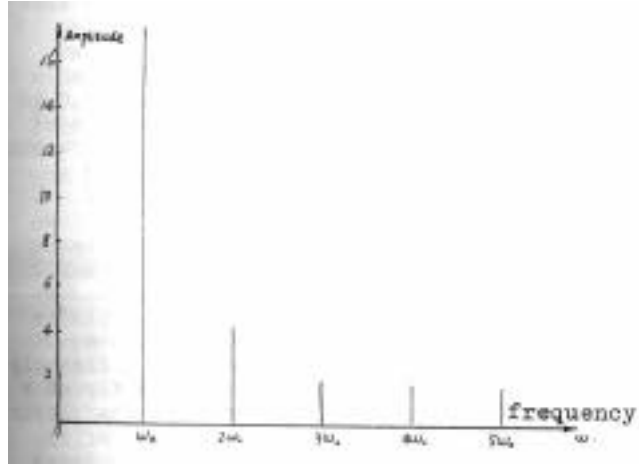


Fig.12 Diagram of Fourier frequency spectrum

Standing for fluctuation quantity is determined by

$$P_{rms} = \sqrt{\frac{1}{T} \int_0^T h^2(t) dt} \quad (18)$$

Equation(18) is integrated numerically with trapezoidal integration, then it's by

$$P_{rms} \doteq \sqrt{\frac{1}{m} \left[ \frac{h^2(0) + h^2(m)}{2} + \sum_{i=1}^{m-1} h^2(t_i) \right]} \quad (19)$$

It follows that we obtain the variational curve for non-dimensional root-mean-square value  $P_{rms} / P_R$  ( $P_R$ : reference value) with  $L/D_1$ , or  $U/U_s$  ( $U_R$ : reference velocity). It is shown in fig. 13,14.

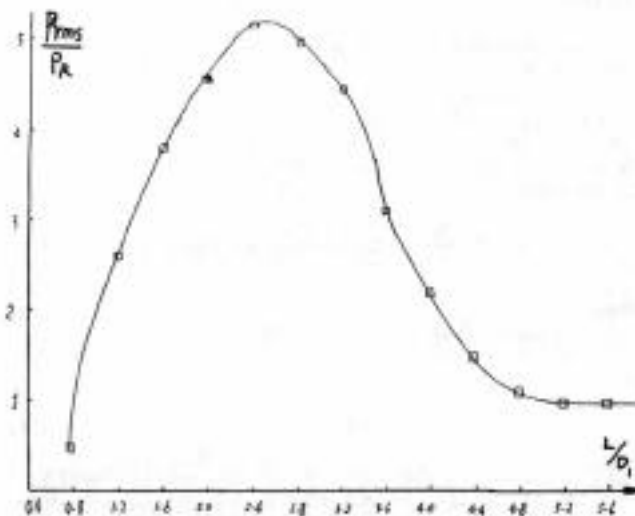


Fig.13 Variation of dimensionless root-square-value of pressure versus  $L/D_1$  for  $u$  is constant

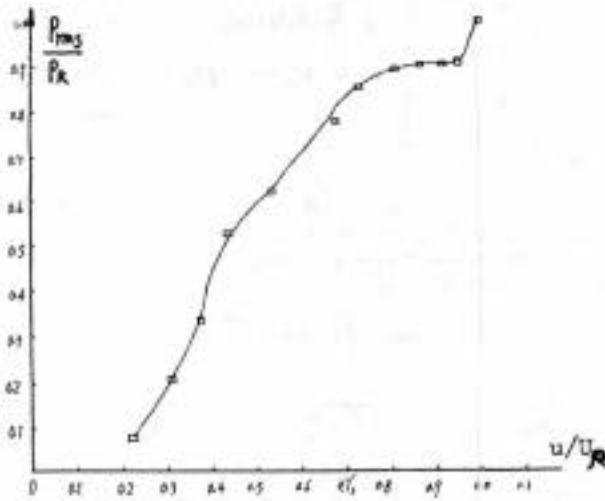


Fig.14 Variation of dimensionless root-square-value of pressure versus  $u/U_R$

To understand the transient pressure, we plotted the curves of  $P_{max}/P_R - L/D_1$ ,  $P_{max}/P_R - U/U_R$  and the curves of non-dimensional Strouhal number  $S_D$  with  $L/D_1$ , or  $U/U_R$ . They are shown in fig.15,16,17 and 18 respectively.

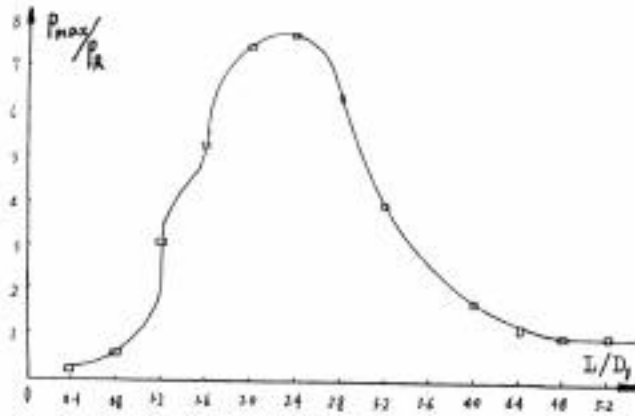


Fig.15 Variation of maximum dimensionless pressure versus  $L/D_1$

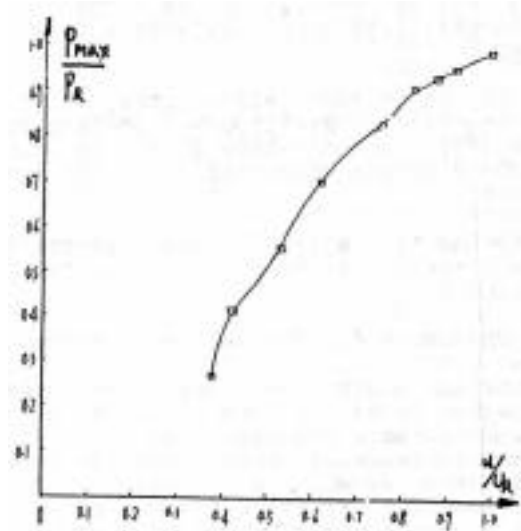


Fig.16 Variation of maximum dimensionless pressure versus  $u/U_R$

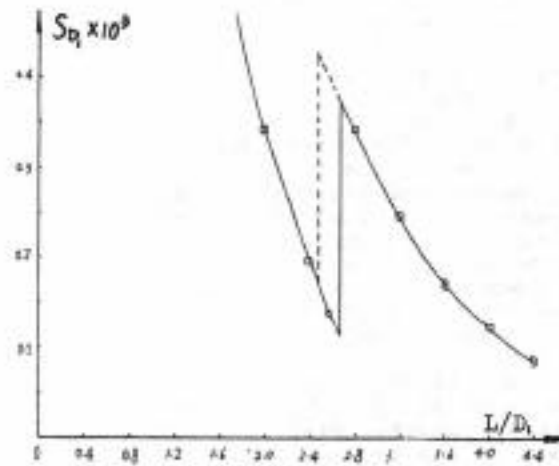


Fig.17 Variation of Strouhal number versus  $L/D_1$

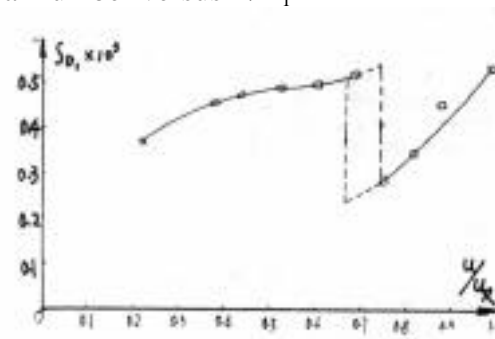


Fig.18 Variation of Strouhal number versus  $u/U_m$

For shorting paper, we only give the experimental data treatment of taper surface.

## EXPERIMENTAL RESULT ANALYSIS

### (1) The Cavity Length For Oscillation To Be Occured

The cavity lengths for oscillating to be occurred are the same corresponding to three different shapes of impinging edge from fig.8, 9 and 10. We know that the shear layer thickness  $s$  of round jet developing region can be calculated by:

$$s=c.x$$

Where

$c$ : experimental const.  $c=0.2-0.3$

Hence we can calculate the cavity length which jet can impinge on impinging edge, i.e.  $L/D_1=0.4$ . At  $0 < L/D_1 < 0.4$ , shear layer impinging on down stream edge don't satisfy oscillation requirement. At  $0.4 < L/D_1 < 0.8$ , although it forms shear layer which can impinge on downstream edge, the disturbances in this scope don't be content with the condition of self-excited oscillation of shear layer instability, and amplification of the perturbances only occurs in certain scope of Strouhal number.

### (2) The Scope of Oscillation To Be Produced

It is seen from fig.8,9 and 10 that the scopes of oscillation to be produced for taper surface,convex spherical surface and plate surface are  $0.8 < L/D_1 < 5.2$ ,  $0.8 < L/D_1 < 5.6$  and  $0.8 < L/D_1 < 2.8$  respectively . It shows in fig.8,9,10 that the self-excited oscillation consists of a lot of frequency components which have different oscillating amplitude respectively. According to shear layer instability theory, the disturbances (vorticity fluctuation) including different frequency components travel to downstream with jet, and lead to every frequency component to be amplified. Roscoe.D and Hankey [5] derived the relationship between amplification factor and wave number from stable equation (fig.19). Because  $w, \theta, s$  varies directly as  $\theta, s, x$  respectively. Then  $w$  varies directly as  $x$  also (where:  $\theta$  , momentum thickness,  $s$ : shear layer thickness,  $x$ : the disturbance between interior nozzle and external nozzle). Comparing indirectly fig. 13 with fig.18, we can see that the theory calculation agrees with experiment data. Exception,vortex running up and unlinear pressure oscillation composition in impinging region make the self-excited oscillation include many high frequency components (fig. 12).

(3) When cavity length  $L/D_1=5.2$  (taper surface),  $L/D_1=5.6$  (convex spherical surface) and  $L/D_1=2.8$  (plate surface), the jet produces sound, some parts of the energy (including pressure energy and kinetic energy) transform into sound energy and make oscillating amplitude reduce abruptly. It must be pointed out that it can produce resonant effects and increase greatly self-excited oscillation amplitude when the disturbances frequency in cavity liquid flow approximate to the frequency of sound effects.

### (4) The Cavity Length For Oscillation To Disappear

When the cavity length  $L/D_1=5.6$  (taper surface),  $L/D_1=5.8$  (convex spherical surface) and  $L/D_1=3$ .(plate surface),the self-excited oscillation disappears completely and strength of oscillation is weaker than strength of turbulent disturbances. It

results from disturbances not to content with condition of feedback for jet varying unregularly.

(5) It is shown in fig.17 that frequency appear to jump at  $2.4 < L/D_1 < 2.8$ , and the position for jumping up differs from the position of jumping down. There exists hysteresis quantity. This is similar to edge-tone and hole-tone and demonstrates their having some approximate oscillating mechanism .it is seen from figure.13 that the oscillating amplitude is a maximum and oscillation is very strong in this scopes.

(6) It can produce self-excited oscillation among the Reynolds  $Re=1.5 \times 10^5 - 4.8 \times 10^5$  from fig.14. They differ from hole-tone that only occur at  $Re=1000-2500$  and edge-tone that only occur at  $Re=80-1300$ .

## CONCLUSIONS

According to the experimental observation and data treatment above, we infer a few results is follows:

### 1: The Cause For The Self-excited Oscillation

During the disturbances developed in separation region travel to downstream certain frequency components are amplified differently for the mechanism of shear layer instability. The disturbances whose  $Sd$  is equal to  $0.5 \sim 0.1$  can be amplified. Arriving the impinging edge, the disturbances are limited and enforce an effective force on the flow fluid and lead to pressure or velocity changing. Oscillating pressure fields are produced in the impinging region. These disturbances propagate to very sensitive region at separation and induce new disturbances at separation region, and they excited jet shear layer to oscillate transversely at impinging region at a time. If the feedback is effective or positive feedback ,it will induce some new disturbances at separation region in phase with original disturbances and enhance instability of disturbances. These can offer energy for maintaining or increasing oscillations.

### 2 The Condition of Effective Feedback Or Positive Feedback

To make the new disturbances induced by the feedback disturbances from the impinging region in phase with original disturbances it is necessary that the disturbances waves near impinging edge exist proper phase difference with disturbances at separation region of shear layer. It has to do with volume fluctuation bounded by separation streamline of shear layer and cavity interior wall as well as deflection of separation streamline of shear layer. Positive feedback must demand that the deflection of separation streamline of shear layer near the separation region of shear layer has an opposite motion (deflection) near the impinging region (fig.19) To cancel volume fluctuation  $V(t)$  dynamic feedback pressure disturbances must be imposed on the jet shear layer. The feedback disturbance is proportional to  $V(t)$  .Therefore the effective feedback condition is volume fluctuation  $V(t)$  in phase with deflection of separation streamline of shear layer at separation region.

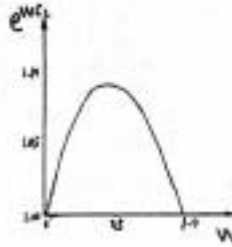


Fig.19 Amplification factor versus wave number according to Ref. (5)

### 3 Effects For The Shapes Of Impinging Edge

It is shown by theory analysis and computation that the pressure disturbance having different strength and frequency is generated for vortex-impinging edge interaction corresponding to different shapes of impinging edge. In the four shapes of impinging edge which we discussed, taper surface is good for generating self-excited oscillation. It has been seen from experimental observation and fig 8,10 and 11 that the amplitude and frequency of self-excited oscillation are different largely each other corresponding to four impinging edges. In the special case, the amplitude of self-excited oscillation is very large corresponding to one impinging edge (e.g. taper surface),but the amplitude of self-excited oscillation is very small corresponding to another one impinging edge(e.g. concave spherical surface).This is agreeable with theory analysis. It is concluded that the shapes of impinging edge have an large effect on self-excited oscillation.

### 4 Helmholtz Excitation Effects

Our physical model by adding a cylindrical cavity on jet-impinging edge (different shapes) in fig.1 to be formed a Helmholtz resonant cavity. The natural frequency  $f_0$  determined by structural parameters of cavity and restrain is approximate to self-excited oscillation frequency, It can amplify the pressure disturbances largely and make oscillation be more strong. Since the production of self-excited oscillation has to do with natural frequency of cavity and structural parameters, the structural parameters which make self-excited oscillation frequency match with natural frequency must be determined. This is what we are studying now.

### REFERENCES

- (1). Z.F. Liao and D.S. Huang, "Nozzle Device For The Self-excited Oscillation Of A Jet", 8th Inter. Symp. On Water Jetting Tech.BHRA 1986.
- (2). D.S. Huang and Z.F. Liao, "The Study Of Self-excited Oscillation Jet Mechanism," J. of Chongqing University, Go.3,1986.
- (3). V.Saroha, "Experimental Investigation of Oscillation In Flows Over Shallow Cavities" AIAA Journal,July,1977.
- (4) E.Naudascher, "From Flow Instability To Flow-induced Excitation," J. of Hydraulic Division,ASCE, July,1967
- (5) W.L. Hankey and J.S. Shang, "Analysis of Yressure Oscillation In Open Cavities," AIAA Journal, Aug. 1980
- (6) C.Knisey and Rockwell , "Self-sustained Low-frequency Components In An Impinging Shear Bayer," Fluid Mech.(1982),Vol 116.

(7) D.Rockwell and E.Naudascher,"ReviewSelf-sustained Oscillation of Flow Past Cavities," J. of Fluids Engineering Vol 100, June 1978.

(8) R.R. Clements,"An Inviscid Model of Twodimensional Vortex Shedding," J. Fluid Mech. Vol 157,1973,pp 321 336

# DYNAMIC CHARACTERISTICS OF WATERJETS GENERATED FROM OSCILLATING SYSTEMS

W.Z. "Ben" Wu, D. A. Summers, and M. J. Tzeng  
Rock Mechanics and Explosives Research Center  
University of Missouri-Rolla  
Rolla, Missouri

## ABSTRACT

In the last two decades, there has been a considerable increase in the use of pressurized waterjets as a novel means of cutting and cleaning surfaces in a wide variety of industrial applications. The fluctuating dynamic force exerted by a waterjet on impact was analyzed both in the time domain and the frequency domain. The effects of pump characteristics, hose and high pressure tubing, support constraints, nozzle geometry, jet velocity or pressure and stand-off distance are ascertained. A magnetic shaker was employed to excite the end of nozzle, both perpendicular and parallel to the ejecting direction of the jet. Correlations between the imposed excitation and the impact force from the waterjet are delineated.

## INTRODUCTION

The ejection of pressurized water through a small nozzle into ambient air will produce a solid jet stream, which rapidly breaks down into high speed droplets containing a high density of energy. The power in the coherent jet is increasingly being utilized as a cutting and cleaning tool in many industries. For example in chemical plants waterjet systems are frequently employed to clean deposits from heat exchangers, both on the shell and tube side. At a higher pressure, and lower flow rate, high pressure waterjets have become an accepted tool for cutting non-metallic materials such as plastic and cardboard. In recent years, this tool has also been considered as an innovative solution for the removal of plastic bonded explosives (PBX) from unwanted locations.

The impact force generated by a waterjet fluctuates; that is it does not apply a steady cutting force. As a consequence, vibration will be induced in any target structure. Under certain circumstances, it is possible to conjecture that a large vibration will develop in this target through resonant amplification, leading to fatigue failure in structures such as the heat exchanging system or leading to an induced explosion due to vibration related friction during the PBX cutting process. Because the fluctuating impact of the jet can be the main excitation source of a target structure, characterization of the waterjet impact is essential to predict and ameliorate unstable cutting or cleaning situations. However, before it is ejected through the nozzle, the water stream must first be pressurized in a pumping system. Thus a combined vibration analysis of the total system is required to give a better understanding of the waterjet impact.

The vibrational characteristics of pumps at various discharge pressures has been investigated by several researchers (1-4). Since the characteristics of a fluctuating waterjet strongly depends upon the choice of the associated pumping system, the objectives of the current research program are extended to include the effects of system

and operational parameters on the fluctuation of the waterjet. Four pumps, connected both with flexible hose, and with rigid metal tubing, to one of five nozzles capable of producing either a fan jet or a round jet, were operated at different pressures. The effects of the standoff distance and boundary constraints of the pipes were also included. Vibrations within the system and the variation of impact force were recorded in terms of time histories and frequency spectra. The correlation of the measured data were then delineated.

Pipe vibrations, both perpendicular and parallel to the ejecting direction of the jet were imposed. A magnetic exciter was applied to drive the nozzle leading to the variations of the waterjet structure. The effects on the impact force due to such oscillations at the nozzle were investigated in the time and the frequency domains. There are some significant correlations obtained.

### EXPERIMENTAL ARRANGEMENTS AND PROCEDURES

The experimental set-up shown in Figure 1 included a choice of a motor and a pump used to generate high pressure water in turn transmitted through either a piece of flexible hose or a length of rigid high pressure steel tubing. The pressurized water was then discharged through a nozzle onto a target plate. A lathe, simulating a rigid support, was employed to hold the target on one end and the supply tube on the other. In order to avoid splash-induced vibrations, a splash-guard plate was used to prevent the jet from hitting places other than the target. A magnetic shaker was employed to excite the nozzle at the end of the tube when necessary.

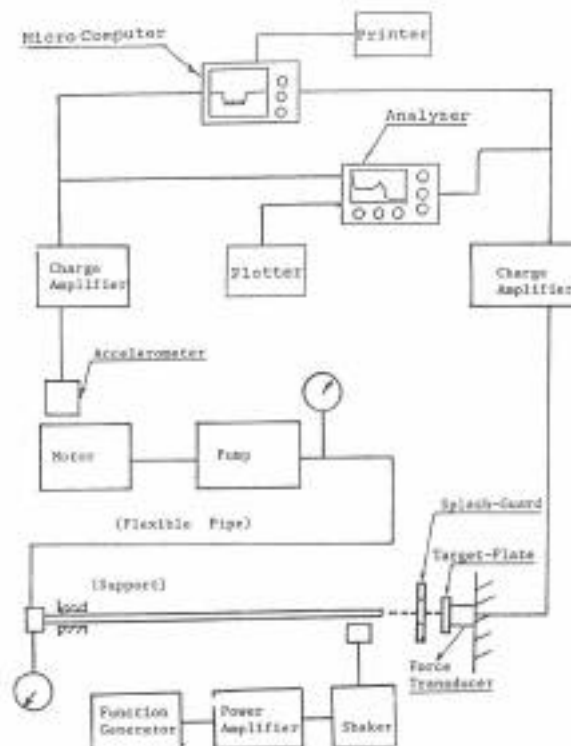


Figure 1. Schematic of the experimental set-up.

A piezoelectric transducer (Kistler-922F3), sandwiched between the target plate and a rigid support frame was used to record the impact force. A thin aluminum plate (0.25 cm thick) was employed as the target. Wave propagation in the plate was neglected which assumes that the force exerted on both sides of the plate was assumed identical. An accelerometer was applied to detect oscillations in the pumping system. Output signals from transducers were enhanced through charge amplifiers and then displayed and analyzed by a Hewlett Packard 3582A spectrum analyzer and an Apple IIe microcomputer. A high-speed (3.5 MHz) A/D converter was installed in the microcomputer which was then able to record the time-varying wave form; that is, the microcomputer was converted into an oscilloscope. An X-Y recorder and a printer were employed to record the displayed signals. Pressure gauges were installed at two locations in Figure 1 to monitor the pressure. An ultrasonic flow meter (Polysonics-DHT) was wrapped around the metal pipe to determine the flow speed of the liquid.

The accelerometer was calibrated by means of a free fall test in which the gravitational acceleration was adopted as a standard factor of calibration. The force transducer was calibrated with a manufacturer-calibrated hammer (Dytran-5850A). When the hammer struck the force transducer, dynamic response signals were displayed on the Apple IIe microcomputer as shown in Figure 2. As a result of comparing the recorded signals, a valid calibration of the force transducer was achieved.

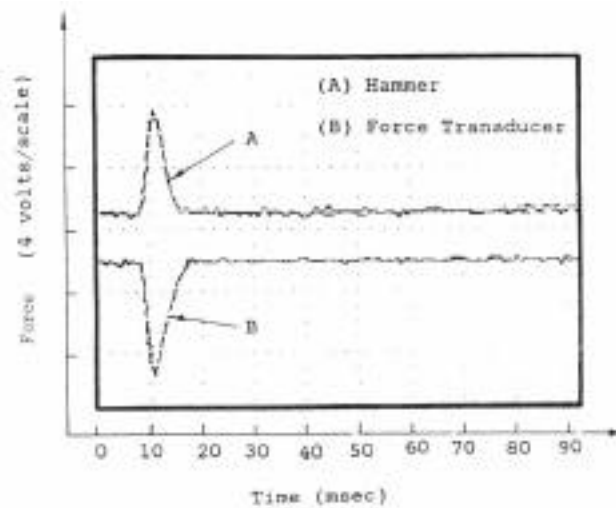


Figure 2. Calibration of the force transducer.

Four different pumps were used in this study; an initial correlative test was conducted using an oral water irrigation device (Water Pik); two three-cylinder positive displacement pumps (Little Giant and Hammelman) and a seven-cylinder pump (Radial) were then used at pressures up to 70 MPa. The flexible hose was lain on the floor while the high pressure tubing was supported with a fixed attachment at one end. An accelerometer was applied at several locations to detect the transverse oscillations of the pipes. Five different nozzles as shown in Figure 3 (two round jet and three fan jet) were attached to one end of the tube. The water pressure in the pipe was changed by adjusting a bypass valve, leading to a change of flow rate. For each test, frequency spectra and time histories were recorded and compared with one another.

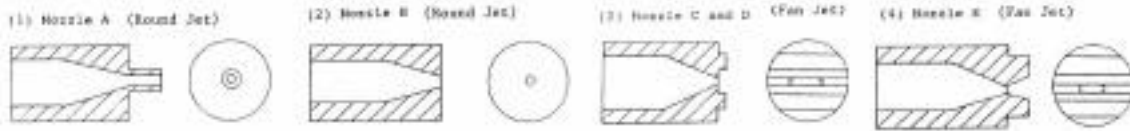


Figure 3. Nozzles used in the experiment.

Referring to Figure 1, in order to study the effects of pipe vibrations on the waterjet impact force, a magnetic shaker (B & K 4810) driven by a function generator and a power amplifier was installed near the nozzle to generate transverse vibration. When the longitudinal excitation, parallel to the ejecting direction of the jet was needed, the end of the pipe was bent at 90 deg. Due to the power limitation of the shaker, several resonant frequencies of the tube were chosen to amplify the oscillation of the nozzle.

### RESULTS AND DISCUSSIONS

Impact forces generated from the four different pumps were first evaluated in the time domain, as shown in Figure 4. The variation of the force was seen to strongly depend on the pumping system used. Major fluctuating peaks become more dominant as the number of pump cylinders decreases. The energy distribution of impact excitation could be easily observed in the frequency domain as shown in Figure 5. It is noted that the Hammelman pump and the Little Giant pump show significant differences in the shapes of the spectra monitored, even though both are three-cylinder reciprocating pumps. The Hammelman pump delivers up to 40 lpm at 70 MPa, while the Little Giant will only produce 20 lpm at 14 MPa.

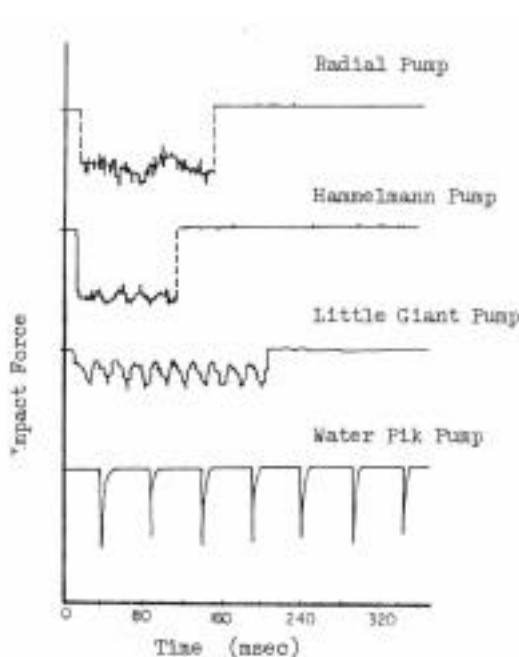


Figure 4. Impact Forces of Waterjets

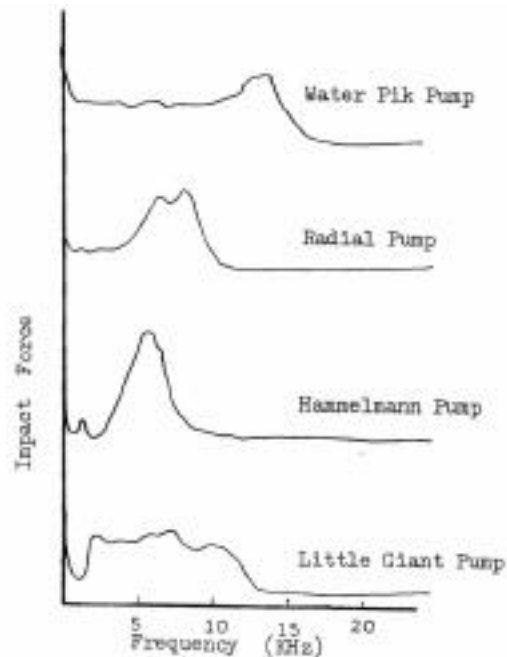


Figure 5. Force Spectra of waterjets.

From the data obtained, it is clear that the frequency range of the fluctuation does not depend on the maximum pressure that the pump can generate, but rather is dependant upon the type of the pump. The ranges of the peak frequencies monitored for the Radial, the Hammelman pump, the Little Giant pump and the Water Pik were 10 KHz, 8 KHz, 14 KHz and 18 KHz, respectively . Although fluctuations were monitored over a wide-band width, there is a dominant peak region for the Hammelman pump (3-8 KHz), indicating the energy concentration in the corresponding range. In the low frequency range, the jet pulsates with the same frequencies as does the reciprocating pump, as shown in Figure 6.

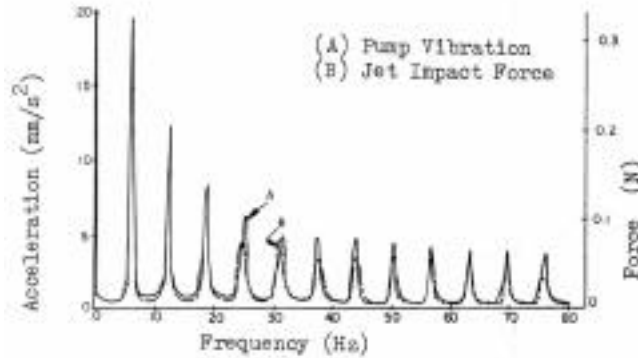


Fig. 6 Correlation of Oscillation Signals

A long flexible feed hose can dampen the pulsations of the fluid flowing through the pipe. That is, the vibration of the pipe became smaller as the location of the accelerometer was moved farther from the pump, along the hose length. However, this only occurs when the length of the hose exceeds some certain critical value. The critical length for such a hose when the Little Giant pump is used was found to be 15 m, for example.

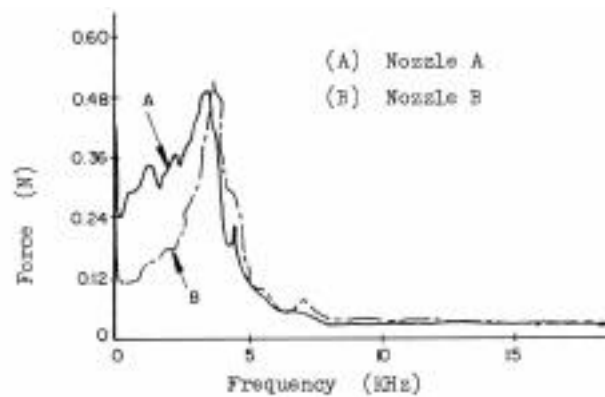


Figure 7. Impact force spectra of waterjets

The orifice diameter of the nozzle was also shown to be an important factor. If the diameter of the orifice is sufficiently small when compared with the inside diameter of the pipe, then the pipe serves as a high pressure liquid reservoir. Vibrations of the waterjet generated from a pump can be dampened out when water passes through such a region. Frequency spectra monitored during impact in Figure 7, were also found to

depend on the types of nozzle used. For nozzles of the same type (round or fan) but different orifice diameters and geometry, the shapes of the spectra in the high frequency range were approximately the same, although some differences did appear in the low region.

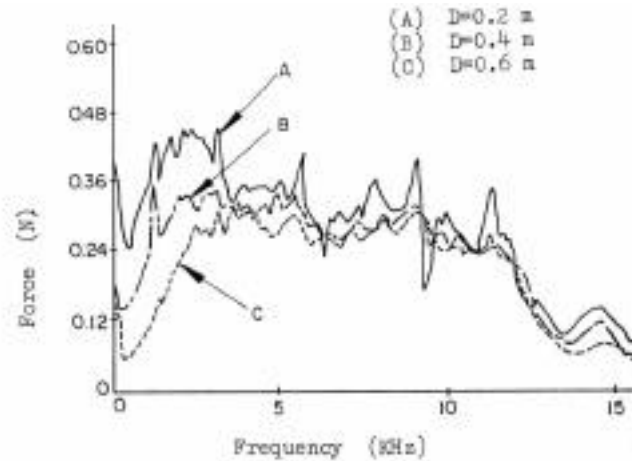


Figure 8. Force Spectra of waterjets from Little Giant

The frequency distribution of the signal was found to change as a function of the distance of the target from the jet nozzle, as shown in Figure 8. The distribution monitored appeared to relate to the structure of waterjet. A proposed jet structure for the three zones is now commonly accepted, as illustrated in Figure 9 (see for example, Ref. 5).

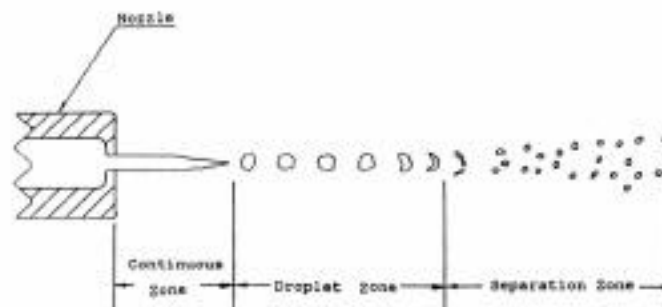


Figure 9. A model of the waterjet structure.

The jet in zone 1 is continuous. In zone 2, owing to the inherent instability of the cylindrical jet, the jet breaks into a series of larger liquid droplets. In zone 3, the droplets are separated into a number of small particles through aerodynamic drag. For different nozzle designs and pressures, the jet structure which is being monitored at a given standoff distance will change, and this will, in turn, be reflected in the distribution of the frequency spectra monitored. Further, each pump at a specific flow rate or pressure has its own optimum standoff distance, as shown in Figure 10. For the cases shown, the optimum standoff distances are 0.13 m, 0.12 m, 0.27 m, and 0.29 m for the Water Pik, the Little Giant pump, the Hammelman Pump and the Radial Pump, respectively. It is

conjectured that this optimum signal occurs at the point at which the jet is breaking into the large droplets, from the solid stream, and before those droplets are, in turn, broken into a fine spray.

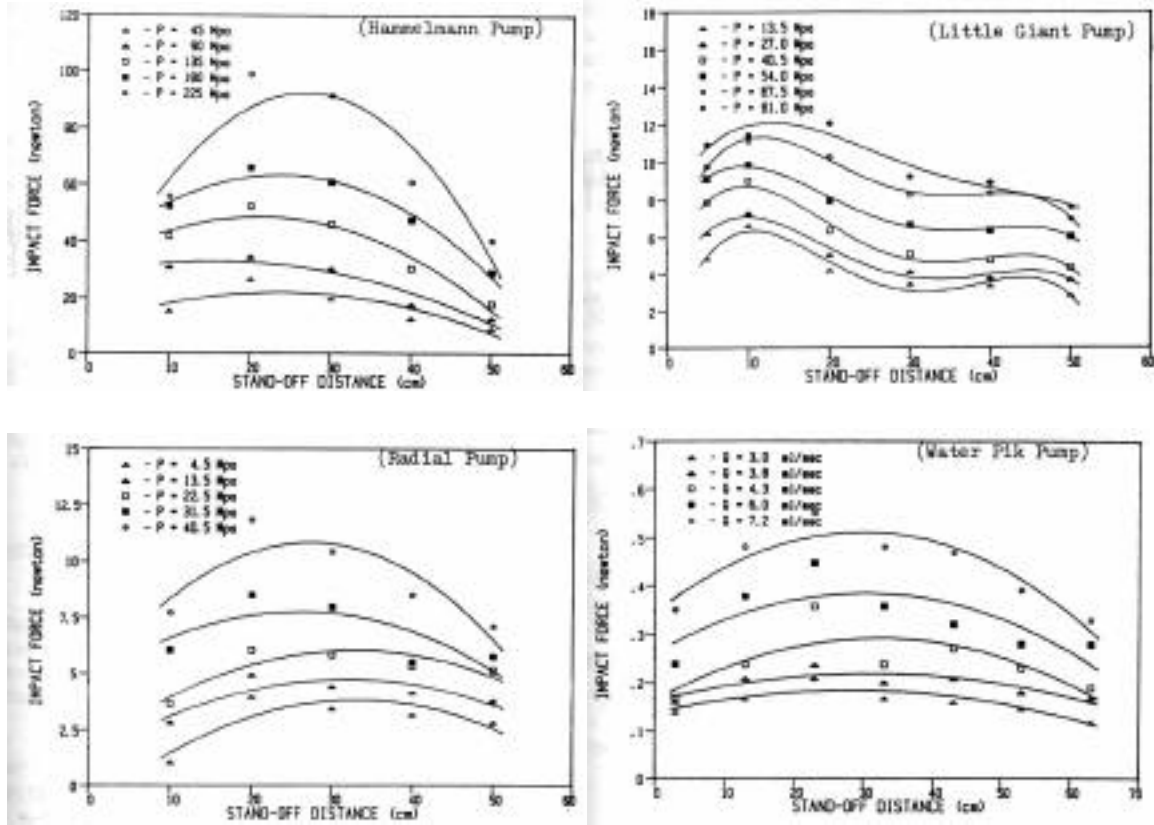


Figure 10. The effects of standoff distance on impact forces.

The impact force exerted by the continuous jet can be estimated by the formula

$$F_c = d Q V \dots\dots\dots (1)$$

Where

- d is the density of the fluid,
- Q is the flow rate and
- V is the flow velocity.

While for the droplet impact, the force can be obtained from the following

$$F_d = d Q C \dots\dots\dots (2)$$

where c is the compressive wave velocity (1435 m/s in room temperature) in the jet fluid. In general, the practical impact waterjet is not continuous nor droplet. The comparison is shown in Table 1. It indicates the impact force could be enhanced through the modification of the jet structure.

The magnitude of the jet pressure influences the magnitude but not the shape of the spectrum, as shown in Figure 11. The higher the flow rate or the pressure is, the greater the impact force will be, as measured in either domain. The constraints imposed upon the feed pipe show a minor effect on the jet pulsation. In this experiment, the highest flow speed measured by a flow meter was 3 m/sec. The oscillation of the metal pipe at that flow speed was not significant. That is, the pipe did not reach a critical instability.

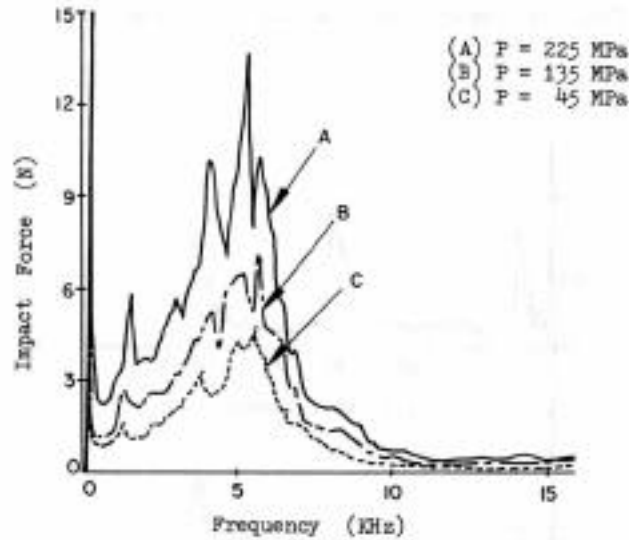


Figure 11. Force Spectra of waterjets (Hammelmann)

Table 1. Impact force of waterjet (Water Pik pump).

STAND-OFF DISTANCE (cm)	FLOW RATE (ml/sec)				
	3.0	3.8	4.3	6.0	7.2
3	0.14	0.16	0.17	0.24	0.35
13	0.17	0.21	0.24	0.38	0.48
23	0.21	0.24	0.36	0.45	0.55
33	0.17	0.20	0.24	0.36	0.48
43	0.16	0.21	0.27	0.32	0.47
53	0.15	0.18	0.23	0.28	0.39
63	0.12	0.17	0.19	0.28	0.33
CONTINUOUS (Eq. 1)	0.020	0.032	0.041	0.079	0.137
DROP IMPACT (Eq. 2)	4.305	5.779	6.171	8.610	10.332

Through the external excitation generated from a shaker, the pipe vibration and the jet impact force is correlated. Referring to Figure 12(a), the oscillation signal of the pipe is transmitted through the waterjet onto the target transducer. While the excitation is stopped, the corresponding fluctuation frequency disappears as shown in Figure 12(b). In the high frequency range, there is an additional significant peak near the 30 KHz shown in Figure 13(a) when the excitation is imposed. It indicates the jet structure is affected through the pipe vibration. In the time histories, as shown in Figure 14, obvious

difference of impact forces with and without the shaking of the pipe is observed. In some stand-off distances, the improvement is very significant (up to 30% increase) as shown in Figure 15.

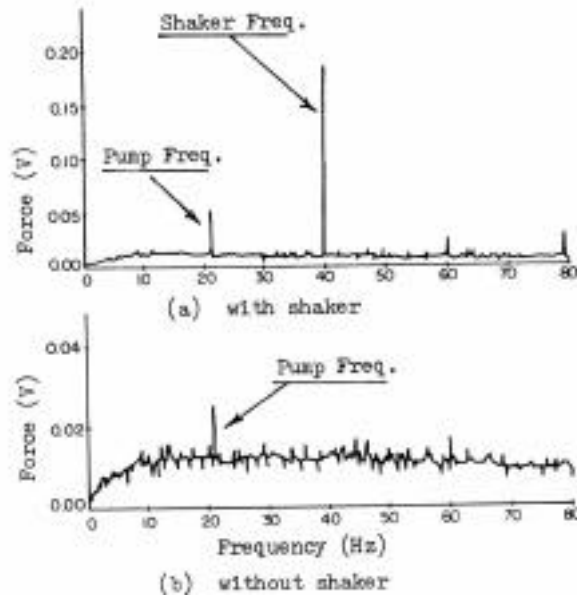


Figure 12 Impact force spectra of waterjets.

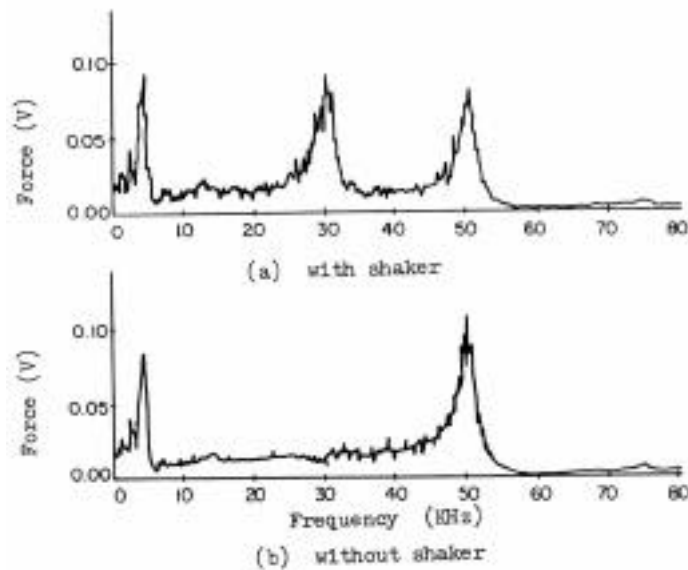


Figure 13 Force spectra of waterjets.

The amplitude of the pipe oscillation plays an important role. Referring to Figure 15, the higher power inducing larger oscillation increases the impact force. When the excitation frequency is increased, the effect is decreased. The oscillation of pipe, either in transverse or longitudinal direction causes breaking of a continuous jet and yields a dominant droplet impact at some stand-off distances. When a pipe is oscillated at a high

frequency with a low amplitude, the structure of the waterjet may be affected insignificantly.

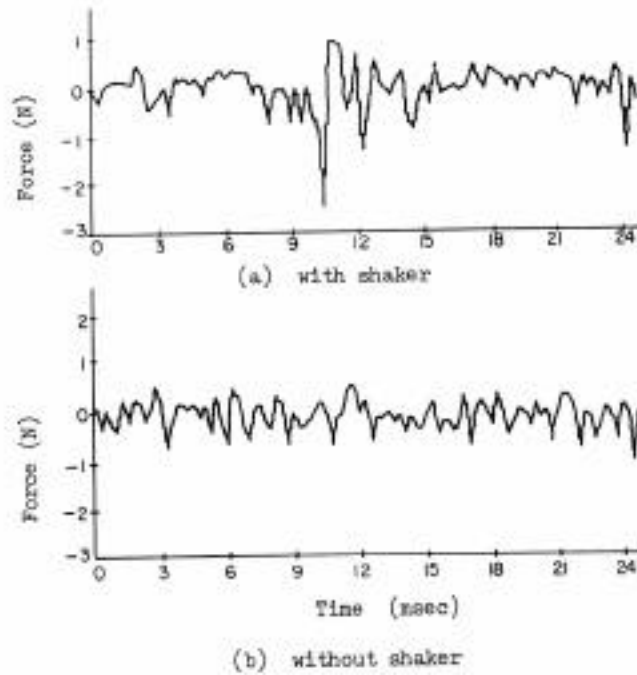


Figure 14. Time histories of impact forces

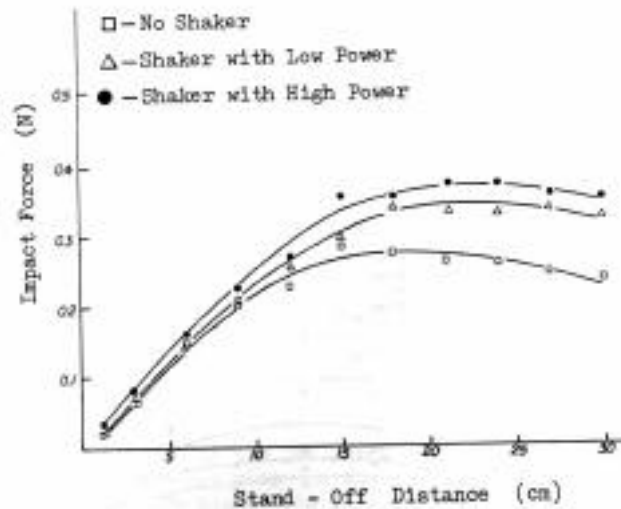


Figure 15. Effect of shaker on impact forces.

#### CONCLUDING REMARKS

The pulsation of the waterjet induced by the components of the associated pumping system can be dampened if the connecting hose section is long enough and the orifice diameter of the nozzle is small. Different pumps, nozzles and standoff distances create different characteristic jet structures and therefore generate different frequency spectra.

The pressure of the jet is not an important factor affecting the jet pulsation frequency but it changes the magnitude of the impact force. An optimum standoff distance with the maximum impact force exists for each pumping system. The way in which the pipe is supported has a limited effect on the jet pulsation for experiments with low flow velocity.

Vibrations induced into the components of the pumping system show a strong correlation with the waterjet pulsation in the low frequency range. When the system resonates with a large oscillation, then the operational parameters (e.g. speed of motor, flow rate, etc.) or the configuration (e.g. length of supply hose, type of nozzle, etc.) need to be adjusted to suppress vibrations.

The oscillation of the pipe shows a strong influence on the waterjet structure. The impact force could be enhanced up to 30% through a significant transverse or longitudinal vibration of the pipe.

Before cutting or cleaning is undertaken, the frequency spectrum of impact force from a waterjet should be measured. The peak frequency in which the energy of the jet is concentrated should be shifted away from the resonant frequencies of any target structure, in order to reduce the possibility of amplified vibrations creating resonance and associated failure or reaction.

#### REFERENCES

1. Nakaya, M., Nishida, N., and Kitagawa, T., "Development of Variable Delivery Triple Reciprocating Plunger Pump for Waterjet Cutting", 2nd U.S. Waterjet Conference Proceedings, Summers, D.A. (Ed.), University of Missouri-Rolla, May, 1983.
2. Gronauer, R., "High Pressure Plunger Pumps", 1st International Symposium on Jet Cutting Technology, England, BHRA, Fluid Engineering, 1972.
3. Heron, R.A., "Interpretation of Dynamic Pressure Ripple Generated by Positive Displacement Pumps with Self-Acting Valves", I. Mech. Eng. Seminar--High Pressure Water Pumps, May, 1986.
4. Tilley, D.G. and Butler, M.D., "The Generation and Transmission of Fluid Borne Pressure Ripple in Hydraulic Systems", I. Mech. Engr. Seminar--Quieter Oil Hydraulics, London, Oct., 1980.
5. Jackson, M.K. and Davies, T.W. "Nozzle Design for Coherent Water Jet Production", Proc. 2nd U.S. Water Jet Symposium, University of Missouri-Rolla, May, 1983.

# FLOW VISUALIZATION OF HIGH-SPEED WATER JETS

M. Szymczak, S. Tavoularis, and A. Fahim  
Department of Mechanical Engineering  
University of Ottawa  
Ottawa, Canada

M. M. Vijay  
Gas Dynamics Laboratory  
National Research Council  
Ottawa, Canada

## ABSTRACT

This paper contains a description of instrumentation and procedures for the visualization of high-speed, submerged water jets of the type used in cleaning, cutting and drilling applications. The use of these techniques in the study of cavitation inception within the jets produced by a plain conical nozzle and a conical nozzle equipped with a transverse pin is also described. The results can be used to identify the regions of cavity generation, growth and collapse. The effect of increased jet speed on cavitation is also illustrated.

## INTRODUCTION

During the past few years, high-speed water jets have found extensive application in industrial cleaning, cutting and drilling. A number of publications have reported tests of the jet performance under different conditions, but fundamental studies dealing with the jet structure and the rationalization of its erosive properties are relatively few. The presence of cavitation (i.e. the formation of vapor-filled cavities in the water) is known to improve jet performance at least in certain applications such as rock cutting (e.g. Refs. 1, 2). Although cavitation might occur within high-speed jets issuing in air, its effects have been mostly documented with the jet operating under submerged conditions. Enhancement of cavitation erosion has been attempted by using special nozzles containing flow obstructions and/or various polymer solutions. The purpose of the present research is to investigate the structure of high-speed, submerged water jets, produced by different types of nozzles, and to document the inception of cavitation and subsequent collapse of cavities. It is hoped that understanding of these phenomena might lead to suggestions for improving the jet cutting ability. This report contains preliminary results describing the development of flow visualization techniques suitable for the study of cavitation in submerged water jets and their application in the jets produced by two different nozzles.

Although acoustical, electrical and other techniques have been used for measuring cavitation, optical means are preferable, when possible, as being non-intrusive and able to provide local as well as global information. Early visual studies of cavitation in submerged water jets by Rouse (3) using full-field and axial plane illumination have demonstrated that inception of cavitation occurred

near the nozzle exit in the mixing layer between the jet core and the surrounding fluid. Direct measurements (see Ref. 4 for a summary) have shown that large pressure fluctuations, associated with turbulence, occur in that region and that negative pressure peaks occur relatively frequently and have a duration that is sufficiently long for cavities to form. It has been suggested that the critical value,  $\sigma_c$  of the "cavitation index",  $\sigma$ , defined as

$$\sigma = \frac{p_o - p_v}{\frac{1}{2} \rho U_o^2}$$

where:

$p_o$ : characteristic static pressure;  
 $p_v$ : vapor pressure;  
 $\rho$ : density;  
 $U_o$ : characteristic velocity) can be related to the r.m.s. pressure fluctuation,  $p'$ , as

$$\sigma = c_1 \frac{p'}{\frac{1}{2} \rho U_o^2}$$

with a value of  $c_1$  about 10 for submerged jets (3).

At the same time, it is well known that  $\sigma_c$  also depends on the concentration and distribution of gas nuclei in the water and on the size of the orifice.

Besides the work of Rouse (3), visual studies of cavitating water jets have been performed by Hoyt and Taylor (5). They utilized a special photographic technique, imaging light from an electronic flash through the flow field directly upon the photographic film and recording two subsequent images on the same frame; this technique has a good temporal resolution but is unable to reveal the three-dimensional distribution of cavities since it provides a projection of the entire flow. More recently, Doi (6) has used holography and Schlieren photography in an extensive study of cavitating, submerged jets; the latter technique provided detailed views of the jet projection, but, again, is unable to resolve the radial distribution of cavities. Among the flow visualization studies of non-cavitating, high-speed liquid jets, one might mention the work of Hiller and Hagele (7) in which they used laser-induced fluorescence, the infrared technique of Nebeker and Cramer (8), the interferometric study of Einfeld (9) and the work of Baev et al. (10) involving microphotography and roentgenography.

## EXPERIMENTAL FACILITY AND PROCEDURES

A sketch of the experimental set-up is shown in Figure 1. High-pressure water flow was produced by a Union Quintuplex pump, rated at 69 MPa and 0.83 x/s.

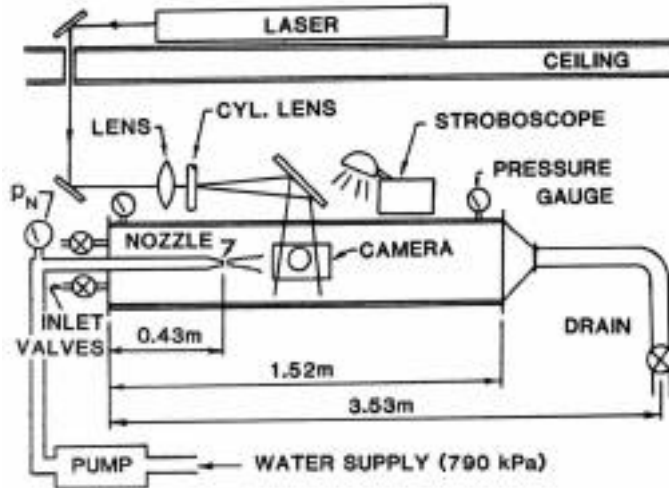


Figure 1. Sketch of the facility

A number of nozzles with different shapes and sizes were available, but results reported here correspond to a) a conical nozzle with orifice diameter  $D=4.0$  mm and b) a similar conical nozzle with  $D=3.0$  mm but equipped with a cylindrical pin mounted transversely near the orifice exit; the two nozzles are sketched in Figure 2.

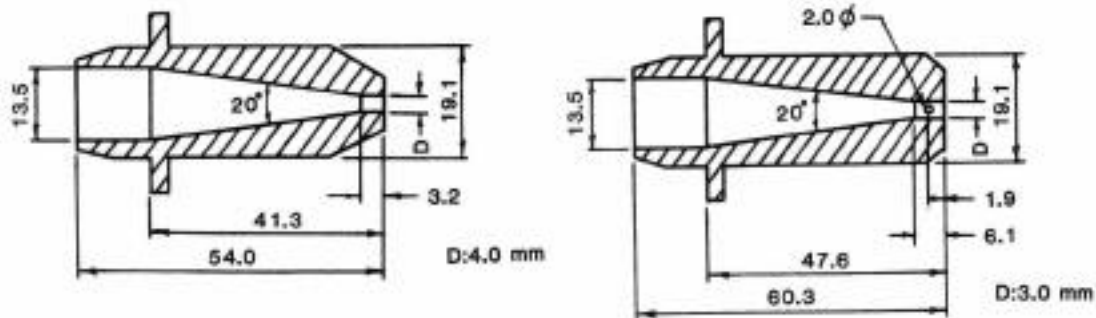


Figure 2. Sketch of the plate nozzle (left) and the obstructed nozzle (right). All dimensions are in millimeters.

The nozzles issued into a channel with a 140 X 140 mm square cross-section and made of clear acrylic material for visual access. Four inlet valves upstream of the jet nozzles were used to fill the channel and to maintain a slow water stream, co-flowing with the jet. The channel could be slightly pressurized, up to about 138 kPa above atmospheric pressure. Although the pump was capable of operating at full capacity for pressures up to about 69 MPa, the maximum pressure at the nozzle and the speed of the jet depended on the nozzle size and shape. Lower pressures could be obtained by opening one or more by-pass valves.

The main source of illumination was a 13 W Ar-Ion laser, whose beam was focussed and then converted into a thin sheet with the use of a cylindrical lens. The thickness of the light sheet, occasionally reduced by a slit, was roughly

between 0.5 mm and 1.5 mm. Full- field illumination was possible with the use of a stroboscope (Strobotac, Type 1538A) The photographs presented here were taken with a 35 mm camera (NIKON F2), equipped with a 50 mm lens and a macro-teleconverter lens, and recorded on black and white recording film (Kodak 2475). Direct observation of the jet was possible through a cathetometer mounted on a vertical vernier scale.

Photographs with an exposure duration between about 0.5 and 3 $\mu$ s of overall views of the jet were obtained by synchronizing the stroboscope with the camera shutter. The internal structure of the jet was observed and recorded by utilizing the lasersheet illumination, either along an axial plane or on a transverse plane forming an angle of 60 degrees with the jet axis. Combinations of the above techniques with room light illumination were occasionally used. The film exposure time, corresponding to the minimum of illumination duration and camera shutter opening, will be presented with each plate.

## RESULTS AND DISCUSSION

### Plain Conical Nozzle

Results were obtained at two nozzle pressures,  $P_N=3.79$  MPa and 1.55 MPa, corresponding to jet exit velocities of 86.5 m/s and 51.5 m/s and Reynolds numbers (based on jet exit velocity and nozzle diameter) of  $2.6 \times 10^5$  and  $1.5 \times 10^5$ , respectively.

Plate 1 shows the jet as seen with room lighting. The parts of the jet that appear as white in the photographs are those containing gas and/or vapor bubbles. It is interesting to note that, when issuing under tap pressure, the jet is invisible, thus indicating absence of cavities. For both nozzle pressures presented here, the visible cross section of the jet grows monotonically in the entire test section and fades into a "milky cloud" of small air bubbles, which are mostly carried through the main discharge or through some of the intermediate valves; larger air pockets sometimes attach to the top of the test section and break into smaller bubbles at random time intervals. The jet appears to start axisymmetrically but evolves into a circular flapping motion further downstream.

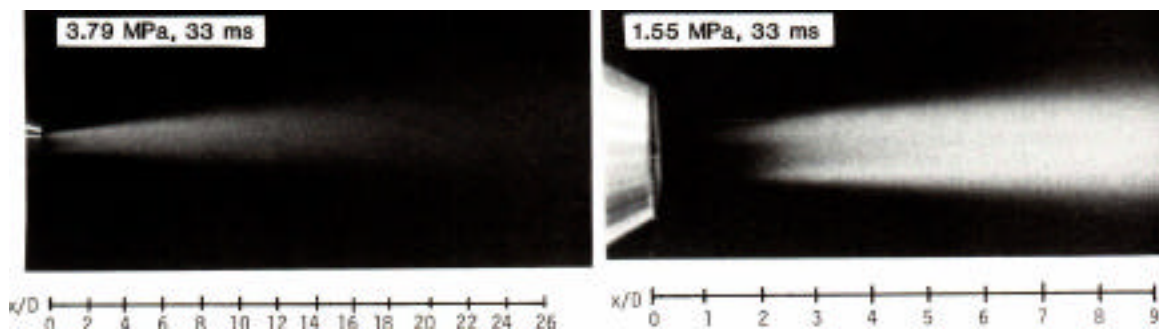


Plate 1. Jet issuing from the plain nozzle, illuminated by room lighting. Numbers on plate indicate the nozzle pressure the film exposure time.

Decrease of nozzle pressure from 3.79 MPa to 1.55 MPa resulted in a general reduction of the bubble density and the formation of an invisible region near the nozzle exit, where, presumably, there are no light scattering bubbles. These effects of pressure decrease became much more obvious when the jet was illuminated with the stroboscope. As shown in Plate 2, at  $P_N=3.79$  MPa the jet appeared as an almost continuous cluster of gas and/or vapor filled cavities, while at  $p_N=1.55$  MPa these cavities formed clusters which were separated by dark regions.

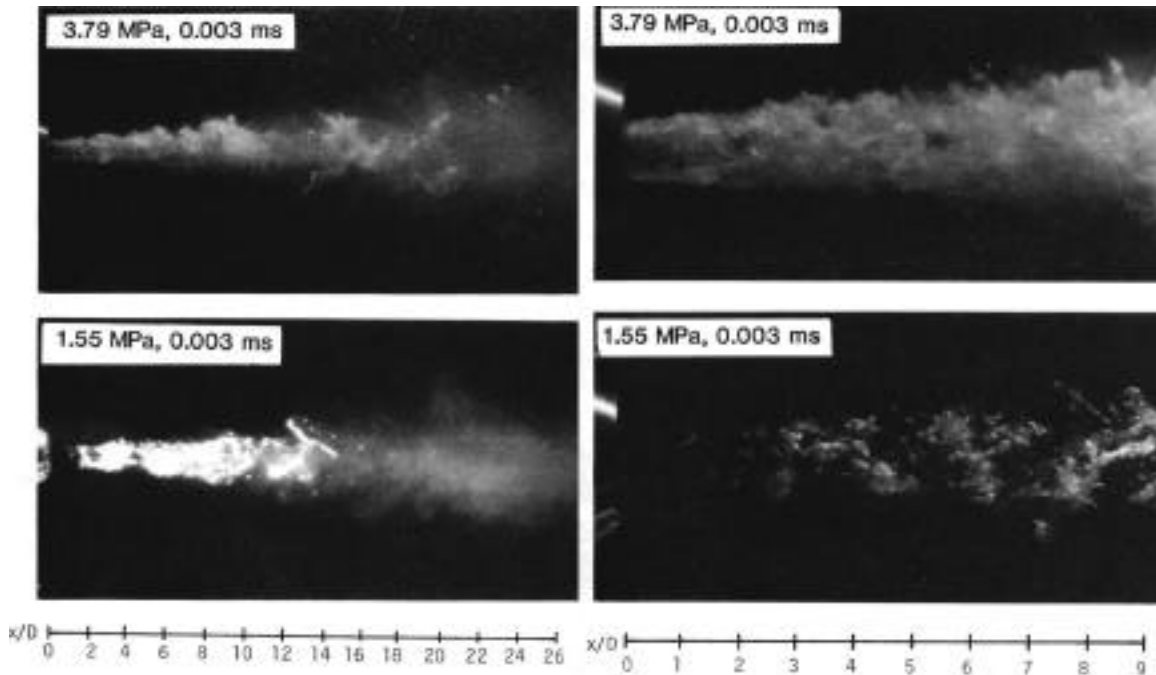


Plate 2. Jet issuing from the plain nozzle, illuminated by the stroboscope.

At least for the  $p_N=1.55$  MPa case, one may speculate that the distribution of cavities near the nozzle exit follows the development of a helical instability of the jet, which produced low-pressure regions within quasi-organized large structures. Another observation in Plate 2 is that the cavities can be divided into two categories: a) those which are relatively small (as demonstrated by the low intensity of scattered light) and persist to the end of the test section, and b) some which are much larger, tend to form clusters and disappear after a certain distance from the origin. A plausible explanation is that the former contain mostly air which was released as the water was depressurized, while the latter contain mostly vapor; it is presumed that the vaporous cavities collapse and are responsible for cavitation erosion.

The internal distribution of cavities was visualized with the use of the thin laser sheet. Plate 3 illustrates views of the jet illuminated along its axial plane. Unlike full-field illumination, plane illumination reveals that cavities first form in the mixing layer of the jet, while the "potential" core is cavity free. This supports

earlier observations that cavitation occurs at regions with large pressure fluctuations (3,4).

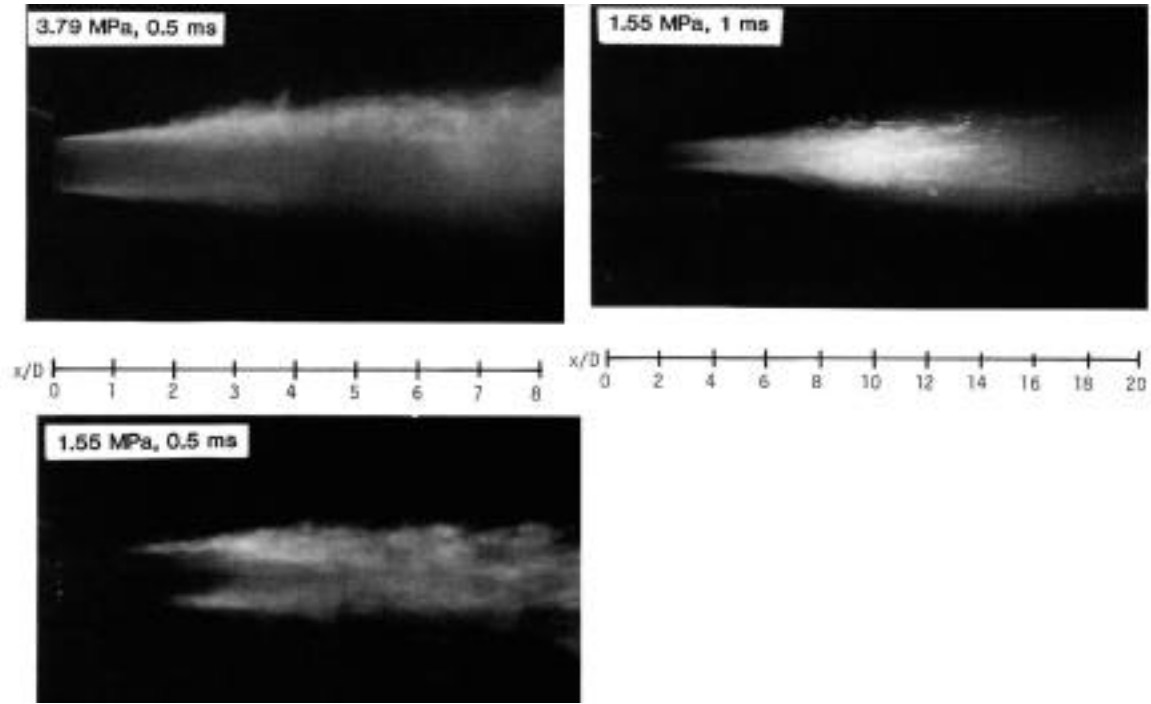


Plate 3. Jet issuing from the plain nozzle, illuminated by an axial laser sheet.

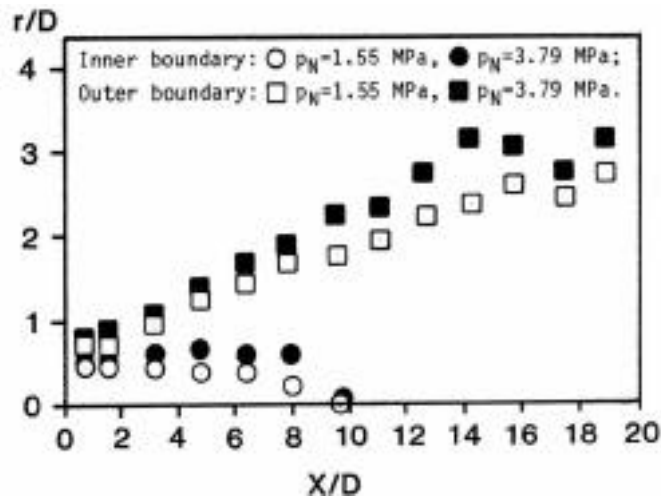


Figure 3. Plot showing the boundaries of the visible part of the jet, determined using the cathetometer.

The distinction between gaseous and vaporous cavities is also apparent, since the latter are much larger and are seen in substantial numbers only for  $x/D \leq 17$ . Plate 4, obtained with transverse plane illumination shows even more clearly the fact that cavitation inception occurs in the jet's mixing layer, that cavities

spread to occupy the entire cross section and that vaporous cavities are not encountered beyond  $x/D=18$  for  $P_N=1.55$  kPa. The boundaries of the visible cross-section of the jet, observed directly through the cathetometer are plotted in Figure 3 for both pressures. It can be seen that, for the same  $x/D$ , the cavitation region is shifted towards larger distances from the axis as the pressure increases.

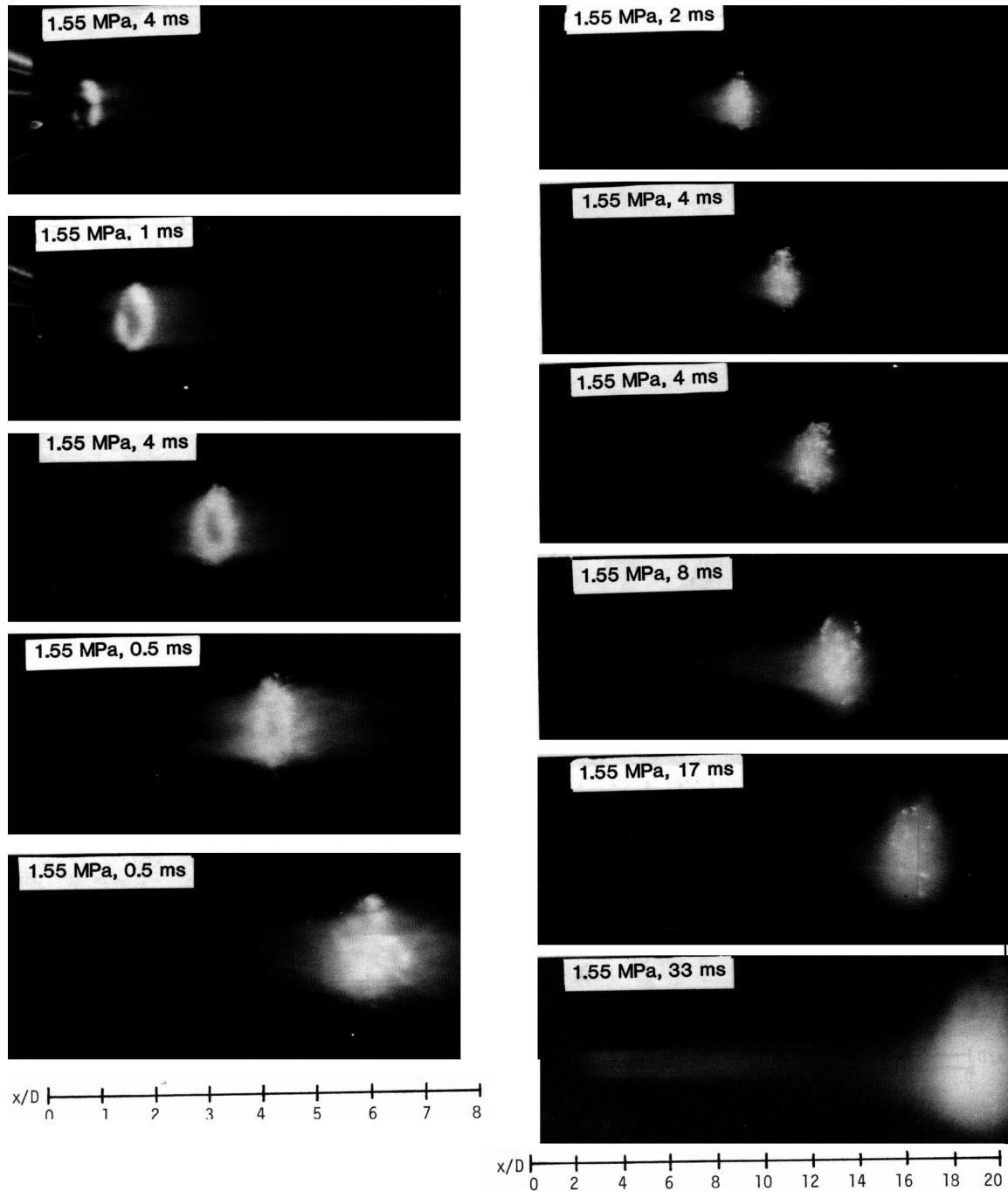


Plate 4. Jet issuing from the plain nozzle, illuminated by a transverse laser sheet.

### Obstructed Conical Nozzle

The nozzle pressure and jet speed obtained with this nozzle were substantially higher than those obtained with the plain nozzle. As Plate 5 shows, the visible region of this jet was much wider than that observed when the plain nozzle was used. Another feature of the obstructed nozzle jet is that cavitation inception occurs in the mixing layer of the jet as well as in the boundary of the wake of the pin. Further studies using special nozzle designs are in progress.

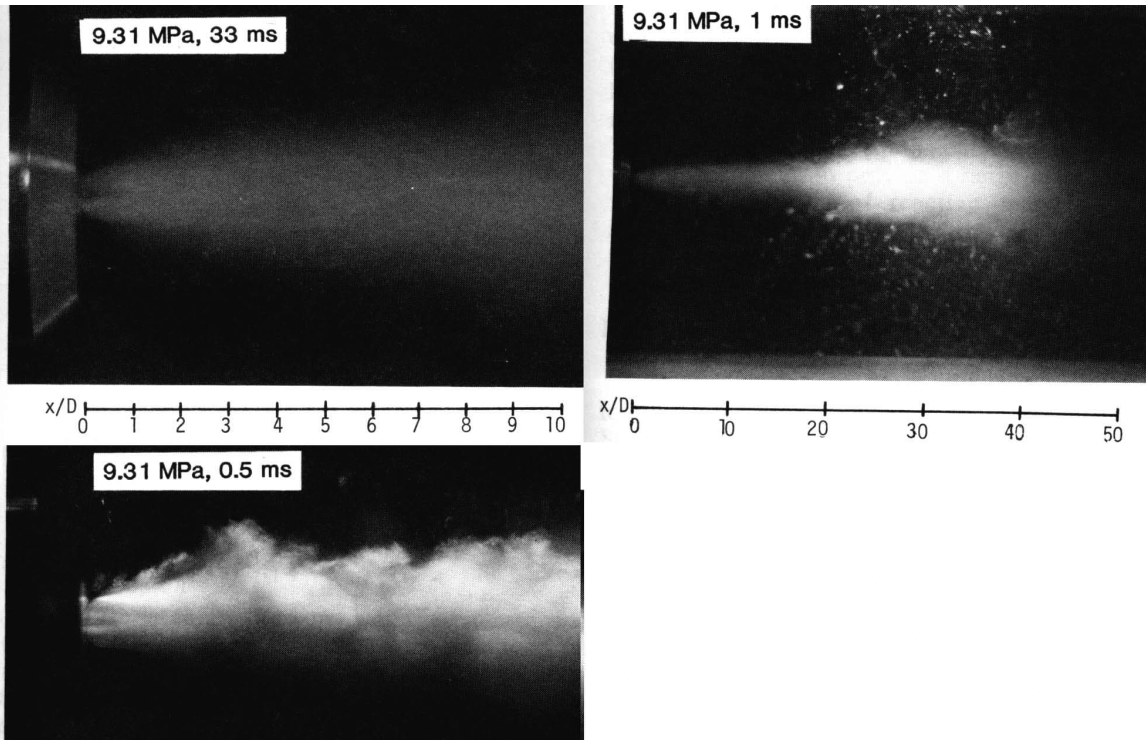


Plate 5. Jet issuing from the obstructed nozzle, illuminated by room lighting (top left) and by an axial laser sheet (right and bottom).

### CONCLUDING REMARKS

The preliminary results presented above have demonstrated that simple flow visualization techniques are adequate in describing inception and collapse of vaporous cavities in high-speed submerged water jets. Further improvements of the technique are possible, since for example it would be desirable to obtain short-duration ( $\sim 1 \mu\text{s}$ ) exposures of the jet using plane illumination. Although only sample results have been presented here, the study will include jets issuing from smaller and specially designed nozzles at much higher speeds than the present ones, which are more relevant to jet cutting technology. The visualization of the combined processes of cavitation and material removal during cutting is a natural extension of the current work and will be, hopefully, pursued later.

## ACKNOWLEDGMENT

Financial support for this project was provided a Graduate Scholarship awarded to the first author by the Natural Sciences and Engineering Research Council of Canada as well as by Research Grants of the same organization to the second and third authors. The use of research facilities and assistance of the technical staff of the Gas Dynamics Laboratory, National Research Council is greatly appreciated.

## REFERENCES

1. Johnson, V.E., Jr., Thiruvengadam, A., and hl, R.E., "Rock Tunnelling with High-Speed Water Utilizing Cavitation Damage", ASME Paper No. 8-FE-42, American Society of Mechanical Engineers, 1968.
2. Vijay, M.M., Brierley, W.H., "A Study of Erosion by High-Pressure Cavitating and Noncavitating Waterjets", Erosion: Prevention and Useful Applications, ASTM STP 664, W.F. Adler, Ed., American Society for Testing and Materials, 1979, pp. 512-529.
3. Rouse, H., "Cavitation in the Mixing Zone of a Submerged Jet", La Houille Blanche, Jan.-Feb. 1953, pp. 9-19.
4. Arndt, R.E.A., "Cavitation in Fluid Machinery and Hydraulic Structures", Ann. Rev. Fluid Mech., Vol. 13, 1981, pp. 273-328.
5. Hoyt, J.W., Taylor, J.J., "A Photographic Study of Cavitation in Jet Flow", Transactions of the ASME, Vol. 103, March 1981, pp. 14-18.
6. Ooi, K.K., "Scale Effects on Cavitation Inception in Submerged Water Jets: A New Look", Journal of Fluid Mech., Vol. 151, 1985, pp. 361-390.
7. Hiller, W.J., Hagele, J., "Visualization of Hypersonic Micro-Jets by Laser-Induced Fluorescence", Proceedings of the Second International Symposium on Flow Visualization, Bochum, West Germany, September 9-12, 1980-, pp. 427-431.
8. Nebeker, E.B., Cramer, J.B., "Visualization of the Central Core of High-Speed Water Jets - An Infrared Technique", Proceedings of the Second U.S. Water Jet Conference, Rolla, Missouri, 1983, pp75 - 80.
9. Eisfeld, F., "The Investigation of the Penetration of Liquid Jets in Gas by the Methods of High Speed Cinematography and Short Time Interferometry", Proceedings of the Society of PhotoOptical Instrumentation Engineers, Vol. Pt 1, 1984, , pp. 329-335.
10. Baev, V.K., Bazhaikin, A.N., Buzukov, A.A., Timoshenko, B.P., Bichenko, E.I., Rabinovich, R.L., "Experimental Study of the Development and Structure of High-Velocity Liquid Jets in Air", Progress in Astronautics and Aeronautics, Vol. 105-, -Pt- 1, 1986, pp. 104-112.

# CONSIDERATIONS IN THE DESIGN OF A WATERJET DEVICE FOR RECLAMATION OF MISSILE CASINGS

D. A. Summers, L. J. Tyler, J. Blaine, R. D. Fossey  
High Pressure Waterjet Laboratory  
Rock Mechanics Facility  
University of Missouri-Rolla  
Rolla, Missouri

J. Short and L. Craig  
Naval Weapons Support Center  
Crane, Indiana

## ABSTRACT

The use of high pressure water as a means of removing explosive and propellant from munitions has several apparent advantages. Experimental programs have been carried out to define the operational range in which equipment can be operated with an adequate level of safety. Potential problems arise, however, when enhancement techniques are included in the jet delivery system. The problems are discussed within the context of the design of a system for missile cleaning.

## INTRODUCTION

The University of Missouri-Rolla is currently under contract to the Naval Weapons Support Center (NWSC), Crane, Indiana to examine means by which high pressure waterjets can be used to completely remove all the explosive contained in military munitions. The experiments and equipment used have evolved, with the program, to provide a range of criteria under which jet cleaning of reactive materials can be successfully achieved. In the process of developing these procedures it has also been necessary to establish the relative safety of the cleaning process.

## EARLY EXPERIMENTS

The use of high pressure waterjets as a cleaning tool has been well established for a number of years. Such usage has, however, been mainly restricted to cleaning of relatively inert materials from a variety of industrial surfaces. Experiments had previously been carried out at a number of military facilities investigating the use of such jets to remove plastic bonded explosive (PBX) with a variety of success. The problem needed evaluation from a number of different viewpoints. The two primary criteria which had to be established were, could such a system effectively clean explosive from casings, and in so doing, would the jets be at a low enough pressure as to not induce a reaction from the jet impact on the target surface.

As an initial set of test criteria, small 0.4 kg charges of explosive of the range of types likely to be encountered were supplied to UMR from NWSC. These charges were placed in a specially prepared facility, with the charges inserted into a small receptacle set in the rock wall of the facility. This location was designed so that any reaction would be confined by the rock, while leaving the front surface of the charge exposed, both for

jet impingement, and so that it would be visible from a television camera, used to provide a visual record of the test. Two high pressure pumps, each capable of producing 40 liters/min at 175 MPa, were manifolded together for this test series.

A sequence of tests at 35 MPa increments, at full fluid flow, up to the maximum pressure of the pumps indicated no discernable reaction to the impact, over the suite of explosives tested. Given that the impact of a fluid can generate greater pressures than those of sustained flow (Ref 1), the experiments also included tests wherein the jet was pulsed, by an interrupter placed between the nozzle and the explosive (Ref 2). No reaction was observed from these tests. Finally cavitation was induced in the jet stream in the manner most commonly suggested by Tracor Hydronautics (Ref 3). This method was chosen over the method for cavitation induction suggested by Daedalean Associates Inc. (Ref 4) based upon an evaluation of probable system performance, and relative simplicity. Testing times for these tests were very short, typically all the explosive was ejected from the casing within a period of seconds, but, based upon an overview of the tests, from the videotape record, and based upon examination of the recovered fragments of explosive, at that time, it was believed that no reactions had occurred on the target surface. Because of their better flow characteristics, it was determined, based upon the comparative results of the experiments carried out in the preliminary series, that conventional, non-cavitated waterjets gave superior performance in removing the explosive suite under test (Fig 1).

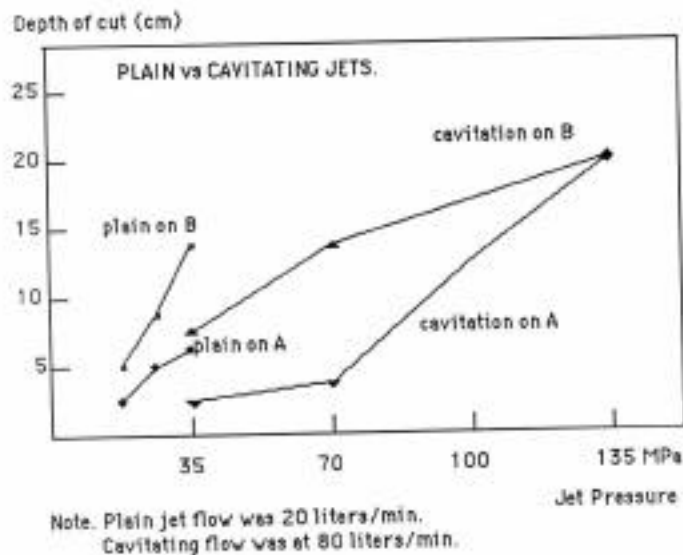


Figure 1. Comparative performance of plain and cavitating jets in penetrating PBX.

### SYSTEM DESIGN

Two considerations, beyond that of reaction sensitivity, predominated in the design of equipment for the cleaning of the casings. The first consideration was to ensure that the surfaces of the casing were completely cleaned of explosives. As a result of tests to determine how best to achieve that objective, a second imperative became ensuring that the explosive was only removed in small pieces.

An experimental mechanism was designed (Ref 2) which moved the cutting jet along the interface between the explosive and the casing. The initial purpose of this test was to determine how wide a swath would be completely cleaned by the jet on the internal casing surface, which would, in turn, control the increment that the cleaning nozzle could be moved forward between sweeps over the explosive surface. It was found that, for some explosive types, where the bond between the explosive and the casing was weak, that a potentially dangerous condition could occur. In this condition the jet would penetrate along the explosive: casing interface, to the back of the casing. Continued jet flow would separate the explosive from the casing across the entire back of the charge, which space would fill with water, which would pressurize at the delivery pressure. Given that this pressure might exceed 100 MPa, and that the area being pressurized could exceed 100 sq cm, a considerable force would be exerted on the explosive billet. Such a force is sufficient to cause the entire explosive billet to be forced, virtually intact, from the casing. This potentially can induce two hazards. The first is from a violent impact with the nozzle or other metal obstruction, potentially inducing reaction. The second is only pertinent when the target material is soft. In that instance the ejected material can flow around the cleaning nozzle orifices, and instantaneously block egress of water. This will induce a water hammer pressure in the system, one obvious indication of which might be the simultaneous failure of hoses and couplings at multiple points. The concomitant dangers of inducing explosive reaction, or severe pump damage should also be recognized,

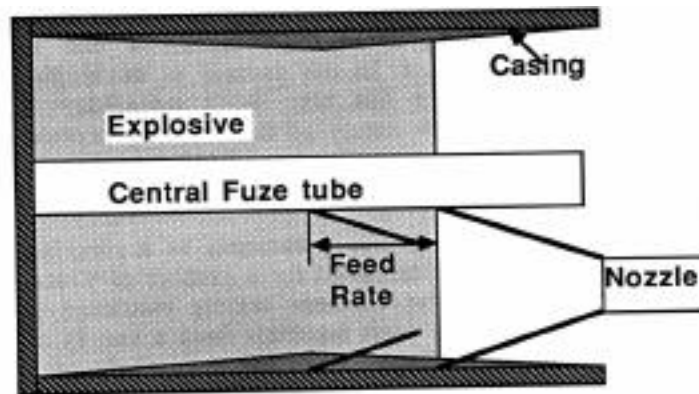


Figure 2. Side view schematic of the jet path, showing that the jets cover the full surface.

Recognition of these dangers led to the recommendation that the removal system be designed so that only relatively narrow depths of explosive be removed at any one time from the casing. This could be achieved by rapidly spinning a lance, fitted with two diverging nozzles, as it was moved over the target surface. A dual orifice system had two advantages, firstly the jets could be designed so that they covered the surface of the target explosive, as they rotated during a single sweep over the face of the material (Fig 2). Secondly with a symmetrical dual orifice design, not only would the jets sweep a clear path, into which the nozzle could feed, but the balanced design would allow the lance to penetrate further into the casing without additional support. For most of the explosives suite tested a feed of between 1.0 and 1.5 cm for each sweep of the nozzle proved most effective. This had the serendipitous advantage of equating to the width of surface which the jet would effectively clean on a single pass.

The choice of depth of material removed was ,considered important, since some explosive types are placed into the casing in billets. If the jet penetrated to the back of a billet, then a similar "push-out" of the remaining thickness of the billet could occur. If the thickness thus removed was kept to less than 1 cm then this would partially fragment under the pressure and would be thin enough not to interfere with the jet flow, or to pose other problems to the lance passage, as the explosive passed out of the casing. In order to further safeguard against problems with the fragments being trapped between the lance and the casing safeguarding software, based upon instrumentation in the line, stopped lance rotation, and reversed the motion if lance interference was detected.

A series of tests, based upon a computer controlled cleaning lance, capable of simultaneous motion in all three orthogonal directions, led to the development of a mechanism referred to as the WOMBAT (Waterjet Ordnance and Munition Blastcleaner with Automated Tellurometry.) This device has been sequentially modified so that it is capable of cleaning the interior of range of different munition casings, each of which can be filled with one of a variety of explosives. In each case jet pressure, lance positioning and movement must be tailored to the combination of explosive and casing encountered. This has been addressed by making the controlling computer program menu-driven, with alternate combinations established by the operator as he initiates the program.

#### REACTION SENSITIVITY

A continuing question, during the course of the program, has been a measure of the safety of the washout process. As with many things the simplest measure to determine how safe the procedure is to establish the point at which the process becomes unsafe. In the case of waterjet impact this is the impact pressure at which reaction is initially observed on the target surface. Initial testing of this sensitivity has been described elsewhere (Ref 5). Of particular concern, however, has been results from a recent late stage part of that sensitivity program.

Equipment has been developed which allows the direction of water, moving at velocities of up to 10 km/sec onto the test sample surface. In order to determine the instant at which reaction occurs it was decided to examine the impact of such jets on very thin layers of explosive. These samples would be prepared on glass slides in order to see reaction both from the direction of impact and also from underneath the sample during the impact. In order to prepare these samples, a technique was used in which small pieces of explosive were disrupted using a cavitation technique. This liberated small particles of explosives which became suspended in the water under which the disruption had occurred. The particles were then allowed to settle onto glass slides, placed on the bottom of the container, so that, after drying, they provided the required samples for the test purposes. Cavitation was used for this program because very low absolute power levels are developed by the cavitating system and these would allow a slow erosion of the explosive at the individual grain level.

The equipment used in this program is a Brunson Ultrasonic Horn, of the type normally used in the standard ASTM vibratory cavitation test, (Ref 6). However, because of the nature of the explosive, it is not possible to machine samples to fit the end of the

horn and the modification of the standard in which the test sample is placed under the horn was used (Ref 7). This procedure was originally developed in the United Kingdom and modified by Dr. Carolyn Hanson (Fig 3).

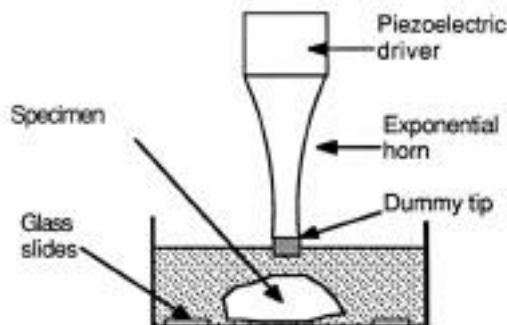


Figure 3. Layout for cavitation dis-aggregation

The equipment consists of an acoustic driver which is vibrated electrically. These vibrations are passed down through a specially shaped horn threaded to the driver and designed to magnify the amplitude of vibration at its further end. Samples located on the end of the horn will thus be induced to vibrate at some 20 kHz with a peak to peak amplitude of 0.005 cm. The horn tip is submerged in water so that as it oscillates up and down, it will induce cavitation in that water. By placing the explosive directly beneath the tip, the cavitation bubbles generated by the vibration of the tip are driven down onto the explosive surface, where they collapse.

The collapse of the cavitation bubbles will cause erosion of the material. It was not originally anticipated that the samples would react during this process because of the relatively low level of energy (500 watts) induced by the horn. However, as with all explosive tests, this procedure was carried out within the explosive test chamber at the Rock Mechanics and Explosives Research Center. After one of the first such procedures had been carried out, a slight odor of reaction was noted in the explosive chamber, when it was opened after the run. While it was considered probable that this had been left from an earlier test program, the explosive samples were closely examined to see if there was any evidence that any reaction had occurred. Several samples of PBXN 5 were found to have been discolored to a grey tone at points around the major erosion area.

This grey zone was then examined under a low powered microscope and relatively small black dots could be identified on the explosive surface. A higher powered microscope was then utilized and it was possible to discern small black circles and other signs of discoloration on the explosive surface (Figures 4 & 5). Because of the relative difficulty in examining the explosive surface in detail with the microscope because of the very limited depth of field and the very varied size of the cavities induced in the explosive, it is difficult to be entirely certain as to the nature of these circles. An initial prognosis has, however, been proposed.

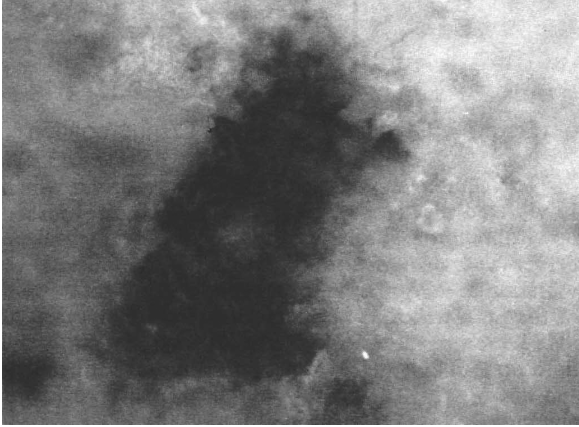


Figure 4. Magnified surface of explosive showing cavitation pits and staining.

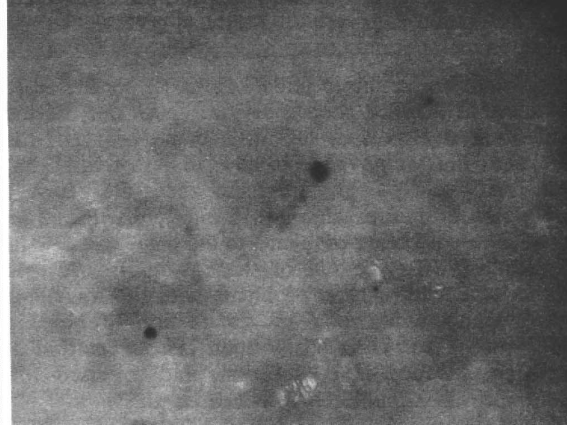


Figure 5. View of smaller reaction pits on explosive surface.

It is believed that the impact of the small waterjet created by the collapsing bubble was of sufficient intensity to induce a microscopic reaction on the explosive surface. This impact pressure can exceed 1.5 million psi as identified experimentally by Ellis (Ref 8) and proposed theoretically by Voinov and Voinov (Ref 9) and by Ellis (Ref 8). This produced a small amount of carbon, as part of the reaction products. While much of this has been removed by the continued cavitation action (a common use for which is in cleaning) nevertheless, particularly in those areas away from the center of the most intense cavitation action, some of the reaction products were retained within the explosive surface. This series of events would explain the circular shape of the blackened zone around the impact point which is, in some cases, only approximately .0005 inches in diameter, although, in others it is significantly larger.

While the identification of these small reaction zones was considered to be primary evidence of reaction, it was necessary to seek additional confirmation of this result. The experiments had been carried out using carefully deionized and filtered water to surround the sample during each cavitation run. This water was sampled and examined using an ion chromatograph to determine if any reaction products were present in that water. Samples from four different tests on separate samples of the same explosive type indicated the presence of such reaction products (Figure 6). Similar evidence of reaction products were then found in subsequent tests on other explosive types.

Because two different reviews of the results of this procedure have indicated the presence of reaction during the course of low power cavitation on samples of explosive, the existence of the small reaction circles on the explosive and the presence of reaction products in the water, it is now believed that sufficient evidence exists to warrant concluding that a reaction has occurred.

The pressures required to initiate reaction by waterjet impact have been found, in earlier tests at UMR, to lie above 1 million psi. Dr. Ellis has shown that such pressures can be generated during the collapse of cavitation bubbles and this would provide additional corroboration to the likelihood of this event occurring. This evidence, which is

based on more detailed examination of the samples, than that carried out earlier, when the very small scale of the reaction would not have been evident in the methods of analysis used, has led to a recommendation that techniques using cavitation not be used in the removal of explosive or propellant, or the cleaning of surfaces on which such reactive materials are found. While this recommendation is subject to review and the results of a more detailed and comprehensive set of experimental findings on this phenomenon, it should be broadened to include all those conditions where, when waterjets are directed at reactive materials underwater, the target surface can be exposed to the impact of cavitating bubbles.

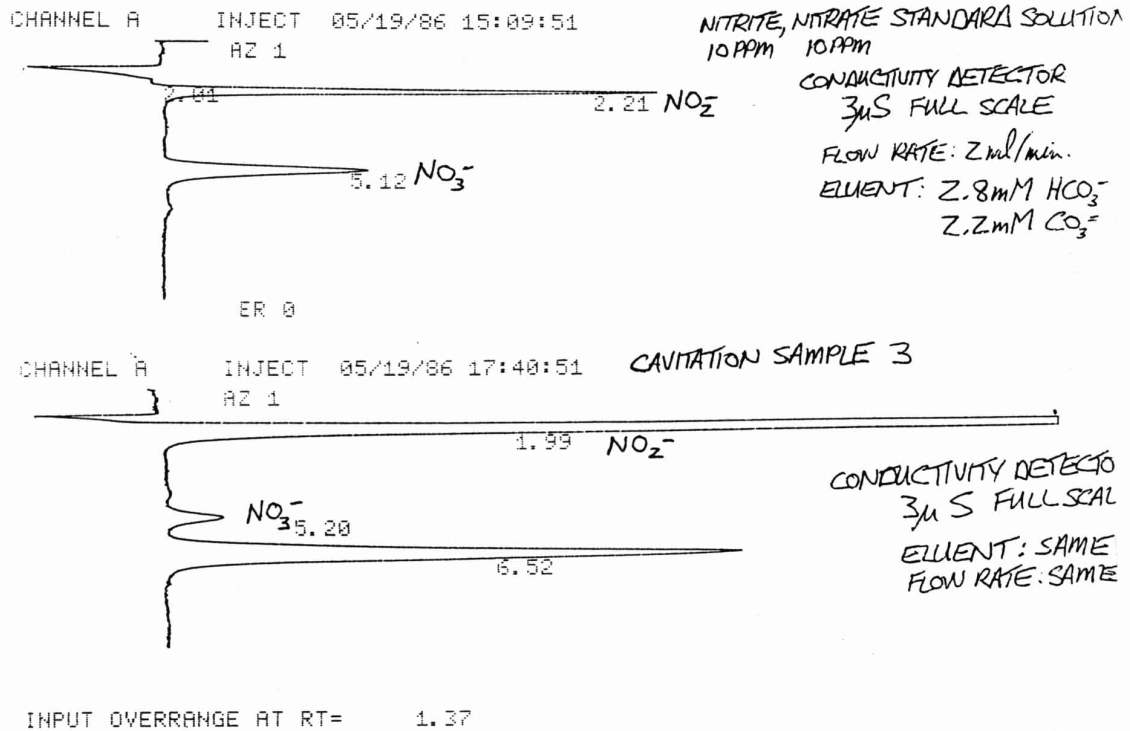


Figure 6. Traces from the Ion chromatograph comparing the cavitation result (lower) with a standard solution.

Input overrange at Rt = 1.36 in the upper figure. The analyst was Jim Rankin

For Sample 2, cavitation sample #3 the IC provided the following information:

Name	PPM	Rt	Areas BC	RF
1	0	1.99	48954595 01	
NO3	2.489	5.2	2215311 01	889954.299
3	0	6.52	30404994 01	
Totals	2.489		81574810	

## REFERENCES

1. Lesser M.B. and Field J.E. "The geometric wave theory of liquid impact" paper 17, Proc 6th Int. Conf. Erosion by Liquid and Solid Impact, Cambridge, UK, 5-8, Sept 1983.
2. Summers D.A. and Worsey P.N. "The Use of High Pressure Water Jets to Wash Out Explosives" paper 35, Proc 6th Int. Conf. Erosion by Liquid and Solid Impact, Cambridge, UK, 5-8, Sept 1983.
3. Conn A.F. and Rudy S.L. "Using Cavitating Water Jets for Demilitarization" Symp. on Demilitarization of Conventional Explosives, Am. Defense Preparedness Assoc, April 20-22, 1976, Hawthorne, NEV
4. Daedalean Associates Inc. "Dynamic Response and Explosive Characteristics of Solid Propellants due to Water and Cavitation Impact during Cleaning Operations at NOS" DAI Technical Report No. RSW8245-002, October 1983.
5. Worsey P.N. and Summers D.A. "High Impact Velocity Testing of PBX Explosive" A progress report on Contract N00164-83-C-0110, submitted to NWSC, Crane IN May 1984.
6. ASTM "Standard Method of Vibratory Cavitation Erosion Testing "Designation G32-72, ASTM Comm G2 on Erosion and Wear, 1972
7. Preece C.M. "Cavitation Erosion" in Erosion vol 16, of the Treatise on Materials, Science Technology, ed. C.M.Preece, Academic Press 1979.
8. Ellis A.T. and Starrett J.E. "A Study of cavitation bubble dynamics and resultant pressures on adjacent solid boundaries." Proc 2nd Int Conf on Cavitation, Edinburgh, 68 Sept., 1983, pp 1-6, IMechE Publications.
9. Voinov O.V. and Voinov V.V. "On the process of collapse of a cavitation bubble near a wall and the formation of accumulation jet." Sov. Phys. Dokl.1 VOIA 21, no. 3, p. 133, 1976.

## ACKNOWLEDGEMENTS

This program was funded through the Naval Weapons Support Center, Crane, IN under contract N00164-85-C-0042, and we are grateful to Mr. Dennis Smith, Contracting Officer and Mr. J. Short and L. Craig, Technical Project Officers for their considerable help which they and their organization provided. This work was carried out with the help of Mr. J. Blaine, Mr. L. J. Tyler, Mr. R. Fossey, Mr. S. Gabel, all of the technical staff of the Rock Mechanics and Explosives Research Center, University of Missouri-Rolla. This paper was typed by Ms. J. Moutray. This help is gratefully acknowledged.

# DEVELOPMENT OF CAVITATING JET EQUIPMENT FOR PAVEMENT CUTTING

A. F. Conn, M. T. Gracey, and W. Rosenberg  
Tracor Hydronautics, Inc.  
Laurel, Maryland

S. W. Gauthier  
Gas Research Institute  
Chicago, Illinois

## ABSTRACT

City streets all over the world are continually being cut open, to allow repairs or maintenance of their the pavement itself or one of the many services gas electricity, telephone, TV cable, water, sewer) buried below. An effort is now underway to develop equipment, using standard pumping units (10,000 psi; 69 MPa) and CAVIJET cavitating water jet nozzles, to replace the mechanical methods now used to cut pavement . Using only water, these nozzles have achieved cutting rates of 8 to 9 in./minute (20 to 23 cm/min) in pavement consisting of 2 in. (5 cm) of asphalt over 6 in. (15 cm) of concrete. Cutting costs -- in comparison to mechanical pavement cutting methods such as diamond saws or pneumatic breakers -- are about one-half with the CAVIJET method. Cost analyses based on laboratory and field tests with experimental equipment and existing gas utility experiences, indicate economical payback period for this type of equipment. Substantial additional savings are achievable if a circular plug of pavement is removed, intact, and subsequently replaced during pavement restoration. Equipment is being developed which can cut linear or circular slots in pavement, and capture, filter, and reuse the cutting water.

## INTRODUCTION

### Motivation

Efficient and safe repair of underground gas piping is a continuing concern of the gas utility industry. The repair process involves pavement removal, soil excavation, pipe repair or replacement and site restoration. A major time, cost, and safety factor in this process is the surface-cutting method applied. Conventional equipment used for cutting pavement includes diamond saws, jack hammers, impacting breakers and large cutting wheels. However, these techniques can be labor-intense, expensive, slow and may be unable to cut the wide variety of pavement surfaces that will be encountered. Most of the currently available methods also produce poor quality cuts that may complicate and increase the cost of the surface restoration process. The many drawbacks of conventional pavement cutting equipment have motivated this effort to develop equipment which uses only water to cut asphalt and concrete, and at a cost less that that of current technology. A primary goal of this project is to help reduce the cost of installing, maintaining, and monitoring the gas distribution system.

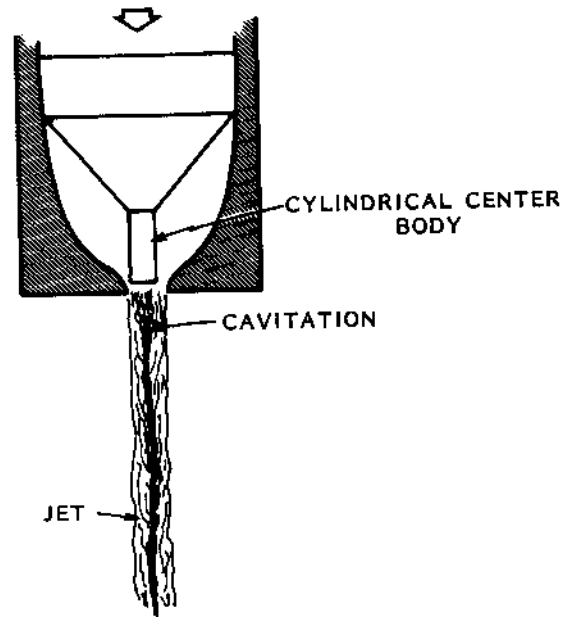


Fig. 1 The centerbody CAVIJET<sup>®</sup> nozzle design. This nozzle system induces cavitation by flow separation.

In response to this need the Gas Research Institute is sponsoring the development of the CAVIJET Pavement Cutter. The CAVIJET cavitating fluid jet harnesses the destructive power of cavitation for useful purposes. The basic concept is to induce explosive growth of vapor-filled cavities within a relatively low velocity water jet. By proper adjustment of the distance between the nozzle and the surface to be cut, the cavities are induced to grow and then collapse on or near the surface where the jet impacts the solid material creating intense localized pressure which quickly erodes the pavement to be cut. This concept provides the cavitating fluid jet with a great advantage over steady noncavitating jets operating at the same pump pressure and flow rates.

### Background

In an earlier phase of this program (1,2), the feasibility of using a cavitating water jet -- having no abrasives or other additives -- to cut pavement was demonstrated during preliminary field experiments in Baltimore, Maryland. It was shown that a centerbody CAVIJET<sup>®</sup> nozzle, Fig. 1, using a conventional, portable 10,000 psi (69 MPa) positive displacement pump, could rapidly cut through a city street. This nozzle had an orifice diameter of 0.106 in. (2.7 mm), and at 10,000 psi (69 MPa) had a flow rate of 19 gpm (72 t 1m) ; delivered hydraulic power was 111 hp (83 kW). A hydraulically-powered linear translator caused the nozzle to repeatedly traverse an 18 (45.7 cm) path at a rate of 9 in./s (22.9 cm/s).

The average pavement cutting rate in these tests was 8.3 in./minute (ipm) (21.2 cm/min) through pavement of varying composition. The overlying asphalt thickness was 3.5 in. (8.9 cm); the concrete varied from 6 to 10 in. (15.2 to 25.4 cm). Total cut time to create a 1.5 by 3 ft (0.46 by 0.92 m) perimeter slot was 13 minutes; adding about 5 minutes to fracture the concrete into liftable chunks, another 5 minutes to clear out the

hole, a total 23 minutes was required. This compared to a 45 minutes, according to a Baltimore Gas and Electric Company (BG&E) representative at the site, typically remove this amount of pavement with pneumatic jack hammer.

The success of this preliminary testing led the continuation of the program, as described in this paper, with the objective of developing and evaluating cavitating water jet pavement cutting equipment which would be:

- Economical in comparison to existing mechanical pavement cutting methods,
- Self-contained and portable,
- Easily deployed and set up, by one man if possible
- Capable of entrapping the effluent (water plus pavement cuttings), circulating it through filters, and thus allowing reuse of a fixed amount of water brought to the site in tanks within the system,
- Able to cut out an intact plug of pavement, which could be removed, and replaced after repairs were completed, and
- Safe to operate, simple, reliable, and easy to maintain.

To date, as described below, the feasibility of all but the last objective has been demonstrated. Prototype equipment, now being developed, will hopefully demonstrate the final objective relating to safety, simplicity, reliability, and maintainability.

#### DESCRIPTION OF EXPERIMENTAL EQUIPMENT

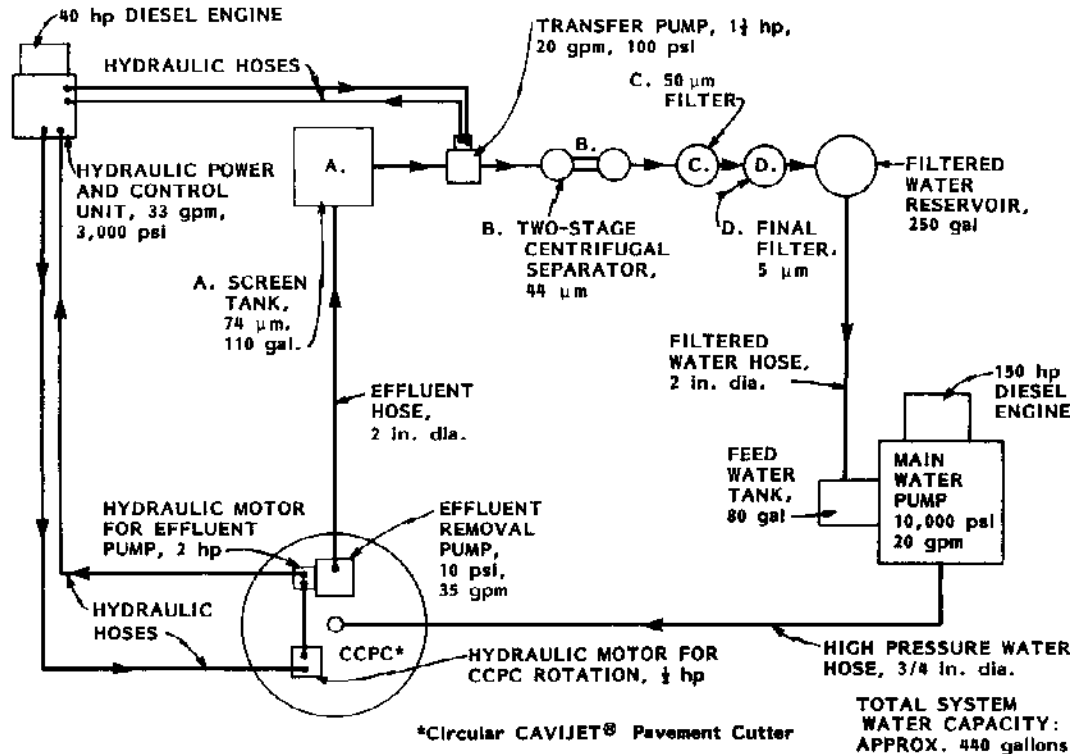


Figure 2. Block diagram of system for laboratory and field test of CAVIJET<sup>R</sup> pavement cutting

In order to learn how to reach the technical and economic objectives specified for this equipment, various experimental modules were designed, built and tested, Fig. 2. Each unit was designed so that it could first be tested at Tracor Hydraulics, Inc. (THI), in the laboratory, and on a 120 ft long (36.6 m) test pavement constructed at THI for this project. These units could then be mounted onto a flat-bed truck, taken to Baltimore, and used to cut holes in city pavements.

### Circular CAVIJET Pavement Cutter (CCPC) Unit

The experimental CCPC unit, Figs. 3 and 4 was designed to allow easy deployment and positioning of the cutter, and to fully entrap the effluent. It cut circular slots from 1.5 to 4 ft (0.45 to 1.2 m) in diameter, and as seen in Fig. 5, the pavement plug could be removed intact. Once placed on the street, the CCPC was rolled to the required cutting site, then lowered into contact with the street surface by the hydraulically actuated wheels. A rubber seal around the CCPC base, squeezed by the weight of the unit, served to keep the effluent fully entrapped within.

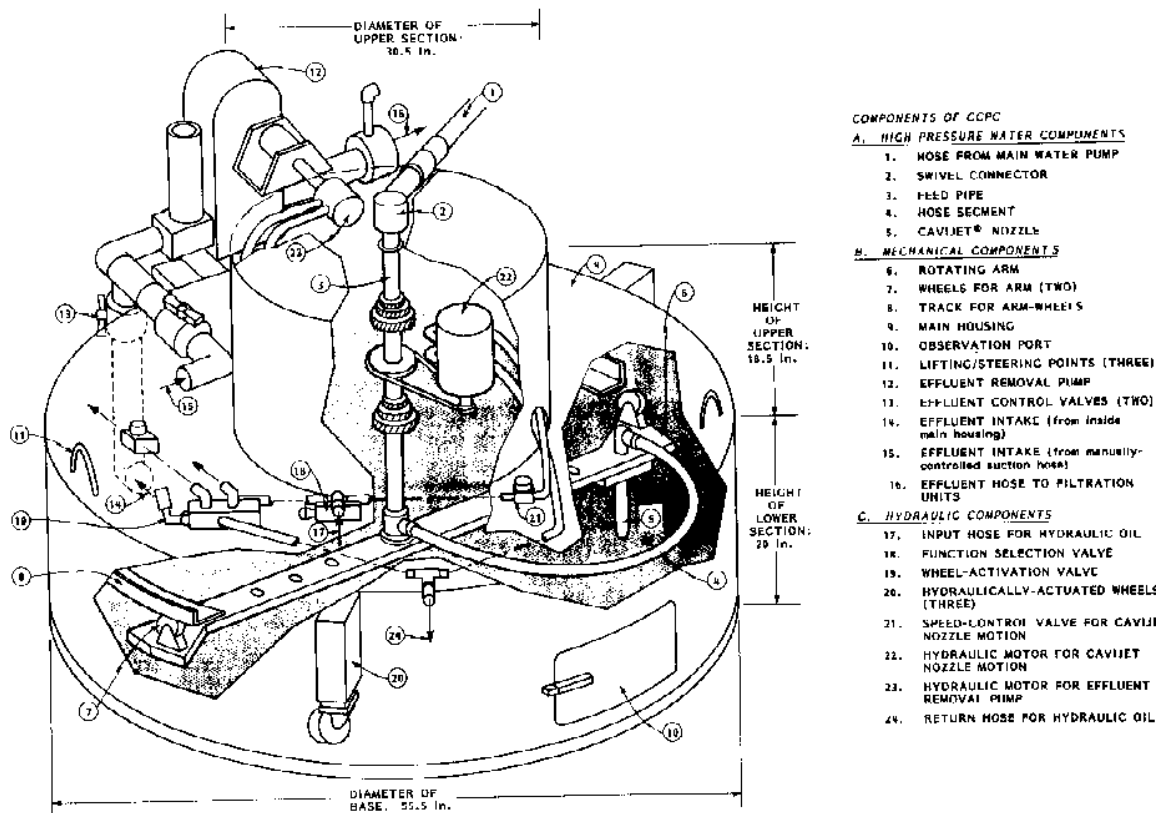


Figure 3. The CAVIJET<sup>®</sup> circular pavement cutter (CCPC) – experimental prototype.

The high pressure (10,000 psi) water entered via the 3/4 in. (19 mm) hose, 1, (Numbers in this section refer to call-outs in Fig. 3). The hose was fastened to a swivel connector, 2, which allowed rotation of the nozzle, 5. The water reached the nozzle through a piece of 3/4 in. (19 mm) diameter feed pipe, 3 (which also served as the central drive shaft for the arm, 6), and then a short segment of hose, 4. The CAVIJET nozzle, 5, could be shifted to various radial positions on arm, 6, thus allowing hole diameters of

from 1.5 to 4 ft to be cut. Other features of this experimental CCPC unit can be seen in Fig. 3.

The diaphragm sump pump, 12, continually removed the effluent during the concrete cutting process. Afterwards, the water trapped in the hole could be drawn out with the same pump by using a manually manipulated suction hose fastened at intake 15.



Figure 4. The circular CAVIJET<sup>®</sup> pavement cutter (CCPC) – hoses are for high pressure water, hydraulic oil, and effluent removal.



Figure 5 Removal of circular plug of pavement cut by CAVIJET nozzle.

#### Main Water Pump Unit

Either of two THI owned trailer-mounted water pumping units were available for pavement cutting trials. Each is powered by a 150 HP (112 kw) diesel engine, driving a five-plunger, positive displacement pump to provide up to 10,000 psi (69 MPa) at 20 gpm (76 elm) flow rate. In addition, one of these units could be fitted for up to 15,000 psi (103 MPa) operation. Although usually only one pump was used, a few runs with two pumps in parallel were made, to achieve total flows rates of up 35 gpm (132 l/m).

#### Hydraulic Power and Control Unit

For these experimental evaluations, a separate hydraulic power and control unit was used to drive the hydraulic motors for the rotation of the CCPC the effluent pump, and the transfer pump. In the prototype system a single diesel engine will power both the hydraulic pump and the main water pump. This experimental unit contained an air-cooled, 40 hp (29.8 kW) diesel engine, directly-coupled to a hydraulic pump capable of up to 33 gpm (125 l/m at 3,000 psi (21 MPa). Also included were a 24 gal (91 l) diesel fuel tank and a 90 gal (341 l capacity hydraulic oil reservoir with filters and oil-cooling units. On-off controls and independent pressure and flow rate variations were provided for each of the three hydraulic circuits.

#### Filtration Units

After experimentation, and analysis of the particle size distributions in the effluent water, a four-step, ever-finer series of filter units evolved. As indicated in Fig. 2, by A, B, C, D, these units were operated in series to finally produce water which was clean enough

to be returned to the main water pump. Over eight hours of cutting time was attained with these filtration units, with differential pressure drops remaining well within allowable limits.

## LABORATORY TESTS

### Test Pavement and Pavement Cutting Trials

The tests at THI were performed on a 120 ft long by 18 ft wide (36.6 by 5.5 m) segment of pavement that was constructed for this project. This pavement had three thicknesses of concrete, each in 40 ft long (12 m) sections, respectively 6, 8, and 10-in. thick (15, 20, 25 cm). Overlaying the concrete was asphalt, in two thicknesses. One half of the 120 ft length had a 2-in. (5-cm) thickness of asphalt covering, the other 4-in. (10-cm) thick. In this manner, a total of six combinations of asphalt and concrete pavement was available. Based on comparative cutting data, it was found that this test pavement concrete was substantially more resistant to erosion than either the test blocks used in earlier laboratory studies or the city street preliminary trials described above. The time required to cut through a 6-in. (15-cm) thickness of this test pavement concrete was about 15 times longer than the laboratory blocks. For this reason, as summarized in Table 1, a wide range of test parameters was examined, seeking the optimum combination for cutting through this difficult material.

Table I Parameters for Laboratory Tests of CAVIJET Pavement Cutting Equipment

Parameter	U.S. Customary Units	SI Units
Nozzle orifice diameter	0.080 to 0.141 in.	2.0 to 3.6 mm
Pump pressure	7,000 to 15,000 psi	48 to 103 MPa
Flow rate	13 to 35 gpm	49 to 132 l/m
Nozzle standoff distance	0.5 to 1.5 in.	13 to 38 mm
Nozzle traverse rate	7 to 15 in./s	18 to 35 cm/s
Jet impingement angle:	Perpendicular, 5* and 10* from perpendicular	

These optimization trials, for the very high erosion strength test pavement concrete, yielded the results summarized in Table 2.

By increasing the flow rate from 20 gpm to 30 gpm (76 to 114 l/m) the cutting time for the 22-in. (56-cm) diameter slot was reduced from over one-half hour to the 8 minutes shown in Table 2. Use of pressures up to 15,000 psi (103 MPa), at a flow rate of about 13 gpm (49 e/m), however, produced about the same cutting rate as when the same hydraulic power was delivered at 10,000 psi, 20 gpm (69 MPa, 76 l/m). Since the pressure of 10,000 psi (69 MPa) was found adequate to cut even this very difficult concrete, it as therefore necessary to deliver the additional flow ,and power in order to increase the cutting rate. A key question remains to be answered, before finalizing the flow rate capability of the production equipment, namely: What is the spectrum of actual pavement erosion strengths, and therefore what system capacity should be provided to produce what rate of cutting in some majority percentage of this range of concrete strengths? Only extended field trials will serve to answer this question.

Table 2 Summary of CCPC Pavement Cutting Results on THI Test Pavement

Parameter	U.S. Customary Units	SI Units
Pavement thickness		
Asphalt:	2 in.	5.1 cm
Concrete:	6 in.	15.2 cm
Cut diameter	22 in.	56 cm
Nozzle orifice diameter	0.141 in.	3.6 mm
Pump pressure	10,000 psi	69 MPa
Flow rate	30 gpm	114 l/m
Nozzle standoff distance	0.6 in.	15.2 mm
Nozzle traverse rate	9 in./s	23 cm/s
Impingement angle	Perpendicular	Perpendicular
Time to initial cut-through	6 minutes	6 minutes
Total cutting time	8 minutes	8 minutes
Cutting rate	8.6 ipm	22 cm/min

As seen in Fig. 5, once the slot had been completed, it was possible to lift out the intact plug of pavement. This was accomplished by drilling three holes into the pavement prior to the cutting operation, using either an electric-powered or airportable drill, equipped with a carbide-insert bit. Threaded lead expansion plugs were then tamped into the drilled holes, and 3/8 in. (9.5 mm) diameter bolts were used to secure a lifting plate. This 0.25 In. (6.4 mm) thick steel plate was affixed with a length of chain, which was fastened to the same chain-fall hoist used to lift the CCPC. For the lab tests, a fork-lift instead of the chain-fall was used. The cut surface, Fig. 6, was somewhat irregular, but smooth enough to allow easy removal of the plug.



Fig. 6 Cut surface: CAVIJET<sup>®</sup> cut is smooth enough to allow plug removal.

#### Effluent Recovery and Filtration

One of the main objectives of this program was to devise methods for trapping the effluent, recovering it, and removing the pavement cuttings so that the water could be recirculated through the high pressure pump. By varying the thickness and softness of the

foamed rubber placed around the base of the CCPC, a seal was developed which had the ability to conform to variations in the pavement surface, and yet was strong enough to withstand the handling and CCPC weight loadings. This seal trapped virtually all of the effluent beneath the CCPC. The effluent removal pump, while removing almost all of the water, left the majority of the cuttings behind. It was estimated from measurements during the lab testing that about 80 percent of the slot-volume cut by the CAVIJET nozzle was left on the pavement, a fortuitous factor, since this served to minimize the burden on the filtration system.

The first unit in the filtration sequence, Unit A, the screen tank (see Fig. 2) received the flow directly from the effluent removal pump. This tank, which was 2 by 2 by 4 ft high (0.6 by 0.6 by 1.2 m), contained two removable, flat, 2 x 4 ft screenholders. Screen meshes ranging from 45 to 149  $\mu\text{m}$  were tested; it was found that a 74  $\mu\text{m}$  (200 mesh) size was optimum for both screens for the first filter unit. However, during the testing it was necessary to manually brush away particles which built up on these screens. Therefore, a commercial unit containing "active filtering," i.e., an automatic continual wiping or periodic back-washing, is being sought for the prototype version of the system.

The other filters (B,C,D in Fig. 2) were standard commercial units, and as cited above, were satisfactory for meeting the objective of removing pavement cuttings from the water. As discussed below, however, the field tests demonstrated the difficulty of avoiding soil particles within the effluent flow. The existing "passive filters", i.e., containing no wiping or backwashing means, were not designed to handle the quantity of particles created when the jet encounters soil. For this reason, "active filtering" is also being sought for the final filter unit.

## FIELD EXPERIMENTS

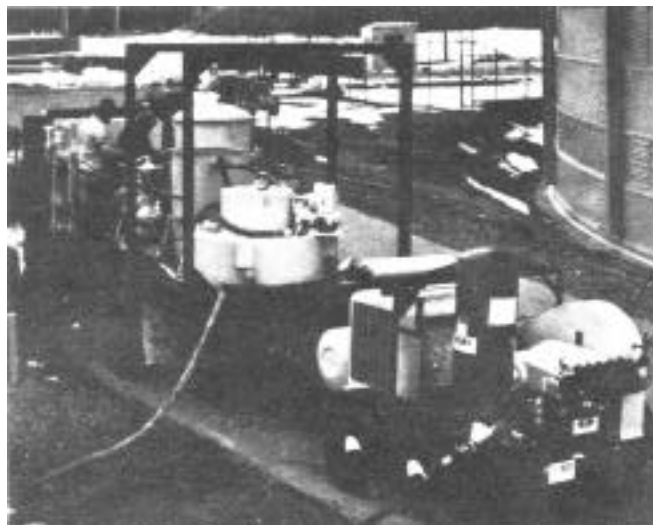


Figure 7. Experimental CAVIJET<sup>R</sup> pavement cutting equipment mounted on flat-bed truck. Main water pump unit is towed by truck.

All of the experimental modules were mounted onto a 20 ft long by 8 ft wide (6.1 by 2.4 m) flat-bed truck, Fig. 7. A framework which supported a two ton (17.8 kN) chain-fall hoist was added, for handling the CCPC unit and lifting pavement plugs. This truck also towed the main pump unit. With support from the BG&E, three field tests were conducted in Baltimore, Maryland at sites of either slow gas leaks or service cutoffs. These tests served to demonstrate several of the stated objectives for this system:

- (a) Deployment and positioning of the CCPC unit by one man under field conditions.
- (b) Full entrapment of the effluent within the CCPC unit on actual city streets.
- (c) Filtration to remove pavement cuttings and recirculation of the water through the main water pump.
- (d) Ability to operate in subfreezing weather.
- (e) Capability of operation in a self-contained, portable mode.

As anticipated, these field experiments also served to define some additional specifications for the prototype design:

- (a) Flow rate/Cutting rate optimization -as discussed above, the erosion strength of concrete, and hence the rate of pavement cutting achieved by a given cavitating jet nozzle, can vary greatly. Therefore, the prototype equipment will be provided with adequate flow rate capacity to allow assessment of the optimum system capacity for achieving cost efficient cutting rates in a majority of concrete types.
- (b) Filtration of solid particles - prior to the field trials, the premise was to design a filtration capability for only the pavement cuttings, i.e., particles of asphalt and concrete. This was accomplished, and a storage capacity had been provided to shunt the effluent into when pavement cut-through occurred and soil particles began to be "mined" by the jet erosion action. The field trials showed that this premise was invalid; it is too difficult to observe the onset of soil particles in the effluent flow, and soil may also be found between the asphalt and concrete layers. For this reason, active filter units capable of handling the soil particles are now being evaluated.

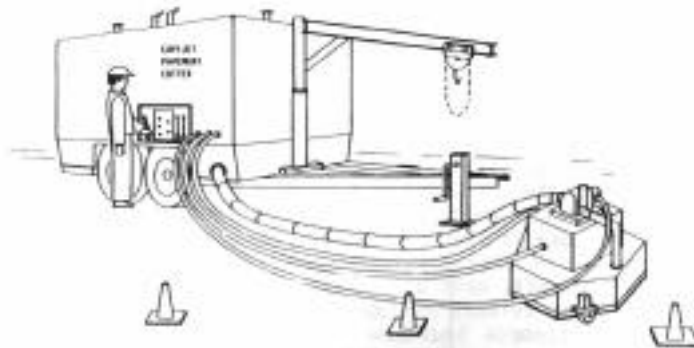


Figure 8. Artist's concept drawing of CAVIJET<sup>®</sup> pavement cutting equipment.

- (c) Configuration of system - to achieve the objectives of safety, simplicity, and reliability, a system configuration as suggested in Fig. 8 will be required. All controls and readouts must be brought to a single panel, where one operator can monitor and

control the cutting operation. Deployment of the cutter unit must be from street level, using a retractable hoist as indicated in this figure. Other cutting units, to provide rectangular slots and linear cuts for trenching, are to be developed. This system design is based on a trailer, which would be brought to the site by any available towing vehicle. Truck mounted equipment could also be provided.

### DISCUSSION OF RESULTS

In several previous publications (1,2,3) cost comparisons were made between mechanical methods (pneumatic pavement breakers, diamond saws), abrasive jets (4,5), and the cavitating water jet method. A summary of this comparison is shown in Fig. 9. Based on the preliminary results available to date, for a two-man pavement cutting operation, it is seen that the cavitating jet method offers the potential of being an economical alternative to existing methods for cutting pavement. It should be emphasized that only costs associated with cutting pavement are considered in this or the following figures, i.e., additional savings associated with pavement removal and replacement, by use of the intact plug created by the CAVIJET method, were not factored into these economic analyses.

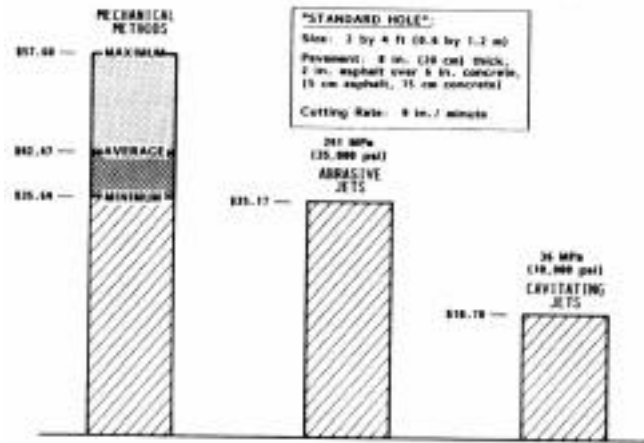


Figure 9. Pavement cutting cost comparison (1985/1986 - \$)

Pavement cutting costs are primarily affected by the rate of cutting, as seen in Fig. 10. For instance, a three-fold change in cutting rate (4 to 12 ipm) (10 to 30 cm/min) will reduce the cost per "standard hole" by a factor of three (from over \$40 to about \$15). System purchase price has a relatively small cost-per-hole effect. As plotted in Fig. 10, a price change of from \$40K to \$70K increases the cost per-hole by only about \$1.

Another important factor that is weighed when deciding whether or not to purchase a new piece of equipment is "payback time." Assuming that the new equipment: (a) will offer a lower cost per-hole-cut, and (b) will cost more to purchase than the currently used equipment, in this case a pneumatic pavement breaker system, Fig. 11 examines how long it will take to recover the added capital outlay for a CAVIJET pavement cutting system. The key parameter here is how many holes per month will be cut. If, for instance, 50 to 75 holes per month are anticipated, and the system price is between \$50K and \$60K, then the payback time would be about 1.25 to 2.25 years, an acceptable time for many organizations.

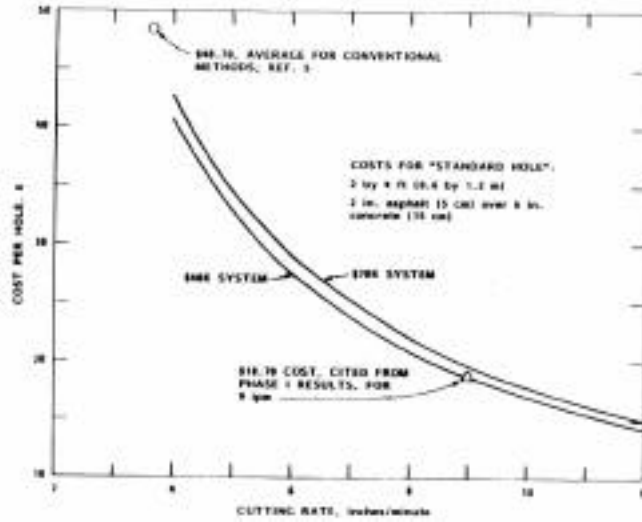


Figure 10. Effect of CAVIJET<sup>R</sup> cutting rate and system cost on cost per hole.

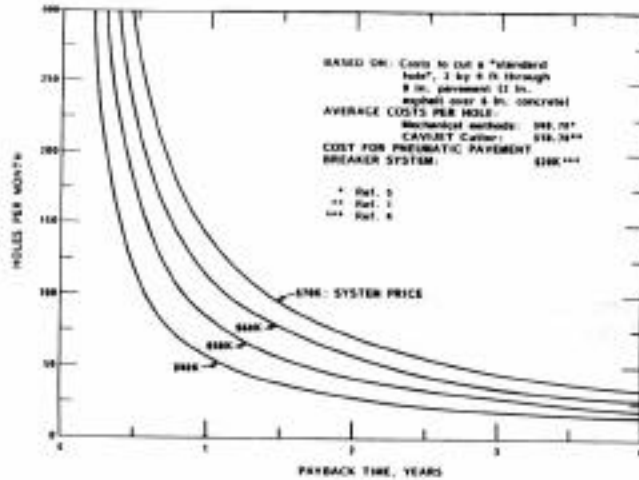


Figure 11. CAVIJET pavement cutter system payback analysis.

## CONCLUSIONS

This paper has described work in progress. Although at this stage an operational prototype has yet to be assembled, each principal component has been built, evaluated, and required changes, if needed, have been identified. The cutting rates, and the anticipated capital and operating costs, as of this time continue to indicate that cavitating water jet equipment should be a viable replacement for the existing mechanical pavement cutting methods.

## FUTURE PLANS

Development will continue for trailer-mounted independent units as shown in Fig. 8, with a Circular CAVIJET Pavement Cutter and a Linear CAVIJET Pavement Cutter. It is envisioned that the circular cutter will be used by utilities to cut an opening in pavement for "key hole" excavation work, when repair and maintenance operations on an

underground pipe would be performed from the surface using long handle tools. A linear cutter would cut pavement in situations where a larger, square pavement opening is required so that a backhoe can be used to excavate a buried pipe and a utility field crewman can get into the excavation pit. The initial work effort will focus on the development of hydraulically-powered units. Consideration is also being given to developing a configuration that will use pneumatic power to move the CAVIJET nozzle, drive the effluent-removal pump, and raise and lower the unit's wheels.

#### ACKNOWLEDGMENTS

This project is being supported by the Gas Research Institute (GRI) under Contract Nos. 5085-271-1064 and 5085-271-1169. The authors would like to thank Mr. Steven R. Kramer, Manager of GRI's Distribution Operations for his continued support, counsel and guidance during this project. Only the generous support of the Baltimore Gas and Electric Company made the field trials possible; a special thanks to Mr. Jerry Fields for his unflagging enthusiasm. Our many colleagues at Tracor Hydronautics who have contributed to this project include: Mr. George Arrington, Mr. Paul Bolander, Mr. Roger Dorsey, Ms. Kae Guy, Mr. Blair Holtschneider, Mr. Cal Lockner, Mr. George Matusky, and Mrs. Donna Vanek. A special acknowledgment is given to Mr. Marcel E. Gres, Applied Science Group, Tracor, Inc.; his technical and administrative guidance is a constant and essential factor to this and all of our jet technology projects.

#### REFERENCES

1. Conn, A. F., "A Preliminary Field Trial Evaluation of the CAVIJET Method for Rapid Cutting of Pavement," GRI Report No. 85/0161 (Tracor Hydronautics, Inc. Report No. TR 85016-1), July 1985, 50 pp.
2. Conn, A. F., "Rapid Cutting of Pavement with Cavitating Water Jets , Proceedings of 8th International Symposium on Jet Cutting Technology BHRA, September 1986, pp. 231-240.
3. Conn, A. F., Gracey, M. T., Rosenberg, W., Matusky, G. E., and Arrington, G. W., "Development of CAVIJET Pavement Cutting Equipment, Phase II: Laboratory Trials," GRI Report 86/0306 (Tracor Hydronautics, Inc. Report No. TR 85023-1), July 1986, 92 pp.
4. Fort, J. A. and Kirby, M. J., "Development of a Waterjet Pavement Removal System, Phase III. Field Testing," GRI Report No. 84/0208 (Flow Industries, Inc. Report No. TR-307), September 1984, 61 pp.
5. Fort, J. A., Kirby, M. J., and Tower, "Development of a Waterjet Pavement Removal System, Phase IV: Extended Field Testing," GRI Report NO. 85/0266 (Flow Industries Inc. Report No. TR- 46), September 1985, 65 pp.

## HYDRO DEMOLITION - TECHNOLOGY FOR PRODUCTIVITY AND PROFITS FOR AMERICA

R. J. Nittinger  
Senior Sales Representative  
Atlas Copco Roctec, U.S.A.  
Wayne, New Jersey

### ABSTRACT

Within the US highway system there are 585,059 bridges inventoried and classified. Of this number 245,817 are classified substandard.

The transportation of people and goods in the US accounts for more than 20% of the gross national product. Transportation affects every element of our economy and every aspect of our daily life. We built the roadways we must now repair them. Without bridges we have no roadways.

Because of the enormous highway program and depleting budgets, efficiency and cost effectiveness are a must, and hydro-demolition can fulfill those demands. In two separate case studies by Indiana DOT, it was proven that hydro-demolition out-produced a 7-man jackhammer crew and a 5-man jackhammer crew by a minimum of 3 to 1 and 5 to 1 respectively.

Time and money were saved for both the State and Contractor alike. Bridges were expeditiously repaired, while stretching the budgetary dollars.

### INTRODUCTION

The US Transportation System is in deep trouble, and as capital construction improvements continue to be deferred, the actual rate of deterioration continues to increase at a rapid accumulative rate. The transportation of people and goods in the US accounts for more than 20% of the gross national product. Transportation affects every element of our economy and every aspect of our daily life. Within this transportation system there is an estimated 3.9 million mile highway system that serves some 170 million vehicles that travel more than 1.6 trillion vehicle miles annually. (1) Eighty percent of the system is surfaced and within this system there are 585,059 bridges inventoried and classified. Of this, more than 42% were classified substandard.(2)

All states recognize the seriousness of the bridge program, and the need to address the situation. Some states categorize their bridges in percentile of deterioration, other states classify them as satisfactory or unsatisfactory, yet others, such as New York, in the heart of climatic changes and chloride attacks categorize it on a scale of 1 to 7, with the number 1 representing "very poor condition" and 7 as "good condition".(3)

With tight budgets and a deteriorating bridge system the need to expedite repairs and keep the cost down by virtually stretching the dollar is welcome. Expanding on this,

is the need to rapidly repair bridges in high traffic areas to minimize delays. Fulfilling all these demands is the utilization of hydro-demolition.

More than a decade ago at the Atlas Copco Research Institute in Ecublens, Switzerland near Lausanne the art of "jet stream technology" was developed.(4) By coordinating a specific pressure of water with an optimum volume of water it was found that concrete could easily be removed while maintaining an astounding cost effectiveness. It was realized that if a high enough pressure of water could be created with a specified volume of water, delaminated and unsound concrete could be removed effectively and easily without damaging the existing rebar. This technique was developed through the utilization of two pieces of equipment. The power pack and the robot both being called hydro-demolition but one cannot work without the other. Hence; the development of a new construction technology.

### THE BRIDGE PROBLEM

When bridges were built the anticipated life was 75 to 100 years before heavy maintenance and/or repairs would be required. However several unexpected factors entered into the picture and created premature deterioration.

1. Geometric increase in traffic volume since World War II
2. The shallow placement of structural reinforcing bars
3. Severe attack of chlorides

Within a forty year period traffic volume has increased thirteen fold since the end of World War II. Traffic grew from an estimated 12.3 million vehicle to over 170 million vehicles per year. This is not to mention the dramatic increase in truck weights and their increased speeds.(5)

In addition during the boom years of the interstate program between the 1950's and 1970's the reinforcement bars were to be placed 1-1/2 in. from the surface. This in itself was not sufficiently deep enough, and the actual placement of the rebars fell anywhere between 3/4 in. to 1-1/2 in. due to the poor construction techniques and/or poor inspection. These bars would react to heavy traffic volume and a harmonic frequency would develop, creating spalled areas and capillary paths for the chlorides and crystals to travel and penetrate.

Although the concrete was air entrained to accept the crystals and allow room for expansion, as illustrated in Figure 1, the chloride attack became so severe that the entrained air voids could no longer accept the expanding crystals and out grew the void sphere, thereby debonding the mortar from the aggregate (Figure 2) and causing pavement cracks. In turn these cracks permit more chlorides to enter thereby compounding the problem. Thus the situation becomes exponentially digressive.

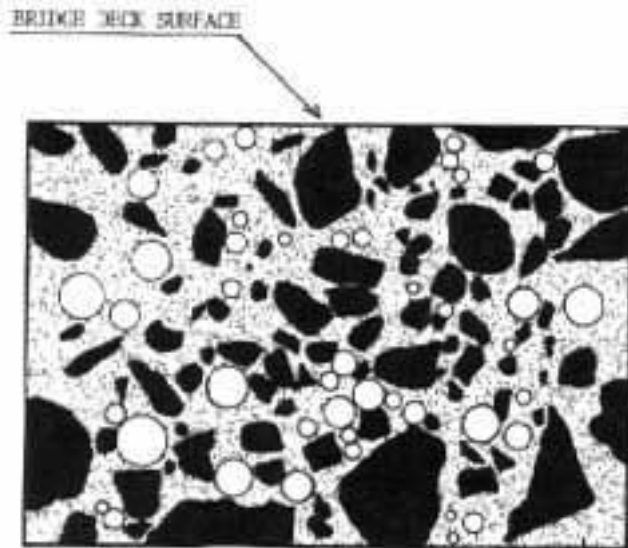


Figure 1. Air entrained concrete profile section. The bubbles illustrate entrained air bubbles or voids within a concrete bridge deck. Entrained air is required to allow for crystal expansion during freeze and thaw thus preventing concrete disintegration.



Figure 2. Entrained air bubble filled with chloride crystals.

#### DATA ANALYSIS – NORTH-EASTERN STATE

Selecting an example State in the heart of the northeastern climate zone, New York was chosen. With bridges subjected to snow, ice, warm, cold and chloride attacks, it was realized that every bridge had to be categorized and classified.

All bridges built between the years 1900 and 1979 were rated on a scale of 1 to 7. The data obtained for these structures were summaries from inventory and inspection files by state forces. The rating numbers are defined as follows: (6)

- 1 - Very Poor Condition
- 2 - Poor Condition
- 3 - Major Structural Repairs Required
- 4 - Structural Repairs Required
- 5 - Repairs Required
- 6 - Minor Repairs Required
- 7 - Good Condition

What was shown in the data was the history of all maintenance, rehabilitation and replacement of structures summed over the past 80 years. The regressions indicate that from 1900 to 1965 all structures on the average declined in condition at the rate of 0.023 rating points per year. Starting about 1965 all structures on the average begin the decline in condition at a faster rate of 0.075 from that year onward.

An example of this occurrence would be to take a group of average structures built in the year 1900 and are rated at 7. At a constant annual rate of deterioration of

0.023 in the year 1910 when they are 10 years old, their rating would be 7 - (10 x 0.023) or 6.77,

As they continue to age, after 80 years their rating would be 4.37 (see TABLE 1).(7)

**TABLE I**  
**Bridge Rating And Corresponding Decade**

Year	Age	Rating
1920	20 Years	6.54
1930	30 Years	6.31
1940	40 Years	6.08
1950	50 Years	5.85
1960	60 Years	5.62
1965	65 Years	5.50
1970	70 Years	5.12
1980	80 Years	4.37

It appears that bridges in this part of the country (Northeast) begin accelerated deterioration after 65 years old. In the NYS Special Research Report - 70, all structures under the NYS jurisdiction from 1900 to 1979 were rated and categorized:

**TABLE 11 (8) Bridge Rating Based On Five Year Intervals**

Interval In Which Structures Were Built (Year)	Number Of Structural	1980 Inspection Mean Rating
1900 - 1904	34	3.91
1905 - 1909	30	3.87
1910 - 1914	90	4.13
1915 - 1919	71	4.25
1920 - 1924	156	4.21
1925 - 1929	494	4.55
1930 - 1934	856	4.80
1935 - 1939	477	5.01
1940 - 1944	155	4.92
1945 - 1949	200	5.22
1950 - 1954	307	5.18
1955 - 1959	593	5.35
1960 - 1964	884	5.34
1965 - 1969	1,024	5.79
1970 - 1974	777	6.14
1975 - 1979	187	6.58

TABLE II used a mean rating because all structures have not been neglected.<sup>1</sup> Based on the deterioration rating illustrated in TABLE II and the rating formula the prediction of the average rating for each 5 year interval will be reduced by 1.22 in the year 1990. New York State like most states, is aware that needed repairs are backlogged, and the overall system condition declines. The analysis shows the mean rating for all structures will reach 3, in less than 20 years.

The state realizes that it might meet its responsibility to the public. On the average, in New York State alone, there is one structure for every three miles of roadway. These structures are becoming deficient at a rapid rate. One half will be deficient by 1994 and 74% by 2000 if the situation stays as is. Posting for reduced load lags behind this, but by 2000 nearly one third will be posted. This means that a posted structure, unable to carry a large truck safely will be encountered on the average of every 10 miles. The impact of this on the state's economy will be significant.

Calculated predictions of posted structures are as follows:

TABLE III (9) Posted Structures - Rating -3 Or Less

Year	Rated 3 Or Less	Total Posted	Average Miles Between Posted Structures
1980	507	109	174
1990	2,280	606	31
2000	4,688	1,838	10
2010	6,018	3,738	5

The NYS Special Research Report concludes the following:

1. New York's structures are experiencing accelerated deterioration. The current rate of decay appears to be five times the historical rate--and may increase still further
2. A rapid response to this problem is needed to prevent an unacceptable decline in the condition of structures, with its attendant economic consequence.
3. Preventive maintenance applied to structures in good condition appears to be a very cost-effective strategy.

---

<sup>1</sup> A example of the mean rating for the interval 1930 to 1934 inclusive. There are 856 structures with a mean rating of 4.80. A breakdown of these show 49 rated 7, 223 rated 6, 279 rated 5, 184 rated 4, 73 rated 3, 33 rated 4, and 15 rated 1.

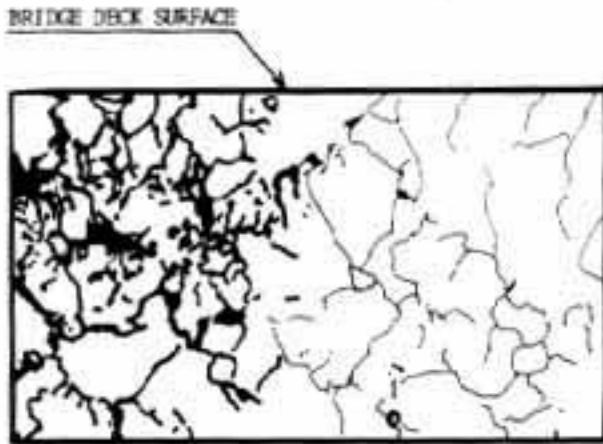


Figure 3. Profile illustrating heavy and light capillary map cracking within a concrete bridge deck.

Left side of the above illustration shows heavy cracking which would yield a hollow sound when chained. The right although showing map cracking would yield a solid sound when chained. The left side would be jackhammered and removed. The right side would be ignored and some three or four years later would have to be addressed for repairs.

#### THE SOLUTION

New York State Special Research Report 70, argues very strongly in favor of early and preventive maintenance. Relatively modest expenditures now to keep a structure at a rating of 5 or better will prevent much larger expenditures from being necessary at a future date.

#### Jackhammers

During the past fifty years, bridge decks were repaired by a single conventional method known as jackhammers. The decks are usually sounded by an inspector manually dragging a group of chains across the deck, and when they hear a hollow sound (Figure 3), the inspector marks it out. These marked out spots are then removed by a crew of seven, ten or more men with jackhammers. The removal is slow but effective, however additional areas that should have been -removed, but were missed, such as slight map cracking (Figure 3), will require repairs in the not to distant future. This has always been a problem with bridge repair in the past and present.

#### New Equipment

Like all existing concepts, new ways are continually being sought after. In the search, with the bridge rehabilitation program being in dire need and the continuous desire to reduce cost, pavement profilers, millers and planers came into their own and were utilized for partial deck removal. Although it enhanced the process, it did not achieve the cost effectiveness required, because jackhammers were still needed to get around and below the reinforcing bars. It complemented the existing conventional method of jackhammer work but was not an end result.

As work loads grew and costs escalated the search continued for new and better ways, until jet stream technology became a reality, thereby introducing hydro-demolition. This technique utilized two pieces of equipment -- the robot and the power pack. Both being called hydro-demolition but one cannot work without the other.

## CONCEPT

### 1. Robot.

The robot can consist of a cutting nozzle or nozzles which can be fixed Or rotate on a transverse feed beam. The transverse speed can be regulated as well as the forward progress speed. In essence the robot can be programmed. The cutting head (transverse) can cut from 8-in. wide to 12'feet in width, and deliver pressures from 10,000 PSI to 30,000 PSI using from 8 gallons to 85 gallons of water per minute. The consumption of water is not necessarily lineal with PSI. An example of this is delivering a pressure of 12,000 PSI using 85 gallons of water per minute while in another location a pressure of 17,500 PSI is delivered with 26 gallons of water per minute.

The robot was designed keeping in mind the surrounding environment, eliminating dust and minimizing noise. Its size of 8 feet plus or minus in length and a width of 5 feet to 12 feet depending on the transverse feed beam is compact. The unit has the capability of working around the clock with only one man operating it, and it will take the place of 8 to 12 men with jackhammers, and even more depending on the situation. It can be hooked up to one or two power packs. When two power packs are connected, the productivity is not leaving the pressure the same and increasing the volume of water productivity in depth and square feet can be tripled and quadrupled.

### 2. Power Pack.

The power pack is connected to the, robot by high pressure hoses and electric cables. power pack is an enclosed 8 foot by 8 foot by 20 foot sound proof container that is filtered and vented for noise containment and can easily be moved or loaded unloaded off a truck. Within the enclosed container consists a delivery high pressure pump, diesel engine, cooling system, water reservoir, filtration system, and electrical circuitry. Water can be supplied to the water reserved either from a tanker truck or a fire hydrant at no pressures. The power pack can be as far as 265 feet away from the robot, and can be placed easily in an "out of the way" location, which was designed to minimize space.

### 3. The Principle.

As the nozzle of the hydro-demolition robot moves transversely across the pavement it delivers a large volume of water at a high pressure, thus forcing the water into the capillaries and air voids, (Figure 4) removing all the unsound and delaminate concrete. The water will travel in the path of least resistance and FIND UNSUSPECTED MAP CRACKS (Figure 3) and remove the concrete. As the water is forced into the concrete, it reaches the point where can travel no further and is forced back out through the top placing the concrete in tension which is only one-tenth of its compressive strength (Figure 4). This in turn will leave a sound, rough concrete surface that can easily accept the bond of the new overlay (Figure 5). The remaining rebar is intact, non-damaged, and relatively clean, thereby minimizing sandblasting, if needed at all. Properly adjusted the

robot can eliminate sounding with chain or other devices and other guess work, while at the same time removing the concrete that should be removed, leaving only the strong, sound concrete in place, clean and ready for overlaying.

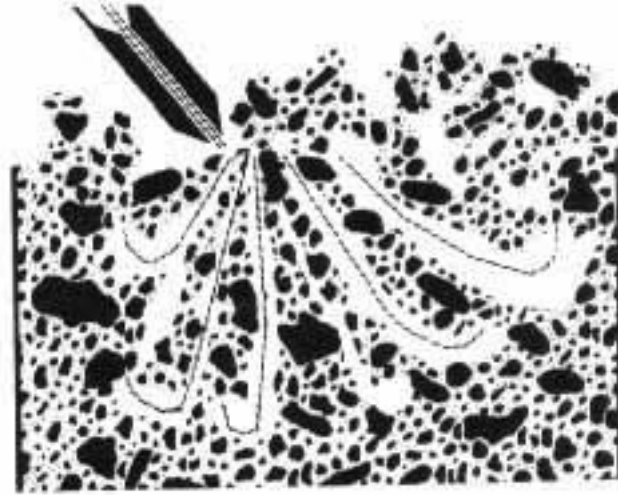


Figure 4. Illustration of water jet stream penetrating concrete bridge deck forcing the concrete upward and putting it in tension.

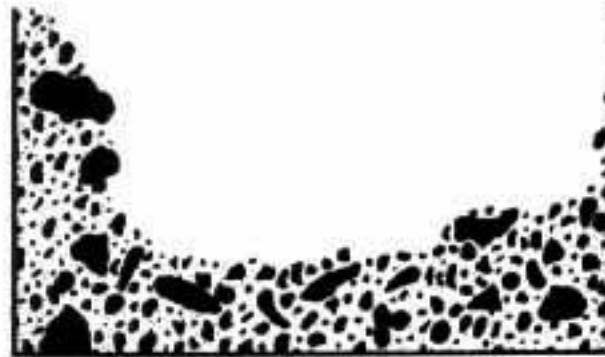


Figure 5. Illustration of deteriorated concrete removed, leaving the strong sound concrete, clean and ready for overlaying.

#### CASE HISTORIES

A. Early in 1985, the New York State Thruway Authority was very impressed with hydro -demolition when it was utilized on a bridge on Interstate 190 near Grand Island in Buffalo, New York.(10) A 4.6 million dollar Contract was awarded to Severson Construction from Niagara Falls, New York. The contract called for removing 14,000 square feet of bridge deck one inch below the top reinforcing steel. The Thruway Authority had allowed 18 months to complete the project. After sounding the deck, they (Thruway Authority) discovered that 75,000 square feet of concrete was unsound and had to be removed. A 500% overrun. Despite this, Severson completed the entire project in only four months--14 months sooner than required. By hooking up a second power pack to a single robot Severson Construction was able to remove up to 2000 square feet, 3 to 6

inches deep of deteriorated bridge deck in a 24 hour work day. Unlike a man the -robot was able to work around the clock.

B. Indiana DOT closely documented a comparison between the conventional jackhammer crew method and hydro -demolition- on two separate project sites.

CONTRACTOR - HYDRO TECHNOLOGY INC., JEFFERSON, INDIANA  
 MANAGER - MR. GARY OTTMAN

- Bridge ID B-15331, Miami County, IN (TABLE IV)
- Bridge ID B-15644, Switzerland County, IN (TABLE V)

The results from these two project sites were outstanding. On the Miami County Project the hydro-demolition unit was compared to a seven man jackhammer crew working a nine hour shift. It took the 7-man crew 12 days to remove 3524 square feet and the hydro-demolition unit took only 6 days to remove 5,193 square feet. The hydro-demolition unit achieved 47% more production than the 7-man crew in one half the time (see TABLE IV). One of the noticeable key ,problems with jackhammers is the fact that they hit rebar, debonding the sound concrete from the rebar and then chase the debonded concrete and going deeper than necessary expanding cost in both time and material.

TABLE IV (11)7-Man Jackhammer Crew Vs. Hydro-Demolition -Bridge B-15331, Miami County, Indiana

ITEM	SOUTHBOUND		NORTHBOUND	
	Drive Lane	Passing Lane	Drive Lane	Passing Lane
	JACKHAMMER	HYDRO	JACKHAMMER	HYDRO
Calendar Days	12	6	17	12
Deck Size (SFT)	12782.7	11178	12782.7	11178
Man Hrs/ Machine Hrs	756	39.5	1071	128
Patching (SFT)	3524	5193	4057	8878
Avg Patch Depth	3.4811	2.0611	3.7211	2.4111
Production (SFT/Hr)	4.66	131.47	3.78	69.36

General Notes:

1. Deck was scarified first by roto mill.
2. Deck was sounded and marked by IDOH personnel.
3. Calendar days based on 7-man working 9 hours per day.

4. Northbound structure was predominately a latex overlay that was removed.
5. These quantities are from the IDOH field reports.
6. Hydro-demolition was performed as a single shift operation with one machine.
7. Water consumption for hydro-demolition was 167,500 gallons.
8. Hydro-demolition was one pass only.
9. Some minor trim work was performed with jackhammers.
10. Cleanup of hydro-demolition was performed by a Vac-All. (Included in Service.)

TABLE V (12) 5-Man Jackhammer Crew Vs. Hydro-Demolition - Bridge B-15644, Switzerland County, Indiana

<u>ITEM</u>	<u>Phase I JACKHAMMER</u>	<u>Phase 2 HYDRO</u>
Calendar Days	20	3
Deck Size (SFT)	5130	5508
Man Hrs/Machine Hrs	728	18
Patching (SFT)	1544	1175.7
Avg Patch Depth	3.76	6.04
Production (SFT/HR)	2.12	65.27
Scarification (SFT/HR)		306

General Notes:

1. Deck was scarified and patching removed in one pass by hydro-demolition.
2. A second pass was made in a extreme deep patch area.
3. Deck thickness is 6-3/4".
4. 411 SF of patching was 6-1/2" deep.
5. 36 SF of full depth patching was done by jackhammers for barrier wall.
6. All patching was filled with latex overlay.
7. These quantities are from the IDOH field reports.
8. Hydro-demolition was performed as a single shift operation with one machine.
9. Water consumption for hydro-demolition was 26,400 gallons.
10. Some minor trim work was performed with jackhammers.
11. Cleanup of hydro-demolition was performed by a Vac-All. (Included in Service.)
12. Scarification depth averaged .33" to .41".

Based on TABLES IV and V it was obvious that hydro-demolition's production rate is far superior to the conventional jackhammer crew method. Although TABLE IV shows less square feet completed it was greater than two inches deeper, and it was accomplished in one-seventh the time.

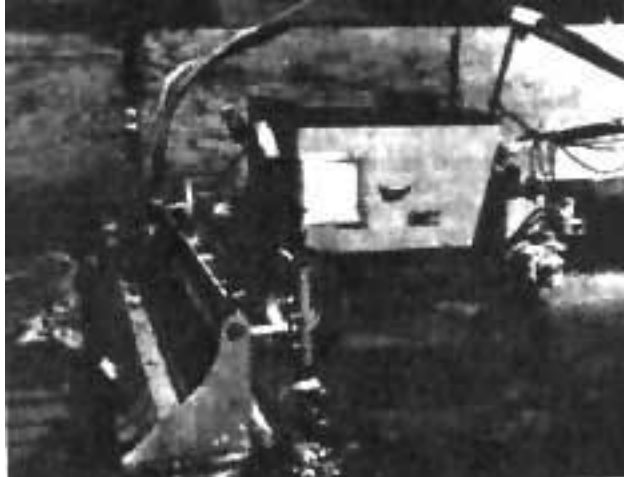


Figure 6. Atlas Copco Conjet removing concrete down to the rebar in a parking garage in Chicago O’Hare Executive Plaza. Contractor – Mid-West Hydro Blasting, Inc., Chicago, IL.

**OPERATING AND OWNERSHIP COST**

**A. Operating And Maintenance Cost**

The daily operating cost of the Conjet has been established based on two years of operation. TABLE VI illustrates the operating cost.

**TABLE VI - Daily Operating Cost - Conjet - With Single Powerpack  
Based On 10 Hour Work Day**

<u>Item</u>	<u>Expense In \$</u>
1. Fuel - 12 Gals/Hr @ 80% Efficiencyx 1.00	\$96
2. Grease and Lube	2.00
3. Oil	.50
4. Filters	5.00
5. Traction System (Robot)	4.00
6. Pump (8 Year Life)	5 .00
7. Engine & Radiator	8.00
8. Pistons (Pump)	20.00
9. Cylinders (Pump)	30.00
10. 5 Meter Hoses	15.00
11. Nozzles	50.00
12. Miscellaneous	<u>2.00</u>
<b>TOTAL MAINTENANCE COST</b>	<b>\$287.50</b>

**Daily Cost - Labor Only**

<u>Item</u>	<u>Expense In \$</u>
1. One (1) - Machine Operator* 60 = Hr/Wk-at \$15 Per Hour With 20 Hrs Overtime	\$262.50

2. Maintenance Man \$150/Wk His	=	30.00
Portion Towards Conjet		
TOTAL LABOR COST	=	\$292.50
TOTAL DAILY MAINTENANCE AND LABOR COST		= \$580.00

\*Machine Operator - Includes time and one half for 20 hours of overtime for the week plus 25% fringe benefits.

As shown in TABLE VI items 5 thru 10 are considered "money for the boot". Money that should be reserved for the day that maintenance will be required. Nozzle life can vary between 80 to 125 hours. The cost to operate the Conjet is estimated at \$580.00 per day. This cost can then be calculated on a square foot basis. A minimum production rate of 800 square feet at an average depth of 2-1/2 inches deep per day should be achieved. Hence:

$$\frac{\$580.00}{800 \text{ Sq Ft}} = \$ .725 \text{ Per Square Foot}$$

#### B. Ownership Cost

With the operating and maintenance cost estimated the cost to own the unit must be determined giving the contractor the knowledge to estimate his bid. The contractor must assume achieving at least 72,000 square feet of work per year. Establishing an 8 year ownership cost, the following calculation can be estimated (TABLE VII).

TABLE VII Ownership Cost - Conjet With Single Powerpack

1.	a. Purchase Price	\$405,000.00
	b. Sales Tax (National Aver 6%)	\$24,300.00
	c. Freight (National Aver)	<u>\$7,000.00</u>
	d. Delivered Price	\$436,300.00
2.	a. Salvage Value (20.0%) 8 Years	(\$ 87,260.00)
3.	Depreciable Value (1d-2a)	\$349,040.00
	a. Depreciable Value Over 8 Years	43,630.00
	b. Based on 90 Days Per Year	\$ 484.78/Day
4.	a. Interest = 12.5%	
	b. Insurance = 1.0%	
	c. Taxes = 1.0%	
	d. Total = 14.5% = .095 Factor Finance Handbook	
5	<u>.095 x \$436,300 =</u>	
	90 Days	\$460.54/Day

6.	Total Ownership Cost Per Day	\$ 945.32/Day
7.	Total Yearly Ownership Cost = \$1.18 - Based on 72,000 Sq Ft Per Year	$\frac{\$945.32 \times 90 \text{ Days}}{72,000 \text{ Sq Ft}}$
8.	Cost of Ownership Per Sq Ft	\$ 1.18

With only an estimated 90 day utilization per year a minimum yearly total of 72,000 square feet can be calculated. As illustrated in TABLE VII the cost to own the unit is reduced to \$1.18 per square foot.

### C. Estimated Bid

With the estimated ownership and operating costs established, the contractor now has the ability to factor in a starting bid. The cost to own and operate the unit calculates at:

$$\$1.18 + \$0.725 = \$1.905 \quad \text{Per Square Foot 2-1/2 Inches Deep}$$

As production rates increase, these figures will obviously reduce considerably thereby increasing the profit margin. Naturally the contractor must add in support equipment such as water tanker, vacuum truck, touch-up jackhammer work, traffic control, etc...and profit margin.

### CONCLUSION

With the vast bridge rehab program that lay ahead not only in the USA but throughout the world, not to mention the multi-story parking garages, hydro-demolition has proved to be not only expedient but cost effective. Unlike the conventional jackhammer method, the use of hydro -demolition is not only quieter, but eliminates pavement micro cracks, will not debond rebars from sound concrete, or damage rebars and will leave a sound clean surface ready for overlay. Hydro -demolition is fast overcoming the famous 3R's of new technologies and concepts -resistance, resentment and revenge to something new.(13) Because of the need and the ability to satisfy this need hydro-demolition is becoming the acceptable answer to the repair program. Not only, does hydro-demolition repair I, bridges and parking garages but it stretches the taxpayers dollar through reduced repair cost while simultaneously yielding profits to the contractor. Within the next two years hydro-demolition will become the "state of the art" and be referred to as the conventional method.

### ACKNOWLEDGEMENTS

A special thanks is to be given to Mr. Gary Ottman and Mr. Jim Hughes of Hydro Technology Inc., Jeffersonville, Indiana for providing the production charts documented by the Indiana Highway Department.

Thanks to Mr. Pete Salamoun of Mid West Hydro Blasting, Inc., Chicago, Illinois for providing photo and information on the Chicago O'Hare Executive Plaza Project.

## REFERENCES

1. American Transportation Advisory Council ATAC III Report, Wash., D.C., April 1986, pp. 3 to 12.
2. Better Roads Magazine, "Exclusive Bridge Inventory Update", Nov. 1986, pp. 42.
3. Fitzpatrick, M.W.; Law, D.A.; Dixon, W.C., "The Deterioration of New York State Highway Structures" Special Report 70 NYS Eng. Research and Development Bureau, Dec. 1980, pp. 2.
4. Atlas Copco Video Tape "Conjet" Copyright Feb. 1986.
5. American Transportation Advisory Council ATAC III Report, Wash., D.C., April 1986, pp. 1.
6. Fitzpatrick, M.W.; Law, D.A.; Dixon, W.C., "The Deterioration of New York State Highway Structures" Special Report 70 NYS Eng. Research and Development Bureau, Dec. 1980, pp. 3 to 16.
10. World '86 of Concrete; Concrete Bridge Repair Seminar 19-34; "Waterblasting Robot Helps Complete Bridge Repair 14 Months Early", Feb. 16-20, 1986, pp. 78 to 79.
11. Hoffman, M.; State Resident Project Engineer, Indiana Highway Department, Miami County, Indiana, Documentation Sept. 1986.
12. Logman, J.; State Resident Project Engineer, Indiana Highway Department, Switzerland County, Indiana, Documentation Oct. 1986.
13. Hegarty, C.; "Managing the Challenges of Change", C.J. Hegarty & Co., Novato, Ca., Copyright 1980, pp. 2.

# ABRASIVE-WATERJET AND WATERJET TECHNIQUES FOR DECONTAMINATING AND DECOMMISSIONING NUCLEAR FACILITIES

D. C. Echert, M. Hashish, and M. Marvin  
Flow Research Company  
Kent, Washington

## ABSTRACT

A deep kerf tool was designed to cut through thick, reinforced, concrete structures to facilitate their decommissioning. It employs the abrasive-waterjet (AWJ) cutting technology. The basis of the system is a rotary nozzle that makes a 25 mm wide slot in the concrete. The tool is inserted into the slot as the concrete is removed. In this program, concrete as thick as 1.5 meters was cut through from one side. The cutting rate of the tool ranges from 0.2 to 0.6 square meters per hour.

The tool employs a computer-controlled traverse mechanism with a simple device to detect obstacles such as uncut reinforcing bars or hard aggregate. An electronic sensor system to identify, in real-time, when rebar is being cut, was developed and tested with good results.

A cleaner/scarifier, a tool for decontamination was also designed and tested to remove the surface layers of contaminated concrete and to decontaminate metal surfaces. It uses ultra-high pressure water jets mounted on a rotating arm to remove or clean the target surface.

Concrete can be scarified to a depth of 7mm at a rate of 11 square meters per hour. Concrete and metal surfaces can be cleaned of paint and corrosion, at a rate of 33 square meter per hour. Spoils recovery with a shroud/vacuum system is over 99% complete, for both tools.

## INTRODUCTION

At the end of their useful lives, nuclear support facilities and reprocessing plants require decommissioning. This involves the orderly disposition of a nuclear facility, taking into account the environment, waste management and safety. The procedure can range from minimum removal of radioactive material to the complete disassembly of a facility and its unconditional release for other uses (1).

A major portion of most decommissioning jobs is the decontamination and removal of concrete. In many facilities, large, thick sections of activated reinforced concrete need to be removed along with contaminated surfaces. To reduce the volume of waste that must be placed in controlled storage, it is desirable to separate the contaminated portion for isolation, while allowing the remainder of the structure to be demolished by conventional techniques.

Concrete decontamination and demolition require special care during decommissioning activities. Precautions must be taken to prevent the release of radioactive particles when activated concrete sections are removed. Sometimes the radiation level is too high to allow Personnel access to the area to be decontaminated. In such cases, the equipment must be operated remotely.

Concrete surfaces are also difficult to decontaminate because concrete is porous and often contains numerous cracks that hold the contaminants. In addition to the problem of radiation, nuclear structures typically contain a large volume of concrete with reinforcing bars. Basemats may be 8 meters thick, and biological shields up to 3 meters thick. Conventional concrete removal methods cannot efficiently remove these structures while containing contaminants from release into the environment (2).

Another facet of decommissioning a nuclear facility is the decontamination of metal parts. The surfaces of such metal parts may have been painted to contain smearable contamination, or coated as a result of accidental releases. Efficient techniques are needed to remove surface contamination, reduce personnel exposure and enable less restrictive proposal requirements.

This report describes a research and development program sponsored by the U.S. Department of Energy. In this program, two systems were designed, built and tested for use by the nuclear industry: a Deep Kerf tool and a cleaner/scarifier. The deep kerf tool will cut through thick concrete structures to facilitate their decommissioning. It is based on the abrasive waterjet (AWJ) cutting technology. The cleaner/scarifier is a tool for decontamination. It uses ultrahigh-pressure waterjets to remove the surface layers of contaminated concrete and to decontaminate metal surfaces. Both systems are equipped with a shroud and vacuum system to contain and recover the cutting and cleaning spoils for proper disposal.

## BACKGROUND

### Facilities to be Decommissioned

Approximately 500 contaminated facilities or sites have been identified for decommissioning and decontamination in the U.S.A. The contaminated locations include reactor buildings, laboratories, fuel reprocessing plants, trenches and burial grounds (3).

The West Valley Demonstration Project is being conducted under the sponsorship of the U.S. Department of Energy. The purpose of this project is to decommission a nuclear fuel reprocessing facility. A significant portion of the project will focus on decontamination of concrete buildings with cell walls up to 1.5 meters thick. Because some cells are highly radioactive, special techniques and equipment will be required to collect and remove the contaminated materials safely. The project will demonstrate almost every aspect of facility decommissioning, including planning, decontamination, demolition and the safe handling, packaging and disposal of high- and low-level nuclear waste. The information developed during this project will help in the planning and execution of future decommissioning projects (4).

Commercial nuclear power plant decommissioning will require a far greater effort than any job attempted to date. As noted by Williams (5), a typical pressurized-water reactor plant contains approximately 130,000 cubic meters of concrete, while the largest power plant dismantled to date (Elk River) had approximately 3600 cubic meters of concrete.

The activated and contaminated structures and surfaces must be removed using techniques that will not breach containment and release contamination into the air. Existing demolition equipment is too slow and cumbersome to perform such work efficiently; new techniques are needed (5).

#### Decontamination and Decommissioning Equipment Requirements

There are certain unique requirements for concrete cutting and surface removal techniques in a contaminated environment (6). The ideal equipment characteristics for performing this work include:

1. Total containment of the cuttings, with
  - no release of airborne contamination, and
  - no recontamination due to the cutting operation.
2. Generate no additional waste in the removal process.
3. Remove only the contaminated surface, leaving radiation-free concrete.
4. Cut concrete and reinforcing bars simultaneously.
5. Perform all cuts on all surfaces (ceilings, walls, floors, contoured surfaces, etc.) without tool changes.
6. Easily adapt to remote operation and automation, and for use in confined locations (7).
7. Generate no shock, vibration or excessive noise while operating.
8. Easy to operate by personnel in protective clothing.
9. Easy to repair.
10. Economically feasible.

A review of conventional concrete demolition and concrete surface removal equipment is found elsewhere (6-10). Conventional demolition and surface removal equipment does not meet many of the ideal features listed.

A study (11) on the use of conventional AWJ techniques for the dismantling of thick concrete structures by cutting out prism-shaped blocks, 0.6 meters on a side, showed that such an approach is possible but slow to dismantle thick concrete structures.

#### Abrasive-Waterjet Cutting

Abrasive-waterjets are formed by mixing small diameter (0.25- to 0.8-mm), high velocity (up to 75 m/sec) waterjets with abrasive particles. The mixing process occurs in a specially designed mixing and accelerating chamber, as shown in Figure 1. The abrasive particles exit the acceleration section with high velocities and become capable of cutting even hardest material (12-15).

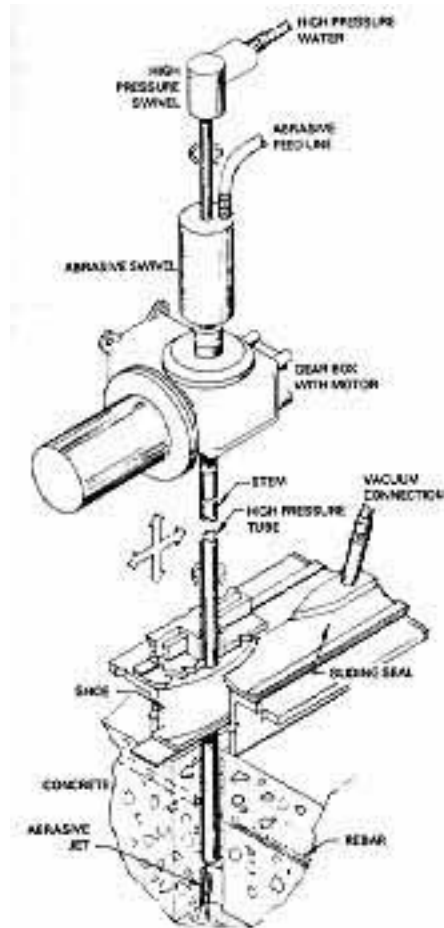
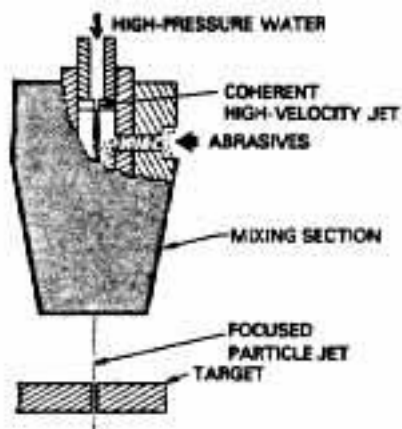


Figure 1. Abrasive-waterjet nozzle concept. Figure 2. Abrasive waterjet deep kerf tool.

### DEEP KERF TOOL

The deep kerfing tool consists of many components that will be classified here as stem, swivel, traverse system, shroud and catcher, and disposal systems. Figure 2 shows some of these components.

#### Nozzle Stem

There are many concepts for a deep kerfing nozzle stem (6,16,17). Because of its versatility, ease of manufacture, and ease of application, the concept of a single angled jet in a circular tube was chosen as the basis for the deep kerf tool. It was also selected because it is the most simple configuration to produce a uniform depth slot over the entire length of traverse. Figure 3 shows a cross sectional of view of the abrasive jet stem and nozzle. Abrasives flow to the nozzle through the annulus between the high pressure conduit and the outer stem. The waterjet nozzle is machined such that the jet exits at the same angle at which the mixing tube is placed. The life expectancy for a mixing tube depends on a number of factors such as water jet pressure and diameter and abrasive flow rate. On average, the mixing tubes used during testing lasted about one hour before being changed. Increased mixing tube life is an area requiring further development.

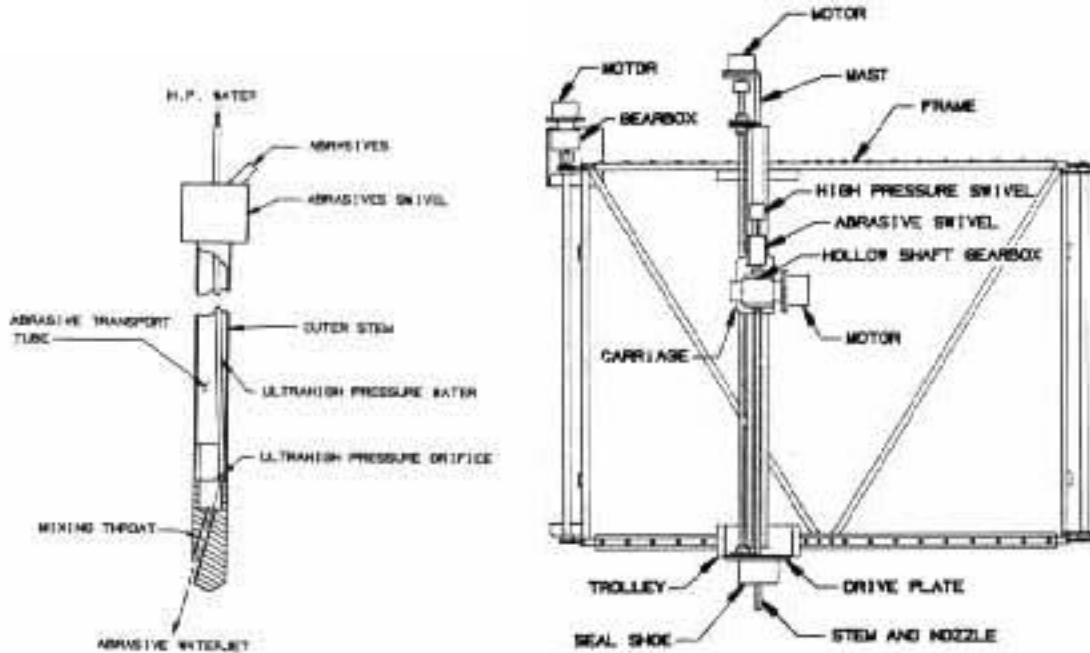


Figure 3. Components of rotating nozzle. Figure 4. Deep kerf traverse mechanism

Theoretically, the stem and nozzle assembly could be any length desired; however, it is limited by stiffness and strength. The outer stem for the deep kerf tool was 22 mm in diameter which was found suitable for depths up to 1.5 meters. For kerf depths exceeding 1.5 meters a larger diameter stem would have to be used.

#### Abrasive and High Pressure Swivels

High pressure swivels are relatively well developed and there are a number of acceptable products for use in this application. The high pressure swivel used on the deep kerfing tool has a speed range of 0-1500 rpm at 380 MPa. Seal and bearing life varies with operating speed and pressure; however, at the relatively low rotational speeds used for the deep kerf tool (0-100 rpm), seal and bearing life should be several hundred hours.

An abrasive swivel was developed in this project to allow the feed of abrasives from a stationary hopper to the rotating stem. In this swivel, the abrasives are introduced into the annular area between the high pressure tube and the outer stem through an angled port. At the upper end of the swivel is a seal and bearing allowing relative motion between the high pressure tube and the housing. At the lower end of the swivel there is another seal and bearing which allows relative motion between the outer stem and housing.

It is estimated that during the test program there were twenty hours of rotary running time on the abrasive swivel and when disassembled there was little detectable wear on the seals.

### Traverse Mechanism and Obstacle Detection

Figure 4 shows the deep kerf traverse mechanism designed and manufactured for this project. The mechanism provides three axes of motion to the stem and nozzle assembly.

The range of traverse motion for this mechanism is 1.5 meters and maximum traverse speed is .5 meters/ minute. Depth motion advances the stem and nozzle into the kerf. The range of depth for this mechanism is 1.5 meters and the maximum speed is 1.5 meters/ minute. The third axis of motion is stem rotation. The mechanism is capable of rotating the stem and nozzle through a range of 0-60 rpm.

Each axis is powered by a stepping motor which facilitates the use of a simple open loop control system when the system is under computer control. The stem and nozzle are connected to the drive plate on the trolley, Figure 4, through a spring centered bushing. If the stem encounters an obstacle during operation the side load pushes the bushing off center and proximity switches positioned adjacent to the bushing detect that an obstacle has been encountered. The control circuit is wired such that the traverse mechanism will not move in the direction in which an obstacle has been detected but rather a different routine will be followed to remove the obstacle which could be a rebar or an aggregate.



Figure 5. View of stem in concrete cut

### Shroud and Catcher

In order to catch greater than 90% of the water and cuttings generated by deep kerf cutting there must be no path through which the jet back-splash can escape. The

shroud and catching system designed for deep kerfing relies on sealing the cutting area or slot in its entirety. Figure 5 is a picture of the deep kerf catcher. The catcher frame is sealed to the concrete with neoprene rubber lip seals which run the length of the frame. Also running the length of the catcher is a pair of seals which can be parted to create an opening in the top of the frame. A wedge shaped seal shoe fastened to the traverse mechanism parts the seals as the stem is traversed along the length of the deep kerf slot and maintains closure of the catcher cavity. The stem is free to move up and down through the seal shoe for cutting at various depths.

Placing vacuum ports at the top and ends of the kerf was attempted for spoils removal. This relies on the jet splash-back to transport the spoils to the top and ends of the kerf to where the air velocity is high enough to carry the material away. When the kerf depth exceeded about 200-250mm it would fill with water and abrasives greatly reducing the cutting rate of the tool.

Two suction tubes were built which could be slipped through the seals of the catcher to the bottom of the kerf and these kept the slot free from water and debris. When the stem approached one end of the slot the suction tool at that end would be turned off and removed allowing the stem and nozzle to cut to the end of the slot. The shroud and catcher system collected in excess of 99% of the spoils produced during both cleaning and light scarifying.

### Spoils Collection

Figure 6 is a diagram of the spoils collection system developed for this project. Water air and solids from the shroud and catcher system enter the primary drum through a cyclone baffle cover. Most of the solids settle to the bottom of the drum leaving water and air to exit through the other port in the lid. This mixture enters the secondary drum through cyclone baffle causing the water to separate from the air. In the bottom of the second drum is a sump pump with a float switch to maintain the water level below the air outlet. The sump pump discharges through a check valve, into a tank, where the remaining solids can settle out over a period of time. The outlet of the second drum has an automatic shutoff float valve to Prevent damage to the vacuum system should the sump pump fail to operate.

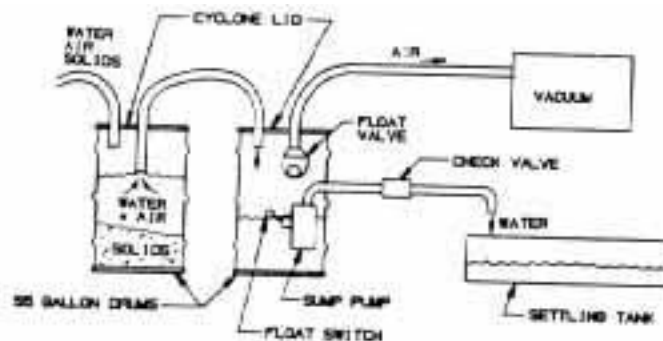


Figure 6. Spoils collection system

## EXPERIMENTAL RESULTS

### Linear Cutting Tests

Parametric linear cutting tests were performed to determine the effect of a number of variables including:

- Abrasive flow rate
- Traverse rate
- Standoff distance
- Mixing tube diameter
- Jet pressure
- Abrasive size
- Abrasive type

The aim of the linear cutting tests was to determine the optimum operating parameters to maximize the volume removal rate of material in the kerf. It was found that most of the material removed from the kerf is due to direct cutting action of the abrasive jet and little material is removed by breakage between adjacent cuts.

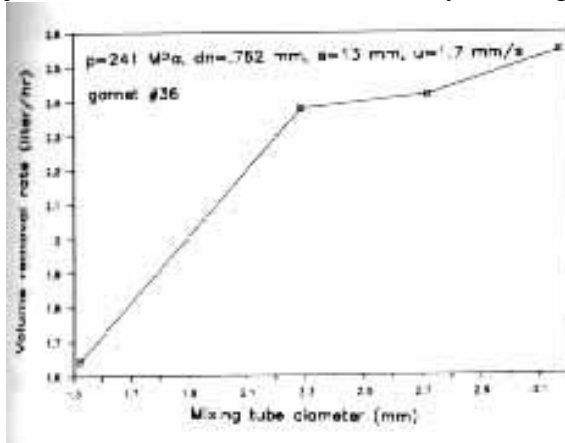


Figure 7. Effect of Mixing tube diameter.

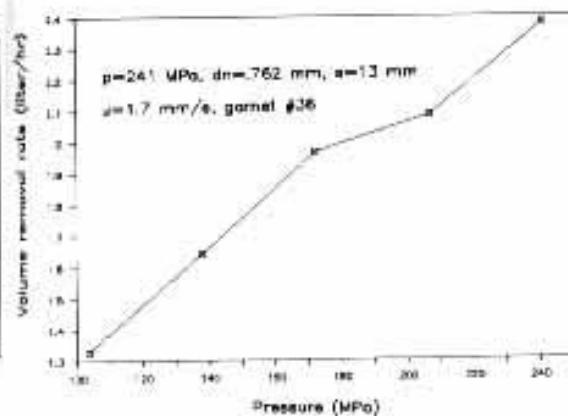


Figure 8. Effect of waterjet pressure.

The effect of mixing tube diameter on volume removal rate is shown in Figure 7. Obviously, the trend shown would reverse if the mixing tube diameter became large enough; however, there are practical limits to the size of mixing tube which can be fit into a deep kerfing tool that is, itself, limited in size.

Figure 8 shows the effect of cutting jet pressure on volume removal rate. As one would expect increasing waterjet pressure increases the volume removal rate of material.

As seen in Figure 9 the size of abrasive particles used has a pronounced effect of the rate of volume removal. As particle size increases it becomes more difficult to transport the abrasives down a compact stem and nozzle assembly and in fact 36 mesh garnet sand was found to be the largest size that could be reliably fed through the kerfing tool.

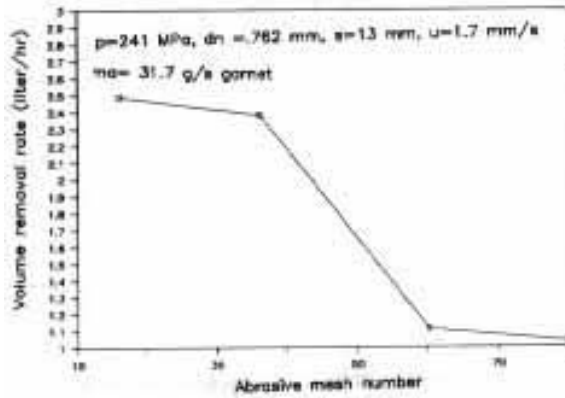


Figure 9. Effect of abrasive size.

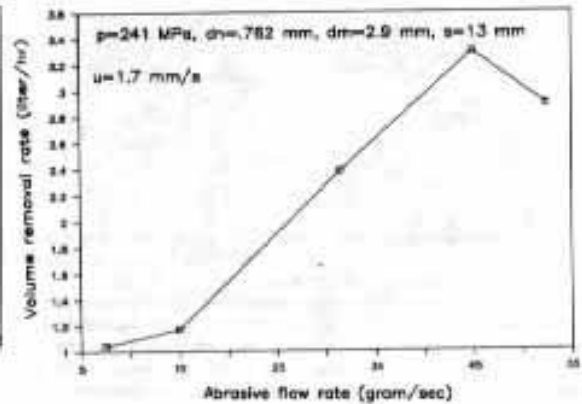


Figure 10. Effect of abrasive flow rate.

Figure 10 shows volume removal rate increasing from abrasive flow rates from 7.5 to 45 grams per second but at 53 grams per second the cutting rate begins to fall off.

The effect of traverse speed is shown in Figure 11. The rate of volume removal increases with traverse rate with a maximum beyond the range of speeds tested. (It was found in a separate later investigation that the kerf area generation rate in concrete was maximized at a traverse speed of approximately 85mm/sec.)

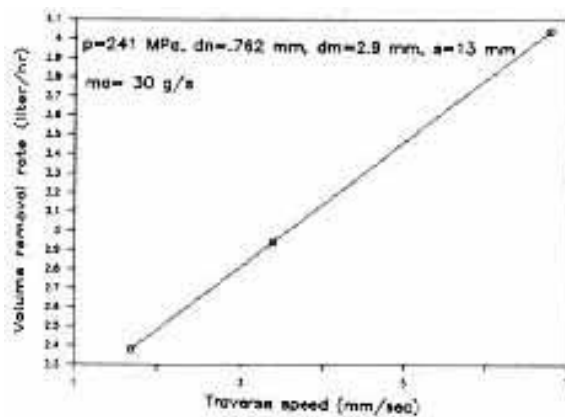


Figure 11. Effect of traverse rate.

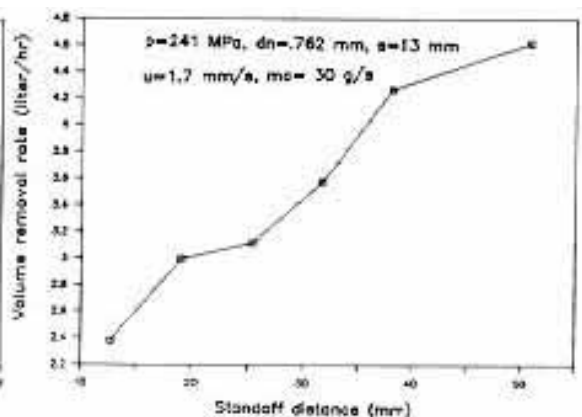


Figure 12. Effect of standoff distance.

Figure 12 shows the effect of varying standoff distance on volume removal rate. The plot shows removal rate to be increasing with increasing standoff distance. This is advantageous when applied to the process of deep kerfing.

The effect of abrasive type was tested using identical conditions. Table 1 compares the volume removal rates for the different materials. The potential advantage to using steel as the abrasive material is that it can be more easily recycled than garnet sand.

Table 1. Abrasive Material Comparison

<u>Abrasive Material</u>	<u>Removal Rate (liter/hr)</u>
Garnet sand	2.42
Silica sand	0.59
Steel shot	2.27
Steel grit	2.22

### Deep Kerf Testing

The emphasis of the deep kerf test program was on creating nozzle motion algorithms that would produce an acceptable kerf through the range of depths specified. Much effort was expended on coping with obstacles, either rebar or pieces of hard aggregate, in the kerf. Also much effort was expended on the removal of spoils from the bottom of the kerf. In all some twenty eight tests were performed producing an estimated 3 square meters of kerf area.

The result of the testing produced an optimum sequence of nozzle motions as follows to produce a deep kerf:

- The nozzle is rotated at 50 rpm and traversed the length of the slot to be cut.
- At the end of each pass nozzle rotation is stopped and oscillated 180 degrees from two to four times to slightly over-cut the slot end. This ensures that the ends of the slot do not slope inward.
- The stem is then indexed downward slightly less than the average depth of cut for the previous pass.
- Every fourth pass the jet is raised up to the height where the first pass of the sequence was made. The nozzle is traversed back and forth to remove the projections from the walls of the slot.
- The nozzle is then lowered to the next depth index and the process is repeated.

The following sequence was developed to remove a detected obstacle:

- The stem is backed up 12mm to free it from the obstruction.
- The stem is raised up 150mm.
- The jet is oriented to one side of the kerf and traversed for about 40mm.
- The jet is oriented at the other side of the kerf and traversed back.
- The stem is returned to the position where the obstacle was encountered.

The deep kerfing system generated kerf face at a rate of 0.1 to 0.5 square meters per hour depending on concrete strength, hardness of aggregate, and density of rebar.

### Abrasive Recycling

It would be desirable to recycle abrasive material to limit the amount of abrasives used and to limit the amount of radioactively-contaminated waste that is produced. The abrasive most commonly used for AWJ cutting, garnet, is nearly totally pulverized during use, thereby rendering it unsuitable for recycling. Steel grit was investigated as an

alternative abrasive material. The magnetic nature of the steel provides a way of separating it from the concrete spoils.

The steel grit, being much more dense than garnet, was not moved to the slot ends by the splashing action of the jet to a satisfactory degree. The suction had to be moved along with closely behind the nozzle to adequately remove grit from the slot. This would have to be accounted for if steel grit were used. It was found feasible to use steel grit as the abrasive media for deep kerf cutting with some modification of the cutting system.

The reuse of steel grit showed that 93% of the unused grit was retained by the 20 mesh screen on successive cycles 78% and 71% were retained by the 20 mesh screen respectively. This represents about a 10% loss of particles of a particular size for each time the material is used. This coupled with a reasonable estimate of 90% recovery from the spoils for a production type system yields an overall recovery of 80% of the abrasive material per use.

Linear test cuts made with unused, once used, and twice used showed a change in cutting performance. The test cut made using once used grit was 13% deeper than the test cut made using unused grit probably because particle size became closer to optimum value. The test cut made using twice used grit was 4% shallower than for unused grit. A test cut was made using 50 grit (smaller particles) abrasives and the depth of cut was 17% greater than for the 25 grit.

This shows that the particle size used for this test was larger than the optimum for cutting concrete. For recycling it is desirable to use grit that is larger than optimum to increase the number of times it can be reused such that optimal performance is obtained during the recycling process instead of only at the beginning.

The results of the laboratory testing were incorporated into an economic model to evaluate the utility and cost-effectiveness of steel grit abrasive recycling for the deep kerf tool. The model includes provision for various costs including: capital equipment, consumables, maintenance, labor, and waste disposal.

The results are sensitive to the cost of solid waste disposal. For example, a disposal cost of over \$600/cubic meter will make recycling of steel grit abrasive a more economic alternative.

#### Forecasting of Rebar Presence

A more efficient approach than obstacle detection would be to sense the presence of the rebar during the normal cutting operation and then immediately adjust the cutting parameters to address the rebar. What is needed is a method of detecting the rebar during cutting. This was one objective of this program.

Several possible means of detecting the presence of or contact with the rebar were considered.

The selected method is based on an observation that there is a difference in noise levels when the impinging jet was cutting concrete as opposed to striking rebar. Simple monitoring of the sounds of cutting should provide the sought after signal.

The tests employed a high frequency response microphone placed 0.3 meter away from the top of the concrete and 75 to 150mm away from the rotating axis of the nozzle. Additionally, a signal was generated by a piezo-electric accelerometer cemented to the concrete. The results of the experiments can be summarized as follows:

- Rebar can be detected when the nozzle head is rotating by noting changes in the acoustic spectrum of the accelerometer signal.
- The microphone provides no useful signal.
- Rebar cannot be detected when cutting narrow slots. The rebar is too well supported for it “ring” with its characteristic signature.
- There is a weak dependence of stand off distance and the acoustic spectrum. It is uncertain because only frequencies in the range of 20 KHz were studied. This was simply due to the accelerometer’s sensitivity band.
- Simple filtering (low-pass, high pass and band pass) is all that is needed to detect the rebar.

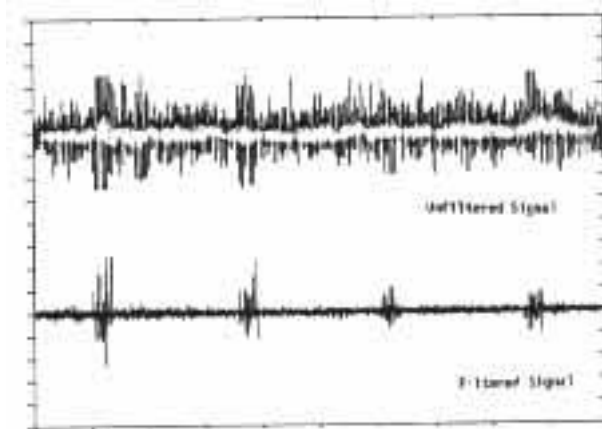


Figure 13. Rebar detection by noise signal filtering.

Figure 13 shows an example of unfiltered and filtered signals from which the existence of rebar is evident.

## CLEANER/SCARIFIER

### Equipment Design

The cleaner/scarifier removes material from a surface by rotating high-pressure waterjets at a radius, creating a circular pattern, and traversing the rotating mechanism across the surface to be cleaned or scarified. A photograph of the cleaner/scarifier is shown in Figure 14.

High-pressure water is fed to a central tube through a high-pressure swivel. The tube carries water through bearing supports to a manifold, which distributes the water to

four arms leading to nozzle holders. Each nozzle holder has two nozzle ports that can accept nozzles of various sizes. Eight jets can be installed in the unit and rotated up to 1000 rpm.

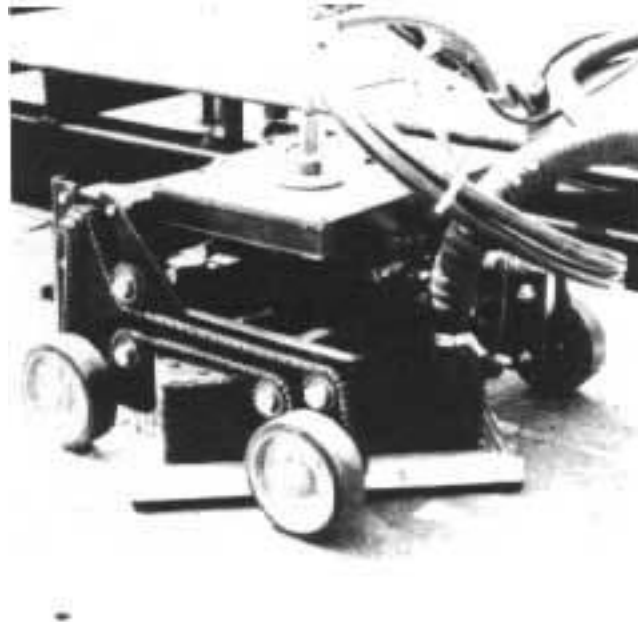


Figure 14. Waterjet cleaner/scarifier device.

The manifold and nozzles are encased in a steel box with a brush sealing system around its perimeter. There is a vacuum port and suction tube located in one corner of the box for connection to the spoils collection system described earlier.

#### Parametric Testing

A series of parametric tests was conducted to determine the optimal configuration and settings for the cleaner/scarifier. The parameters varied included rotational speed, traverse speed, number of jets, size of jets, water pressure and target material.

The tool had four nozzle heads, each equipped with two nozzles. Two of the nozzle heads were mounted on a diameter of 350 mm, and the other two were mounted on a diameter of 25 mm. The outer jets were 0.010 inch in diameter, and the inner were 0.008 inch in diameter. It was found that the parameters described below produced light concrete scarification (approximately 3 mm of surface removal) and provided good cleaning of rust and paint from metal surfaces.

Water Pressure:	241 MPa
Water Flow Rate:	9.7 liter/min
Jet Power:	38 kW
Rotational Speed:	1000 rpm
Traverse Speed:	20 mm/s
Production Rate:	26 m <sup>2</sup> /hr

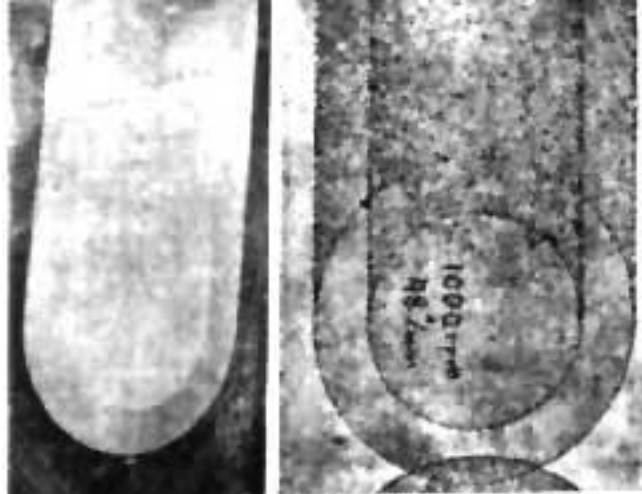


Figure 15. Cleaned surfaces with cleaner/scarifier.

Figures 15a and 15b show examples of a concrete surface and a rusted steel surface after operation of the tool. Greater depths in concrete surface removal were accomplished by increasing the water flow rate, decreasing the rotational and traverse speeds and reducing the number of jets. Concrete was scarified to an average depth of 7 mm under the following conditions:

Water Pressure:	241 MPa
Jet Diameter:	0.356 mm
Water Flow Rate:	11.5 liter/min
Jet Power:	45.5 kW
Rotational Speed:	50 rpm
Traverse Speed:	8.5 mm/s
Production Rate:	11 m <sup>2</sup> /hr



Figure 16. Light scarified concrete surface to 7 mm. Depth.

Figure 16 shows an example of this depth of surface removal on very hard concrete (69 MPa compressive strength). The cleaner/scarifier vacuum system did not provide enough air velocity to remove the pebbles. Even after being freed of the

surrounding grout, they tended to remain in place, protecting the underlying concrete from attack. After slow passage of the tool, the concrete surface was covered with loose, well cleaned pebbles. The cleaner/scarifier was used on vertical surfaces to test the ability of the shroud to contain and remove the water and spoils. On both steel and concrete, the tool left the surfaces nearly dry with no spray.

#### FIELD DEMONSTRATION AT WEST VALLEY NUCLEAR FACILITY

The Deep Kerf system and the cleaner/scarifier were taken to the West Valley Nuclear Facility in West Valley, New York, to demonstrate their capabilities. The test specimen for the deep kerfing was a concrete slab that measured approximately 1.5 x 1.5 x 0.3 meters. The slab was set upright on one edge with the Deep Kerf tool mounted above it. The test cutting, was done vertically, into the block. A kerf measuring 1.2 meters deep and 1 meter long was cut into the block. This kerf was made at an average rate of 0.46 square meters per hour. The cleaner/scarifier was demonstrated on a rusty steel surface, a painted steel surface and a painted concrete slab. Additionally, two stripes of duct tape were placed on the steel surface for removal. The majority of the tests were conducted under the following conditions:

Water Pressure:	241 Mpa
Flow Rate:	9.8 liter/min
Jet Hydraulic Horse Power:	39 kW
Rotational Speed:	1000 rpm
Number of Jets:	8, 2 jets per arm
Translational Speed:	20 mm/s
Production Rate:	26 m <sup>2</sup> /hr

Under the above conditions, the steel surface was cleaned of rust and paint, and the duct tape was removed. The concrete was cleaned of paint, and the concrete surface was removed to a depth of 3 mm in the center of the swath to 4.7 mm at the outer edge of the swath.

#### CONCLUSIONS

- Deep kerfing with abrasive-waterjets is technically, economically and environmentally feasible for many nuclear decommissioning applications. Kerfing rates up to 0.6 m<sup>2</sup>/hr were achieved and can be improved upon by further optimization.
- The recycling of abrasives is technically feasible for steel grit or shot. However, the economic feasibility depends upon the cost of disposal. An economic evaluation showed that recycling will be feasible if the cost of disposal is greater than \$600/m<sup>3</sup>.
- Rebar detection can be accomplished with either an obstacle detection arrangement or through forecasting based on noise level changes. Both methods were demonstrated, and the latter proved more efficient to employ.
- The cleaning of metal surfaces and shallow scarification of concrete were demonstrated with a lawn-mower-like waterjet system. Rates of cleaning of around 33 m<sup>2</sup>/hr were achieved, while scarification of concrete to 7 mm depths can be accomplished at rates of 11 m<sup>2</sup>/hr.

- The containment and catching efficiencies of the deep kerf tool and cleaner/ scarifier are greater than 99%. However, monitoring of the surrounding air needs to be conducted.
- Further work is needed on hardware improvement regarding:
  - Wear of mixing nozzles
  - Reduced stem diameter versus stiffness
  - Quick change of mixing nozzles
  - Development of high-pressure fan jets.

## ACKNOWLEDGMENTS

The authors acknowledge the support of the DOE/SBIR program under Contract No. DE-AC03-84ER80192. Thanks are due to Dr. Henry Walter, DOE, for monitoring the Project and to Mr. L. Weidemann, West Valley Nuclear Services, West Valley, New York, for assisting in the field demonstration tests.

## REFERENCES

1. Maestas, E. and O. Ilari "An Overview of Decommissioning Policy, Standards and Practices in NEA Member Countries," Proceedings of the International Decommissioning Symposium, Seattle, WA., 1982 p. 11-3.
2. LaGuardia, T. S. "Concrete Decontamination and Demolition Methods," in Proceedings of the Concrete Decontamination Workshop, A. J. Currie, ed., PNL-SA-8855, U.S. Department of Energy, prepared by Pacific Northwest Laboratory, Richland, WA, 1980 p. 2.
3. Kluk, A. F. "Management of the DOE Inventory of Excess Radioactively Contaminated Facilities," in Decontamination and Decommissioning of Nuclear Facilities, M. M. Osterhout, ed., Plenum Press, New York, NY, 1980.
4. Woods, P. G. "The West Valley Demonstration Project ... A Nuclear Success Story," West Valley Nuclear Services Company, Inc., West Valley, NY, 1984.
5. Williams, D. H. "A Utility Perspective on Needs for Technical Advances in Nuclear Decommissioning," ASME paper No. 83-JPGC-NE-17, 1983
6. Hashish, M., M. McDonald and M. Halter "Abrasive Waterjet Technique for Decommissioning Nuclear Facilities" 3<sup>rd</sup> U.S. Waterjet Symposium, Pittsburgh, PA, 1985.
7. Toto, G. and H. R. Wyle "Remote Machine Engineering Applications for Nuclear Facilities Decommissioning," ASME paper No. 83-JPGC-NE-23, 1983.
8. Nemec, J. F., and T. Mooers "Contaminated Concrete Removal Techniques for Nuclear Plant Decommissionings," ASME paper No. 83-JPGC-NE-19, 1983.
9. Manion, W. J. and T. S. LaGuardia "Decommissioning Handbook" prepared by for the U.S. Department of Energy, DOE/EV/10128-1, Section 7, November 1980.
10. Halter, J. M., R. G. Sullivan and J. L. Bevan "Surface Concrete Decontamination Equipment Developed by Pacific Northwest Laboratory" PNL-4029, U.S. Department of Energy, prepared by Pacific Northwest Laboratory, Richland, WA., 1982.
11. Arasawa, H., K. Matrumoto, S Yamaguchi, and K. Sumita "Controlled Cutting of Concrete Structure with Abrasive-Waterjet" in proceedings of 8<sup>th</sup> International Symposium on Jet Cutting Technology, Durham, England, 9-11 September, 1986.

12. Hashish, M. "Steel Cutting with Abrasive-Waterjets" 6<sup>th</sup> Int. Symposium on Jet Cutting Technology, BHRA, Guildford, England, April 1982, pp. 465-487.
13. Hashish, M., "The Application of Abrasive-Waterjets to Concrete Cutting", 8<sup>th</sup> Int. Symposium on Jet Cutting Technology, BHRA, Guildford, England, April 1982, pp. 447-464.
14. Hashish, M., "Cutting with Abrasive-Waterjets", Mechanical Engineering, March, 1984.
15. Hashish, M., et al., "Development of a Waterjet Concrete Cutting System", EPRI EL 3601, Vol. 2, Project 7860-1, Final Report, Sept, 1984.
16. Hashish, M., "Deep Kerfing Concepts with Penetrating Abrasive-Waterjet Nozzles", Proceedings of the Canadian Conference of Applied Mechanics, Edmonton, Alberta, 1987.
17. Hashish, M., "Aspects of Abrasive-Waterjet Performance Optimization", Proceedings of the 8<sup>th</sup> International Symposium on Jet Cutting Technology, BHRA, Durham, England, September, 1986. pp 297-308

## JET KERFING PARAMETERS FOR CONFINED ROCK

J. J. Kolle  
FlowDril Corporation  
Kent, Washington

### ABSTRACT

A test stand for jet kerfing under conditions simulating those in a deep well has been used to determine kerfing parameters for Wilkeson Sandstone, Indiana Limestone and Mancos Shale. The threshold pressure for kerfing the impermeable shale increased significantly at moderate overbalance pressure. The permeable limestone was not affected by overbalance pressure while the sandstone was affected only when kerfing with Kerf volumes are substantially reduced in all rock types due to the suppression of cavitation at high ambient pressure.

### INTRODUCTION

Attempts to use jets in oil field applications at depths greater than a thousand meters have been less successful than would be expected from submerged jet kerfing performance at the surface. This can be attributed to degradation of the jet at high ambient pressure and to increased rock strength due to confining stresses and overbalance pressure. These circumstances combine to increase the threshold pressure of the rock at depth and to reduce the effective dynamic jet pressure. Higher pressure jets using standard oilfield drilling equipment are impractical because of the large volume of fluid required to transport cuttings to the surface; the power requirements for such a system are unrealistically high.

A new dual conduit technique has been developed which overcomes this objection and other problems related to the safety of large volumes of high pressure fluid. This system uses a low volume high pressure inner conduit to carry jet cutting fluid. The annular space surrounding the inner conduit carries low pressure high volume mud for cuttings transport. Effective use of this system will require jet pressures high enough to kerf rock at depths from 1,500 to 5,000 meters.

A test stand has been built to observe jet kerfing in rock samples subject to the high confining stresses and mud overbalance pressures found in deep wells. This test stand has been used to observe the kerfing properties of three common sedimentary rock types. Results from these tests are presented and a model for submerged non-cavitating jet kerfing is discussed.

### KERFING TEST STAND

The kerfing test stand used to carry out these experiments is illustrated in Figure 1. This test stand was designed to allow kerfing experiments in a chamber at high confining stress and ambient pressure. A pore pressure port was provided in order to subject the samples to a high differential pressure. The pressure controls allow simulation of conditions in a well up to 5000 m deep.

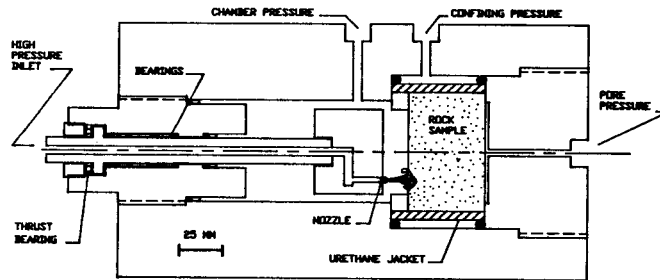


Figure 1 Kerf test stand pressure vessel.

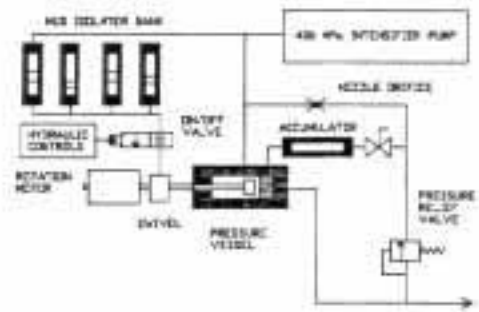


Figure 2 Kerf Test Stand Hydraulic Pressure Control System

### Hydraulic Pressure Controls

The surface of the sample is exposed to an ambient pressure of up to 133 MPa (20,000 psi) in the main chamber of the pressure vessel. A pore pressure port can be either plugged or left open for a drained or undrained test when the port is left open there is a pressure gradient from the chamber ambient pressure to zero pore pressure in the permeable rock samples. This is analogous to the overbalance condition which exists when a well is drilled with weighted mud (1).

A continuous flow of fluid from the main pump is used to maintain pressure within this chamber through a relief valve. A schematic of the hydraulic pressure control system for this stand is given in Figure 2. During a test the high pressure kerfing jet is discharged into the pressure vessel. The flow rate from the kerfing jet is much lower than the pressure relief flow rate so that chamber pressure does not change appreciably. Both mud and water were used as fluids in these tests.

Confining stresses of up to 133 MPa (20,000 psi) are provided by pressure in an annulus around the jacketed sample. During a test this pressure is maintained by an accumulator.

A high pressure jet nozzle is mounted on a rotating head inside the pressure vessel. Leach and Walker 13 degree inlet nozzles were used for these tests. High pressure mud was supplied from a series of isolators pressurized by a 400 MPa intensifier pump. The jet can be turned on and off with a high speed servo valve. Tests were accomplished by setting rotary speed and activating the servo valve with a timer.

Pressure transducers were used to monitor jet pressure and chamber pressure during a test. A tachometer records the rotary speed. Confining stress was obtained from a hydraulic gauge.

### Instrumentation

Data were recorded on two digital oscilloscopes. When the jet is activated the ambient chamber pressure increases slightly due to increased flow rate. There is also a short 10 millisecond period of high frequency ringing in the high pressure line. Also the pressure causes an increase in friction in the swivel which causes the rotary speed a to slow.

### RESULTS OF LABORATORY TESTS

Kerfing tests were carried out on three different rock types: Wilkeson Sandstone, Indiana Limestone and Mancos Shale. The shale samples were sealed immediately after coring and kept in plastic bags until the test to prevent dehydration. Cylindrical rock samples for the tests are 76 m in diameter and 50 mm thick. A polyurethane jacket is cast around each sample to provide a seal for confinement stress pressure.

Table 1 Properties of rock samples

Rock Type	Compressive Strength MPa	Threshold Pressure MPa	Ref
Wilkeson Sandstone	100	48	(2)
Indiana Limestone	55	55	(2)
Mancos Shale	60	NA	(3)

### Wilkeson Sandstone

This material is a medium hard fine grained sandstone obtained locally. A total of 21 tests were carried out on this rock type. All tests were done with a dynamic jet pressure of 172 MPa which is well above the reported unconfined threshold pressure. Tests were done using water and a low solids bentonite mud with a specific gravity of 1.09. Two nozzles were mounted on the rotating head to give two traverse rates for each test.

The nozzles were 0.36 m in diameter and were mounted at a standoff distance of 2.5 mm which is roughly 7 nozzle diameters. Two tests were carried out at a higher and lower standoff distance as indicated in Figure 3. After each test the width and depth of the resulting kerf were measured in eight locations using a depth gauge and calipers. The kerf area and volume were computed by assuming that the kerf profile is elliptical. At 14 nozzle diameters no kerf was produced while the kerf area at 3.5 diameters was slightly larger than at 7 diameters.

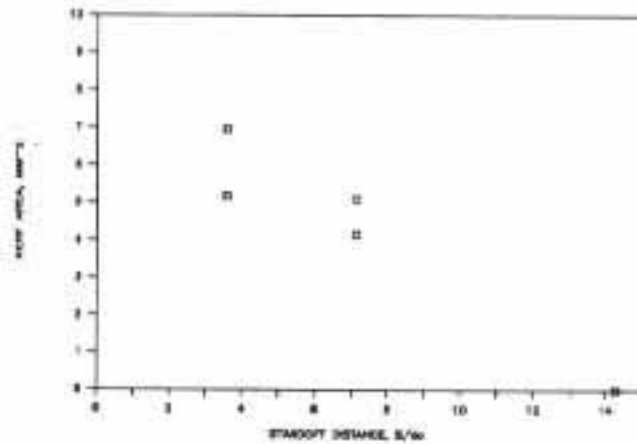


Figure 3 Kerf area versus standoff distance  
Standoff has been normalized by nozzle diameter.

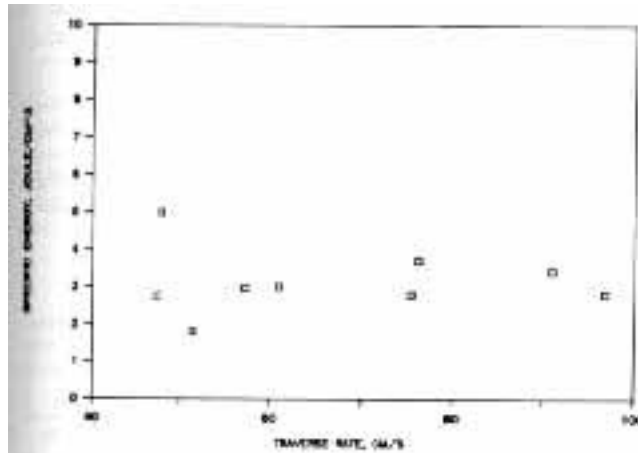


Figure 4 Specific Energy as a Function of Traverse Rate in Wilkeson Sandstone

The specific energy required to remove a fixed volume of rock was computed from the jet power and traverse rate. Figure 4 shows the specific energy as a function of traverse rate for a series of tests carried out with water at constant confining stress and overbalance pressure. These tests show that over a limited range of traverse rates the specific energy is a constant.

Overbalance had a strong effect on specific energy as shown in Figure 5. This is similar to the behavior reported by several authors during drilling tests at different overbalance conditions (4), (5), (6). Water overbalance has no apparent effect on kerfing performance but mud overbalance causes a large increase in the specific energy. It is also interesting to note that the specific energy for mud is consistently higher than for water. This plot may be compared with a similar plot of specific energy versus confining stress, Figure 6. Confining stress has no apparent effect on the specific energy.

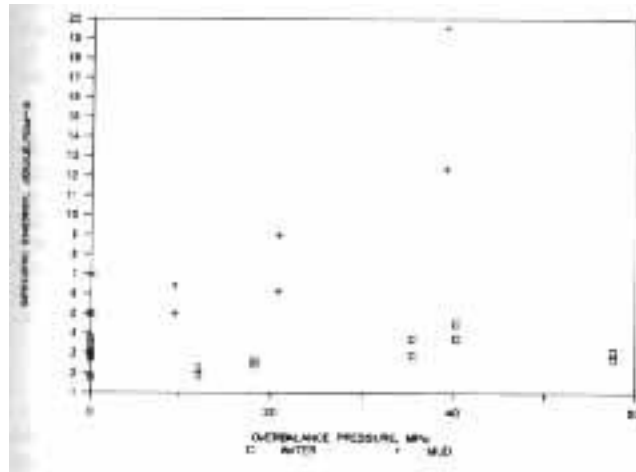


Figure 5. Specific energy as a function of overbalance pressure in Wilkeson Sandstone.

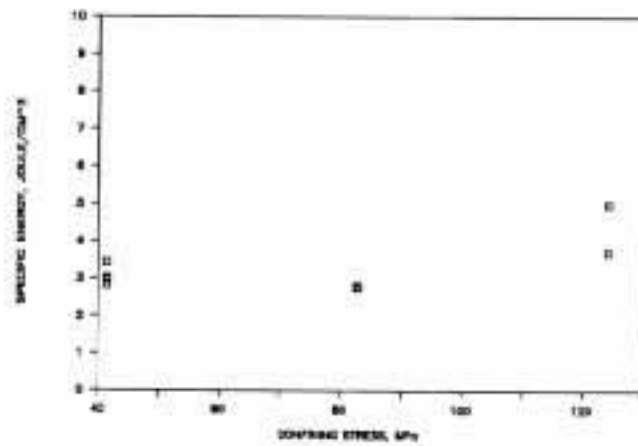


Figure 6 Specific Energy as a Function of Confining Stress in Wilkeson Sandstone

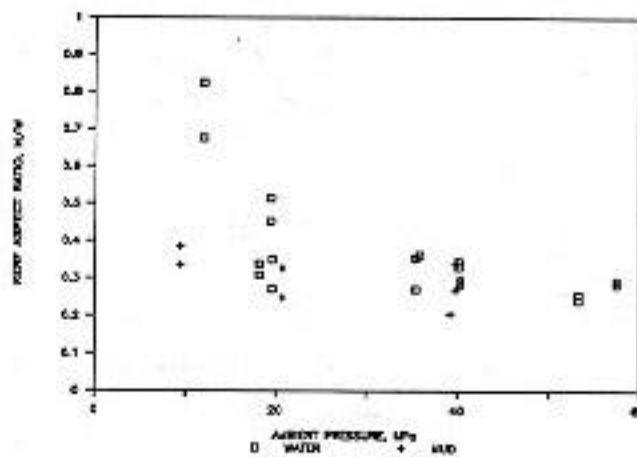


Figure 7 Kerf Aspect Ratio as a Function of Ambient Chamber Pressure

The ratio of kerf depth to width or kerf aspect ratio was averaged for each test. A plot of aspect ratio versus ambient pressure is given in Figure 7. The aspect ratio for mud was a relatively constant 0.3 for all kerfing conditions. However the aspect ratio for water increases substantially at lower ambient pressure.

Indiana Limestone

A smaller number of tests were run using Indiana Limestone. Figure 8 shows the effect of overbalance on specific energy. In this highly permeable material there was no consistent effect observed for either mud or water. The kerf aspect ratio in this material was also sensitive to ambient pressure as shown in Figure 9.

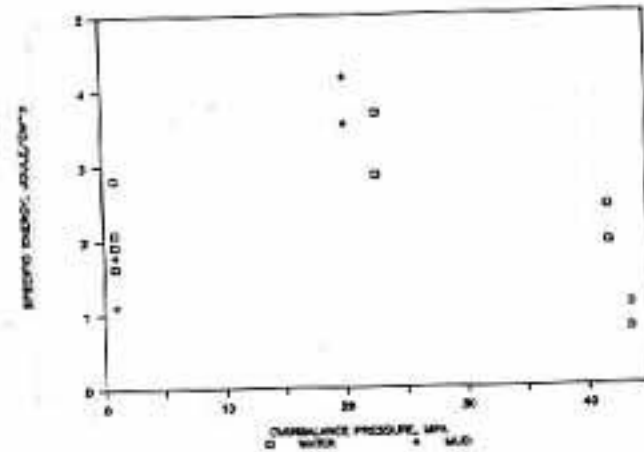


Figure 8. Specific energy as a function of underbalance pressure in Indiana Limestone.

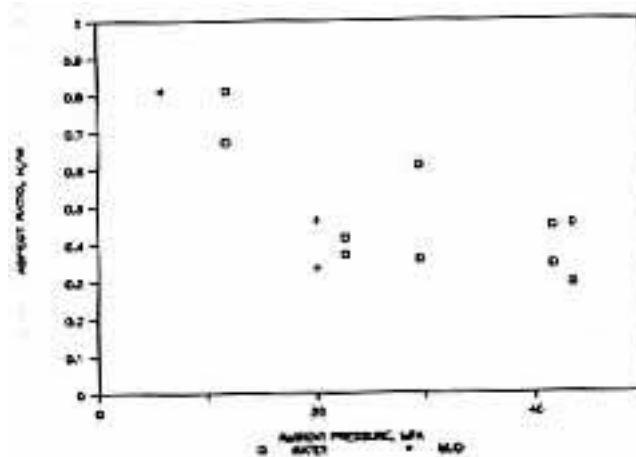


Figure 9. Aspect ratio as a function of ambient pressure in Indiana Limestone.

Mancos Shale

The final series of tests were run on Mancos Shale. This material is essentially impermeable on the time scale of these tests so that overbalance equals ambient pressure. The jets did not produce uniform kerfs in the shale. Instead the surface was spalled to form large chips and a shallow wide kerf. Because the kerfs were so wide it was not possible to use two jets as in the previous tests. A single jet 0.64 m in diameter was

used at a standoff distance of 3.8 mm. Kerf volume was measured directly by filling the kerf with fine glass bead sand and weighing.

The variation in kerf volume with overbalance is shown in Figure 10. At 173 MPa dynamic jet pressure and an overbalance pressure greater than 14 Mpa, no kerfing was observed in this material. At slightly lower overbalance pressures the kerf volume was very small. Only at zero overbalance was a large kerf observed at 172 MPa jet pressure. At a higher jet pressure 193 MPa significant kerfing was observed at an overbalance of 7 MPa.

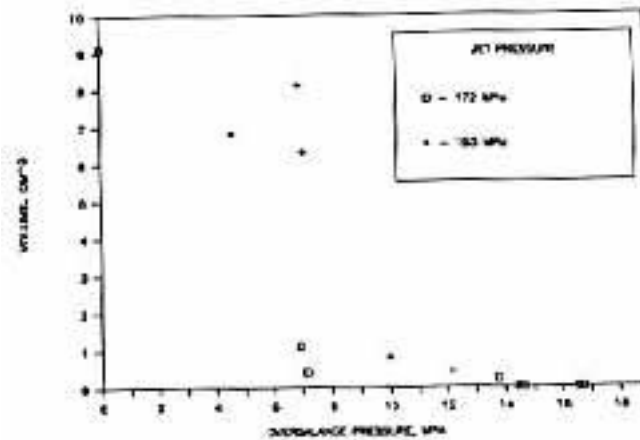


Figure 10. Kerf volume as a function of overbalance pressure in Mancos shale.

### KERFING MODEL

The observations given above may be understood in terms of a non-cavitating submerged jet operating on confined rock. Cavitation is known to significantly enhance the performance of submerged jets at high standoff distances by limiting entrainment of the surrounding fluid. When cavitation is suppressed fluid entrainment dissipates the energy of the jet by turbulent mixing. We first discuss suppression of cavitation by ambient pressure and then the theory of jet dissipation.

#### Cavitation of Submerged Jets

A submerged waterjet will cavitate when the difference between jet dynamic pressure and ambient pressure is greater than the vapor pressure. For water or mud at room temperature or above, the vapor pressure is small compared to Flowdril System pressures or ambient mud pressure in a well. The jet will therefore always cavitate in the immediate exit region of the nozzle. Submerged jets are covered with a shroud of cavitation bubbles which can extend a considerable distance from the nozzle exit and act to enhance erosion of the rock.

Cheung and Hurlburt (7) provide a theory predicting the extent of the cavitation shroud as a function of ambient pressure. Cavitation occurs when the turbulent jet entrains water at velocity higher than the gradient between ambient pressure and vapor pressure can sustain. The extent of the cavitation shroud is given by

$$x_c = \frac{u_o d_o}{4 v_e \ln(1.113 u_o / v_e)} \quad (1)$$

where:

$u_o$  is the jet exit velocity

$d_o$  is the nozzle diameter and

$v_e$  is the entrainment velocity given by the ambient pressure.

$$v_e = \sqrt{\frac{2(P_a - P_c)}{\rho}} \quad (2)$$

where:

$\rho$  is the density of the fluid In our case  $P_a$  is much greater than the cavitation pressure  $P_c$ . The jet exit velocity is

$$u_o = \sqrt{\frac{2 P_j}{\rho}} \quad (3)$$

where

$P_j$  is the differential jet pressure.

Equation (1) reduces to

$$\frac{x_c}{d_o} = \sqrt{\frac{P_j}{P_a}} \ln 0.113 \frac{P_j}{P_a} / 4 \quad (4)$$

Plots of the normalized shroud length versus ambient pressure for three jet pressures are given in Figure 11. Even at the highest pressure the cavitation shroud collapses within one nozzle diameter at ambient pressures above 1.7 Mpa. This corresponds to a depth of only about 150 meters in a water filled well.

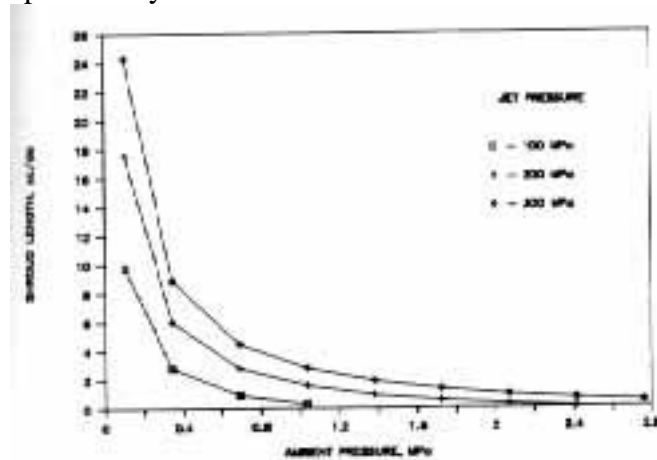


Figure 11. Cavitation shroud length as a function of ambient pressure for three dynamic pressure levels.

In general oil and gas wells are greater than 500 meters deep. As shown the ambient pressure below this depth is high enough to prevent propagation of a cavitation shroud around the jet. Jets at this depth may thus be considered to be non-cavitating

#### Dynamic Pressure and Maximum Kerf Depth

A basic assumption used here is that kerfing occurs only when the dynamic jet pressure exceeds the rock kerfing threshold pressure. A submerged non-cavitating jet decays rapidly with distance from the nozzle. The equations for velocity in the far field of a turbulent axisymmetric jet are derived by Schlichting (8) by assuming conservation of momentum.

The expression for velocity along the centerline of the jet is

$$u_m = \frac{6.57d_o u_o}{x} \quad (5)$$

This equation tell us that the jet does not begin to decay until the jet extends 6.57 nozzle diameters from the exit. Beyond this distance the jet velocity decays as 1/x. The dynamic pressure distribution in the jet can be found from

$$P_j = \frac{\rho u^2}{2} \quad (6)$$

along the middle of the jet,

$$P_{jm} = \frac{43.16P_{jo}}{(x/d_o)^2} \quad (7)$$

At less than 6.57 nozzle diameters the jet velocity may be assumed constant and equal to the exit velocity.

#### Confining and Overbalance Stress Effects

Kerfing threshold pressure is related to compressive rock strength. A general observation can be made that the threshold pressure is always equal to or less than the compressive strength. The observations made in the kerf test stand indicate that the threshold pressure required to kerf increases with mud overbalance pressure. This is consistent with a model in which threshold pressure also varies with overbalance pressure in the same way that compressive strength varies.

In a low permeability rock assume that the jet acts as an indenter on the surface so that kerfing will not begin until the mechanical load exceeds the compressive strength. If the threshold pressure in low permeability rock is linearly related to compressive strength it will vary with confining stress in the same way as the confined compressive strength.

$$P_{th} = P_{tho} + \gamma S_2 \quad (8)$$

Depending on the rock type can vary between 4 and 6 (9). . If the confining stress is significant it can easily dominate the threshold pressure.

Observations of both drilling and kerfing under downhole conditions have shown that it is not the overburden stress but the overbalance pressure between mud pressure and pore pressure that acts to provide confinement, increasing the strength and threshold pressure. During indentation by a cutter or a jet material removal occurs by shear along a wedge of material extending to the surface. The maximum principle stress in this region is roughly parallel to the surface and the minimum principle stress is perpendicular to it.

## CONCLUSIONS

Several of the observations made during the kerfing tests can be explained in terms of a simple theory of jet kerfing:

- The reduction in jet effect with standoff distance is a consequence of the turbulent dissipation of a non-cavitating submerged jet.
- Overbalance pressure acts to increase the threshold pressure for kerfing a low permeability material like Mancos Shale. This is consistent with the effect of confining stress on compressive strength.
- Mud overbalance pressure increases the specific energy required to kerf Wilkeson Sandstone, while water overbalance has no effect. This is consistent with the formation of an impermeable filter cake layer when kerfing with mud and an increase in compressive strength due to overbalance confining stress.
- Neither mud or water overbalance had an appreciable effect on kerfing a high permeability material like Indiana Limestone.

The effect of confining stress on compressive strength is relatively large implying that jet kerfing will be sensitive to overbalance pressures. Typically an oil well is drilled at an overbalance of about 10% of ambient pressure. At 5,000 meters this is an overbalance of only 5 Mpa. If there is potential for a blowout however drilling may proceed with heavily weighted muds and an overbalance of 10 MPa in a shallow well would not be unusual. If as suggested the threshold pressure increases with overbalance in the same way as compressive strength the threshold pressure would increase by 20 to 50 MPa which is a significant fraction of currently available jet pressures.

## REFERENCES

- 1 Gray G R and H C H Barley "Drilling problems related to drilling fluids " Composition and Properties of Drilling Fluids Gulf Publishing Company Houston 1986 pp 391-475
- 2 Veenhuizen S D and T A O Hanlon "Development of a System for High-Speed Drilling of Small-Diameter Roofbolt Holes " RTD Report #117 Flow Industries Kent Washington 1978
- 3 Rock List TerraTek Drilling Research Laboratory Salt Lake City Utah March 1987
- 4 Maurer W C "Bit tooth penetration under simulated borehole conditions " J Pet Tech Dec 1965, 1433-1442.
- 5 Garnier A J and N B van Lingen "Phenomenon affecting drilling at depth" Trans AIME, V 216, 1959, 232-239.

6 Cunningham R A and J G. Benink " Laboratory study of overburden formation and mud column pressures on drilling rate of permeable formations ' Trans AIME V 216 1959, 9-17.

7 Cheung J B and G Hurlburt "Submerged water-jet cutting of concrete and granite " Proc Third International Symposium on Jet Cutting Technology Chicago BHRA Fluid Engineering 1976 E5-E49

8 Schlichting H Boundary Layer Theory McGraw-Hill New York 1960

9 Jaeger J C and N G W Cook, Fundamentals of Rock Mechanics, Chapman and Hall London (1976)

## CONICAL WATER JET DRILLING

W. Dickinson, R. D. Wilkes, and R. W. Dickinson  
Petrolphysics, Ltd.  
San Francisco, California

### ABSTRACT

A laboratory program to develop a family of conically shaped water cutting jets for earth and rock penetration is underway. These systems show significant advantages where continuous penetration of a formation is required. The system under development to date uses flow rates of up to 13 liters per second, and pressures up to 82 MPa, with nozzle orifices 6.35 mm in diameter.

The conical geometry allows the cutting of a hole much larger than the nozzle orifice diameter, without the use of any rotating components. A vane assembly in the nozzle produces the conical shell of fluid, which at low ambient pressure breaks up into many discrete droplets. The included angle of the conical shell can be varied by altering the assembly of vanes, located upstream of the nozzle orifice.

Experimental results on the cutting of a variety of materials are presented, with comparisons drawn to similar work.

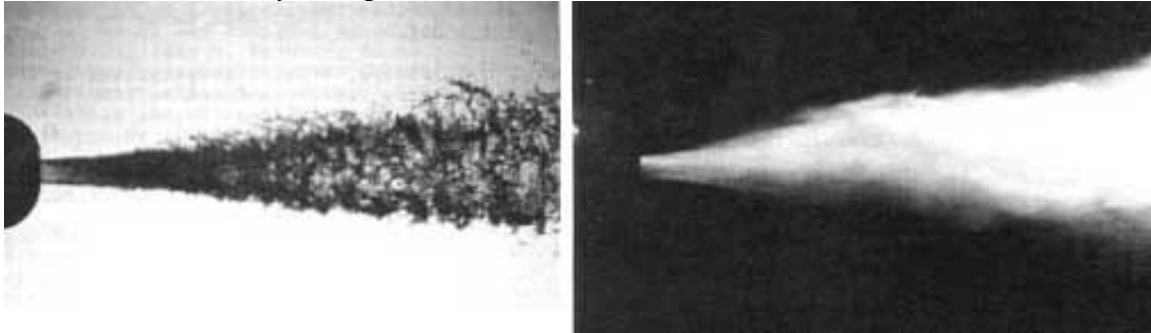
### INTRODUCTION

A nozzle family, the "Conical Jet" nozzle, is currently under development for use with high pressure, high flow systems. Typically, 54 to 68 MPa water (8,000 to 10,000 psi) is used at 9.5 to 13 liters per second (150 to 200 gpm) with a 6.35 mm (0.25 in.) diameter nozzle orifice. These nozzles are primarily intended for drilling all types of consolidated and unconsolidated earth formations. Laboratory testing has been done on a wide variety of rock types, including limestone, chalk, granite and basalt.

The primary advantage of these Conical Jet nozzles is that they produce a bore hole much larger than the nozzle orifice. This action occurs because the cutting fluid exits the nozzle in a hollow conical shell. The conical geometry is obtained by placing an assembly of vanes upstream of the nozzle orifice to introduce a rotational component to the fluid. The fluid exits the nozzle orifice in an expanding conical shell, which concentrates the cutting fluid on the periphery of the hole. As the nozzle advances into the formation, the region of rock contained within the boundary of the jet cone is removed.

The geometric advantage for material removal of this nozzle design over the collimated } solid stream jets of Leach and Walker (1), among others, is apparent. In order to achieve a similar hole diameter, the collimated jet would have to be mounted eccentrically or at an angle, then rotated.(2)(3)

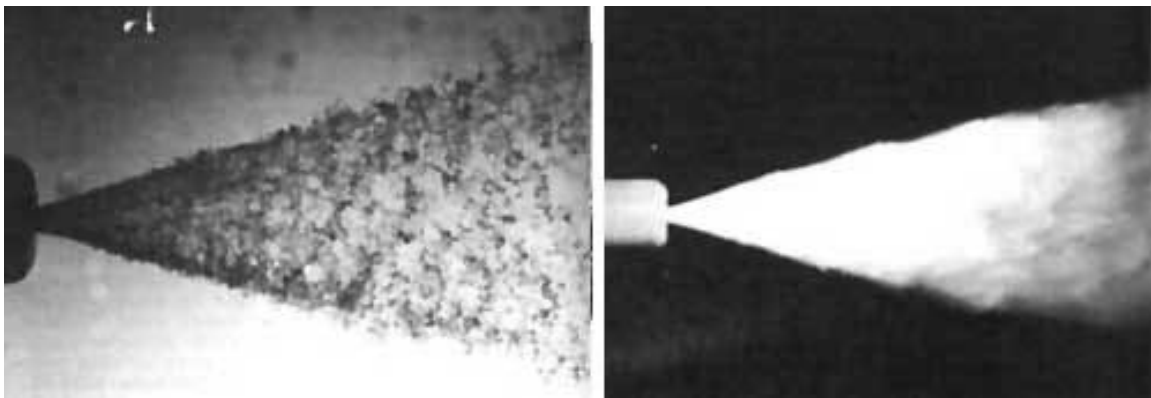
Figures 1 and 2 show stroboscopic photographs of two different conical jet nozzles with varying fluid exit angles. As can be seen from the figures, the exit angle of the fluid does not vary with pressure.



a) 0.4 MPa line pressure.

b) 20 MPa line pressure.

Figure 1. 10° Conical Jet nozzle with a 10  $\mu$ sec strobe duration



a) 0.4 MPa line pressure.

b) 20 MPa line pressure.

Figure 2. 30° Conical Jet nozzle with a 10  $\mu$ sec strobe duration.

Note the change in droplet size and that there is no change in cone angle.

The Leach and Walker nozzle is clearly superior for drilling small holes or slotting at large distances from the nozzle, as it was designed to do. The Conical Jet nozzle, however, is better suited for removing material from a larger area, allowing continued penetration by the nozzle and its feed line.

#### DESIGN BASIS

To continuously penetrate a formation with a water jet, the cutting of a bore hole from 3 - 6 times the nozzle orifice diameter is desirable. This permits a feed line to be used that will have fluid velocities at an order of magnitude less than the nozzle orifice velocity. Low feed line velocities are desired from a system efficiency point of view, as head loss in the feed line will then be a smaller percentage of the pump output. The head delivered to the nozzle is thusly increased as the feed line velocity decreases. These feed line losses become substantial as long distances (1000+ meters) are penetrated. Bore hole diameter becomes even more critical in the case of homogeneous hard formations, where the only method of cuttings removal is along the annulus between the bore hole and the

feed line. A conical cutting fluid geometry was sought to accomplish large diameter cutting action without the use of any rotating parts, which are mechanically complex and provide a potential source of failure. To obtain the conical shape with minimal head loss, the "Conical Jet" nozzle was conceived.

### NOZZLE CHARACTERISTICS

The Conical Jet nozzle is composed of three distinct regions, a vaned inlet, a conical constriction, and a straight exit. The conical constriction/straight exit geometry was chosen based on the work of Leach and Walker (1). Figure 3a shows the geometry used in all the testing reported herein. Figure 3b shows how the basic Leach and Walker design is modified to produce a conical cutting jet. The vane assembly imparts the rotational component, which is introduced in the low fluid velocity region (less than 30 meters per second). Many vane assemblies have been tested, from two to eight blades and a variety of different entrance and exit geometries. Two examples of vane geometry are shown in Figures 3c and 3d.

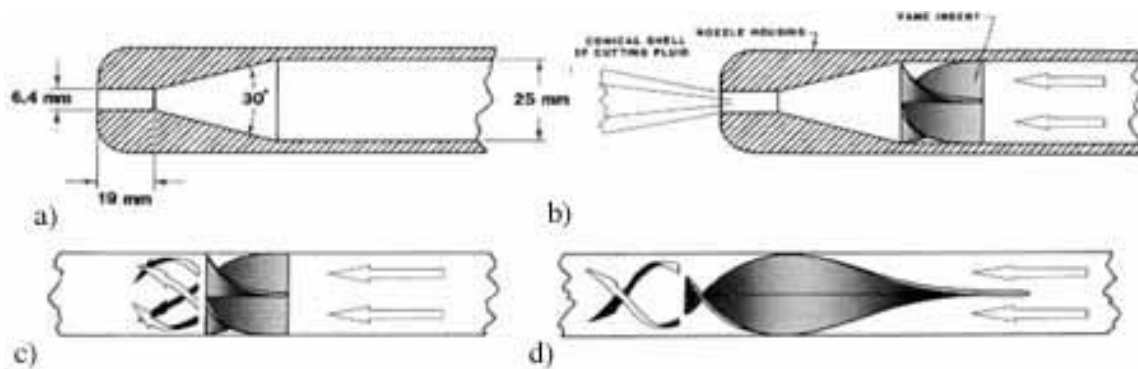


Figure 3. a) Leach and Walker configuration b) A Conical Jet nozzle in section  
c) Vane used in a 30° Conical Jet nozzle. D) Vane used in a 10° Conical Jet nozzle.

The spinning fluid then enters the conical constriction which accelerates the cutting fluid to up to 390 meters per second. Constriction angles of 14° and 30° have been tested with negligible difference in the fluid cone shape. A straight nozzle section of 2-3 nozzle diameters then carries the spinning fluid to the exit, where the fluid rotation causes an expanding conical shell of fluid to be formed. Above a certain threshold pressure (usually < 1 MPa), which varies with fluid cone angle, the hollow cone of the exiting fluid establishes itself within the straight exit section itself. The fluid exiting the nozzle does so in an annular region, so the cross sectional exit area actually decreases.

At very low fluid pressures (less than 0.07 MPa) the surface tension of the water is strong enough to maintain the fluid in a solid sheet. Above these pressures, and certainly at operating pressures, the cone is formed of discrete water drops. It is believed that water droplet impact effects are a predominant factor in the material removal rate of Conical Jet systems.

## EXPERIMENTATION

In air, the conical shell of fluid produced by the nozzle is composed of discrete drops. The time average of the drop stagnation pressure was measured by traversing a pitot tube across the conical shell of fluid. The plot of stagnation pressure for the conical jet nozzle at low pressure and varying standoff is given in Figure 4. As can be seen from the figure, an exponential decay exists in delivered stagnation pressure. The hole diameter, however, increases approximately linearly with distance. This yields a standoff distance for maximum material removal rate, which will be dependent on the formation properties, the Conical Jet included angle and the fluid pressure. Figure 5 shows this maximum for the case of a 10° Conical Jet at 68 MPa on White Granite.

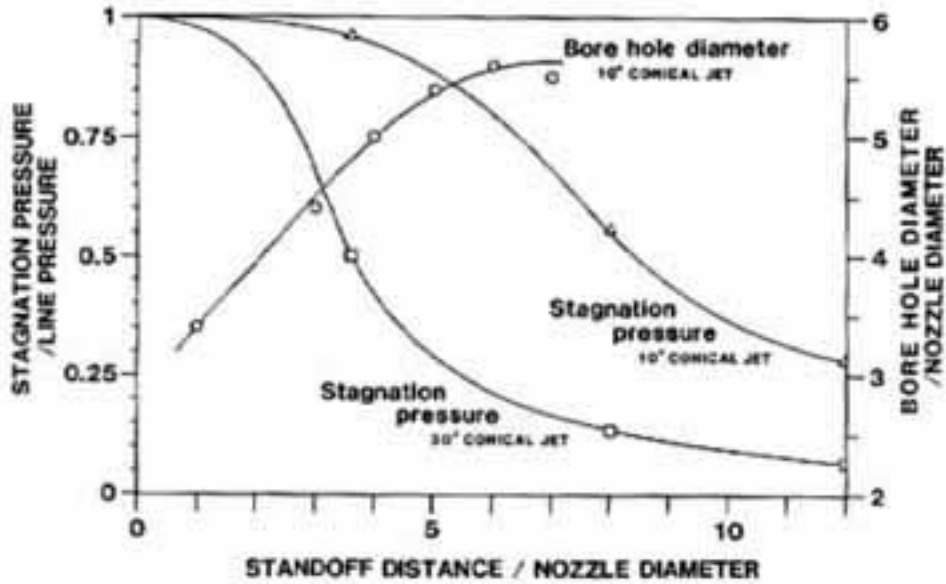


Figure 4.

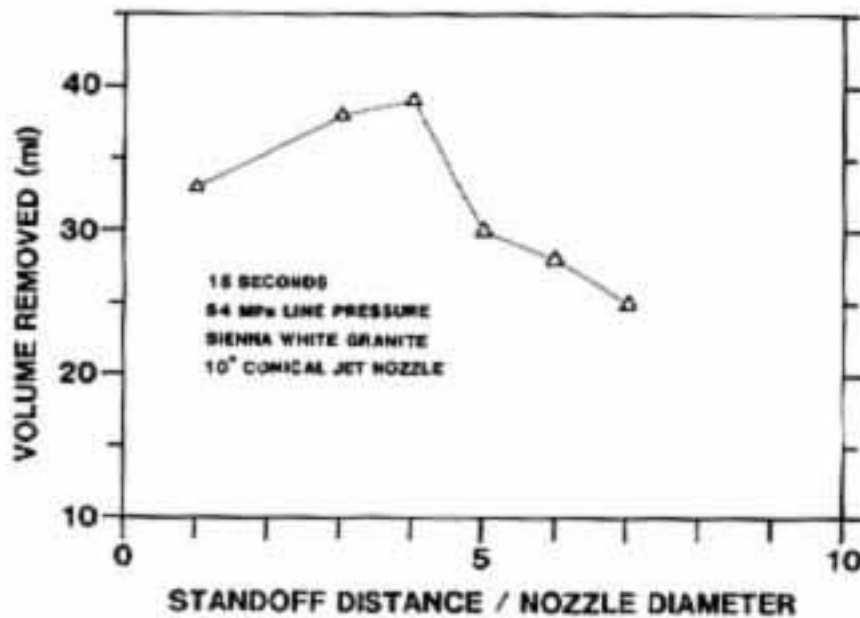


Figure 5.

A second series of tests at the full operating pressure (68 MPa) were performed on a variety of samples of 75 -100 mm diameter by about 150 mm long. To preclude shattering, the samples are contained in a steel pipe and held therein by expanding cement. The nozzle was fed by a 32 mm outside diameter, 25 mm inside diameter pipe, within a coaxial 75 mm diameter pipe. The 75 mm pipe was one meter long and was used to obtain a submerged condition on the jet. Figure 6 is a schematic of the fixture used in the testing.

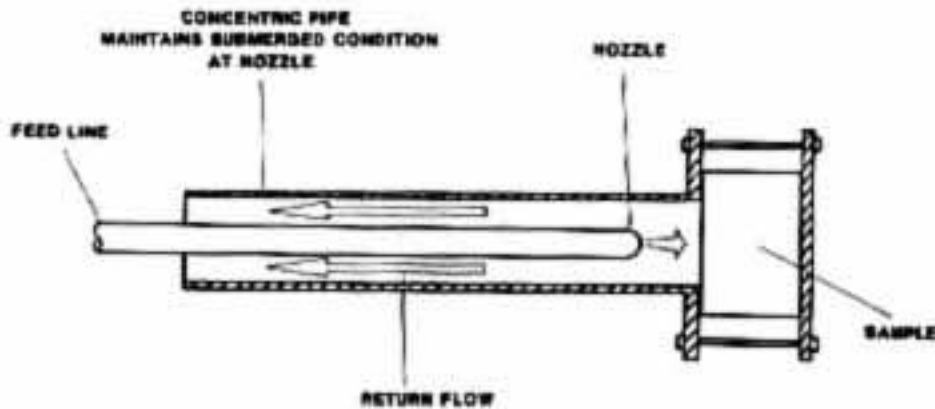


Figure 6. Test fixture.

Table I gives a summary of some of the test results with rocks from various world sources.

Figures 7 and 8 show samples cut with a 10° Conical Jet nozzle. Heavy pitting of the surface is indicative of a fracture failure which is consistent with droplet erosion as observed by Bowden and Field (4) and Adler (5).

## CONCLUSIONS

A water jet nozzle has been developed for continuous penetration of consolidated and unconsolidated earth formations. It produces a conically shaped cutting jet which allows a hole much larger than the nozzle orifice diameter to be cut. This characteristic is particularly desirable for continuous penetration, as it provides an adequate size hole for the nozzle feed line to advance with the nozzle.

These "Conical Jet" nozzles have been tested at pressures up to 68 MPa and have successfully cut materials such as limestone, granite and basalt.

The included angle of the conical cutting fluid can be varied by changing the geometry of an assembly of vanes within the nozzle. This allows the hole diameter cut by the Conical Jet to be controlled.

Table 1. 10° Conical Jet test results.

Material	Compressive Strength (MPa)	Test Time (sec)	Initial Standoff (mm)	Depth of Penetration (mm)	Hole Diameter (mm)	Volume Removed (ml)	Line Pressure (MPa)
1. Homogeneous basalt (Richland, WA)	270 (est.)	214	25	51	32	100	65
2. Coarse grained, layered granite, and quartz (Canadian Shield)	119	20	25	43	32	50	54
3. Homogeneous Sienna White Granite	112	15	25	30	32	39	54
4. Homogeneous Sienna Pink Granite	112	15	25	41	32	34	54
5. Austin Chalk (Carrollton, TX)	-	15	25	152	32	300	54
6. Stevens Sandstone (Eik Hills, CA)	-	15	25	127	64	310	54
7. Khuff Limestone (Abu Dhabi, UAE)	-	15	25	140	32	280	34
8. Limestone (Quintuco, Argentina)	-	15	25	127	32	380	54
9. Aluminum (6061-T6)	306	129	50	10	34	4.3	54

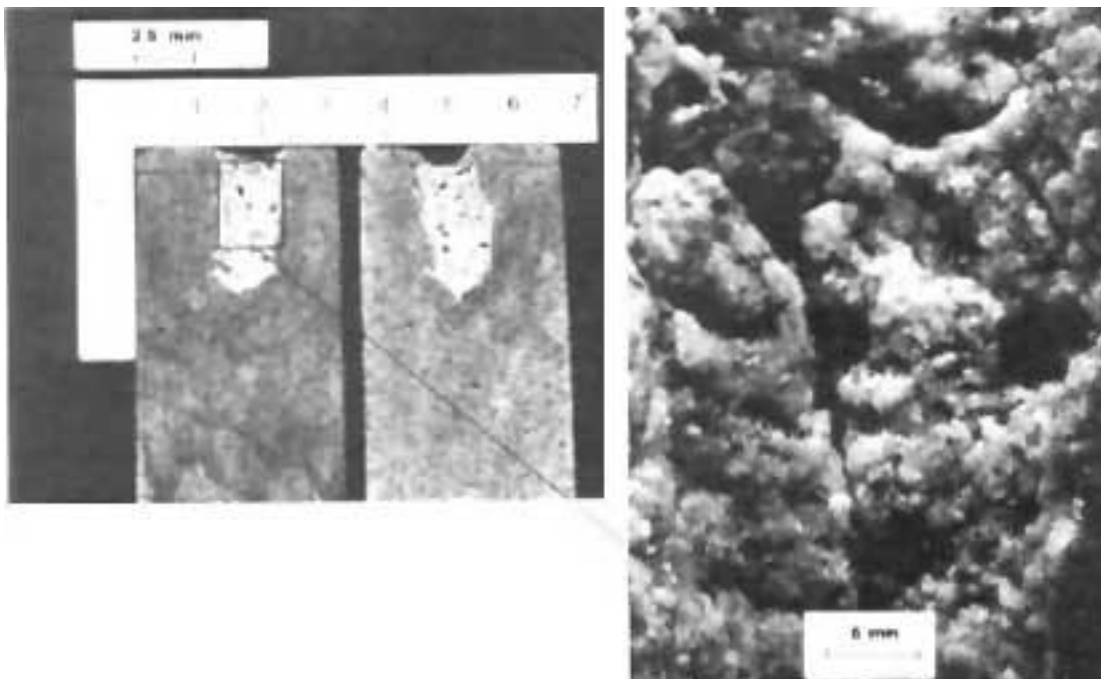


Figure 7. Sierra White granite cut with a stationary 10° Conical Jet nozzle, at an initial standoff of 25 mm, for 15 sec, at 54 MPa line pressure.

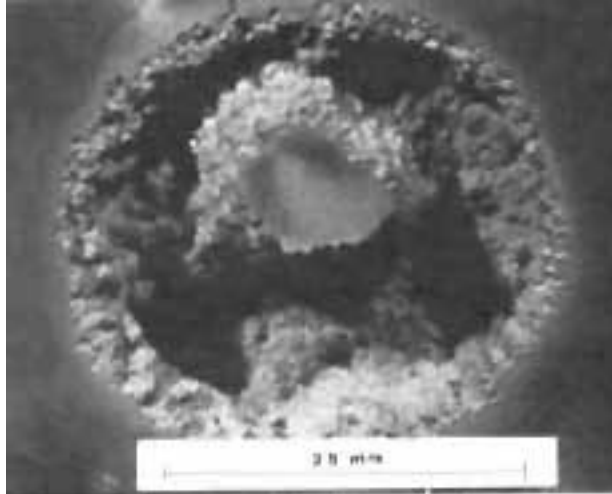


Figure 8. 6061-T6 aluminum cut with a 10° Conical Jet nozzle, 2 minutes at 54 MPa, with an initial standoff of 50 mm.

#### REFERENCES

- 1 Leach, S.J., and Walker, G.L.' "Some Aspects of Rock Cutting by High Speed Water Jets," 1965, Phil. Trans., Royal Society, London, Ser A, U260.
- 2 Pols, A.C., "High Pressure Jet-Drilling Experiments in Some Hard Rocks", 1977, Journal of Pressure Vessel Technology, The American Society of Mechanical Engineers, U.S.A., No. 76-PET-50.
- 3 Vijay, M.M. and Brierley, W.H.' "Drilling of Rocks with Rotating High Pressure Water Jets: An Assessment of Nozzles", Proc. 5th. Int. Symp. on Jet Cutting Technology, Paper G1. Organized by BHRA Fluid Engineering, Cranfield, Bedford, England (June 2-4, 1980).
- 4 Bowden, F.P., FRS and Field, J.E., "The Brittle Fracture of Solids by Liquid Impact, by Solid Impact, and by Shock", 1964, Proc. Roy. Soc., A, Vol. 282, 331f.
- 5 Adler, W.G., "Investigation of Liquid Drop Impact On Ceramics", Office of Naval Research, Final Report for Contract No. N000 14-76C-0744 NR 032-565, May 1982.

# THE EFFECT OF PRE-WEAKENING A ROCK SURFACE, BY WATERJET KERFING, ON CUTTING TOOL FORCES

J. E. Geier and M. Hood  
University of California, Berkeley  
Berkeley, California

## ABSTRACT

Empirical models are developed to describe the influence on the cutting process of pre-weakening a rock, by cutting a series of parallel kerfs in the surface with high pressure waterjets, prior to excavating the rock with a PDC drag bit. These models show that both the bit cutting and the bit normal forces are reduced substantially (by as much as a factor of four) when the spacing and the depth of the kerfs is appropriate to the depth of cut taken by the bit. The mechanical specific energy, or the mechanical energy applied to the bit to excavate a unit volume of rock, is also reduced dramatically when the rock is pre-kerfed.

## INTRODUCTION

Although waterjets at very high pressures (of the order of 380 MPa) are capable of eroding almost every type of rock, it is widely accepted that in most cases the use of these jets by themselves for this purpose is inefficient in that this method of excavation is very energy intensive (1). Despite this disadvantage, interest in this approach to rockbreaking persists. The reason lies in the fact that present day methods of rock excavation are dominated by mechanical tools. For any breaking process the rate of excavation is a function of the power applied to the rock. However, the strength and the wear resistance of tool materials is an inverse function of the power transmitted through the tools (2). Consequently a fundamental restriction on excavation rate using mechanical tools is given by the maximum power that can be applied to the rock through the tools without causing unacceptably high rates of tool wear. High pressure waterjets overcome this restriction by applying power to the rock other than through mechanical tools.

Three approaches to overcome the energy intensive nature of waterjet rock cutting have been investigated. In one of these approaches an abrasive material is entrained within the high velocity water stream (3). This method is termed "abrasive jet cutting". The use of this abrasive substantially enhances the cut depth made by the jet. This technique offers the potential as the key element in a system for selective mining wherein deep kerfs are made on both sides of a vein and the ore then is removed from the face separately from the waste rock (4). In this case the breaking efficiency is enhanced because only a small fraction of the rock (the kerfs) is excavated by the jets, the remaining rock, now weakened, is removed by some secondary system.

Another approach, termed "waterjet assisted cutting" employs jets at moderate pressures, typically 35-140 MPa, directed immediately adjacent to the cutting tools (5, 6, 7). These jets are found to act synergistically with the cutting tools to substantially reduce the forces acting on these tools and to provide cooling at the rock:tool interface, which

serves to reduce tool wear (8). It is argued (9) that the breaking efficiency using this approach is of the same order as the present systems that employ mechanical tools because, although the jet power often is of the same order as the power to the tools and so the total power applied to the rock face is doubled, the rate of rock excavation can be enhanced by a factor of two or more (9). In this case the jets do not serve to kerf the intact rock (5), indeed when they are used in this manner the result is detrimental (10). Rather they are believed to act to flush away the crushed rock that always is formed adjacent to cutting tools and thereby enable the tool to press directly, and thus more effectively, onto the intact rock (10).

A third approach, termed "mechanically assisted cutting", employs high pressure jets to pre-weaken the rock surface by cutting a series of shallow kerfs in the face. A mechanical tool then is used to break off the ridges between these kerfs. Here the ratio of the power applied by the jets to that applied by the tools is more likely to be in the range 4:1- 10:1, rather than the 1:1 ratio noted above for jet assisted cutting. This approach has been used for drilling both small (11) and large (12) holes.

An alternative, and simpler approach, to enhancing the rate of rock excavation could be accomplished by strengthening and improving the wear resistance of the cutting tool materials. The cutting material of choice in present day rock machining applications is cemented tungsten carbide. The properties of this material that make it so attractive are high hardness combined with high toughness. Unfortunately the hardness of this material decreases rapidly with increasing temperature (13, 14) and when this happens during the cutting process wear of the tool accelerates rapidly (8, 13). A more wear resistant and harder material is polycrystalline diamond. This man-made diamond is manufactured as thin wafers which then are bonded onto cylinders of cemented tungsten carbide. In this form the tools are known as polycrystalline diamond compacts (PDCs). This material is more susceptible to brittle fracture than cemented tungsten carbide. Despite this serious disadvantage, laboratory and field experience with PDC drill bits has shown that the drilling rates that can be achieved with these bits are 2-3 times more than conventional tungsten carbide bits and 80-100 times more than conventional roof bolt bits (15). Furthermore, the wear rate of the PDC bits often is as much as 1,000 times lower than the cemented tungsten carbide bits (15). Unfortunately the susceptibility of PDCs to brittle failure restricts their use to weak and medium strength rocks.

This paper is a preliminary investigation of the benefits that might be gained through a combination of two of the advances in excavation technology described above. Specifically this study looks at the magnitude of the force reductions achieved when PDC bits are used to cut rock that has been pre-weakened, in a mechanically assisted cutting operation, by kerfing the rock with high pressure waterjets. The purpose of this hybrid approach was to determine whether the range of rock types where PDC bits are employed might be extended by reducing the forces acting on these tools and thereby reducing their tendency to fracture.

## APPROACH

A factorial approach to the experimental design was adopted for this study because this both facilitated the construction of an empirical model to describe the relative importance of the various parameters investigated and ensured that the data taken was sufficient for a soundly based statistical analysis. The parameters of greatest interest for this investigation are:

- depth of cut ( $\delta$ )
- waterjet kerf depth (h)
- waterjet kerf spacing (s)
- waterjet kerf width (w)
- PDC bit rake angle ( $\alpha$ )
- PDC bit side rake angle ( $\beta$ )
- traverse speed (v)
- PDC bit wear (W)
- rock type (R)
- rock conditions (D)

The first six of these parameters are defined in the sketches, Figures 1 and 2.

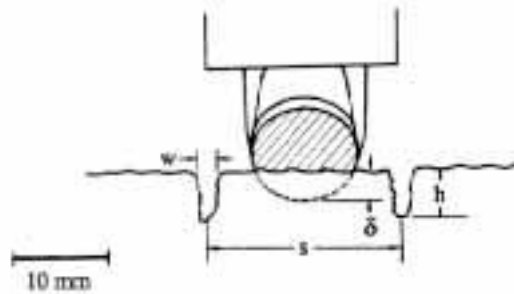


Figure 1: Definition of the parameters  $\delta$ , h, s, and w

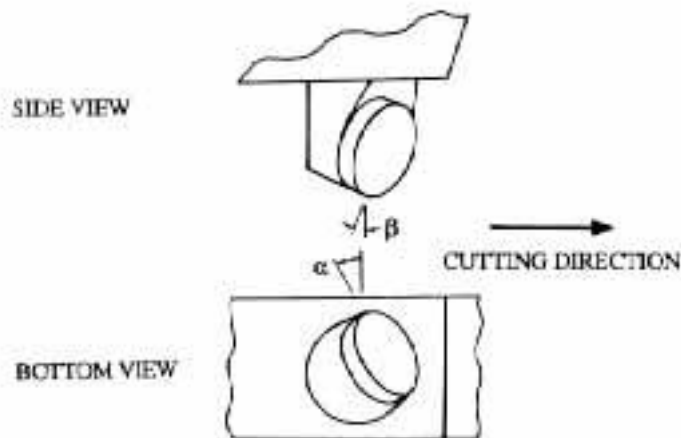


Figure 2: Definition of the parameters  $\alpha$  and  $\beta$

Traverse speed is the velocity of the bit travelling through the rock. Bit wear is a parameter describing the size of the bit wear flat. Rock type obviously refers to the type of rock that is cut. Rock conditions refer to the loadings, other than the bit loading, applied to the rock. These are:

- the thermal loading,
- the fluid pressure loading including pore pressure and mud pressure, and
- the mechanical loading from the rock confining stress.

A single program designed to investigate all of these parameters simultaneously would be unwieldy and for this reason this approach was not followed for this study. An understanding of the influence of many of these parameters on the cutting process, where the rock has not been pre-weakened using waterjets, has been developed over the past three decades and this subject was reviewed by Roxborough (16). In this paper Roxborough notes that the bit forces increase approximately linearly with the depth of cut. These forces are high for negative rake angles and decrease monotonically as the rake angle changes from negative through zero to positive values. The traverse velocity is found to have little effect on the bit forces provided that this velocity is below a critical value where the rate of bit wear becomes significant. Bit wear is reported to increase the values of the bit forces during the cutting process. Hood (17) identifies the reason for this increase in forces with the greater volume of crushed rock material formed by blunt (worn) bits. Roxborough (16) points out also that the efficiency of the cutting process is increased when deep, widely spaced grooves are machined in the rock face. Most of these findings would not be expected to change when the rock is pre-weakened.

In this test program only one rock type, Indiana Limestone, was cut. This rock is well characterized and its properties are given in Krech et al, (18). The condition of this rock (D) was not varied during these experiments. Tests were conducted at ambient laboratory temperatures and no attempts were made to artificially influence the rock pore pressure. No mud pressure was applied to the rock surface and the rock confining stress was zero. Bit wear, the influence of the bit rake angles, and the effects of the kerf width, were not studied here. For these tests only sharp (unworn) bits were employed. The rake angles of these bits were  $\alpha = -15$  degrees and  $\alpha = 0$  degrees. These angles are typical of those employed on the bit inserts currently used for oil and gas drill bits.

The responses measured during the experiments were:

- mean bit cutting force ( $F_c$ ) and mean peak bit cutting force ( $F_{cp}$ )
- bit normal force ( $F_n$ ) and mean peak bit normal force ( $F_{np}$ )
- bit side force ( $F_s$ )
- mean cross-sectional area of cut ( $A_c$ )

The cutting force is defined as the force acting on the bit in the direction of bit travel through the rock. The normal force acts on the bit perpendicular to the planar rock surface. The bit side force acts orthogonally to these other forces. The mean cross-sectional area of the cut is defined as the volume per unit length of cut made by the

PDC bit. This area was measured by filling the cut with a known volume of fine glass beads.

The linear cutting apparatus used for these experiments has been described elsewhere (19). Because the depth of cut taken in many of these tests was small, of the order of a few millimeters, careful measurements of this depth were taken after each cut was made. A custom designed instrument was constructed for this purpose. This instrument employed a direct current linear differential variable transformer (DCDT) to measure the difference between the surface of the rock and the bottom of the kerf or groove made by the waterjet or PDC bit, respectively. Considerable care was taken in preparing a smooth rock surface prior to conducting these tests so that the cut depth was not influenced by an uneven surface.

The experiments were conducted in two suites. The first suite, termed Phase 1, was a reconnaissance investigation covering a broad region of the parameter space in a somewhat cursory manner. The second suite, Phase 2, was an in-depth study to determine more precisely the effects of the variables  $h$ ,  $s$ ,  $v$ , and  $C$  on the responses  $F_c$ ,  $F_{cp}$ ,  $F_n$ ,  $F_{nps}$  and  $E_s$ , where  $E_s = \text{Mechanical Specific Energy} = F_c/A_c$ . It should be noted that it is possible to calculate specific energy in four ways; including or excluding the energy expended by the waterjets in cutting the kerfs, and including or excluding the contribution to  $A_c$  made by these waterjet cut kerfs. In this analysis the waterjet energy was excluded and hence  $E_s$  refers to the mechanical energy required at the bit to excavate unit volume of rock. Also in the calculations of rock volume the contribution to  $A_c$  made by the kerfs was included. The reason for calculating  $E_s$  in this manner follows from the argument given in the introduction, namely that the fundamental limitation on the rate of rock excavation by mechanical tools is a restriction on the power that can be applied to the rock through these tools. Consequently the primary concern is to minimize this power component of the tool. The waterjet power component, while interesting, is of lesser concern; hence the exclusion of the waterjet energy. Also, the point of interest is the tool rate of rock removal, rather than the individual rates of rock erosion by the jets and rock cutting by the bit. Therefore the contribution to  $A_c$  by the jets is included.

In Phase 1 two strategies for kerfing the rock (illustrated in Figure 3) were investigated. In one of these strategies,  $C = 1$ , the bit was positioned halfway between two kerfs. In the other strategy,  $C = 2$ , a kerf was cut along the center of the groove to be cut by the bit. The experimental plan for Phase 1 is given in Figure 4. This was a fractional factorial constructed under the hypothesis that the effect of traverse speed,  $v$ , is negligible. The + and - signs next to the circles indicate the fast (424 mm/s) and the slow (160 mm/s) traverse velocities, respectively.

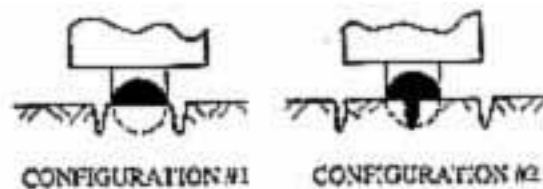


Figure 3: Representation of the two cutting strategies employed

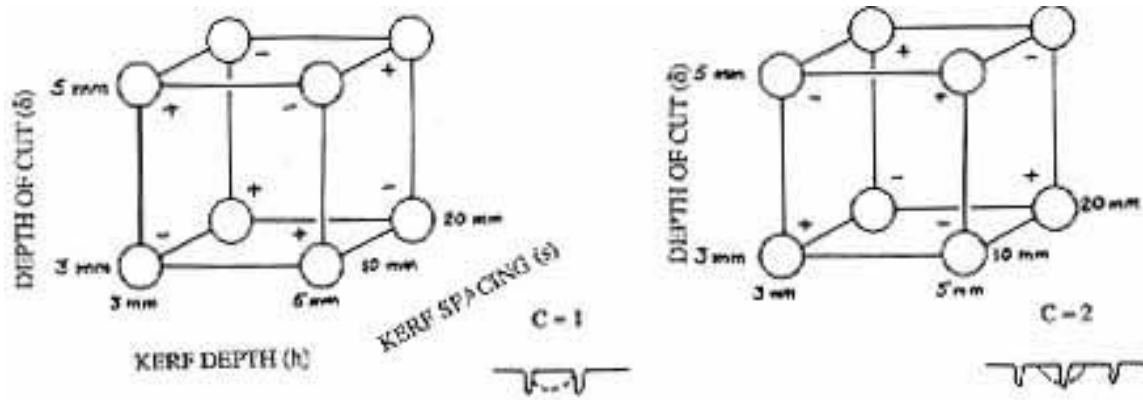


Figure 4: Diagram illustrating the experimental plan for the Phase 1 tests

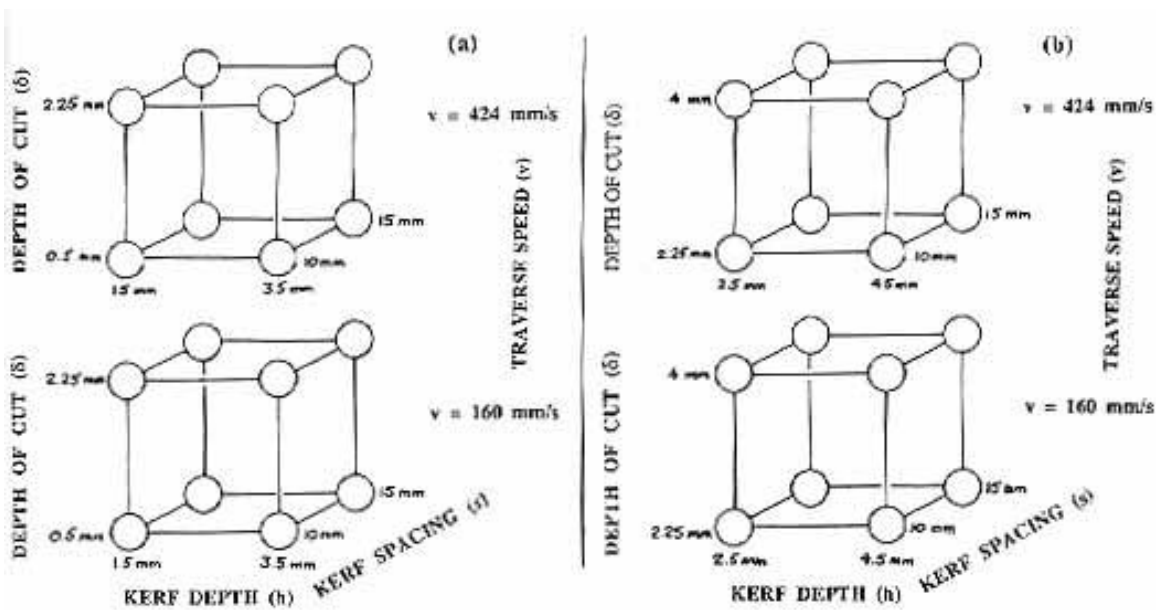


Figure 5: Diagram illustrating the experimental plan for the Phase 2 tests

The experimental plan for Phase 2 consisted of two factorials shown in Figure 5. These cover two separate regions of interest. The first (Figure 5a) represents shallow kerf and shallow groove depths while the second (Figure 5b) covers deeper cuts. Because the results from Phase 1 indicated that  $C = 1$  was the superior kerfing strategy, only this approach was employed during the Phase 2 tests. The influence of traverse velocity was examined explicitly in this second test suite by conducting separate factorials for both the shallow and the deep cuts at the fast and the slow speeds. This was done because results from Phase 1 did not unambiguously support the hypothesis that this velocity had negligible influence on the cutting behavior.

## RESULTS

Results from the Phase 1 tests are given in Figure 6. At this reconnaissance stage the instrumentation to accurately measure  $\delta$  and  $h$  was not available. Consequently the

values presented here are not as accurate as those given under the results of the Phase 2 study. Also, at this stage the importance of the kerf spacing,  $s$ , on the results was not appreciated fully and for this reason the measurements of this parameter were not as accurate as in the later Phase 2 investigation. Despite these limitations the results show interesting trends.

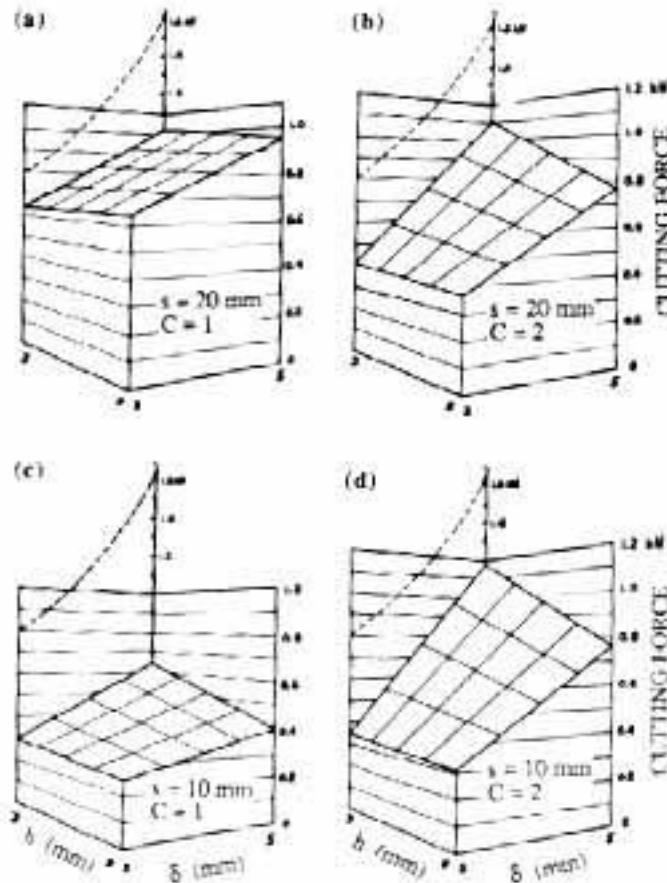


Figure 6. Perspective plot from Phase 1 tests showing mean cutting force  $F_c$ , as a function of depth of cut,  $\delta$ , and kerf depth,  $h$ .

Figure 6 plots the mean cutting force,  $F_c$ , as a function of the kerf depth,  $h$ , and the groove depth,  $\delta$ . In all of these plots the dashed curve indicates the value of  $F_c$  when the rock is not pre-weakened by kerfing with jets. Figures 6a and 6b compare the two kerfing strategies  $C = 1$  and  $C = 2$  when the spacing between waterjet kerfs was 20 mm. From these plots it can be seen that the second approach,  $C = 2$ , produces generally lower cutting forces, except when  $\delta > h$  and at high values of  $\delta$ . When conducting these experiments the reason for this result was apparent from visual inspection of the groove following the cut. When  $s = 20$  mm and  $3$  mm  $< \delta < 5$  mm, rock chips from the groove being machined by the bit only infrequently broke into the kerfs cut by the jets. Consequently for  $C = 1$ , the benefit of these kerfs was only minor. For  $C = 2$ , on the other hand, the kerf in the center of the groove provided some relief for the chip formed by the bit to break to and thus the forces were reduced more substantially.

The picture changes dramatically when Figures 6c and 6d are examined. Again these plots compare  $C = 1$  with  $C = 2$ , but here  $s = 10$  mm. It should be remembered (Figure 1) that the diameter of the bit face was also 10 mm. Thus for  $C = 1$  the kerfs exactly define the outside diameter of the bit. In this situation  $C = 1$  represents the optimal kerning strategy everywhere in this space. Furthermore the magnitude of these force reductions are not much affected by  $h$ .

Over the range of the parameter values studied, the preliminary conclusions from these Phase 1 tests are that for the  $C = 1$  kerning strategy, kerf spacing has a substantial influence on the achievable bit force reductions. The kerf depth is of lesser importance when this strategy is employed. For the other kerning strategy,  $C = 2$ , on the other hand, the kerf spacing is relatively unimportant but kerf depth has significant influence on the force reductions, especially for the deeper cuts. These findings have important practical implications because in a situation such as the drilling of a hole, the kerf depth,  $h$ , will be greatly affected by changes in the rock properties with hole depth. In general it will not be possible to constantly adjust the jet pressure and jet flow rates to ensure that the required value of  $h$  is always achieved. Consequently, the slotting strategy adopted needs to yield benefits to the cutting process which are mostly independent of  $h$ . Kerf spacing, on the other hand, can be easily controlled by simply rearranging the mountings of the waterjet nozzles on the cutter head. Based on these considerations only the kerning strategy  $C = 1$  was selected for further testing in Phase 2.

Results from the Phase 2 experiments are illustrated in Figures 7 and 8. These experiments were conducted in two sets with overlap between the sets in the kerf depth variable (see Table 1). Data obtained from these sets were analyzed by fitting a linear model through the parameter space. Initially the data from both sets were combined and the model was fitted. However, a regression analysis demonstrated that the model fitted to these data was not good, indicating the need for a higher order model. The approach then adopted was to analyze the results for each data set separately. The linear models for  $F_c$  are shown in Figure 7 and are given in algebraic form in Table 1. An excellent fit to the data was now achieved yielding a multiple correlation coefficient of  $r = 0.98999$ .

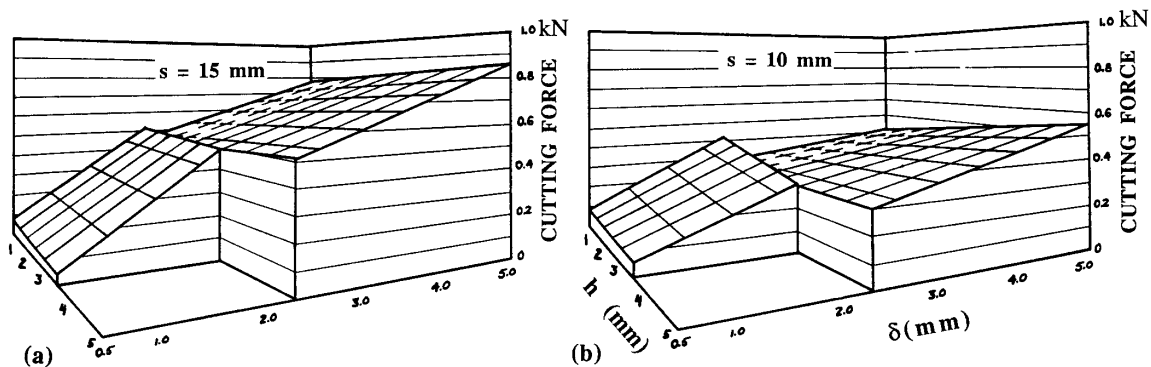


Figure 7: Perspective plot from Phase 2 tests showing mean cutting force  $F_c$ , as a function of depth of cut,  $d$ , and kerf depth  $h$ .

From Figure 7 it is apparent that good conformity was achieved between the two domains. It should be noted however that a significant difference in gradient exists between these domains explaining why a single linear fit through both domains was inaccurate. It is evident that substantial force reductions are observed when the rock surface is pre-kerfed with the waterjets. The magnitude of these force reductions increases as the spacing between the kerfs is reduced from 15 mm to 10 mm and that the percentage force reduction increases as the cut depth,  $h$ , increases. From this figure it is apparent that the effect of kerf depth is very slight over the range of  $h$  studied. This confirms the finding from Phase 1.

Similar trends were found and conclusions drawn from the analysis of the data for the bit normal force. Because this force component was smaller, by about an order of magnitude, than the cutting force, the signal-to-noise ratios were correspondingly lower and consequently the errors in these data were more significant. For example, the estimated standard deviation of the  $F_c$  measurements was approximately  $0.03 F_c$ , whereas the standard deviation of the  $F_n$  measurements was about  $0.08 F_n$ . Consequently the models for this latter force component, presented in Table 1, should be treated with some caution.

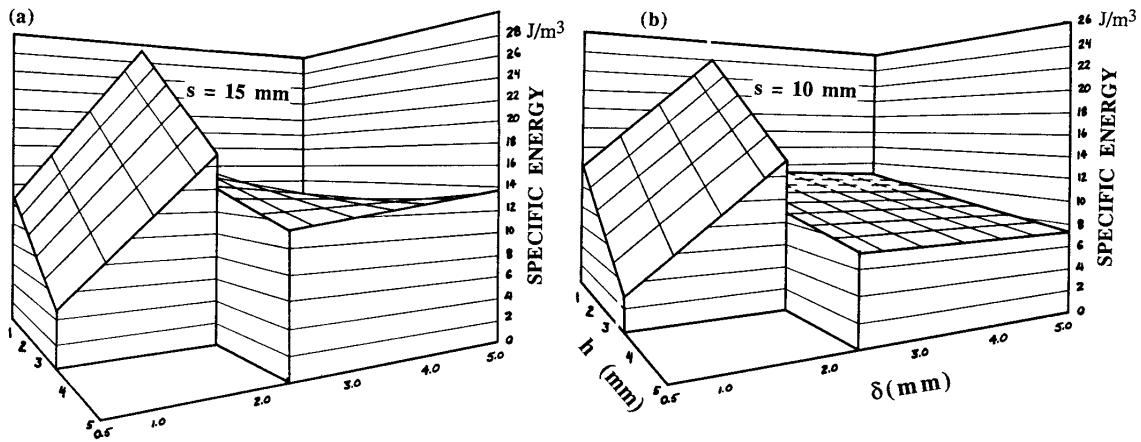


Figure 8: Perspective plot from Phase 1 tests showing mechanical specific energy  $E_s$ , as a function of depth of cut,  $\delta$ , and kerf depth,  $h$ .

Figure 8 illustrates linear models fitted for the results of mechanical specific energy. Again these models are presented in algebraic form in Table 1. It is evident that the conformity at the interface of the two domains is less good than for the cutting forces. This was attributed to the difficulties of accurate measurements of rock volume, particularly at shallow cut depths. For the deeper cuts the worst-case error in  $A_c$  was  $0.03 A_c$ , whereas for the shallowest cuts this worst-case error was as high as  $0.13 A_c$ . Despite this problem the important trends are apparent, especially for the deeper cuts where the measurements are more accurate. The figure shows that the most efficient cutting is achieved at close kerf spacing and with deep kerfs. When these conditions were met, the cut depth taken by the bit, was found to have little influence on the mechanical specific energy.

Analysis of the residuals of these models showed no significant correlation of these residuals with  $v$ . Hence it was concluded that traverse speed has no effect on the bit forces over the ranges of the parameters investigated. This finding is in accordance with similar results obtained from cutting experiments conducted when the rock is not pre-weakened by waterjets (16).

## SUMMARY AND CONCLUSIONS

It was demonstrated that the forces acting on a PDC drag bit can be reduced by as much as four times when the rock is weakened prior to the cutting operation by kerfing the surface using high pressure waterjets. This finding has important practical applications because, as noted above, PDC bits while more wear resistant than cemented tungsten carbide bits, suffer from the disadvantage of susceptibility to brittle fracture. This feature limits the range of rocks in which they can be employed. The lower forces applied to the bits with this mechanically assisted approach to the cutting operation, should make it possible to greatly expand the rock types that can be excavated using these tools.

It was shown that when the waterjet kerfs are cut parallel to the direction of bit travel and are spaced evenly across the rock face, the cutting strategy in which the bit is centered along a kerf was effective in reducing the bit forces. In this case the fracture that forms the rock chip tended to break to this center kerf, rather than to the two neighboring kerfs. The magnitudes of these force reductions were observed to be very dependent on the depth of the kerf and almost totally independent of the spacing between the kerfs. An alternative cutting strategy in which the bit was centered between two kerfs was even more effective in reducing bit forces. Here the rock chip was observed to form by the fracture from the bit intersecting the two kerfs, provided that these kerfs were spaced close to the outside diameter of the bit. In this case the magnitudes of the force reductions were largely independent of the kerf depth but were quite dependent on the kerf spacing. This latter cutting strategy was adopted for the more detailed Phase 2 tests. All of these results were obtained over a range of cut depths (taken by the bit) and kerf depths (taken by the waterjets), from 3 mm to 5 mm with a bit diameter of 10 mm.

Empirical models were derived for the bit cutting force, the bit normal force and the mechanical specific energy of the cutting process in terms of the cut depth, the kerf depth and the spacing between the kerfs. These models were developed for the second cutting strategy described above, and for the following ranges of parameters: cut depths from 0.5 mm to 4.5 mm kerf depths from 1.5 mm to 3.5 mm, and kerf spacings from 10 mm to 15 mm. From these models it was confirmed that the most important parameters were the cut depth and the kerf spacing. The mechanical specific energy was shown to be largely independent of cut depth. This finding is in contrast with results derived from cutting research where the rock is not pre-weakened by kerfing. In these circumstances it is accepted that deep cuts increase the efficiency of the cutting process (16). On the other hand, the present study demonstrated that traverse speed in the range 160424 mm/s had no influence on the cutting process. This finding is in accordance with earlier work cutting in rock that is not prekerfed.

TABLE 1 Algebraic Form of Models Fitted to the Phase 2 Experiments

<i>Mean Cutting Force, <math>F_c</math></i>	<i>Region within which model is valid</i>
0.239 - 0.124 - 0.00317s - 0.077h + 0.157 s + 0.024 h + 0.00554sh 0.00139 sh	2.25mm < < 4.5mm 2.25 mm < h < 4.5 mm
0.0329 + 0.124 - 0.00444s + 0.0259h + 0.00844 s - 0.0614 h - 0.00271sh + 0.00421 sh	0.5mm < < 2.25mm 1.5 mm < h < 3.5 mm
<i>Mean Normal Force, <math>F_n</math></i>	<i>Region within which model is valid</i>
3.157 - 0.996 - 0.226s - 0.934h + 0.077 s + 0.289 h + 0.072sh 0.021 sh	2.25mm < < 4.5mm 2.25mm < h < 4.5mm
-0.264 + 0.3 + 0.017s + 0.236h - 0.008 s - 0.18 h - 0.017sh + 0.0126 sh	0.5 mm < < 2.25 mm 1.5 mm < h < 3.5 mm
<i>Specific Energy, <math>E_s</math></i>	<i>Region within which model is valid</i>
-1.689 + 0.69 + 0.321s + 0.392h - 0.0773 s - 0.17 h - 0.0554sh + 0.0188 sh	2.25 mm < < 4.5 mm 2.25 mm < h < 4.5 mm
-1.586 + 0.0313 - 0.0405s - 0.557h + 0.0708 s + 0.108 h + 0.0204sh 0.0144 sh	0.5 mm < < 2.25mm 1.5 mm < h < 3.5 mm

#### ACKNOWLEDGEMENT

This work was carried out under a grant from FlowDril Corporation.

#### REFERENCES

1. Cook, N.G.W. and Harvey, V.R., "An Appraisal of Rock Excavation by Mechanical, Hydraulic, Thermal and Electromagnetic Means" *Proceedings of the Third Congress of the International Society for Rock Mechanics*, Denver, Colorado, in *Advances in Rock Mechanics* Vol. 1, Part B. National Academy of Sciences, Washington D.C., 1974, pp. 1599-1615.
2. Cook, N.G.W., "Wear on Drag Bits in Hard Rock", *Proceedings of the 14th Canadian Rock Mechanics Symposium*, Vancouver B.C., May 13-14, 1982.
3. Hashish, M., "Experimental Studies of Cutting with Abrasive Waterjets", *Proceedings of the 2nd U.S. Water Jet Conference*, Rolla, Missouri, May 1983, pp. 379-390.
4. Marlowe, A.C., Worsley, S.L., and Price, C.J., "The use of Abrasive Entrained High Pressure Water Jets as a Tool for the Non-Explosive Winning of Gold Bearing Quartzites", *Proceedings of the 8th International Symposium on Jet Cutting Technology*, BHRA, Durham, U.K., September 1986, pp. 113124.

5. Hood, M., "Cutting Strong Rock with a Drag Bit Assisted by High Pressure Water Jets", *Journal of the South African Institution of Mining and Metallurgy*, 77, No. 4, 1976, pp. 79-90.
6. Dubugnon, O., "An Experimental Study of Water Assisted Drag Bit Cutting of Rocks", *Proceedings of the 1st U.S. Water Jet Conference*, Golden Colorado, 1981, pp. II-4.1 to II-4.11.
7. Fenn, O., Protheroe, B.E. and Joughin, N.C., "Enhancement of Roller Cutting by means of Water Jets", *Proceedings of the Rapid Excavation and Tunneling conference*, New York, N.Y., June 16-20 1985, pp. 341-356.
8. Hood, M., "A Study of Methods to Improve the Performance of Drag Bits used to cut Hard Rock", Ph.D. Thesis Department of Mining Engineering, University of the Witwatersrand, Republic of South Africa, 1977.
9. Hood, M., "Water Jet Assisted Rock Cutting - The Present State of the Art", *International Journal of Mining Engineering*, 3, No. 2, 1985, pp. 91-113
10. Geier, J.E., Hood, M., and Thimons, E.D., "Waterjet- Assisted Drag Bit Cutting in Medium Strength Rock: A Fundamental Investigation", *Proceedings of the 28th U.S. Symposium on Rock Mechanics* University of Arizona, Tucson Arizona, June 29 July 1, 1985.
11. O'Hanlon, T., "An Overview of Current and Future Applications for Ultra High Pressure Waterjets in Mining" *The 86th Annual General Meeting of the Canadian Institute of Mining*, Ottawa, Canada, 1984
12. Henneke, J and Baumann, L., "Jet Assisted Tunnel Boring in Coal Measure Strata", *Proceedings of the 4th International Symposium on Jet Cutting Technology*, BHRA, Canterbury, U.K., April 12-14, 1978, pp. J1-1 to J1-12.
13. Roxborough, F.F., "Cutting Rock with Picks", *The Mining Engineer*, Vol. 132, No. 153, pp. 445-455.
14. Morris, C.J. and MacAndrew, K.M., "A Laboratory Study of High Pressure Water Jet Assisted Cutting", *Proceedings of the 8th International Symposium on Jet Cutting Technology*, BHRA, Durham U.K., September 1986, pp. 1-8.
15. Green S., Personal Communication.
16. Roxborough, F.F., "Research in Mechanical Rock Excavation: Progress and Prospects", *Proceedings of the Rapid Excavation and Tunneling Conference*, New York, N.Y., June 16-20, 1985, pp. 225-244.
17. Hood, M., "Phenomena Related to the Failure of Strong Rock Adjacent to an Indenter", *Journal of the South African Institution of Mining and Metallurgy*, 78, No. 5, 1977, pp. 113-123.
18. Krech, W.W., Henderson, R.A., and Hjelmstad, K.E., "A Standard Rock Suite for Rapid Excavation Research", *Bureau of Mines Report of Investigations 7865* 1974, 29 pp.
19. Tuduoglu, L., "Mechanical Rock cutting with and without High Pressure Water Jets", Ph.D. Thesis, University of California, Berkeley, 1984, 165 pp.

# STUDY OF PARTICLE VELOCITIES IN WATER DRIVEN ABRASIVE JET CUTTING

R. K. Swanson, M. Kilman, S. Cerwin, and W. Tarver  
Southwest Research Institute  
San Antonio Texas

R. Wellman  
U. S. Government  
Washington, D. C

## ABSTRACT

In water/abrasive jet cutting, abrasive particles are accelerated to high velocities by a high pressure water jet. This paper describes an investigation into abrasive particle behavior based on experimental determination of particle velocity. In these experiments, conventional garnet sand is mixed with magnetic particles of comparable size. This mixture is injected into a conventional waterjet and the resulting cutting stream directed through a pair of current-carrying coils spaced a fixed distance apart. The magnetic particles induce a signal in each of the coils in turn, which is recorded on a digital transient recorder. Measurement of the time between the signal response from each of the coils yields a measure of the particle velocity. Typical results show that, with a waterjet stream velocity of 1800 feet-per-second, for example, injected abrasive particles achieve average velocities of only about 400 feet-per-second indicating incomplete mixing. The relatively low overall efficiency of the water jet as an accelerating medium is explained by the failure of the particles to be effectively embedded into the jet stream.

## INTRODUCTION

Water/abrasive jet cutting is a technique in which abrasive particles are accelerated by a small diameter, high velocity water jet and directed at the material to be cut. The water jet alone is capable of cutting a variety of soft materials including fabric, plastics, rubber, and soft rock. With the addition of abrasive particles, the technology can be expanded to cut almost any material including concrete, rock, and even metals including hardened steel.

Cutting with an abrasive water jet is essentially an erosion process. Erosion is a word used today to describe a broad range of similar mechanisms relating to material removal by a series of independent, but similar impact events. Two common mechanisms of particle erosion are abrasion and fracture. Abrasive erosion is typically associated with shallow angles, while fracturing is usually associated with large angles of particle impact. A critical parameter, in any case, is particle velocity. This paper presents the results of an experimental program of particle velocity measurement in abrasive cutting streams.

## ABRASIVE WATER JET CUTTING

Theoretical models for erosion fall into several broad categories, based upon the nature of the eroded and abrasive materials, and the velocity of the abrasive particles. In abrasive jet cutting, particle velocities are moderately high, in the range of several

hundred feet-per-second. At these velocities erosion involves two distinct processes depending upon whether the eroded material is brittle or ductile in nature. Ductile erosion is defined as a cutting process in which the abrasive particles cut or gouge the eroded material, eventually causing volume loss. Brittle erosion is described as a deformation or cracking process in which abrasive particles remove material by forming a network of intersecting cracks from which material eventually breaks out as a result of direct particle impact.

Separate theories for brittle and ductile erosion are based upon the ideal situation in which erosion is purely ductile or purely brittle. In reality, erosion of any material is a combination of brittle and ductile erosion mechanisms. For most materials, however, one or the other may dominate the erosion process. It is unlikely that in any material erosion is completely ductile or completely brittle. For materials such as soft steel, erosion is predominantly due to cutting wear; while for hard steel, the process is predominantly brittle erosion. For glass, ceramics, and rock, erosion is best described as primarily a brittle erosion process.

For the particular case of abrasive water jet cutting, at least two authors have attempted to establish cutting models based on the physical parameters involved. Hashish (1) has published an abrasive jet cutting model for predicting the depth of cut for brittle materials. His simplified equation of kerf depth (h) is as follows:

$$h = \frac{2(1-c)\dot{m}v^2}{\pi d_j \epsilon \mu} \quad (1)$$

where:

$$c = \mu / N$$

$\mu$  = traverse rate of the jet

N = number of passes

m = abrasive mass flow rate

V = velocity of abrasive particles

$d_j$  = water stream diameter

= energy required to remove a unit volume of metal (specific energy)

G. A. Bitter (2) has published a study of erosion phenomena wherein he presents the following equation for the volume of material removed (w) in erosion of brittle materials:

$$w = \frac{1}{2} \frac{m[(v \sin \alpha) - K]^2}{\epsilon} \quad (2)$$

where

$m$  = total mass of impinging particles

$v$  = velocity of particles

$E$  = specific energy of material

$\theta$  = angle of particle impingement

$K$  = a constant dependent on the material properties of the abrasive particles and eroded material.

Specific energy ( ) of a material is defined as the amount of energy required to remove a unit volume of material by deformation wear also known as the deformation wear factor. Specific energy for cement, for example, is given by:

$$= A y^2/E \quad (3)$$

where:

$A$  = a constant

$y$  = elastic load limit (strength) of cement

$E$  = elastic modulus of cement

In both these models, the cutting performance is a function of the total mass of impinging particles and the square of their velocity. Experimentally, the mass of the particles can be measured and the velocity of the water jet itself can be calculated from pressure-volume relationships. The actual velocity of the abrasive particles, however, must be inferred. Experimental determination of actual particle velocity has not been reported.

## PARTICLE VELOCITY MEASUREMENTS

Currently the water/abrasive stream is achieved by feeding a measured amount of abrasive particles into a mixing chamber through which the high velocity water jet is made to flow. This general process is illustrated in Figure 1 in which the abrasive is drawn into the flowing high velocity water stream and the combined mixture is then redirected through a larger diameter nozzle to the work piece. The average velocity of the total mass of abrasive particles is the quantity of interest.

## EXPERIMENTAL VELOCITY MEASUREMENTS

To make actual measurements of the particle velocities, a method illustrated in Figure 2 was developed. Here, the cutting stream immediately below the director nozzle is encircled by two small coils of wire connected to sensing electronics and timing circuitry. Magnetic particles of the same general size as the abrasive particles are mixed with the abrasive and accelerated in the same stream. When one of the magnetic particles passes through the repeated a short time later as the particle passes through the second coil. The transit time between the fixed coil spacing distance can be measured accurately and this value used to calculate the individual particle velocity.

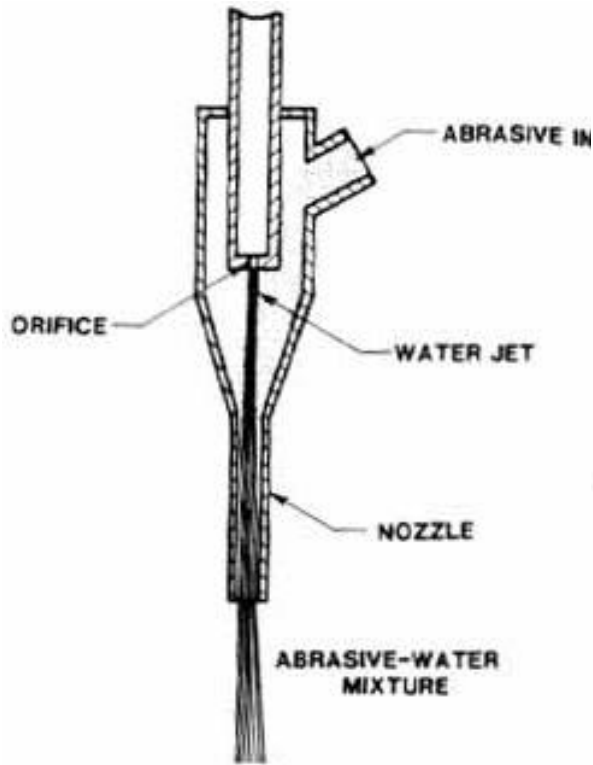


Figure 1. Typical Nozzle Configuration for Mixing Abrasive with Water Jet in an Abrasive Water Jet Cutting Head. (Adapted from Hashish, Reference (1)).

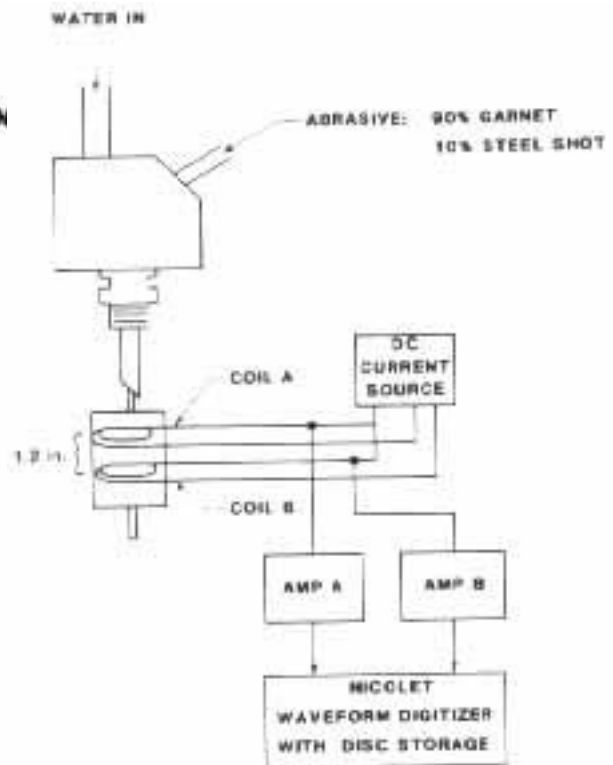


Figure 2. Experimental arrangement for measuring particle velocity in an abrasive waterjet cutting stream.

Initial experiments with the method are illustrated in Figure 3. Here, an air driven pellet from a pellet gun was fired through the coil assembly, and the transit time determined by means of a Nicolet transient recorder. The signal from the spherical pellet is shown by the repeated waveform, displaced by the transit time. The velocity of the pellet, approximately 252 feet-per-second is calculated from the measured transit time of 397 microseconds.

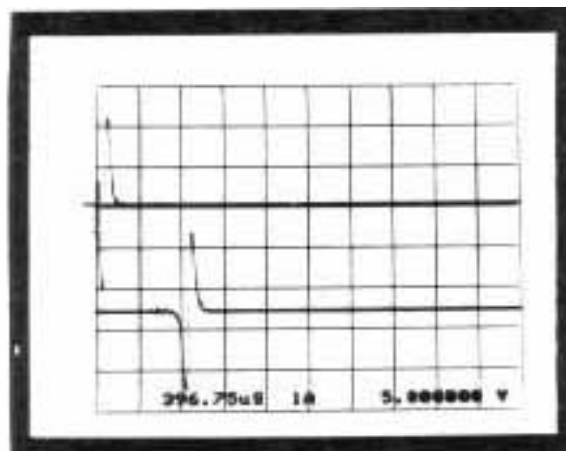


Figure 3. Signal Produced by a Lead Pellet Fired by Pellet Gun Through the Coil Assembly Shown in Figure 2.

An abrasive frequently used in abrasive water jet cutting is garnet sand, which is nonmagnetic and non-conducting and, consequently, will not produce a signature from the measurement coil system.

Furthermore, the large number of particles in an effective cutting stream makes it impractical to detect individual particle velocities in the manner just described. Consequently, it is desirable that the abrasive stream be “seeded” with a few particles to which the instrumentation will respond. A number of materials were tried, but the one most effective was ordinary chilled steel shot, which can be obtained in any mesh grade. These magnetic particles were mixed with the garnet abrasive in ratios typically in the range of 10% of the total mass.

### EXPERIMENTAL RESULTS

Typical results of the particle velocity measurements are illustrated in Figure 4. Here, the top trace represents signals from the first coil, while the bottom trace represents signals from the second coil. The record has been triggered by a particle in the first coil at  $T = 0$ . This particle, marked “1a” in the figure, is recorded by the second coil, marked “1b”, 397 microseconds later. A later signal, marked “2a”, coincidentally occurred during the sweep period, and is also seen by the second coil as signal “2b”. These two particles have calculated velocities of 252 and 243 feet-per-second, respectively. A third particle, “3a” is repeated by the second coil at “3b”.

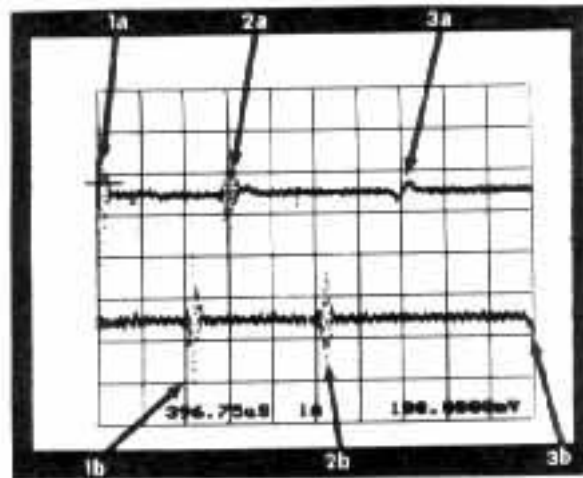


Figure 4. Signals from magnetic Particles in an Abrasive Water Jet Stream at a Water Pressure of 20 ksi.

Notice that the signals produced by these particles also have distinct temporal characteristics. When the sweep time is increased to show the individual signals in detail, their exact nature can be observed. In Figure 5, one such signal appears as a sinusoidal burst. We believe this is characteristic of a rotating particle, which in this case, has a rotational period of 13.5 microseconds, equivalent to a rotational velocity of 4.4 million rpm. Rotational velocities ranging from a few thousand rpm to more than five million rpm have been recorded. These apparent rotational characteristics are interesting, but no particular physical significance is attached to the phenomenon as a cutting parameter at this time.

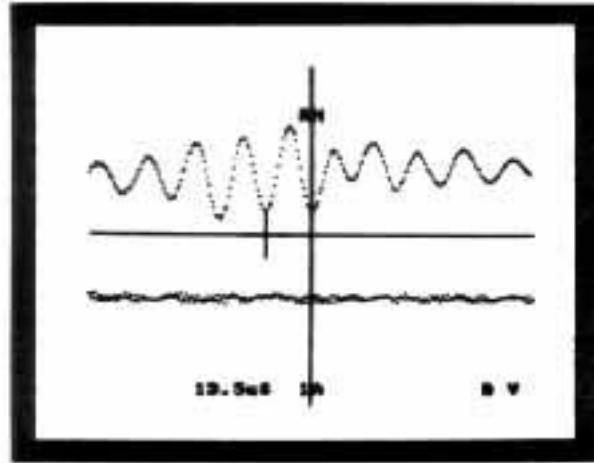


Figure 5. Expanded Signal from an Individual Particle Showing the Modulation Produced by Rotation.

Figures 6 and 7 present additional particle signatures of the same type. The velocity among individual particles detected was found to vary widely under similar pressure and flow conditions.

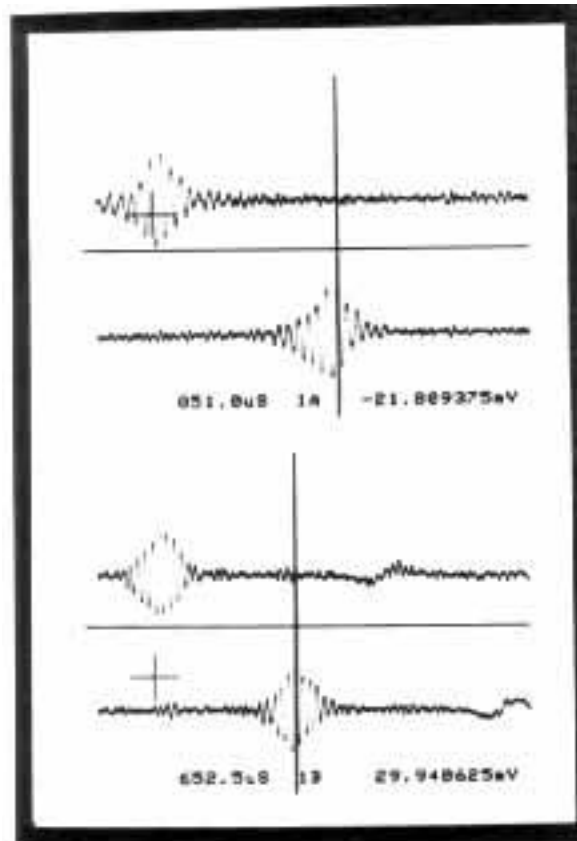


Figure 6. Signal from Individual P particles at Water Pressure of 10 Ksi. The Transit Times are Indicated on the Photos.

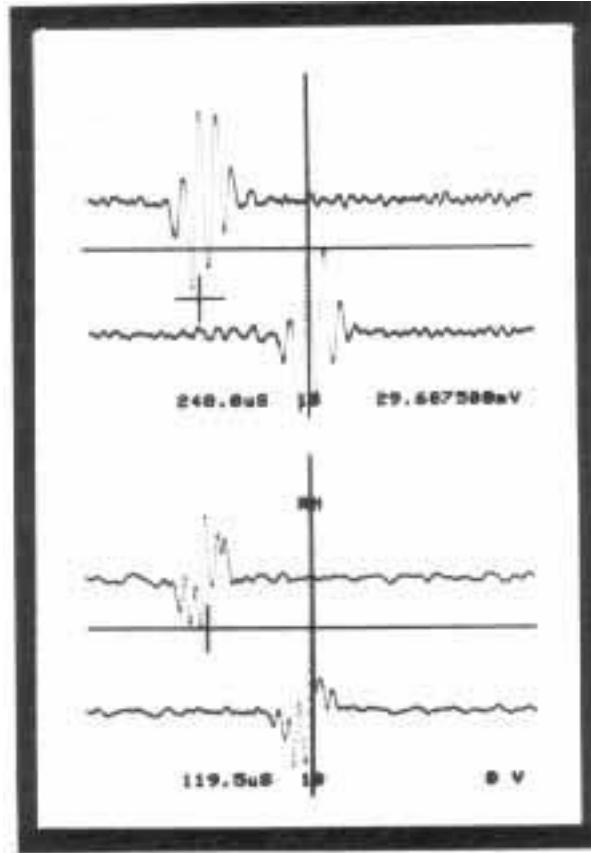


Figure 7. Individual Particle signatures at Water Pressure of 30 Ksi.

Average velocity and minimum and maximum values of particle velocity were tabulated for cutting streams at various pressures up to 35,000 psi. At least twenty individual cases at each pressure formed the statistical basis for calculating the average values.

#### WATER JET VELOCITY

To evaluate the velocity of the water jet prior to injection of abrasives, two methods were employed. First, the stream velocity was calculated theoretically from Bernoulli's equation as follows:

$$V_w = \sqrt{\frac{2P}{\rho}} \quad (4)^1$$

where:

P = pressure drop across orifice

The force of the water jet stream was also measured with a load cell, and this value used to calculate the water jet velocity using the equation

$$V_w = \frac{F}{\rho A} \quad (5)$$

<sup>1</sup> An error in the manuscript was corrected by the transcription for this equation

where:

- $V_w$  = water velocity
- $F$  = measured force of water jet
- $\rho$  = water density
- $A$  = axial surface area of water jet

These two methods of calculating the water jet velocity produce results which generally agree as shown in Figure 8. In this figure also appears a plot of the results of the particle velocity measurements described in the previous section. Notice that at a representative pressure of 30,000 psi, the water jet velocity is in the range of 2,000 feet-per-second, while the corresponding average velocity of the steel shot, mixed with 60 - 80 mesh garnet sand, is only about 500 feet-per-second.

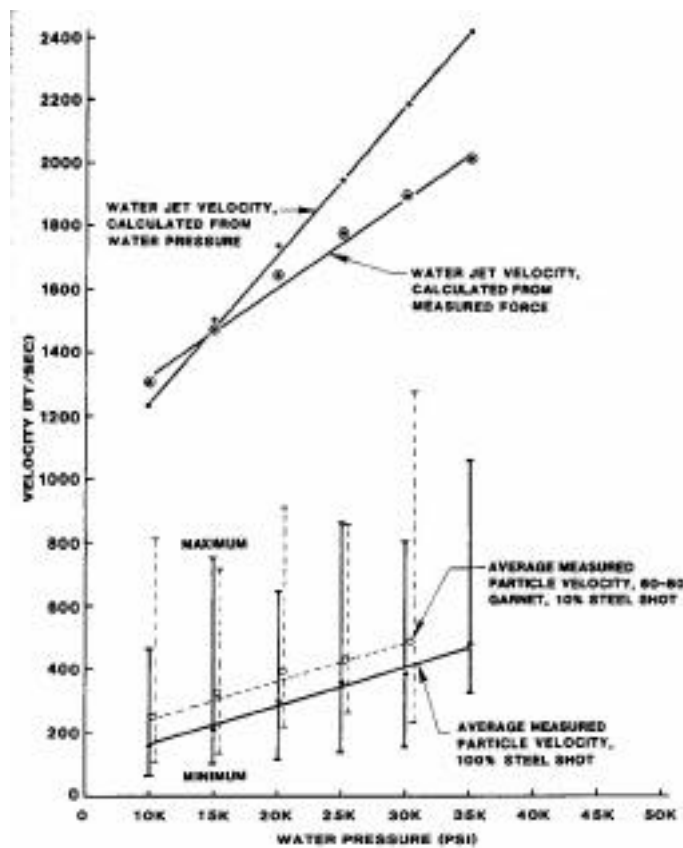


Figure 8. Summary of Abrasive Particle Velocity measurements with Corresponding Calculated water Jet Velocities. Each Bar Represents the Spread of at Least 20 Individual Measurements at each Pressure.

## CONCLUSIONS

The current method of mixing abrasive particles with a high velocity water jet stream has limited effectiveness. Abrasive particles enter the mixing chamber at essentially zero velocity and encounter the water jet which has a velocity ranging up to 2,000 feet-per-second or more. The majority of particles have no chance of penetrating the jet and instead bounce off into the nozzle walls. Particles which enter the jet at its

periphery tend to stay at the periphery without further penetration. If the particles could be injected directly in the center of the jet, they should acquire essentially the full jet velocity within an inch or less of travel. Since no particle velocities of this order have been observed, it is fair to assume that present mixing and acceleration of the abrasive by means of the water jet is a superficial and relatively inefficient process. Considerable gain in the effectiveness of abrasive water jet cutting can be expected as more effective means of accelerating the abrasive particles are developed.

REFERENCES:

1. Hashish, M., "A Modeling Study of Metal Cutting with Abrasive Water Jets" Trans. ASME, Vol. 106, January 1984, pp. 88-100.
2. Bitter, J.G.A., "A Study of Erosion Phenomena-Part I," Wear, Vol. 6, 1963, pp. 5-21.

# HYDRO-ABRASIVE CUTTING HEAD—ENERGY TRANSFER EFFICIENCY

G. Galecki and M Mazurkiewicz  
High Pressure Waterjet Laboratory  
University of Missouri-Rolla  
Rolla, Missouri

## ABSTRACT

Both the abrasive particle milling effect and the transfer of energy that take place between the water nozzle exit and the slurry nozzle inlet are introduced as criteria that can be applied in the evaluation of the effectiveness of the hydro-abrasive cutting head design. This paper presents the results and general conclusions drawn from a test program designed to investigate both of these effects.

## NOMENCLATURE

d	water jet nozzle diameter/injection nozzle diameter
D	slurry nozzle diameter/receiving pipe diameter
S	standoff distance between waterjet nozzle exit and slurry nozzle inlet
M	abrasive mass flow rate
$P_1$	supply system pressure
$P_2$	slurry nozzle inlet dynamic pressure
PT1	pressure transducer for $P_1$
PT2	pressure transducer for $P_2$

## INTRODUCTION

The hydro-abrasive jet has now been accepted as a cutting tool by a wide variety of industries. The ability of an abrasive waterjet to cut materials traditionally considered difficult to machine, such as titanium, ceramics or honeycombed components is unmatched by alternative mechanical or thermal cutting techniques - the problems of material de-lamination and thermal deformation along the cutting path being eliminated.

The effectiveness of hydro-abrasive jets in such cutting applications depends on the energy which can be imparted to the abrasive particles. Many existing cutting head designs are based on the concept of entraining the abrasive grains in either single (See Fig. 1) or multiple water jets within the head.

In both cases the relatively low velocity abrasive grains are accelerated to the resultant velocity of the slurry jet. This process can be compared to that of a collision between the granular and water streams. The resulting reduction in abrasive particle size absorbs a portion of the water jet's kinetic energy. Thus the efficiency of the abrasive acceleration process is reduced as is the maximum slurry jet velocity attainable.

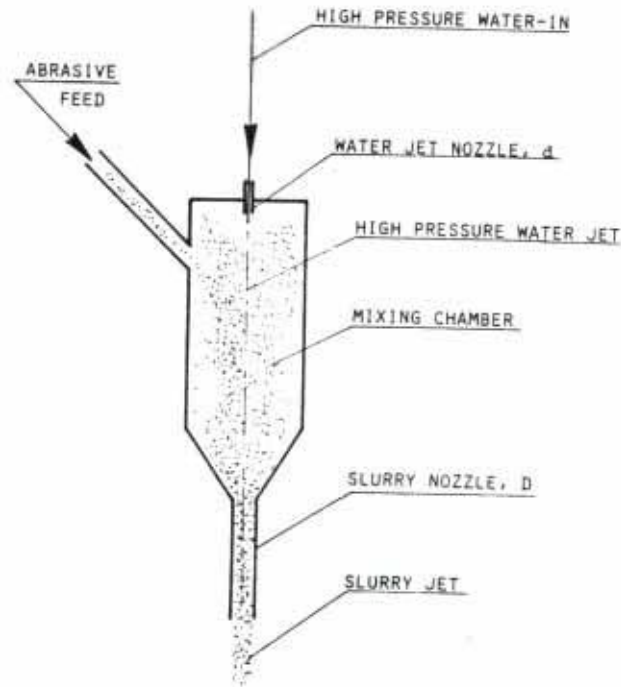


Figure 1. Single jet, side feed hydro-abrasive cutting head.

#### MILLING EFFECT - APPARATUS, PROCEDURE AND EXPERIMENTAL RESULTS

This effect was investigated by conducting a series of tests for each of the three initial main fraction garnet grit sizes of 425  $\mu\text{m}$ , 250  $\mu\text{m}$  and 150  $\mu\text{m}$ . The slurry ejected from the horizontally mounted side feed type cutting head was directed into a PVC pipe, 4.2 m long and of diameter, 0.152 m (See Fig. 2).

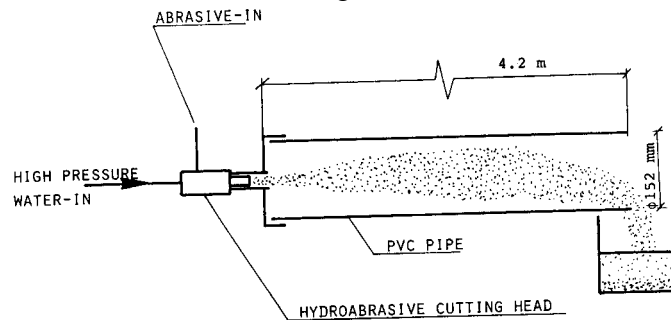


Figure 2. Ejected abrasive particle collection in PVC pipe.

The ejected particles were collected and dried out. A sieve analysis was then made to determine the ejected particle size distribution by weight. Both the test conditions and the corresponding distributions obtained are shown in Fig. 3.

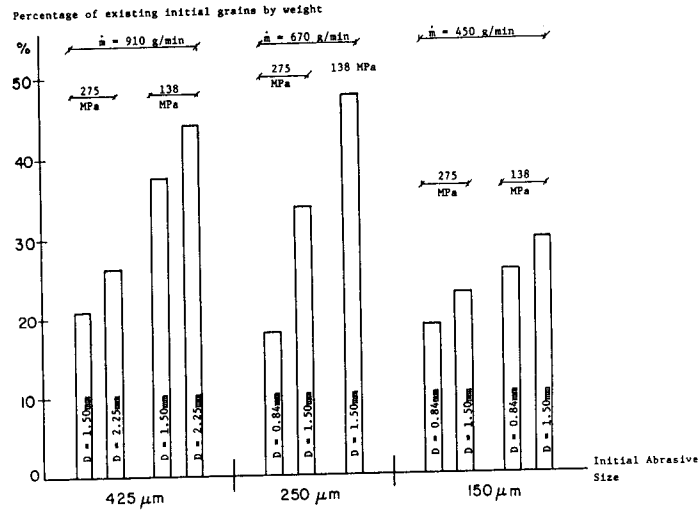


Figure 3. Percentage of initial abrasive particles remaining intact after ejection from slurry nozzle - for various test conditions.

All tests were conducted with a water nozzle diameter  $d$ , of 0.35 mm. The slurry nozzle diameter,  $D$  was varied according to the abrasive grit size used. A McCartney Streamline unit was used to supply the cutting head with water at the two pressure settings investigated - 138 MPa and 275 MPa.

From this part of the test program the following conclusions can be drawn:

- as the slurry nozzle diameter is increased, the disintegration of the abrasive particles within the head becomes less intensive.
- 70% to 80% of the initial abrasives were disintegrated.

Thus, for the given test conditions, only 20% to 30% of the particles, completed the acceleration and ejection process intact.

## PRESSURE TRANSFER - APPARATUS, PROCEDURE AND EXPERIMENTAL RESULTS

As stated earlier, many existing cutting head designs employ a small diameter water jet to accelerate the abrasives. The water is pressurized and then expelled through a sapphire nozzle of diameter  $d$ . This water jet and a secondary stream of abrasives are then introduced into the carbide abrasive nozzle of diameter  $D$ . The momentum transfer between the waterjet and the abrasives is a very complicated phenomenon. The dynamic stability of the high pressure waterjet is one of the system parameters on which this transfer process depends. Hence, the distance between the exit of the water nozzle and the inlet of the slurry nozzle is critical. This stand-off distance  $S$  plays a very important role.

Investigation of the importance of this distance began by conducting a series of tests in which a pure waterjet was injected into a receiving pipe the standoff distance test-parameter being varied from 0 to 24 mm,(2). Each test run was conducted with a receiving pipe diameter,  $D = 0.80$  mm and a series of high pressure water nozzle diameters,  $d = 0.53$  mm, 0.81 mm and 1.04 mm. Both the injection pressure  $P_1$  and the

receiving pressure  $P_2$  were recorded using the special apparatus illustrated in Fig. 4. Results of these tests are presented in Fig. 5.

The pressure ratio,  $P_1/P_2$ , has been found to depend on the accuracy of the nozzle and pipe alignment. The optimum position for the receiving pipe was determined by a step by step positioning of the X-Y table as shown in Fig. 4. This optimum position is defined as that point at which the receiving pressure  $P_2$  is a maximum, (see Fig. 6).

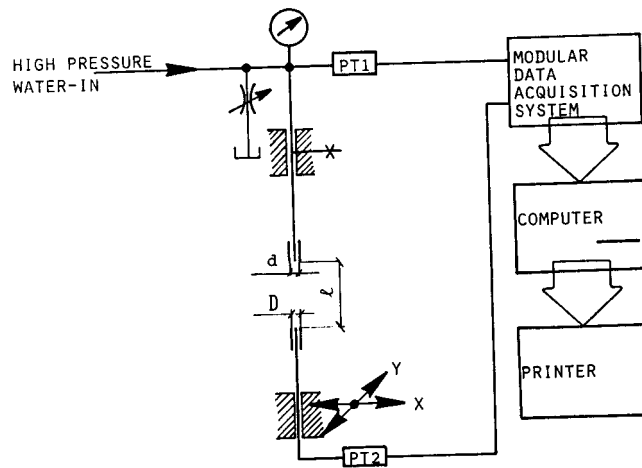


Figure 4. Schematic of test rig arrangement for pressure transmission measurements.

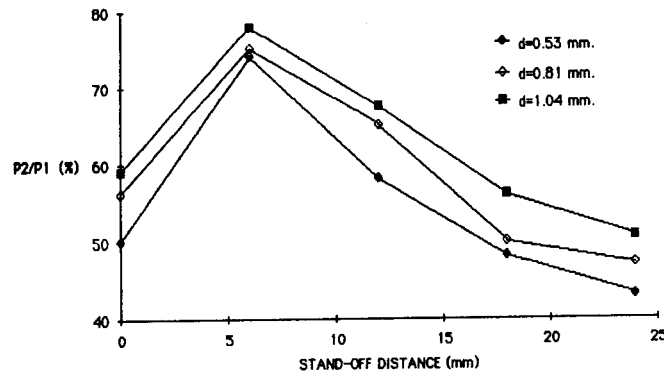


Figure 5. Pressure transmission ratio,  $P_1/P_2$ , as a function of stand-off distance,  $S$ .

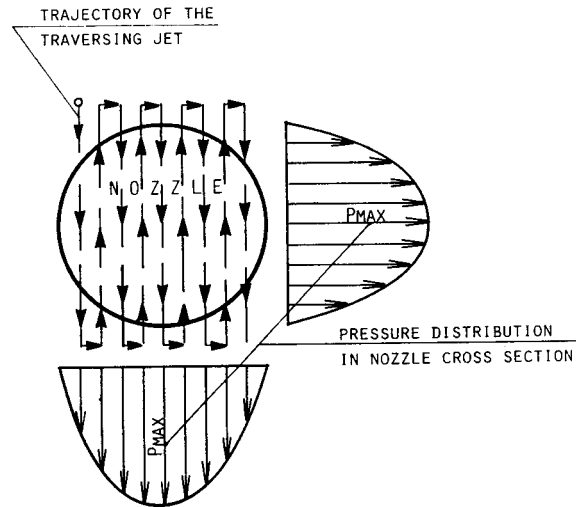


Figure 6. Location of optimum receiving pipe position relative to water nozzle - using receiving pressure,  $P_2$  as selection criterion.

All tests utilized water jets generated by a Hammelmann pump. This limited the tests to a single operating pressure of 84 MPa.

The following remarks can be made concerning the results obtained in this part of the investigation:

- the pressure within the receiving pipe,  $P_2$ , depends on the ratio of the injection nozzle and receiving pipe diameters.
- as the ratio,  $d/D$ , is increased the receiving pipe pressure  $P_2$  increases up to a maximum of 80% of the injection pressure,  $P_1$ , for the given test conditions.
- the pressure  $P_2$  is strongly dependent on the standoff distance,  $S$ , between the water nozzle and the receiving pipe. The above conclusion is very important from the point of view of optimizing the hydro-abrasive head design.

## CONCLUSIONS

Based on the experimental results presented in this paper the following conclusion can be formulated:

Both the disintegration of the abrasive particles prior to ejection from the cutting head and the pressure transfer that takes place between the water nozzle and the slurry nozzle can be used as criteria in evaluating the effectiveness of the hydro-abrasive cutting head design.

These factors should be considered in future cutting head design evaluations (3) in order to optimize the many technical and economic advantages associated with this rapidly growing technology.

## ACKNOWLEDGEMENTS

This work was supported both by the McCartney Manufacturing Co. Inc., Kansas and the Department of Energy, Pittsburgh. Special thanks are due to Lalith Wijeratne and Louis Finucane for their technical assistance.

## REFERENCES

1. Mazurkiewicz, M., Galecki, G., Olko, P., "Testing and Development of a Data Base for a High Pressure Hydro-abrasive Cutting System and its Improvement", Final Report for McCartney Manufacturing Co. Inc., Division of Ingersoll Rand, March 1986, University of Missouri-Rolla, USA.
2. Mazurkiewicz, M., Galecki, G., Technical Progress Report #1 for Department of Energy Contract, DOEDE-AC22-86PC91271, October 1986, University of Missouri-Rolla, USA.
3. Mazurkiewicz, M., Galecki, G., "High Pressure Hydro-abrasive Cutting Head", Patent disclosure 87UMR-007, University of Missouri-Rolla.

## WATER JET ASSISTED LONGWALL SHEARER: DEVELOPMENT AND UNDERGROUND TEST

E. D. Thimons, Supervisory Physical Scientist  
Pittsburgh Research Center, Bureau of Mines  
Pittsburgh, Pennsylvania

K. F. Hauer, Technical Director  
Geswerkschaft Auguste Victoria  
Marl, Federal Republic of Germany

K. Neinhaus, Project Supervision  
Gebr Eickhoff Maschinenfabrik u.  
Eisengie Berei mbH  
Bochum, Federal Republic of Germany

### ABSTRACT

About 20 percent of the underground coal production in the United States comes from longwall mining and indications are that the number of longwall shearer operations will increase significantly over the next 10 years. The productivity advantages of longwall shearer operations over continuous miner operations have been well documented. However, longwall shearers experience many of the same problems as continuous miners in the process of cutting coal. Chief among these are a high percentage of down time due to vibrational wear and tear on the machines, high cutting tool wear, unacceptable dust levels, and a high percentage of product fines. When a longwall shearer cuts coal, the cutting forces are usually more than adequate to keep vibration to a minimum and cutting tool wear is not too high. However, when the shearer encounters rock bands in the coal or rock intrusions, or when rock must be cut in the roof or floor, there is a marked increase in machine vibration and in tool wear and failure. Cutting rock also increases the quartz content of the generated dust.

Research has shown that water-jet-assisted cutting, the process of using a moderate pressure water jet to assist a mechanical cutting tool, can improve cutting in the same harder rock types, reduce cutting tool wear and failure, reduce the percentage of product fines, and result in significant reductions in airborne respirable dust. To date, most water-jet-assisted cutting research has been done in the laboratory, often under conditions not representative of the underground mining environment. The U.S. Bureau of Mines, through a contact with Eickhoff Corporation, has retrofitted a longwall shearer with water-jet-assisted cutting capabilities up to 700 bar (10,000 psi) for testing in underground coal mines. This contract calls for an inmine evaluation of this machine in two mines, one in West Germany and the second in the United States.

The first underground test of this machine took place in the Auguste Victoria Coal Mine in Marl, West Germany from June through November, 1986. During the course of this test the shearer's performance at various water jet pressures was recorded in terms of shearer energy consumption, dust generation, product fines, and bit wear. These results

were compared to the shearer's performance at its conventional water spray pressure. Operating the shearer at the higher water pressures did not result in any statistically significant reduction in the shearer motor energy consumption, although there was a great deal of scatter in the data. However, an 80 percent reduction in respirable dust generation occurred. This was realized at a water jet pressure of only 155 bar (1,800 psi). Increasing the water pressure above this level did not result in any further dust reduction. Operating at water-jet-assist pressures also resulted in an increase in the average size of coal cut, which translates into a decrease in product fines. Finally, while no controlled measurement of bit wear as a function of water jet pressure was made, the mine personnel reported that the shearer bits lasted longer when water-jet-assisted cutting was being done.

## NOMENCLATURE

°C	degree Celcius
ft	foot
fpm	foot per minute
gpm	gallon per minute
gal/yd <sup>3</sup>	gallon per cubic yard
in	inch
kW	kilowatt
l/mln	liter/minute
l/m <sup>3</sup>	liter per cubic meter
m	meter
mm	millimeter
m/s	meter/second
psi	pound per square inch
rpm	revolution per ,minute

## INTRODUCTION

In 1984, Gebr. EICKHOFF Maschinenfabrik und Eisengie Berei mbH received an order from the U.S. Bureau of Mines under a research project to equip a shearer with a high-pressure water supply system and to carry out two underground trials. The first of these trials took place in the second half of 1986 at the Auguste Victoria Coal Mine in Marl, West Germany.

This order must be seen against the background of the numerous international research and development activities in the field of jetassisted cutting which serves the purpose of assisting the mechanical cutting tool with a high-pressure water jet which is directed immediately in front of the pick tip (Fig. 1). The effects expected from the high-pressure water assistance are:

- reduction of the pick wear and extension of the pick life by cooling and "lubricating" the tip of the pick;
- reduction of the cutting and thrust forces by flushing the cushion of fines away from the tip of the pick;

- reduction of the proportion of fines in the coal cut due to the possibility of increasing the penetration depth and the cutting line spacing;
- smooth operation of the machine due to reduced vibration and lower dynamical forces;
- reduced hazard of methane ignition by cooling the pick tips and extinguishing sparks;
- reduction of the dust make by the immediate suppression of the dust at the point where it is produced.

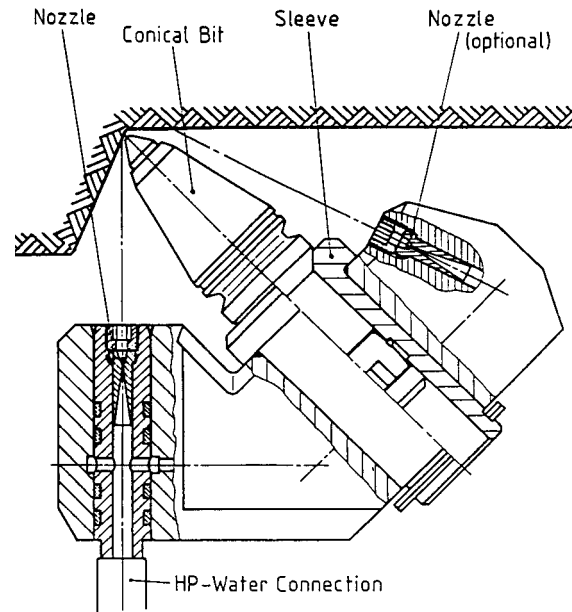


Figure 1. Pick boxes for high-pressure water jet assistance.

## BACKGROUND

The research results obtained in the laboratory (1) were so encouraging that the Bureau of Mines decided to award a research contract in order to have the known positive effects confirmed underground on a shearer and to render them serviceable.

The aim of the research project was to develop a high-pressure water supply for longwall shearers for a pressure up to 700 bar, and to manufacture and install it underground. An essential part of the effort was to provide a phased high-pressure water supply to the picks, so that the water is only supplied to those picks which are engaged in the coal at any given time in order to keep the water consumption and the necessary pump power as low as possible (Fig. 2).

The circumferential speed of the water jet assisted picks had to be reduced as far as possible. In order to achieve this, a reinforced ranging arm for a low drum speed was to be used without an increase of the motor power. Moreover the necessary measuring technique had to be provided and installed in order to evaluate and to quantify the effects of the high-pressure water jet assistance.

The first trial was carried out in cooperation with Gewerkschaft Auguste Victoria Mine in Marl, West Germany.

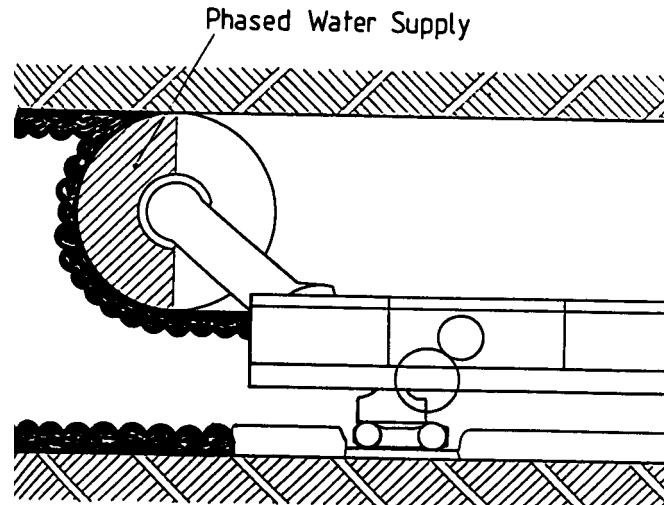


Figure 2. Phased water jet assistance.

### SHEARER DESIGN

The concept of the trial equipment was based on the use of a single-ended ranging drum shearer loader in order to keep the technical scope of the conversion within admissible limits and in order to find an easier solution for the problems involved with the high-pressure water and power supply. Therefore an EW200/170-L shearer of the proven series 200-L powered by a 170 kW drive motor was chosen. At the Auguste Victoria Mine, machines of this type have been successfully operating for many years and used for many different tasks in the face end area.

As the available research results did not give a clear indication as to the water pressure and flow rate required, the trial equipment was designed for an upper limit of 700 bar (10,000 psi) and 120 l/min (31.7 gpm). The necessary space for the drive motor and the pump had to be provided.

All components of the high-pressure water supply system were combined in a package mounted on a trailer which was pulled by the shearer. The high-pressure station included the following main components:

- fine filter in the entry
- 5-piston high-pressure pump
- drive motor
- automatic pressure regulator with safety device
- electrical monitoring with switchgear
- detection and transmission of measured values.

The low-pressure water supply was ensured by the water distributor of the shearer at a pressure of approximately 25 bar (362 psi). The increased requirements which had to be met by the filtering system for the water for the high-pressure station were taken into account by the installation of an automatic back flush filter in the headgate roadway and a standard back flush filter on the shearer with 50 micron fineness.

The conversion set for the shearer included a new ranging arm with double planetary gearing for a drum speed of only 23.6 rpm, a phasing valve and a new cutting drum.

The development of the new phased water supply system for a pressure of up to 700 bar (10,000 psi) required a lot of preparatory work and a great number of test stand examinations. Different concepts were developed and tested:

- a) single pick control whereby the pick force is used for opening the associated valve;
- b) mechanical sector control whereby a slide valve feeds the high pressure water to one half of the cutting drum which is divided into sectors;
- c) electrical or hydraulical sector control whereby electrically or hydraulically controlled high-pressure water feed the necessary sectors of the cutting drum.

The criteria for the selection, i.e., reliability, water consumption, expense, and efficiency, resulted in the installation of the so-called mechanical sector control (Fig. 3).

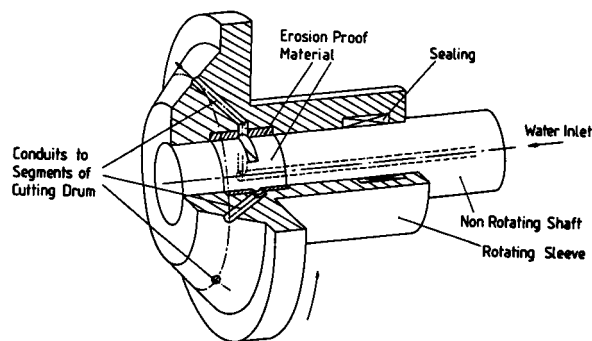


Figure 3. Phased rotary bushing (phasing valve).

The cutting drum with high-pressure water supply represents a completely new design with regard to the water channeling and the pick lacing plan.

The drum having a diameter of 1700 mm (67 in) and a web depth of 850 mm (33.4 mm) was divided into 10 sectors in which the water supply was ensured by manifolds and high-pressure hoses. The sector control was arranged to feed the water to five of the ten sectors. Fifty of the 51 picks on the cutting drum were connected to the high-pressure water supply.

The measured average feeding angle amounted to 195 degrees which means that only 54 percent of the water which would have been required to provide water to every pick was needed.

The pick box (Fig. 4) was especially designed for the requirements of the research installation. The high-pressure water emerged via a connection piece in each box directly in front of the pick.

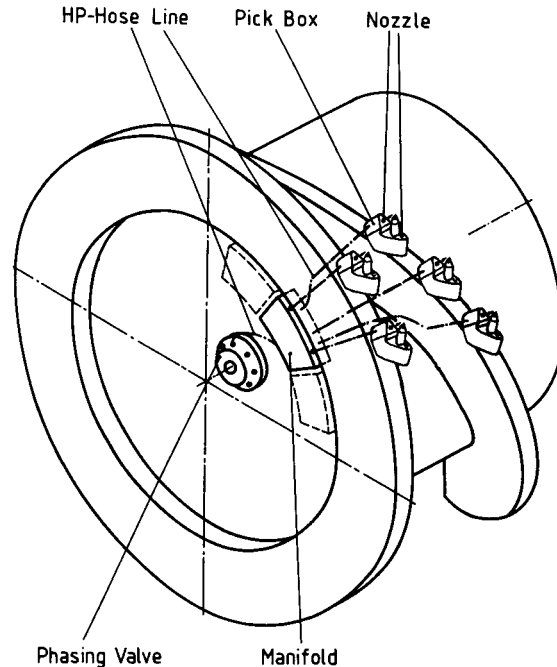


Figure 4. High-pressure cutting drum

A nozzle was screwed into each of these connection pieces leaving the required small distance to the pick tip. In addition, the pick box was provided with a water channel for pick back flushing in order to assess the effectiveness of this type of water supply as an alternative.

As the high-pressure equipment had to be installed on a production face, all elements had to be extremely reliable right from the beginning, and it was necessary to operate alternatively with and without high-pressure water supply.

#### DATA COLLECTION

The success of an underground trial depends highly on the measuring techniques applied to assess the results.

The data collection and transmission system was therefore carefully selected and installed. The measured values - i.e., cutting motor performance (amperage and voltage), haulage pull, traveling speed and incident signals - were recorded on the surface.

All other data - such as water pressure, nozzle diameter, actual cutting depth of the machine, etc., were measured on the face. Cutting samples for a screen analysis were taken from the conveyor.

The respirable dust produced by the shearer loader with high-pressure water assistance was measured in front of and behind the machine in the direction of the ventilating current by means of two dust measuring devices. The absolute and specific dust make was obtained by subtraction of the two dust concentrations whereby the volume of the ventilating current and the quantity of the material extracted were taken

into account. As far as possible no other work producing dust, such as shifting of the roof supports, was carried out during the dust measurements.

[The main department for dust control and the prevention of pneumoconiosis of the BergbauForschung GmbH and the dust control department of Gewerkschaft August Victoria were in charge of the dust measurements.

## SHEARER INSTALLATION

The high-pressure equipment was installed in district 58, seam D/C (general designation C 1/ 2/B) of Auguste Victoria Mine in the middle of June 1986. The main data on the face and the face equipment are summarized in table 1. The face is 2.3 m (7.54 ft) in thickness and is worked on the retreat.

The working range of the face end machine had a length of about 50 m (164 ft) and, as planned, this machine had to cut through a fault.

Prior to the installation of the high-pressure equipment, the face end machine, EW-200/ 170-L, was equipped with a ranging arm which had an output speed of 48 rpm, and which carried a cutting drum with exponential base body. The drum had a diameter of 1600 mm (63 in) and a web depth of 850 mm (33.5 in). For dust suppression it was equipped with conical spray nozzles fed with a pressure of less than 25 bar (362 psi) at a flow rate of approximately 40 l/min (10.6 gpm). Forty-one of the 55 radial picks of the cutting drum were equipped with water sprays.

After the installation of the high-pressure equipment, the system was immediately ready to start operation.

In order to avoid any danger for the personnel at very high pressures, an automatic face end switching off system was provided. The trailer with the high-pressure station proved to be no hindrance despite this being an initial concern.

The annoyance due to water mist and additional noise as well as the danger due to high-pressure jets were at a minimum at pressures of below 200 bar (2,900 psi) as the water was only sprayed off in the direction of the face. It was therefore possible to permanently operate the system at a pressure ranging from 100 to 150 bar (1,450 to 2,175 psi).

During the trial operation at pressures of 500 and 700 bar (7,250 and 10,000 psi) the machine operator was provided with protective glasses and the face team had to keep a safety distance of about 4 m (13 ft) ahead of the cutting drum.

The risk or danger did not emanate that much from the high-pressure water jets but rather from the coal and rock particles which were carried along by the water jets. However, owing to the phased water supply system this danger only arose in the working direction in front of the machine. The face end switch or facility ensured that the machine

could not enter, under any circumstances, the roadway with the high-pressure water supply system operating.

The installation of two safety valves on the one hand and the provision or adequate precautions on the other protected the staff from the risk arising from high-pressure parts bursting solely due to the internal pressure. Likewise, the danger or leakage or cracking caused by additional, external influences could virtually be excluded since all parts were positioned under solid covers. The high-pressure hose for the connection from the ranging arm to the pump was additionally fitted with a protective sheath for protection against wear.



Figure 5. High-pressure water jet assistance in operation.

## TEST RESULTS

All measurements were taken when the upper section was cut traversing towards the tail gate. The traveling speed of the machine was kept constant as far as possible.

The measured results of the respirable dust make are shown in Fig. 6. Owing to the installation of the new equipment, a drastic reduction in the dust make was evident. A relatively low pressure of about 125 bar (1,812 psi) and a water quantity of about 42 l/min (11.1 gpm) was sufficient for dust control. This is equal to the usual quantity of water required for conventional dust suppression with a low-pressure water supply system.

An increase of the pressure to 500 bar (7,250 psi) and the concurrent increase of the water quantity to 79 l/min (20.9 gpm) did not result in any considerable improvement in dust control. The slight increase in the dust make at 125 bar (1,812 psi) and 80 l/min (21.1 gpm) was probably due to the failure of two water sprays as a result of plugging.

The dust make on this face was extraordinarily high. This was confirmed by measurements on other faces. Nevertheless the new equipment with high-pressure full jets managed to suppress 70 to 80 percent of the dust produced by the conventional equipment. An important contributory factor might have been the phased water jet assistance which only feeds water to the dust producing picks. At a feeding quantity of 42 l/min (11.1 gpm), the additional water content of the coal amounted to 12.5 l/m<sup>3</sup> (2.52

gal/yd<sup>3</sup>). Another important influencing variable for the dust make was certainly the low speed of the cutting drum and the resulting cutting speed of the picks of 2.1 m/s (413 fpm).

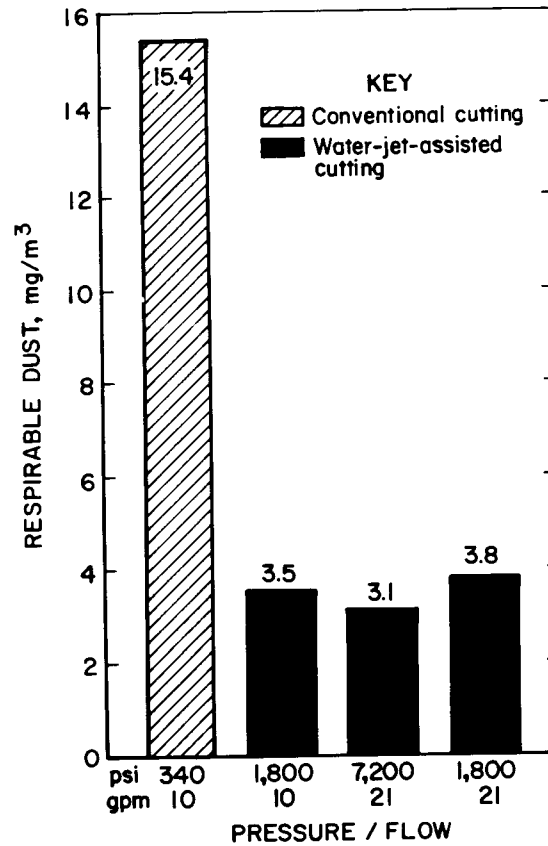


Figure 6. Fine dust make with the shearer loader EW 200/170-L with the conventional equipment and with high-pressure water jet assisted cutting drum.

To summarize, it can be said that a number of measures enabled a drastic reduction in the dust make of the shearer. Since these measuring results were obtained on a specific face, they naturally cannot be universally transferred to other mining operations. However, the magnitude shown in this paper has been confirmed by other researchers (2,3,4).

The screen analysis of coal samples taken from the conveyor indicates an improved grain structure owing to the use of the new cutting drum. The grain proportion below 6.3 mm, for example, could be reduced from 37 to 28 percent. The loading characteristics of the three start cutting drum at a speed of 24 rpm were judged to be considerably superior to those of the previously used drum and cowl.

In the absence of an adequate, easily applicable criterion for the loadability of a drum, the statements must be restricted to subjective impressions at this point.

The measurements of the cutting power and of the haulage pull as well as the resulting specific energy and the specific drum thrust were characterized by an extraordinarily wide dispersion of the values measured.

It is likewise problematic to give a differentiated statement on how far these values are dependent on the water supply pressure. As an example, Fig. 7 shows the specific cutting energy (kilowatt hours per cubic meter) of the mining operation as a function of the nozzle pressure.

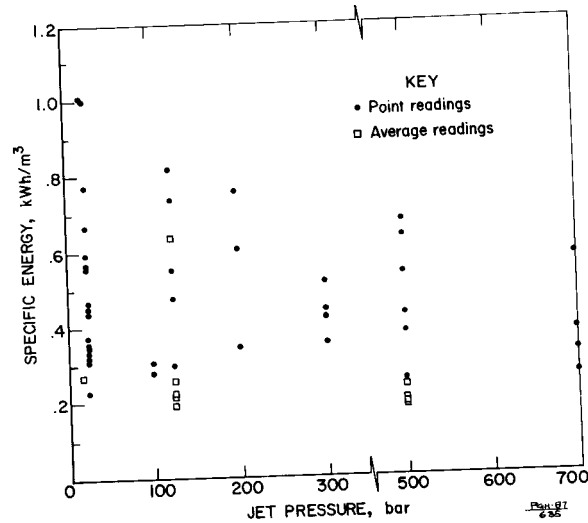


Figure 7. Specific cutting energy of the high-pressure assisted cutting drum as a function of the nozzle pressure.

Regression analysis and careful studies lead to the conclusion that only a very slight reduction in the specific energy results from the water supply pressure. In this case, the power required to supply the water jets has not yet been taken into account. The measurements are divided into short and long period readings.

The tendency noticed here of an only minor influence exerted by the nozzle pressure can be similarly discovered in the other measured values. Neither the cutting power, nor the haulage pull with the resulting specific drum thrust show a meaningful reduction with the nozzle pressure increasing.

To summarize, it can be said that the high-pressure water jet assistance only has minimal direct influence on the forces at the pick of a cutting drum. This result comes as no surprise. Concurrently with this project, single pick trials with high-pressure water jet assistance have been carried out in cooperation with the department for mining and face conveyor technique of the Bergbau-Forschung GmbH (5). These trials clearly showed that the direct influence of the high-pressure water jets on the force reduction at the pick is reduced with the increase of the cutting speed of the pick.

At approximately 2 m/s (393 fpm), as in the present case, the force reduction is below 15 percent. This result is confirmed by the underground trials.

However, the high-pressure water jet assistance considerably influences the wear of the picks and particularly when harder rocks, such as were seen in the fault zone, are cut.

Fig. 8 shows the wear conditioned force increase at a dry cutting pick and at a high-pressure water jet assisted pick. The cutting forces are scarcely influenced. The thrust forces, however, show a difference of about 25 percent, with increasing tendency, after only 1600 m (5,250 ft) of cutting, which corresponds to 13 minutes of shearer operations. In line with this curve, decisive differences in the lifeline of the picks are to be expected. Measurements have shown that the temperatures of the pick tip can be reduced from more than 350° to 120° C (Fig. 9).

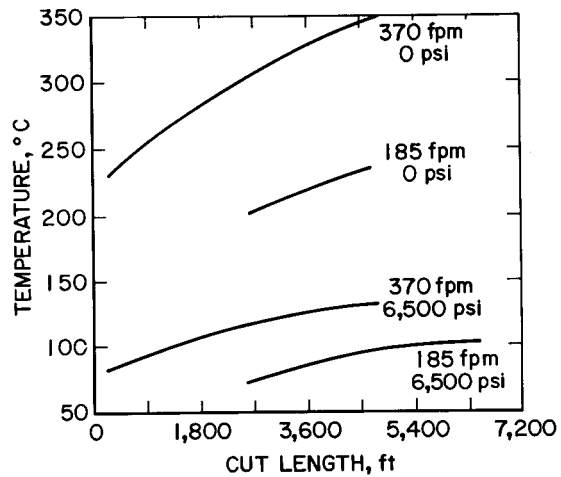
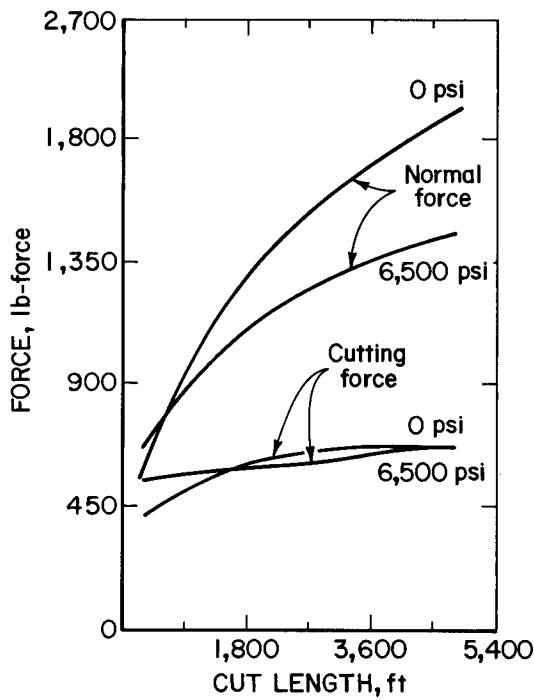


Figure 8. Wear conditioned force increase at cutting pick with and without high-pressure water jet assistance.

Figure 9. Pick temperature as a function of water jet assistance.

During the trial operation of the high-pressure water jet assisted shearer, the high-pressure equipment has proved its reliability. Major problems did not occur. Filters, pumps, valves, sector control and the high-pressure drum operated satisfactorily.

Several of the initially used full jet sapphire nozzles clogged externally, which always became apparent after the operation without high-pressure water jet assistance. In each case, however, the clogging could be eliminated again by switching on the pump

and by setting a pressure of about 150 bar (2,175 psi). The subsequently used full jet nozzles did not show this problem.

The fitting of the high-pressure connection in the pick boxes proved to be a weak point. Unexpected, high axial forces due to coal fines and rock occasionally resulted in the fitting being sheared off. This problem was overcome by the reinforcement and modification of the axial lock.

## CONCLUSIONS

The water jet assisted cutting results summarized in this paper were obtained in an underground trail at the Auguste Victoria Coal Mine in Marl, West Germany. The system tested consisted of the following:

- High-pressure water jets to assist in the cutting operation and directed immediately in front of the pick tip;
- Phased high-pressure water only to those picks which are engaged in the coal;
- Reduction of the drum speed and consequently of the pick speed;
- Pick lacing plan on the drum to optimize cutting.

The results of the trial show that the respirable dust is drastically reduced with water pressures around 125 bar (1,812 psi). The grain size distribution of the coal improved while the pick wear and the temperature of the picks were considerably lowered.

A direct reduction of the pick forces and consequently a reduction of the specific cutting energy and of the drum thrust only occurred to a negligible extent, if they can be proved at all.

A pressure of up to 200 bar (2,900 psi) seems to be reasonable for the high-pressure water supply system where the required water quantity approximately equals that of a conventional dust suppression system. This finding is encouraging since a system of this type can be integrated into a shearer quickly, reliably, and operationally safe. The first steps have already been made.

The second underground trial called for under this research project will be conducted in the U.S.A. It is planned to equip a double-ended ranging shearer with the high-pressure water supply system.

## REFERENCES

1. Handewith, H. J., Evans, R. J., Thimons, E. D. An Overview of Water Jet Assisted Rock Cutting at the Pittsburgh Research Centre. Proceedings of the 3rd U.S. Water Jet Conference, Pittsburgh, PA, 1985.
2. Haslett, G. A., Corbett, G. R., Young, D. A. An Investigation into the Effect of Varying Water Pressure and Flow Rates Upon the Release of Airborne Respirable Dust by a Dosco MKIIB Roadheader Equipped with a Water or Jet Assisted Cutting Head.

Proceedings of the 8th International Symposium on Jet Cutting Technology. Durham, England, Sept. 1986.

3. Morris, A. H., Tomlin, M. G. Experience with Boom-Type Roadheaders Equipped with High-Pressure Water Jet Systems for Roadway Drivage in British Coal Mines.

Proceedings of the USBM Open Industry Meeting: Water Jet Assisted Cutting, Pittsburgh, PA, June 1984.

4. Kovscek, P. D., Taylor, C. D., Kissell, F. N., Thimons, E. D. Longwall Shearer Performance Using Water jet Assisted Cutting. Proceedings of the 8th International Symposium on Jet Cutting Technology, Durham, England, Sept. 1986.

5. Investigation Into the Influence of High-Pressure Water Jets on the Forces, Temperatures and Wear Of Cutting Picks. Investigation Report Of the Department for Mining and Face Conveyor Technique of the BERGBAUFORSCHUNG GmbH, Essen, 1985 (not published).

TABLE 1. - Data of the face and of the face equipment, district 58, seam D/C, Auguste Victoria Mine

General Information

Seam thickness	:	2.3 m (7.54 ft)
Partings	:	approx. 0.7 m (2.29 ft)
Faults	:	two fault zones each of them with a throw of approx. 2.7 m (8.86 ft)
Method of mining	:	retreat mining
Panel length	:	850 m (2,789 ft)
Face length	:	280 m (919 ft)
Face supports	:	THYSSEN shield supports RHB 10/27
Face conveyor	:	double inboard chain DKMF 3.3 x 125/250 kW

Mining Equipment

Face	:	double-ended ranging drum shearer EDW-200/230-L
Face end	:	single-ended ranging drum shearer EW-200/170-L
Haulage system	:	Eicotrack Ventilation
Ventilation	:	homotropical ventilation, approx. 1500 m <sup>3</sup> /min (53,000 cfm)

# CONSIDERATIONS IN THE USE OF HIGH SPEED WATER JETS FOR DEEP SLOTING OF GRANITE

M. M. Vijay  
Gas Dynamics Laboratory  
National Research Council of Canada  
Ottawa, Ontario Canada

J. Remisz, B. Hawrylewicz, and R. J. Puchala  
Indescor Hydrodynamics Inc  
Concord, Ontario, Canada

## ABSTRACT

Experiments were conducted in the laboratory on the slotting of Barre granite with rotating high-pressure water jets. The work was conducted in support of an industrial project in which, among other things, a prototype rock slotter was required to be manufactured for quarrying and mining applications. The objective of the experiments was to arrive at the optimum operating conditions for the slotter.

Tests were conducted on samples of Barre granite embedded in a matrix of concrete. Six nozzle body designs, with and without carbide cutting tips, were investigated. Nozzle pressure was maintained constant at 103.5 MPa (hydraulic power = 105 kW) and the traverse and the rotational speeds were varied within the range of 0.6-6.6 cm/s and 100-800 RPM respectively. Best results of exposure rate (1.2-1.4 m<sup>2</sup>/hr) and the specific kerfing energy (3.5X10<sup>4</sup> J/cm<sup>2</sup>) were achieved with a carbide-tipped nozzle. These results show that slotting with rotating water jets is feasible.

## NOMENCLATURE

a,b	= empirical constants
D	= diameter of the nozzle body, mm
D <sub>1</sub> , D <sub>2</sub> , D <sub>3</sub>	= diameter of orifices in the nozzle body, mm
d <sub>e</sub>	= equivalent diameter of the orifices, mm
D <sub>s</sub>	= nozzle step down into the slot, mm
E <sub>A</sub>	= specific kerfing energy, J/Cm <sup>2</sup>
E <sub>v</sub>	= specific energy, J/cm <sup>3</sup>
f	= porosity of rock sample, %
h	= depth of slot per pass, mm
H <sub>p</sub>	= total hydraulic power of jets, kW
N	= rotational speed of the nozzle body, RPM
P	= pressure at the nozzle, MPa
p	= pitch of the trajectories of the jets
S	= standoff distance, mm
S <sub>o</sub>	= exposure rate of the sample, cm <sup>2</sup> /min -velocity of the jet, m/s
V <sub>j</sub>	= velocity of the jet, m/s
V <sub>tr</sub>	= traverse speed of the rock under the jets, cm/s
W <sub>s</sub>	= width of the slot, mm
σ <sub>c</sub>	= uniaxial compressive strength of rock, MN/m <sup>2</sup>
σ <sub>t</sub>	= uniaxial tensile strength of rock, MN/m <sup>2</sup>

$\kappa$  = permeability of rock at atmospheric pressure,  $\mu\text{D}$   
 $\lambda$  = mean grain size of rock,  $\mu\text{m}$   
 $\alpha, \beta, \gamma$  = angles of inclination of the nozzle body, degree

## INTRODUCTION

The interest in the use of high speed water jets for cutting of rocks in the mines and quarries has increased considerably during the last ten years. Starting from the early laboratory studies with single jets (1), where the interest was mainly in obtaining experimental results to explore the basic jet cutting relationships (2,3), work has advanced to the stage where actual field trials are in progress to assess the potential of water jets for such diverse applications as soil cutting (4), coal mining (5) and tunneling (6). The techniques of water jets for cutting of soft materials, such as coal, has proven to be commercially viable (5); however as far as cutting of hard rocks (for example, granites) is concerned, there is a paucity of information, and a great deal of further work is required to establish their technical or commercial viability, before they can replace the existing technologies .

This paper is concerned with the use of rotating jets for deep slotting of Barre granite, which is a semi-homogeneous material with fairly well defined properties. The work conducted in the laboratory was in support of an industrial project in which, among other things, a prototype rock slotter (Fig. 1) was required to be manufactured for quarrying and mining applications. The objective of the experiments was not only to arrive at the optimum operating conditions for the slotter, but also to consider other factors such as the quality of cut, surface finish, etc.

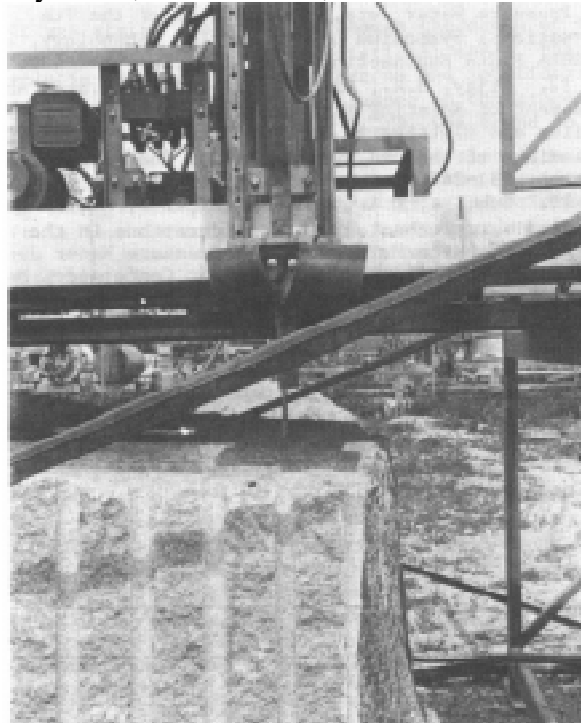


Figure 1. A general view of the rock slotter.

Prior to conducting this work in the laboratory, a search of the literature was made. Results reported by other investigators (7 to 13) were quite interesting, but very

limited and often ambiguous, especially with respect to the magnitudes of pressure and power. Harris and Brierley (7), for example, demonstrated that rotating water jets at relatively low pressures (< 69MPa) and hydraulic powers (435kW) could be used for cutting wide slots ( $W_s = 40$  and  $250$  mm) in Berea sandstone. They reported specific kinetic energy values in the range of  $1.12$  to  $4.53 \times 10^3$  J/cm<sup>2</sup>, achieved with a rotating jet device containing two orifices (orifice diameter varied from  $0.203$  to  $1.02$  mm), at traverse speeds in the range of  $1.71$  to  $26.8$  cm/s.

Hilaris and Bortz (8), on the other hand, carried out both laboratory and field trials on slotting granite at ultra high pressures ( $P = 206$  to  $275$  MPa) with a rotating ( $N = 300$  to  $600$  RPM) twin jet (diameter of each orifice =  $0.5$ mm) device. Laboratory tests were conducted on Barre granite and the results were correlated by the following equation:

$$\frac{h}{d_e} = 3.9 \left[ \frac{d_e}{s} \frac{P}{\sigma_c} \left( \frac{V_j}{V_{tr}} \right)^{0.5} \right]^{0.983} \quad (1)$$

Field tests were conducted at Blue Granite Quarry at Elberton, Georgia (it is not clear if this granite was similar to Barre granite) at a pressure of  $207$ MPa ( $H_p = 52$  kW). The maximum depth of cut obtained was  $3.48$  m (length =  $0.608$  m) and the average exposure rate was  $1.17$  m<sup>2</sup>/hr, which gave a specific kerfing energy of  $1.87 \times 10^4$  J/cm<sup>2</sup>. The authors also compared the water jet technique with a flame jet cutter and showed that the cost, based on power alone, of the latter was about  $2.5$  times higher than the former; furthermore, the total time taken to cut a typical block of size  $3.7 \times 3.7 \times 6$  m by the flame jet was about  $3$  times that taken by water jets. As these estimates were based on a number of assumptions, further work is required to support such claims.

A manufacturer specializing in water jet systems, has claimed that their specialist system could cut slots  $30$ m long,  $4$ m deep and  $7.5$ cm wide in hard granite (the type of granite was not specified) employing rotary water jets operating at a pressure of  $124.2$ MPa and a power of  $313$ kW (9). Since no other details were given, it was not possible to evaluate the merits of this system vis-a-vis the conventional techniques.

Raether, Robison and Summers (10) have reported on a rotary high pressure water jet device for deep slotting of granite ( $\sigma_c = 180$  MN/m<sup>2</sup>). The potential of the device was demonstrated by cutting a  $3.7$  m deep,  $18.3$  m long and  $5.1$ cm wide slot in a quarry. The rotating jet device incorporated a balanced nozzle body consisting of two orifices (diameter of each orifice =  $1.194$  mm) with an included angle of  $30^\circ$  to  $40^\circ$ . The power loading at a pressure of  $103.5$ MPa was  $105.3$ kW. The traverse speed ( $5.1$ cm/s) was matched with the rotational speed ( $360$  RPM) so that no uncut webs were left in the slot. Under these conditions, the rate of area generation ( $S_o$ ) was  $1.49$ m<sup>2</sup>/hr corresponding to a specific kerfing energy of  $2.54 \times 10^4$  J/cm<sup>2</sup>. No detailed results were reported, except that the water jet technique was demonstrated to be a viable and better technique than the flame jet or the wire saw techniques.

Vijay, Grattan-Bellew and Brierley (11) and, Vijay and Grattan-Bellew (12) have reported experimental results on slotting of Muskoka pink granite, Ottawa Limestone, Nepean sandstone (11) and an ore-bearing (Noranda) rock sample (12) with rotating high speed water jets. They thoroughly investigated the effect of the nozzle body design,

operating parameters ( $P$ ,  $V_r$ , etc.) and the properties of rocks and, showed that they all had significant influence on slotting performance. For instance, whereas granite could be cut fairly easily with a plain nozzle at a pressure of 69MPa ( $H_p = 58$  kW,  $V_r = 2.54$  cm/s and  $N = 240$  RPM), the ore bearing sample required a carbide-tipped nozzle and a minimum pressure of 82.8 MPa ( $H_p = 75$  kW,  $V_r = 2.54$  cm/s and  $N = 240$  RPM). At these operating conditions  $S_o = 1.16$  m<sup>2</sup>/hr.,  $E_a = 1.78 \times 10^4$  J/cm<sup>2</sup> for granite and,  $S_o = 0.18$ m<sup>2</sup>/hr and  $E_a = 1.5 \times 10^5$  J/cm<sup>2</sup> for the ore-bearing sample. Based on these results and also the information received from a granite quarry (11), the authors concluded that water jets have a good potential for slotting applications and deserved further study.

Summers and Mazurkewicz (13) have described the carving of granite prisms with rotating high-pressure water jets used in the construction of UMR (University of Missouri-Rolla) Stonehenge. A total of 53 stones (surface area = 251 m<sup>2</sup>) were cut by the water jets. The nozzle body (diameter = 37 mm ) employed incorporated two orifices (diameter of each orifice = 0.94 mm ) at 45° angle. The operating pressure and the hydraulic power were 100 MPa and 62kW respectively. The width of the slot was 50 mm . The authors stated that the equipment operated for a total of 1000 hours and the nozzles needed to be replaced 20 to 30 hours after the cutting had taken place. A long chain polymer was added to the water in order to maintain an exposure rate of approximately 1.8m<sup>2</sup>/hr (specific kerfing energy was about  $1.24 \times 10^4$  J/cm<sup>2</sup>).

Although the main concern of this paper is slotting with rotating water jets, it should be noted that oscillating water jets have also been used for slotting (5 and 14). More recently, abrasive-entrained water jets have become very popular in cutting a variety of materials, including hard rocks (15). The authors feel that deep slotting (> 1 m) of rocks with abrasive entrained water jets is impracticable at the present stage of their development. Nonetheless, experiments with abrasive-entrained water jets are presently in progress and, if proved feasible, it would be a simple matter to incorporate an abrasive feeding system into the rock slotter shown in Fig. 1.

It is clear from this brief review of the literature that although the potential of rotating water jets for deep slotting of rocks has been demonstrated, there is a paucity of experimental data that could be used for designing new systems. Therefore, the present laboratory investigation was undertaken to generate data required for the design and manufacture of a commercial rock slotter (Fig. 1). Tests were conducted on Barre granite, assuming that it fairly well represented the spectrum of rocks encountered in the mines or quarries. It is shown that a number of factors come into play in slotting a rock with rotating water jets. These are discussed in this paper.

## EQUIPMENT AND PROCEDURE

The equipment and some of the nozzles used in the present investigation were the same as those employed in the previous investigations (11 and 12). The pump was a triplex pump capable of delivering 76 liter/min of water at the rated pressure of 103.5MPa. The maximum power available from the pump was 132kW; actual power used in the experiments was 105kW. As shown in Fig. 2, six different nozzle bodies with

varying configurational parameters (Table 1) were used in the program. The first four, designated as A6, 6BTP, 6TS and C2 were thoroughly tested in the laboratory in the previous investigations (11 and 12) on drilling and slotting. The last two, designated as TB/RS and DB/RS were typical commercial nozzles supplied by the company. Of the six nozzles, only 6BTP and 6TS were equipped with carbide cutting tips. The testing rig consisted of an electrically driven traverse trolley on which the test samples were placed, a nozzle holder and a rotating and shifting mechanism.

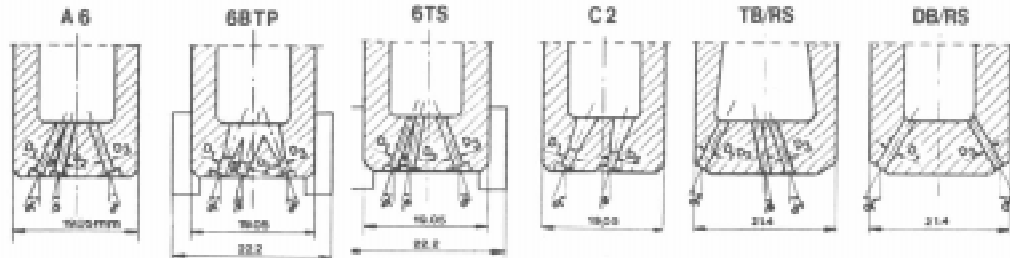


Figure 2. Nozzles employed in the investigations.

The experimental procedure was quite simple. Once the operating variables ( $N$ ,  $P$  and  $V_{tr}$ ) were set at the desired values, the rock sample was traversed underneath the nozzle. After each pass, the nature of the slot was noted, the width and the depths were measured, and the nozzle was lowered into the slot by a predetermined value (nozzle step down =  $D_s$ ) and the test was repeated.

This procedure was continued until the desired depth of the slot was achieved. The total volume of the slot was then measured to calculate the specific energy ( $E_v$  = Energy/volume of material removed). During the program, test parameters were maintained within the following ranges:

$P$  - pressure at the nozzle inlet (constant) = 103.5Mpa,  $N$  = nozzle rotational speed = 100 to 800,  $V_{tr}$  = traverse speed = 0.6 to 6.6 cm/s

#### TEST MATERIAL

The test materials were confined blocks of Barre granite (average size = 80 X 5 5 x 40 cm). They were confined in a matrix of concrete to eliminate edge effects and to impose in situ stress conditions. The structure and composition of the specimens were determined by taking optical and electron micrographs of several thin sections taken from the samples (Figs. 3A and 3B). The rock is a muscovite biotite granite of medium grain size and consisted mostly of feldspars (64%) and quartz (21%). Other minerals were biotite (7%), muscovite (7%), chlorite (0.4%) with some accessory minerals such as apatite (0.5%). As shown in Fig. 3B, open cracks were common around the grain boundaries, and some through the grains themselves (Fig. 3A). Examination of the cuttings indicated that generally the fractures induced by the water jets followed around grain boundaries rather than cutting across them. A number of properties of the rock were measured in the laboratory and these are listed below:

$$\sigma_c = \text{compressive strength} = 146\text{MN/m}^2, \sigma_t = \text{tensile strength} = -8.0\text{MN/m}^2,$$

$\kappa$  = permeability at 1 atm. pressure =  $160\mu\text{D}$ ,  $\lambda$  = grain size =  $976 \pm 614$  (mean +1 standard deviation) and  $f$  = porosity = 1.4%.

A discussion of the influence of these properties on the process of cutting is beyond the scope of this paper (11,12).

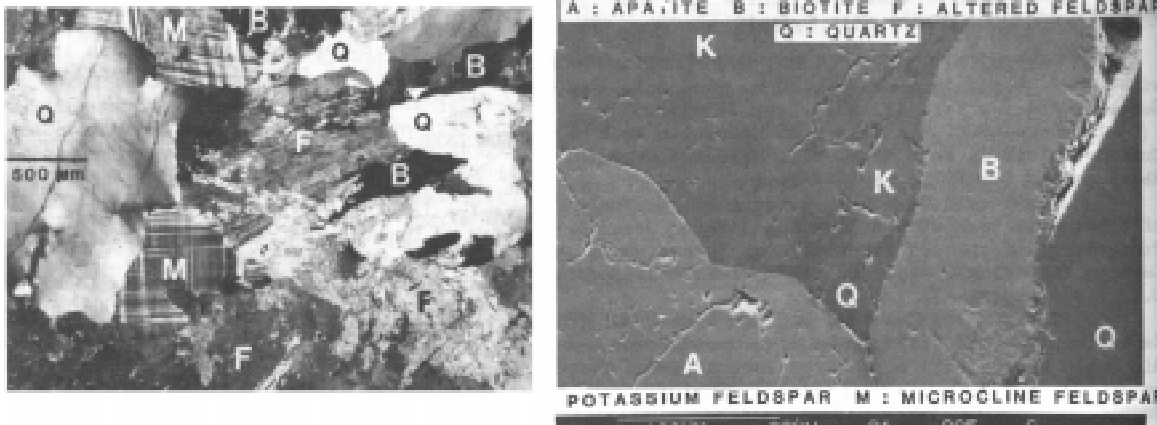


Figure 3. Optical and electron micrographs of Barre granite.

### EXPERIMENTAL RESULTS

Experimental results are plotted in Figs. 4, 5, 6, 9 and 10. In Figs. 7, 8 and 11 some qualitative observations, useful in the discussion of results, are depicted. The dependent variables of interest were  $h$ ,  $S_o$ ,  $E_a$  and to a lesser extent specific energy  $E_v$ . These were calculated as follows:

$$h = \text{mean depth of slot} = \text{total depth of slot/no. of passes} \quad (2)$$

$$S_o = \text{exposure rate} = hV_{tr} \quad (3)$$

In slotting work,  $E_a$  is a more important parameter than  $E_v$ . Therefore, values of  $E_v$  are not plotted. The values of  $h$  were non-dimensionalized with respect to  $d_e$  where:

$$d_e = \sqrt{(D_1^2 + D_2^2 + D_3^2)}_e \quad (4)$$

For the sake of clarity, not all the results are plotted in the figures.

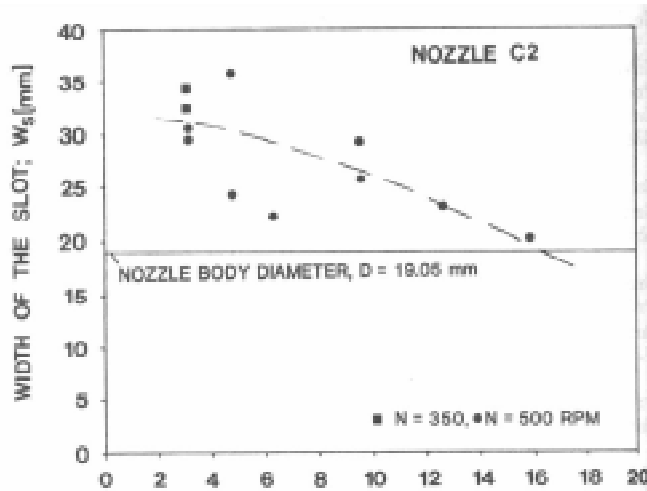


Figure 4. Plot of the width of the slot against the nozzle step down.

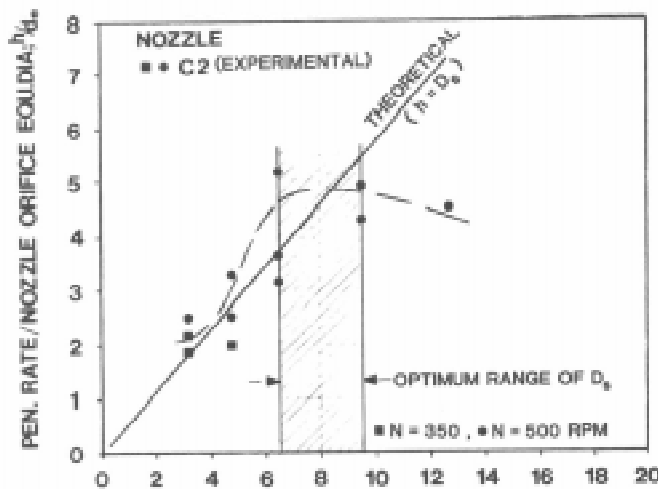


Figure 5. Plot of  $h/d_s$  against nozzle step down.

## DISCUSSION

The important factor in deep slotting of rocks with rotating water jets is that the nozzle body has to step down freely into the slot by a certain value after each pass. In order for this to happen, the width of the slot should be larger than the nozzle body. The standoff distance between the nozzle and the bottom of the slot during the second and the subsequent passes depends upon the width, depth and the nature of the cut achieved during a previous pass. In order to maintain a constant standoff distance, the nozzle has to step down a certain distance which, in principle, should be equal to the depth of penetration (see Fig. 5). However, due to the conflicting requirements of depth and width, the stepdown value ( $D_s$ ) will generally vary from one pass to the other.

Figures 4 and 5 show the effect of nozzle step down (from some reference standoff distance) on the width and depth of cut respectively, for the nozzle body C2 (similar observations were made for other nozzle bodies also). At low values of  $D_s$ , the width of cut was fairly large ( $W_s/D_s=1.84$ ), but at the cost of depth of penetration. As the values of  $D_s$  were increased up to 10 mm, the width of cut was reduced slightly, but there

was substantial gain in the depth of penetration; actually it reaches a maximum in the neighbourhood of  $D_s = 8$  mm. Therefore, the optimum value of  $D_s$  appears to lie between 6.5 - 9.5 mm. This is one of the important considerations in slotting with rotating water jets. Or else, a host of problems, such as nozzle jamming and lance bending, etc., would occur and hinder the rate of production. A slight influence of the rotational speed on the width (Fig. 4) and depth (Fig. 5) should be noted.

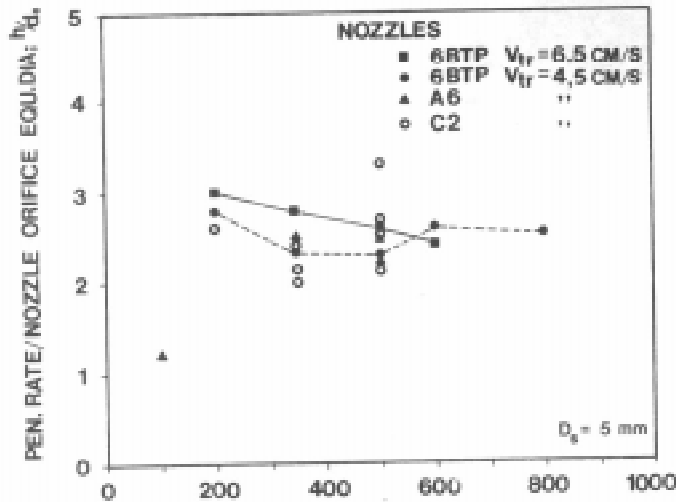


Figure 6. Plot of  $h/d_c$  against  $N$ .

The influence of the rotational speed on the depth of the slot is indicated explicitly in Fig. 6. Statistically, there appears to be no effect of the rotational speed on the depth of penetration. However, rotational and traverse speeds seem to be related, from several stand points, and will be discussed later. There is a great deal of scatter in the results obtained with the plain water nozzles, A6 and C2. Carbide-tipped nozzle 6BTP produced consistent results, and for this nozzle, higher depths of penetration were achieved at rotational speeds below 500RPM. As high rotational speeds ( $> 500$  RPM) impose severe technical problems on the rotating systems, it is better to run the rotating devices below 500 RPM.

It was stated above that although the depth of the slot was not influenced by the rotational speed, there is a relationship between the traverse and rotational speeds that has a significant influence on the process of slotting. In fact, the ratio  $V_{tr}/N$ , was found to have a great effect on the quality of the slot (see also Ref. 10), depth of penetration and hence the specific kerfing energy. As pointed out by Harris and Brierley (7), it is very important to match the traverse speed with the rotational speed to avoid uncut webs over the length of the slot. Figure 7a, taken from their work (7) shows clearly the uncut webs at the bottom of the slot for the worst condition. This problem is not so severe when the widths of slot are small (2.5cm). Figures 7B and 7C show the nature of the bottom of the slot obtained with the plain nozzles. However, with the carbide-tipped nozzles, the bottom of the slot had no uncut webs, even when the rotational and traverse speeds were not properly matched (Fig. 7D). It is possible to estimate the optimum value of the ratio,  $V_{tr}/N$ , by examining the trajectories of the jets over the rock sample (Fig. 8). For a two-jet nozzle, Harris and Brierley (7) have shown that the pitch,  $p$ , is proportional to  $V_{tr}/N$ . This pitch can be measured approximately from Fig. 7C. These qualitative

observations and the experimental results indicate that the optimum value of  $V_r/N$  is in the neighbourhood of 0.3 (0.25 to 0.35).

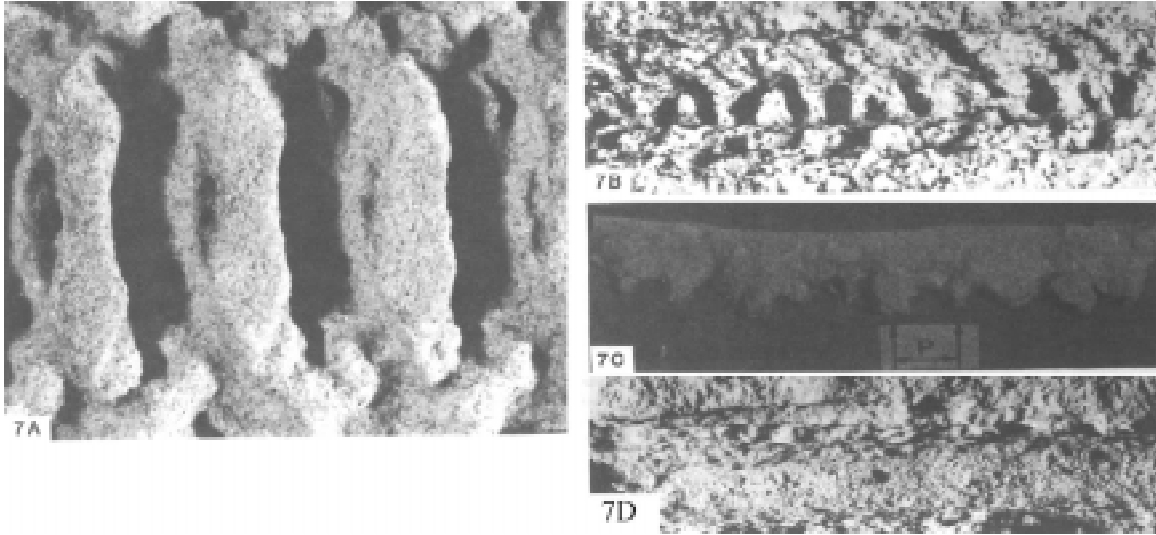


Figure 7. Nature of the slots in rocks cut with rotating water jets.  
 a) close-up view of uncut webs in Berea sandstone b) view of the bottom of the slot cut with plain nozzles. c) A rubber molding of the slot shown in 7B. d) View of the bottom of the slot cut with the carbide-tipped nozzles.

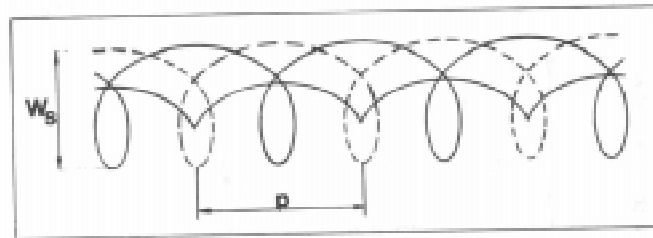


Figure 8. Sketch of the trajectories of rotating jets.

The relationship between the surface exposure rate ( $S_o$ ) and the traverse speed is depicted in Figs. 9A and 9B, with nozzle step down ( $D_s$ ) as a parameter (for the sake of clarity, two separate graphs have been plotted). Surface exposure rate,  $S_o$ , is more important than the depth of penetration in slotting applications. The figures show that the exposure rate increases linearly with the traverse speed, over the range of traverse speeds investigated. The figures also show that the type of the nozzle body and step the down value have significant effects on the exposure rate. Best results were obtained with the carbide-tipped balanced nozzle, 6BTP. Further discussion on nozzles is given below.

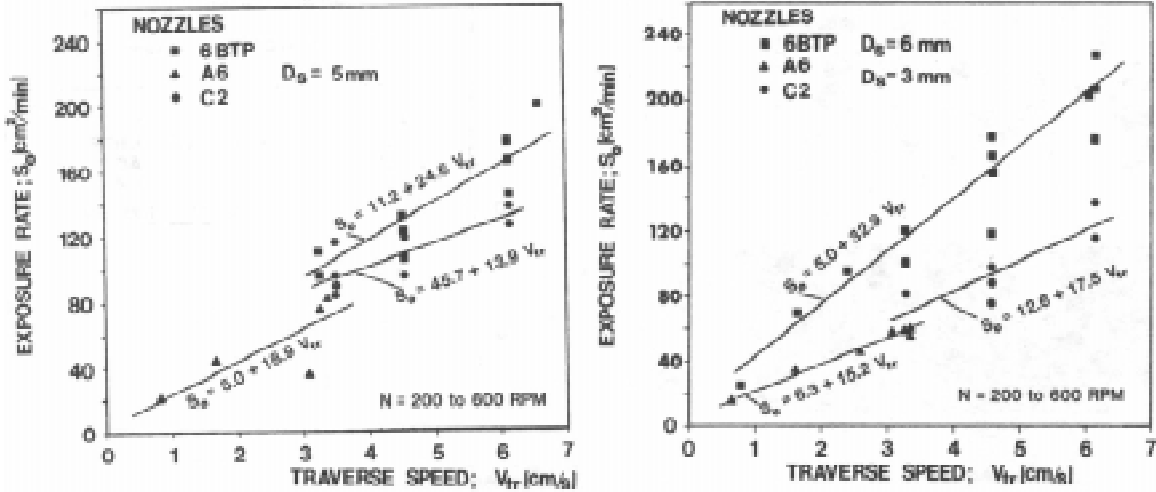


Figure 9. Plot of exposure rate against  $V_{tr}$  for differing nozzle step-downs.

The most important parameter for evaluating the nozzle performance for deep slotting of rocks is the specific kerfing energy, defined in Eq. (3). The influence of the traverse speed on specific kerfing energy is depicted in Figs. 10A and 10B, with  $D_s$  as a parameter. The specific kerfing energy decreases rapidly as the traverse speed is increased up to 3 cm/s and then decreases more slowly as the traverse speed is increased beyond this value. As the curves almost flatten out at a traverse speed of 6 cm/s (it should be noted that different curves will be obtained at different pressures), there is no particular advantage in increasing the traverse speed beyond this value.

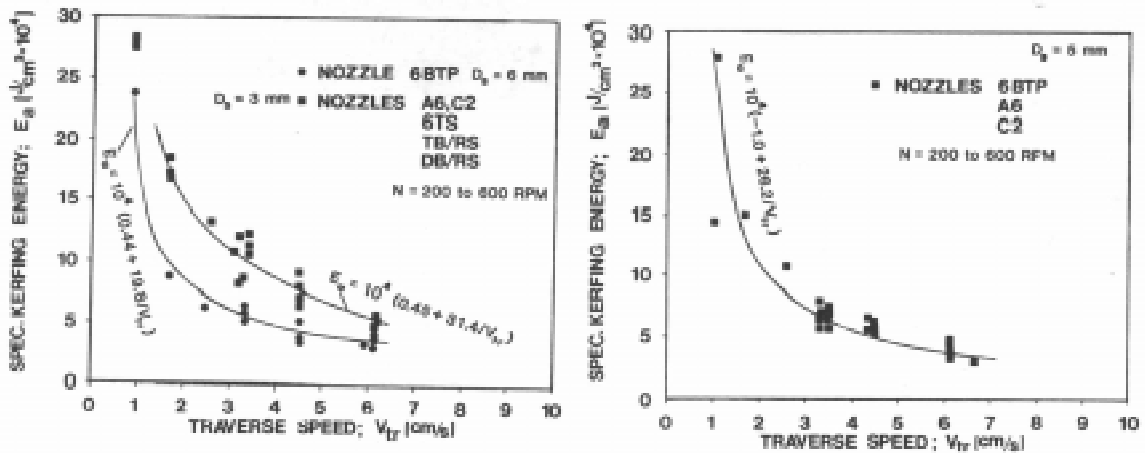


Figure 10. Plot of  $E_a$  against  $V_{tr}$ .

Once again, the superior performance of the nozzle 6BTP should be noted. Although not shown explicitly in the figure, the performance of the commercial nozzles, TB/RS and DB/RS was very poor. The explanation for this is simply that the quality of the jets produced by these nozzles was poor, with the result that the penetration depth per pass was almost zero. Probably, the configurational parameters, that is, orifice diameters, angles of inclinations, etc., for these nozzles, were far from optimum. As far as the plain nozzle bodies, A6 and C2, were concerned, they performed fairly well, except when they

encountered uncut protrusions over the length of the slot. When this happened, the nozzles could not be lowered into the slot for the next pass. The tests had to be repeated several times at the same standoff distance, to remove the uncut protrusions, thereby yielding relatively high specific kerfing energy values. In the case of the carbide-tipped nozzles, the actual cutting was still done by the water jets. The usefulness of the carbide-tips was in removing the uncut protrusions, leaving a smooth wall over the length of the slot. It was, therefore, possible to lower the nozzles into the slot in each successive pass, at relatively large step down increments. Nozzle 6TS did not perform as well as 6BTP, probably because of the straight entry orifices incorporated into this nozzle body (Fig. 2). In any case, the carbide-tipped nozzles are recommended for slotting of rocks, for they not only perform better compared to the plain nozzle bodies, but also improve the surface finish of the blocks. General views of the surface and also the slots cut in the samples are shown in Figs. 11A, B and C.

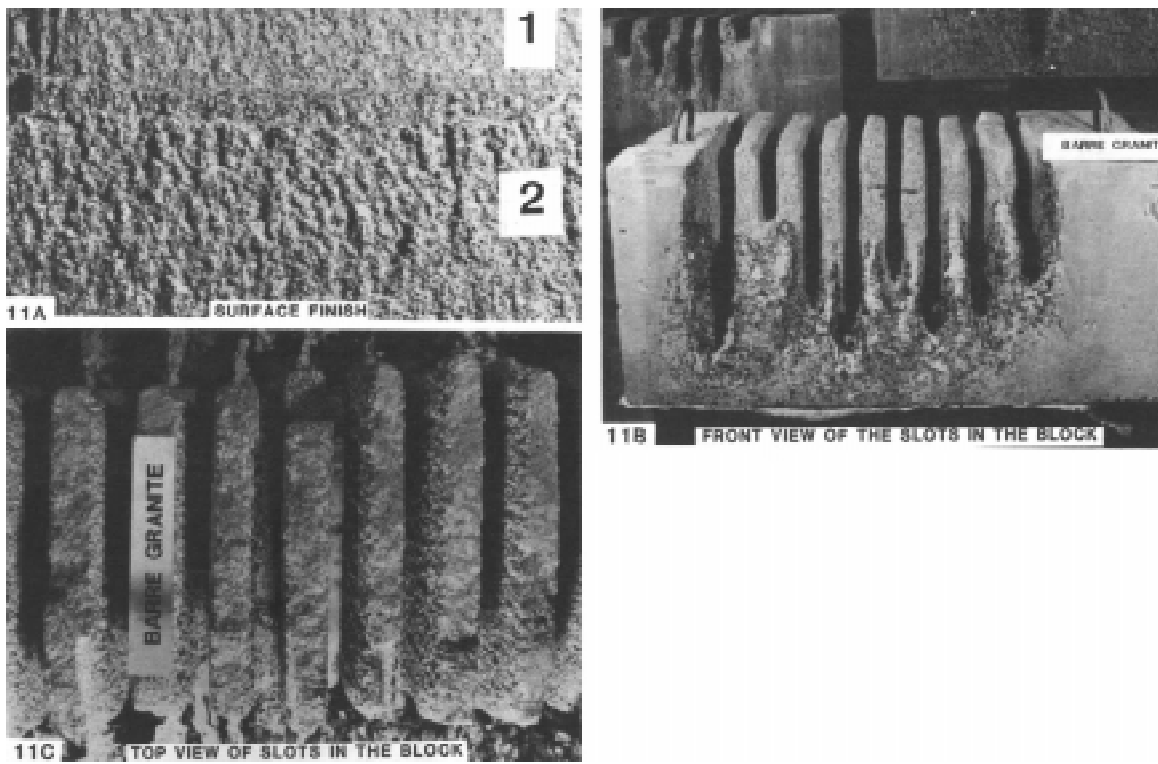


Figure 11. Views showing the surface finishes and the slots cut in Barre granite with rotating water jets.

The equations indicated on Figs. 9A to 10B were obtained by regression analysis and appear to fit the data quite well. Since these equations were obtained at 95% confidence level, extrapolations might be made, if required, to predict the performance of the rock slotter. Although values of specific energy based on volume ( $E_v$ ) are not plotted, the results could be fitted by similar equations. For instance,  $E_v$  was related to the traverse speed by the following equation:

$$E_v = a + b/V_{tr} \quad (5)$$

For nozzle C2,  $a = 0.5 \times 10^4$  and  $b = 4.3 \times 10^4$ , and for nozzle 6BTP,  $a = 0.5 \times 10^4$  and  $b = 4.0 \times 10^4$ .  $E_v$  is in  $J/cm^3$  and  $V_{tr}$  in  $cm/s$ .

## CONCLUSIONS

The following conclusions can be drawn from the 7 tests conducted in the laboratory:

1. It is possible to employ mechanically assisted 13 (carbide-tipped nozzles) rotating high speed water jets to cut deep slots in Barre granite and other type of rocks similar to granite at relatively moderate pressures (100 MPa) and hydraulic powers (100 kW).
2. The surfaces of the blocks could be rendered smooth and even by giving careful considerations to various parameters, for example, ratio of traverse speed to the rotational speed ( $V_{tr}/N$ ), that influence the process of cutting.
3. The optimum values of the independent variables, at 103.5MPa, were:  
 $D_s$  = nozzle step down = 7 to 9mm  
 $N$  = rotational speed = 300 to 500RPM  
 $V_{tr}$  = traverse speed = 6cm/s
4. The best results obtained with the carbide-tipped nozzles were:  
 $h$  = depth of penetration per pass = 0.5 cm  
 $S_o$  = exposure rate = 1.2 to 1.4  $m^2/hr$   
 $E_a$  = specific kerfing energy =  $3.5 \times 10^4 J/cm^2$
5. Regression equations were obtained at 95% confidence level and could be used to predict the performance of the water jet slotting systems, such as the rock slotter, shown in Fig. 1.

It is believed that the performance of water jets, based on the parameters listed above, is comparable to or better than those of conventional systems, such as flame jet cutter. Experiments to establish the commercial viability of the water jet system (the rock slotter) are in progress.

## ACKNOWLEDGEMENTS:

The authors are very grateful to Mr. N. Paquette (Gas Dynamics Laboratory) and Mr. M. Szymczak (University of Ottawa) for rendering assistance in carrying out the experiments and, to Dr. P.E. Grattan-Bellew (Institute for Research in Construction, N.R.C.) for providing the information on the properties of rocks. It is a pleasure to acknowledge Mr. J. Ploeg and Dr. R.G. Williamson, Director and Assistant Director of the Division of Mechanical Engineering, N.R.C., and Mr. J. Stirling, President, Indescor Hydrodynamics, Inc., for their continued interest in this program. Partial funding for this work was received from the Industrial Development Office of N.R.C. This is gratefully acknowledged. Thanks are also due to Mrs. L. Charbonneau for typing the manuscript of this paper.

## REFERENCES

1. Harris, H.D., and Mellor, M., "Cutting Rock with Water Jets," *Int. J. Rock Mech. Min. Sci. and Geomech. Abstr.*, Vol. 11, 1974, pp. 343-358.
2. Crow, S.C., "A Theory of Hydraulic Rock Cutting," *Int. J. Rock Mech. Min. Sci. and Geomech. Abstr.*, Vol. 10, 1973, pp. 567-584.
3. Reh binder, G., "Some Aspects of the Mechanisms of Erosion of Rock with a High Speed Water Jet," *Proceedings of the 3rd International Symposium on Jet Cutting Technology*, Paper E1, BHRA Fluid Engineering, U.K., 1976, pp. 1-19.
4. Yahiro, T., Yoshida, H., and Nishi, K., "Soil Improvement Method Utilizing a High Speed Water Jet and Air Jet," *Proceedings of the 6th International Symposium on Jet Cutting Technology*, Paper J2, BHRA Fluid Engineering, U.K., 1982, pp. 397-428.
5. Ben-Zhoa, T., Jia-Jun, S., and Chen-Lung, Z., "Development and Basic Regularities of Water Jet Cutting Technology in China Coal Industry," *Proceedings of the 3rd U.S. Water Jet Conference*, the University of Pittsburgh, Bureau of Mines and the U.S. Water Jet [ Technology Association, May 1985, pp. 181-193. L
6. Baumann, L., and Koppers, M., "State of Investigations on High-Pressure Water Jet Assisted Road Profile Cutting Technology," *Proceedings of the 6th International Symposium on Jet Cutting Technology*, Paper G2, BHRA Fluid Engineering, U.K., 1982, pp. 283-300.
7. Harris, H.D., and Brierley, W.H., "A Rotating Water Jet Device and Data on its Use for Slotting Berea Sandstone," *Int. J. Rock Mech. Min. Sci. and Geomech. Abstr.*, Vol. 11, 1974, pp. 359-366.
8. Hilaris, J.A., and Bortz, S.A., "Quarrying Granite and Marble using High Pressure Water Jet," *Proceedings of the 5th International Symposium on Jet Cutting Technology*, Paper D3, BHRA Fluid Engineering U.K., 1980, pp. 229-236.
9. Anon, "Aqua-Dyne High Pressure Jet Technology," *Proceedings of the 6th International Symposium on Jet Cutting Technology*, BH RA Fluid Engineering, U.K., 1982.
10. Raether, G.A., Robison, R.G., and Summers, D.A., "Use of High Pressure Water Jets for Cutting Granite," *Proceedings of the 2nd U.S. Water Jet Conference*, University of Missouri-Rolla, Rolla, U.S.A., May 1983, pp. 203-209.
11. Vijay, M.M., Grattan-Bellew, P.E., and Brierley, W.H., "An Experimental Investigation of Drilling and Deep Slotting of Hard Rocks with Rotating High Pressure Water Jets," *Proceedings of the 7th International Symposium on Jet Cutting Technology*, Paper H2, BH RA Fluid Engineering, U.K. 1984, pp. 419-438.
12. Vijay, M.M., and Grattan-Bellew, P.E., "An Assessment of Rotating High Pressure Water Jets for Drilling and Slotting of Hard Ore Bearing Rocks," *Proceedings of the 3rd U.S. Water Jet Conference*, May 1985, pp. 231-247.
13. Summers, D.A., and Mazurkiewicz, M., "Technical and Technological Considerations in the Carving Of Granite Prisms by High Pressure Water Jets," *Proceedings of the 3rd U.S. Water Jet Conference*, 1985, pp. 272-287.
14. Reichman, J.M., and Cheung, J.B., "An Oscillating Waterjet Deep-Kerfing Technique," *Int. Rock Mech. Min. Sci. and Geomech. Abstr.*, Vol. 15, pp. 135-144.
15. Savanick, G.A. Krawza, W.G., and Swanson, D.E. " An Abrasive Jet Device for Cutting Deep Kerfs in Hard Rock," *Proceedings of the 3rd U.S. Water Jet Conference*, May 1985, pp. 101-122.

Table 1. Design Specification of Nozzle Bodies Used in the Investigation

TYPE OF NOZZLE	DIMENSIONS					
	D <sub>1</sub>	D <sub>2</sub>	D <sub>3</sub>	α	β	γ
	mm			deg		
A6	0.742	1.067	1.067	20	10	20
6BTP	0.742	1.067	1.067	20	10	20
6TS	0.742	1.067	1.067	20	10	20
G2	1.332	1.092	-	20	10	-
TB/RS	1.092	0.787	0.991	20	10	20
DB/RS	1.092	-	1.092	30	-	30

## AN ABRASIVE WATER JET ROCK DRILL

G. A. Savanick, Supervisory Physical Scientist, W. G. Krawza, Mining Engineering Technician  
Twin Cities Research Center  
Bureau of Mines  
U.S. Department of the Interior  
Minneapolis, Minnesota

### ABSTRACT

An abrasive water jet rock drill has been designed, built, and tested at the Bureau of Mines Twin Cities Research Center. The drill incorporates three new hydraulic components: a collimator, jet deflectors, and an un-pressurized swivel

Drilling occurs through the action of a 10,000 psi, 20 gpm waterjet into which is entrained 22 lb/min of abrasive. The pump, hoses, and fittings are those commonly used in the waterjet cleaning industry. Only inexpensive common sandblasting abrasives are used. The drill can drill hard rock such as 73,000 psi compressive strength quartzite with 10,000 psi water pressure. The drill can collar a hole at any angle, can drill through fractured material, and can chamber holes.

The concept of abrasive jet drilling of hard rock has been demonstrated. The abrasive jet drill has been shown to represent a significant advance in the state of the art of hard rock drilling. The Bureau of Mines is now actively attempting to transfer this technology to industry.

### INTRODUCTION

Water jet and water-jet-assisted rock drills can be used for rock bolting and other mining and construction applications (1). These drills have a number of advantages over rotary or percussive rock drills including relative lightness and portability the ability to collar a hole at any angle, and the ability to operate in low headroom.

One disadvantage of water jet drills is that extremely high pressures are required to drill hard rock (2). This disadvantage can be neutralized by incorporating abrasives into the cutting jet. This has the effect of greatly enhancing the cutting ability of the jet so that relatively modest pressures can be used to cut very hard rock, e.g., a 10,000 psi abrasive water jet can cut a quartzite with an unconfined compressive strength of 73,000 psi.

Abrasive jets are in common use in cutting hard material (3,4), but heretofore abrasive jets have not been used to drill deep holes or to cut deep slots in hard materials. There are many engineering applications where it is desirable to drill or kerf in hard materials. These include drill holes for rock bolts and for the placement of blasting agents. Kerfs are desirable in mining to prevent blast damage to the roof and to isolate ore from waste rock for selective extraction.

Deep drilling or slotting requires that the jet cut enough clearance for the drill pipe to follow into the hole. This, in turn, has required in past designs that the drill string be rotated. This requirement has been an impediment to the use of abrasive jets in drills or slot cutters. Given the state of the art, this requirement meant that a rotary coupling would be required to pass a pressurized abrasive slurry and a multiple orifice nozzle would be required to pass a high velocity abrasive slurry. This high velocity slurry would cause rapid erosion leading to the destruction of the nozzle.

The purpose of this paper is to introduce Bureau of Mines' research on the concepts of collimation, the jet deflector, and the non-pressurized swivel and to show how these concepts can be used together to form an abrasive water jet rock drill.

This drill is a byproduct of a Bureau of Mines research paper aimed at enhancing the efficiency of metal mining. The purpose of this program is to develop a water jet cutting device to cut deep slots along the ore/waste contact to enable the ore to be selectively removed.

### Collimation

A water jet formed by the discharge of a nozzle into a pipe (fig. 1) will not dissipate. It will retain its cutting ability significantly beyond the distance at which jets passing through air are effective [5]. The jet is constrained to flow parallel to the pipe axis, i.e., it is collimated. This collimated flow reduces the rate of loss of momentum of the jet, as compared with a water jet in air. A water jet in air loses its rock cutting ability shortly after exiting the nozzle, whereas the collimated abrasive jet has cut hard rock (a dolomite with a compressive strength of 20,000 psi) 5 ft from the nozzle. Experiments have shown that a collimated abrasive jet retains 75 pct of its energy after passing through a 10-ft length of collimating pipe.

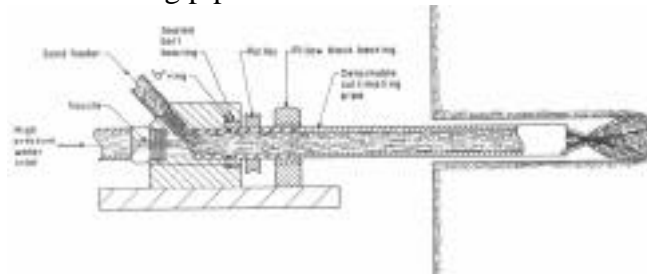


Figure 1. Schematic diagram of a collimator with deflectors.

Water from a 10,000 psi, 20 gpm pump is accelerated to 1,250 ft/sec through a 0.080-in diameter nozzle. It then entrains sand and air, and the resultant slurry enters the collimator. The collimator is a schedule 160 steel pipe. Lengths of pipe from 2- to 6-ft have been used as collimators. Abrasive particles are accelerated by the jet and retain most of their kinetic energy as they pass through the collimator. Sand particle velocities as high as 1,000 ft/sec have been measured at the outlet of the collimator pipe by double exposure high-speed photography.

Since a collimating pipe situated downstream of a high-pressure nozzle permits a high-velocity jet to retain its cutting ability for several feet, the collimating pipe can serve as a drill rod. In the Bureau of Mines abrasive waterjet rock drill, the nozzle is situated several feet upstream of the end of the drill so that it never enters the drill hole. The drill stem downstream of the nozzle is not pressurized. This is in contrast to conventional water jet drills where a multiple pass nozzle is situated at the bottom of the hole at the end of the string of pressurized pipe.

### The Jet Deflector

Drill pipe must be capable of following into a drill hole as the hole deepens. The drill must cut a hole wider than the diameter of the drill stem. Conventional water jet drills accomplish this by using rotating multiple orifice nozzles at the downstream end of the drill string.

This arrangement has not proved practical for an abrasive jet drill because the multiple orifice is quickly destroyed by wear. Instead, with the Bureau of Mines' drill, clearance is cut by deflecting the jet with two 1-in by 0.25-in by 0.125-in tool carbide plates silver soldered into slots at the end of the collimating pipe (fig. 1). These plates are positioned so that a portion of the jet is deflected and cuts wider than the pipe diameter, while the remainder of the jet passes undeflected. Between the deflectors and cuts the central portion of the drill hole.

The carbide deflectors are placed at an angle of  $15^\circ$  to the center plane of the collimator. This placement permits the abrasive jet to cut a hole wide enough for the collimating pipe to enter and deep enough to maintain a steady advance into the drill hole.

The deflection angle chosen is a compromise between the competing needs for axial and radial cutting. High angles of incidence of the abrasive onto the carbides engender wide, shallow cuts while low angles of incidence give narrower and deeper cuts. Of course, the collimating pipe and the deflectors exhibit wear, but both the pipe and plates are low cost, expendable items. The wear process is such that both the pipe and the deflector plates are worn out after about 2 hrs of abrasive jetting at 10,000 psi, 20 gpm.

### The Non-Pressurized Swivel

Present state of the art requires that the drill string of a water jet drill be rotated in order to cut clearance. Rotation of a conventional water jet drill requires that the pressurized water pass through a swivel. This swivel must contain high pressure (10,000 – 50,000 psi) while rotating at high speeds (500 - 2,000 rpm). Because of these requirements, the high-pressure swivels are apt to be expensive and unreliable.

The Bureau of Mines' abrasive jet drill avoids this problem because the fluid in the collimating pipe downstream of the nozzle is not pressurized. The pipe is rotated inside a sealed ball bearing and a pillow block bearing (fig. 1). The rotary motion is

imparted by an air motor coupled to the pipe by a chain and sprocket. The simple bearing swivel is very inexpensive (\$8 in 1986).

### Equipment Design

The drill, as described above, is essentially a rotating collimating pipe terminated by silicon carbide deflectors (figs. 2,3). The drilling apparatus is composed of these essential parts and various means of activation and control.

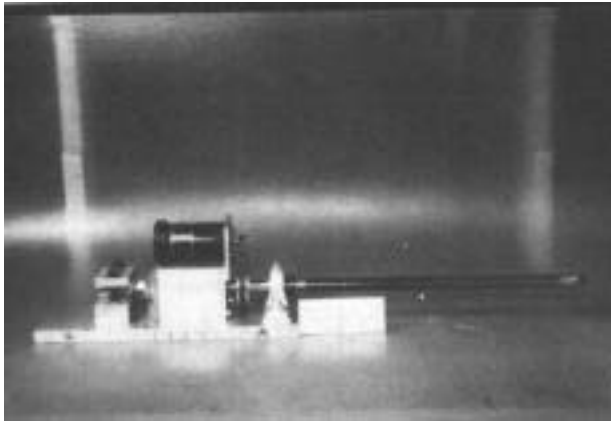


Figure 2. Photograph of the drill.

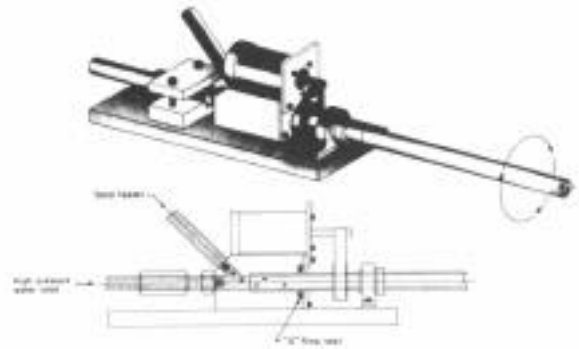


Figure 3. Schematic diagram of the drill.

Water (20 gpm) is pressurized (10,000 psi) by an Aquadyne model GE150 DT triplex pump and fed through waterblaster hoses to a 0.080-in diameter 3D Leach and Walker nozzle (6). This nozzle has a 13° conical taper downstream from the incoming conduit and terminates in a straight section with a length equal to three outlet diameters.

The pressure is dropped across this nozzle as the jet discharges into a mixing chamber. The venturi effect thus created entrains 22 lb/min of sand and air into the mixing section through hoses connected to a sand lance in a barrel. Sand, air, and water are mixed and flow at 1,000 ft/sec through the collimating pipe. The drill is carried on a Cleveland Rock Drill Co. carriage (fig. 4), upon which is mounted controls for the air and hydraulic systems. The drill is remotely controlled from an operator's station.

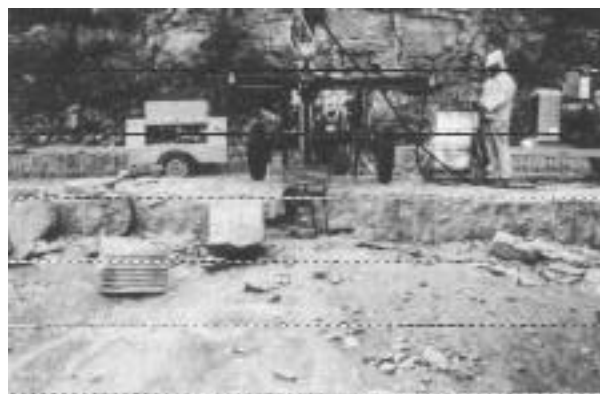


Figure 4. Drilling through loose rock.

The collimating pipe is rotated at 600 rpm by an air motor coupled to the pipe by a chain and sprocket. The drill rides on two orthogonal screw driven mounts. This permits the drill to be translated along the surface of the rock as well as to penetrate into the rock. The ability permits the drill to be used to cut kerfs as well as to drill holes.

### Drilling

Test holes were drilled in samples of Salem limestone, charcoal granite, Oneota dolomite, and Sioux quartzite. Test data are given in table 1. All tests were conducted with a 10,000 psi, 20 gpm water jet, a rotational speed of 600-700 rpm, and an entrainment rate of 22 lb/min of dry sand. Deflectors were set at 15° to the axis of the pipe.

These data show that hard rock can be drilled with an abrasive jet drill, but the penetration rate attainable varies with rock hardness. Table 1 gives the maximum penetration rate attained for each rock tested.

Table 1. - Penetration rate in four rocks

Rock	Compressive Strength, psi	Penetration <u>rate in/min</u>
Sioux quartzite....	73,000	4
Charcoal granite...	30,000	4
Oneota dolomite....	20,000	6
Salem limestone....	8,000	30

The abrasive drill offers the following advantages over other rock drills:

1. The operating pressure of the Bureau of Mines' abrasive-enhanced water jet drill is far lower than that of conventional water jet drills. The abrasive water jet drill can cut hard rock with a compressive strength of 70,000 psi with 10,000 psi water pressure. Other water jet drills must use a pressure approximately equal to the compressive strength of the rock. The water jet drill uses only commercially available hoses and fittings commonly used in the water jet cleaning industry.
2. This drill does not physically contact the rock and, thus, does not have to absorb the force of the rock pushing back on the drill rod. This permits the drill to be built of much lighter materials than ; conventional drills.
3. The drill does not require a bit.
4. The drill can enlarge (chamber) selected parts of the drill hole by slowing the penetration rate. This capability would be helpful to mine operators who must blast tough rock. The chambers can be loaded with extra explosive to put increased rock breaking power where it is most needed.
5. The drill can penetrate rubble or loose rock (fig. 5). This ability could be used to drill probe holes or blast holes in gob areas of mines.
6. The drill can drill holes which overlap (fig. 6). Overlapping holes can be strung together to create a kerf.
7. The drill can make small diameter (less than 1 in) holes. These small notes are ideal for resin-grouted rock bolts because it decreases the volume of grout required.

Conventional rotary or percussive rock drills are incapable of performing the functions described under 5, 6, and 7 above.



Figure 5. Hole drilled through loose rock

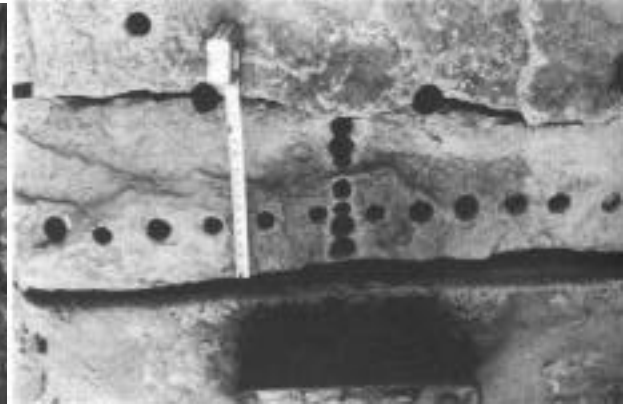


Figure 6. Overlapping drill holes

### Kerfing

Long, narrow kerfs (fig. 7) can be cut if the collimating pipe is rotated and translated simultaneously. If the pipe is fed into the kerf as cutting proceeds, the kerf can be cut deep.

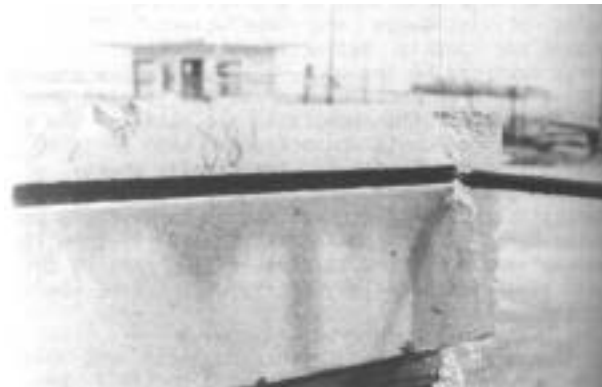


Figure 7. Narrow kerf cut 34 inches deep into Salem limestone.

Kerfs have been cut 34 in into Salem limestone and 19 in into Oneota dolomite. However, kerf cutting is a less efficient process than drilling, e.g., it took 2 hrs to cut a 1-1/2-in by 19-in by 56-in kerf in Oneota dolomite. This inefficiency results from nonuniform cutting caused by inhomogeneities in the rock. Harder material cuts slower than the adjacent softer material, creating high spots in the kerf. The collimating pipe cannot penetrate deeper than the depth of these high areas. This causes a longer than optimum standoff distance because the collimating pipe is not able to penetrate to within an inch of the bottom of the cut in the softer areas.

Another problem arises when surfaces are created in the walls of the kerf which require the incident jet to impinge upon them at a grazing angle. Grazing angles of

incidence are inefficient for cutting because the jet is deflected rather than having its energy absorbed by the rock. Surfaces which present a grazing angle of incidence to the jet created when the depth cutting by the undeviated jet outruns the width cutting by the deviated portion of the abrasive jet. In this instance, most of the kinetic energy of the deviated jet is wasted and the cuts are too narrow for the collimator to advance within an inch of the bottom of the kerf. The stand off distance is then longer than optimum resulting in drastically reduced cutting rates and consequent lengthening of the time needed to cut the kerf.

## SUMMARY

An abrasive jet rock drill has been built and tested. The drill uses a 10,000 psi, 20 gpm water jet which entrains 22 lb/min of sand. The drill incorporates three novel components, a collimator, jet deflectors, and an unpressurized swivel.

The drill has been used to drill rock as hard as quartzite with a compressive strength of 73,000 psi. It penetrates this quartzite at a maximum rate of 4 in/min.

Other rocks drilled include the charcoal granite (compressive strength 20,000 psi) which can be drilled at 6 in/min, and the Salem limestone (compressive strength 8,000 psi) which can be drilled at 30 in/min.

The abrasive jet drill has some unique and useful features as compared with mechanical drills. It can drill small holes, can collar a hole at any angle, can drill through fracture zones, can drill holes which overlap, can be translated perpendicular to the direction of drilling to produce a narrow kerf, and can chamber holes.

## REFERENCES

1. Walgomott, J. E. and G. P. Zink. Water Jet Assisted Drilling for Tieback Anchors. Proceedings of the Third U.S. Water Jet Conference. University of Pittsburgh, PA, 1985, pp. 353-365.
2. Vijay, M. M. and P. E. Gratton-Bellow. An Assessment of Rotating High Pressure Water Jets for Drilling and Slotting of Hard Ore Bearing Rocks. Proceedings of the Third U.S. Water Jet Conference. University of Pittsburgh, Pittsburgh, PA, 1985, pp. 231-247.
3. Kirby, M. J. and S. R. Kramer. Successful Application of an Abrasive Water Jet to Cut Concrete Pavement Under Actual Field Conditions. Proceedings of the Third U.S. Water Jet Conference. University of Pittsburgh, Pittsburgh, PA, 1985, pp. 83-100.
4. Yie, G. G. Cutting Hard Rock with Abrasive Entrained Waterjet at Moderate Pressures. Proceedings of the Second U.S. Water Jet Conference, University of Missouri-Rolla, Rolla, MO, 1983, pp. 407-420.
5. Savanick, G. A., W. G. Krawza, and D. E. Swanson. An Abrasive Jet Device for Cutting Deep Kerfs in Hard Rock. Proceedings of the Third U.S. Water Jet Cutting Conference. University of Pittsburgh, Pittsburgh, PA, 1985, pp. 101-122.
6. Leach, S. J. and G. L. Walker. Some Aspects of Rock Cutting by High Speed Water Jets. Phil. Trans. Royal Soc. (London), v. 260, series A, 1965, pp. 295-308.

## A RELATIVE CLEANABILITY FACTOR

A. F. Conn, M. T. Gracey, and W. Rosenberg  
Tractor Hydronautics, Inc.  
Laurel, Maryland

### ABSTRACT

An approach is described for developing a way to standardize the evaluation of water jets for their relative ability to clean. An "erosion strength for cleanability,"  $S_c$ , is proposed for characterizing any substance-to-be-removed/substrate-to-be-cleaned combination. Jet cleaning would be qualified by an "area cleaning effectiveness,"  $e_a$ , which rates a nozzle in terms of unit of area cleaned per unit of energy expended by that nozzle.

### INTRODUCTION

One of the most important commercial uses of water jets is for cleaning, i.e., removing an unwanted substance from a substrate, preferably without damage to the latter surface. However, unless side-by-side comparative tests are run, in situ, on the actual cleaning challenge, it is very difficult to assess the relative ability of two different jet cleaning devices. This is because of the incredibly wide range of "cleanabilities" or "erosion strengths" represented by the myriad of substance-to-be-removed/substrate combinations. Unless all of the conditions which led to that unique substance/substrate combination (time, temperature, condition of substrate surface; perhaps pressure, sun exposure, chemical environments) are reproduced -- usually an impossible task -- then any attempt at a laboratory evaluation will probably yield very misleading conclusions.

The purpose of this paper is to briefly suggest some ideas which -- by hopefully initiating discussion and further testing within the water jet community -- may lead to some standard methods for performing laboratory evaluations of the cleaning capabilities of water jet nozzles.

### AREA CLEANING EFFECTIVENESS

The concept of  $e_a$ , an "area cleaning effectiveness", is analogous to the "specific energy" factor used to assess the ability of a device to remove a volume of material. The  $e_a$ , however, is an inverse figure of merit in comparison to specific energy. That is, smaller specific energies (energy required per unit volume of material removed) are better, whereas a bigger  $e_a$  describes a better nozzle in an area cleaning challenge.

We have defined (1,2)  $e_a$  as:

$$e_a = \frac{\text{Area cleaned per unit time}}{\text{Power delivered by the nozzle}} \\ = A/P \quad (1)$$

In "U.S. Customary Units":

Area cleaning rate: A, can be in ft<sup>2</sup>/hr,

and

$$P = \frac{\Delta p \cdot Q}{1714} \text{ [hp]} \quad [2]$$

where:  $\Delta p$  is the pressure drop across the nozzle and  $Q$  is the flow rate in gpm.

Thus:

$$e_a = A/P = [\text{ft}^2/\text{hp-hour}] \quad [3]$$

is a suggested dimensional form for this parameter, namely unit of area cleaned per unit of energy expended by the nozzle.

In SI units,  $e_a$  as  $[\text{m}^2/\text{kW-hr}]$  could be used, with pressure in MPa, flow rate in liters/s, power in kW. Incidentally, to convert from  $e_a$   $[\text{ft}^2/\text{hp-hr}]$  to  $e_a$   $[\text{m}^2/\text{kW-hr}]$  multiply the former by 0.1246.

#### CLEANABILITY FACTOR (OR EROSION STRENGTH)

The concept of characterizing a material's ability to resist erosion by some sort of strength is far from new. Thiruvengadam (3), in his studies of cavitation erosion, suggested a set of absolute values for an erosion strength,  $S_e$ , which was originally based on a strain-energy absorption concept. Strengths,  $S_e$ , ranged from about 4,000 psi for 1100-0 aluminum to about 70,000 psi for stellite. Heymann (4) felt that a relative strength concept, based on a compilation of observed liquid impact erosion responses, was more general. Hence,  $N_e$ , a "normalized erosion strength" was derived, using  $N_e = 1$  for an 18Cr-8Ni austenitic stainless steel.  $N$  ranged from about 0.03 for soft aluminum to about 68 for stellites and hard tool steels, a range of about 2000:1.

In examining the erosion of substances from a substrate, some of the ideas of both Thiruvengadam and Heymann were utilized. Following the former investigator, a simple relationship has been proposed between area cleaning rate,  $A$ ; an erosion strength for cleaning,  $S_c$ ; and an erosive intensity,  $I$ , for a given water jet nozzle, when operated under a fixed set of conditions (pressure, flow rate, standoff distance, rate of nozzle traverse, angle of impingement, inair or submerged):

$$A = I/S_c \quad (4)$$

Substituting [3] into [4]:

$$e_a = \frac{I/P}{S_c} \quad (5)$$

or

$$e_a = S_c^{-1} \quad [6]$$

for a given nozzle and fixed set of operating conditions .

Relation [6] was used to derive the curves shown in Fig. 1, based on both laboratory and field tests with CAVIJET cavitating water jet nozzles. In the next section the derivation of Fig. 1 will be described.

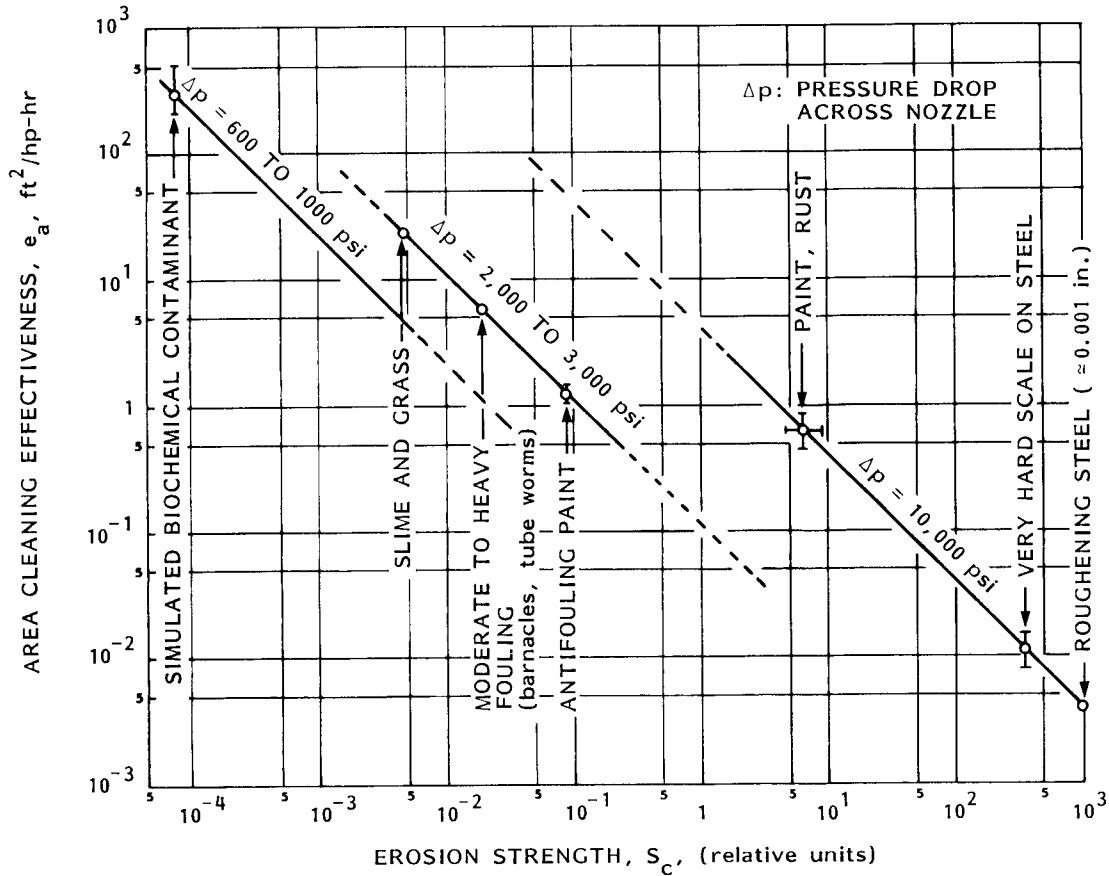


Figure 1. Relative erodability of materials cleaned with CAVIJET<sup>R</sup> cavitating jets (values shown are estimates; to be used only for order of magnitude comparisons).

As indicated on the abscissa in Fig. 1, a relative scale was chosen for  $S_c$ . This scale was arbitrarily based on a value of  $10^3$  for the eroding of steel to a roughness profile of about 0.001 in. (0.025 mm).

### SOME CLEANING EXAMPLES

To derive the curves shown in Fig. 1, a number of cleaning examples were used. These examples are summarized in Table 1. It is seen that a wide variety of nozzle sizes, pressures, and substance/substrate combinations were compiled for this derivation. Since this was existing "historical" data, no planned systematic variation of parameters was available. Despite this lack of coordinated testing, it was found that the  $e_a$  values for comparable substances to be cleaned tended to group closely together.

Table 1. Cleaning examples used to derive relation between  $e_a$  and  $S_c$  (Fig. 1)

Item	Substance/Substrate	CAVIJET Nozzle, Diameter, Type*	Nozzle Pressure Drop, $\Delta p$ ,		Area Cleaning Rate, A,		Power Delivered by Nozzle, P		Area Cleaning Effectiveness, $e_a$		Erosion Strength, $S_c$
			ksf	MPa	ft <sup>2</sup> /hr	m <sup>2</sup> /hr	hp	KW	ft <sup>2</sup> /hp-hr	m <sup>2</sup> /hp-hr	
1	Roughening of steel (=0.001 in.), in air	0.086 in. (2.2 mm), W/CB	10.0	68.9	0.31	0.029	73	54	$4 \times 10^{-3}$	$5.0 \times 10^{-4}$	$1 \times 10^3$
2	Hard rust from steel; submerged	0.107 in. (2.7 mm), plain			1 to 2	0.09 to 0.19	129	96	0.8 to $1.5 \times 10^{-2}$	$1.0 \times 10^{-4}$ to $1.9 \times 10^{-3}$	$3.5 \times 10^2$
3	Paint removal; steel; in air	0.073 in. (1.8 mm), W/CB			32	3.0	53	40	0.61	0.076	$6.2 \times 10^0$
4	Paint, rust; steel; in air	0.086 in. (2.2 mm), W/CB			46	4.3	73	54	0.63	0.078	
5	Paint; steel; in air	0.047 in. (1.2 mm) W/CB			18	1.7	22	16	0.83	0.10	
6	Paint; steel; in air	0.086 in. (2.2 mm) W/CB			42	3.9	73	54	0.58	0.072	
7	Rust from steel; in air	0.086 in. (2.2 mm) W/CB			31	2.9	73	54	0.43	0.054	
8	Paint; steel; in air	0.107 in. (2.7 mm) W/CB	9.7	66.9	66	6.1	124	92	0.53	0.066	$6.5 \times 10^{-1}$
9	Paint; steel; submerged	0.107 in. (2.7 mm) plain	8.4	57.9	75	7.0	100	75	0.75	0.093	
10	Antifouling paint; steel; submerged	0.107 in. (2.7 mm) plain	3.0	20.7	22 to 30	2.0 to 2.8	21	16	1.1 to 1.4	0.14 to 0.17	$9.0 \times 10^{-2}$
11	Heavy fouling (tube worms, barnacles); bronze; submerged	0.107 in. (2.7 mm) plain	3.0	20.7	120	11.1	21	16	5.6	0.70	$1.9 \times 10^{-2}$
12	Moderate to heavy fouling; bronze, submerged	0.107 in. (2.7 mm) plain	2.0	13.8	69	6.4	12	9	5.9	0.74	
13	Moderate to heavy fouling; bronze, submerged	0.107 in. (2.7 mm) plain	3.0	20.7	120	11.1	21	16	5.6	0.70	
14	Slime, filmy growth; bronze; submerged	0.107 in. (2.7 mm) plain	3.0	20.7	480	45	21	16	22.5	2.8	$4.6 \times 10^{-3}$
15	Grasses, heavy film; bronze; submerged	0.107 in. (2.7 mm) plain	3.0	20.7	360	33	21	16	16.9	2.1	
16	Simulated biochemical contaminant; painted steel; in air	0.086 in. (2.2 mm) W/CB	0.6 to 1.0	4.1 to 6.9	300 to 600	28 to 56	1 to 2	0.75 to 1.15	300 to 500	3.7 to 6.2	$8.0 \times 10^{-5}$

\* Type of CAVIJET nozzle: "W/CB" is a centerbody type nozzle.  
 "Plain" is a nozzle without centerbody or other insert.

The point of departure for the 10,000 psi (68.9 MPa) line in Fig. 1 was the data for Item 1, with  $S_c = 10^3$ . This line, per Relation [6], was graphed at a slope of 1:1 on log-log paper. Using this line, and the measured  $e_a$  values, the other points were located at the thus derived  $S_c$  values shown in Fig. 1.

To obtain the line for  $\Delta p = 2000$  to  $3000$  psi (13.8 to 20.6 MPa), the data from Items 14 and 9 were compared, since the same nozzle was used for both of these tests. Using the relation:

$$I = (\Delta p)^3 \quad (7)$$

which has been observed for much of the work with CAVIJET nozzles, the  $S_c$ -value of  $4.6 \times 10^{-3}$  was derived for Item 14. The line was then graphed for this pressure range at a 45 degree slope, and the required  $S_c$  values located as above for the higher pressure line. The line for AP = 600 to 1000 psi (4.1 to 6.9 MPa) was similarly extrapolated from the intermediate pressure line in Fig. 1.

It should be emphasized that the relations between  $e_a$  and  $S_c$  shown in Fig. 1 are presented for illustrative purposes only, and represent at best only an order of magnitude comparison of these parameters.

#### CONCLUDING REMARKS

A concept for comparing the relative ability of water jet nozzles to clean has been described. Although in a very preliminary status, this concept will hopefully begin to stimulate other investigators to examine their data and make some comparisons. This may in the future lead to inter-laboratory comparative testing, and perhaps eventually to a standard method for comparing various cleaning jets. A parallel developmental need is for standard "targets", i.e., simulated substance/substrate combinations that anyone can create and use to make comparisons. An example we have found useful for simulating  $S_c$  in the range of roughly 1 is given in Appendix A.

#### REFERENCES

1. Conn, A. F. and Rudy, S. L., "Parameters for a Ship Hull Cleaning System Using the CAVIJET' Cavitating Water Jet Method," HYDRONAUTICS, Incorporated Technical Report 7510-1, (also National Maritime Research Center Report No. NMRC-275-44210-RI), July 1975.
2. Conn, A. F., Johnson, V. E., Jr., Lindenmuth, W. T., and Frederick, G. S., "Some Industrial Applications of CAVIJET Cavitating Fluid Jets," Proceeding's of First U.S. Water Jet Symposium, Golden, Colorado, pp. V-2.1 to V-2.11, April 1981.
3. Thiruvengadam, A., "The Concept of Erosion Strength," Erosion by Cavitation or Impingement, ASTM STP 408, American Society for Testing and Materials-, pp. 22-41, 1967.
4. Heymann, F. J., "Toward Quantitative Prediction of Liquid Impact Erosion," Characterization and Determination of Erosion Resistance, ASTM STP 474, American Society for-Testing and Materials, pp. 212 - 248, 1970.

#### APPENDIX A

A simulant which has proven capable of reproducible results, and which appears to provide an erosion strength of about 1 (see Fig. 1) was prepared as follows:

Substrate: panel of 6U61-T651 aluminum alloy. Use a powered wire brush to remove all dirt and to very slightly roughen the surface. A final cleaning, to remove any oily residues is then made with acetone, applied with a soft cloth.

Substance-to-be-removed: commercially available flat-primer in spray can format. The particular gray paint used was alkalyd-based, and was manufactured by Illinois Bronze Paint Co. as their "Weekend Spray Paint" brand. An evenly coated, single application is sprayed onto the aluminum surface, until a dry film thickness of about 1 mil (0.025 mm) is achieved.

# THE DEVELOPMENT OF A HIGH PRODUCTION ABRASIVE WATER JET NOZZLE SYSTEM

M. J. Woodward, System and Product Development Manager and R. S. Judson, Engineer  
Weatherford Water Jetting Systems  
Weatherford, Texas

## ABSTRACT

This paper describes a novel abrasive water jet nozzle designed for high production surface preparation of steel structures prior to painting.

This nozzle resulted as part of a two year project to develop the most cost-effective method of pre-paint surface preparation of carbon steel.

The program included a series of parametric experiments that quantitatively evaluated the effect of water jet pressure; water jet flow; abrasive feed rate and nozzle stand-off distance on the economic efficiency of the nozzle system. The text also examines factors that should be considered when designing an economically efficient surface preparation system.

It concludes by comparing the operational cost of an optimized high production dry abrasive blasting unit with that of an optimized high production abrasive water jet system, and shows the economic advantages for abrasive water jet units.

## INTRODUCTION

Steel surface preparation methods pursuant to painting includes scraping, brushing and blasting. The most common blasting technique is the dry abrasive method. Advantages of dry abrasive blasting over scraping and brushing are: speed of operation; the excellent anchor pattern that is achieved provides a good coating adhesion and the cleanliness level that is achieved. The major problems associated with dry abrasive blasting are the cost and generation of dust which can cause silicosis when silica sand is used. A water ring is sometimes placed around the abrasive blasting nozzle to spray water on to the abrasive stream to minimize or eliminate the dust cloud that is produced by the abrasive. (1).

Some steel surface preparation prior to painting is done using abrasive water jet systems where an abrasive material is entrained into a high velocity water jet. (2). The high velocity water jet accelerates the abrasive particles to a velocity capable of removing rust and deposits from the steel structure.

To the authors' knowledge very little technical information (such as 3) has been published on quantitative evaluation of abrasive water jet cleaning. There does not appear to be any published information on "wide path" abrasive water jet cleaning systems. The authors, therefore, elected to publish this paper on the results of quantitative tests to date on single nozzle path tests. It is intended that future tests on multiple nozzle path testing can be accomplished to evaluate the effects of multiple nozzles in close proximity.

As part of a project to develop the most cost-effective method of pre-paint surface preparation of carbon steel structures with an abrasive water jet system, several different types of abrasive water jet nozzles were evaluated. One of the requirements of the project was to clean relatively wide paths. This involved using a number of abrasive water jet nozzles operating simultaneously (10-20). This required that the nozzles be reliable and easy to maintain. Tests under field conditions revealed that nozzles using multiple water orifices (typically six (6) holes) were plagued with plugging problems even when water filters were used.

A novel abrasive water jet nozzle was developed and tested. This nozzle (shown in Plate 1) is simple, reliable and easy to maintain. It has a single water orifice therefore, the orifice is larger than the orifices of a multiorifice nozzle for a given water flow rate and is less likely to plug. Experiments were run using this nozzle to evaluate the effect of water jet pressure; water jet flow; abrasive feed rate and nozzle stand-off distance on the economic efficiency of the nozzle system.

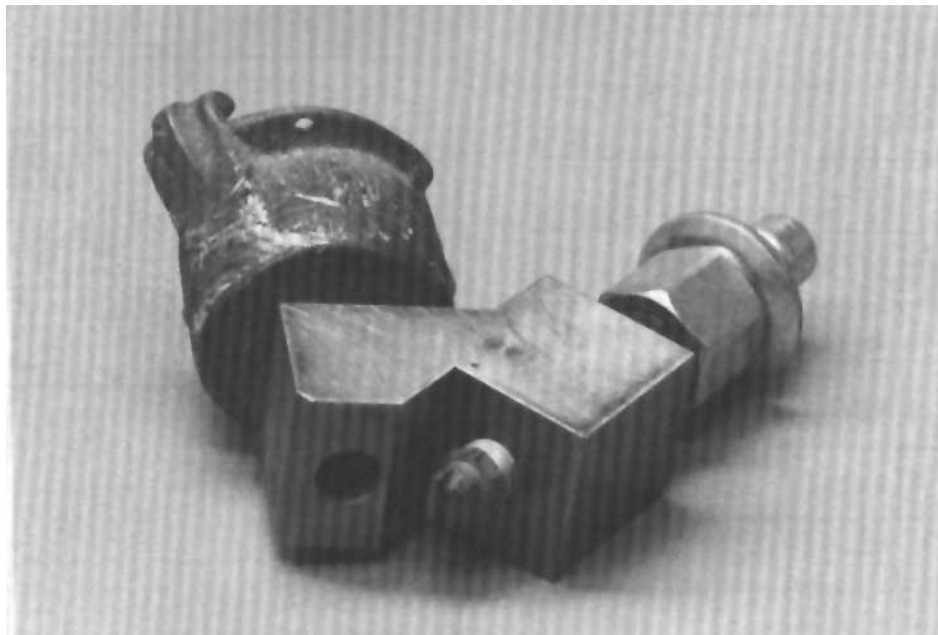


Plate 1. Water/Abrasive nozzle.

#### Test Procedure

The tests were conducted in a test cabinet. The test cabinet had a movable fixture for mounting the sand nozzle. The movable fixture was traversed in the cabinet by a hydraulic cylinder. Hydraulic fluid was supplied to the hydraulic cylinder by an electrically powered variable flow hydraulic pump. This arrangement allowed variable travel speed of the sand nozzle across the test sample, which was mounted in the cabinet below the sand nozzle. The stand-off distance between the sand nozzle and the test sample was variable. All tests were run with the incidence angle between test sample surface and the jet stream at 45D. Sand was supplied to the sand nozzle from a conventional pressurized sand blast machine with a sand flow control valve.

Air to the sand blast machine was supplied from plant air pressure through an air pressure regulator valve. High-pressure water for the water jet was supplied from a diesel power water jetting unit with a quintuplex pump capable of delivering up to 20 gpm at 10,000 psi. Sand flow rate was determined by placing the sand head in a closed container suspended from a spring scale and measuring the weight increase for a fixed time. Water jet nozzle flow rates were determined by timed flow into a calibrated tank.

The mild steel test samples were made from eleven (11) gauge sheet steel cut in one foot by three feet sections (1' x 3'). These samples were placed in the open air to age three (3) months prior to the tests.

### Test Procedure

Tests were conducted by adjusting the water pressure; water flow rate; abrasive feed rate and stand-off distance to the desired values for the particular test run. Test samples were then blasted at different traverse speeds until a SA 2-1/2 surface finish was obtained. The cleaning rate was then calculated using the measured traverse speed and cleaned path width.

### RESULTS

The effect of jet pressures between 200 psi and 7,400 psi on the cost per square foot (\$/ft<sup>2</sup>) was examined. During this series of tests, the following conditions were maintained:

Flow	= 5 gpm
Stand-off	= 2-1/4 inches
Abrasive Feed Rate	= 50 lbs/min
Type of Abrasive	= Black Grit Size BG-4 (20-40 Mesh)
Nozzle Incidence Angle	= 45°

The cost per square foot of surface cleaned decreased rapidly as pressure was increased from 1,000 psi to 4,000 psi. As pressure was increased above 4,000 psi, very little decrease in cost was achieved. The results of these tests are shown in Figure 1.

### Water Jet Flow

The effect of water jet flow between 2.5 gpm and 20 gpm on the cost per square foot (\$/ft<sup>2</sup>) was examined. The following conditions were maintained during these tests:

Water Jet Pressure	= 4,000 to 5,000 psi
Stand-Off Distance	= 2" to 5"
Abrasive Feed Rate	= 50 lbs/min
Type of Abrasive	= Black Grit Size BG-4 (20-40 Mesh)
Nozzle Incidence Angle	= 45 °

The cost per square foot of surface cleaned decreased gradually as flow was increased from 2 gpm to 12 gpm. The results of these tests are shown in Figure 2.

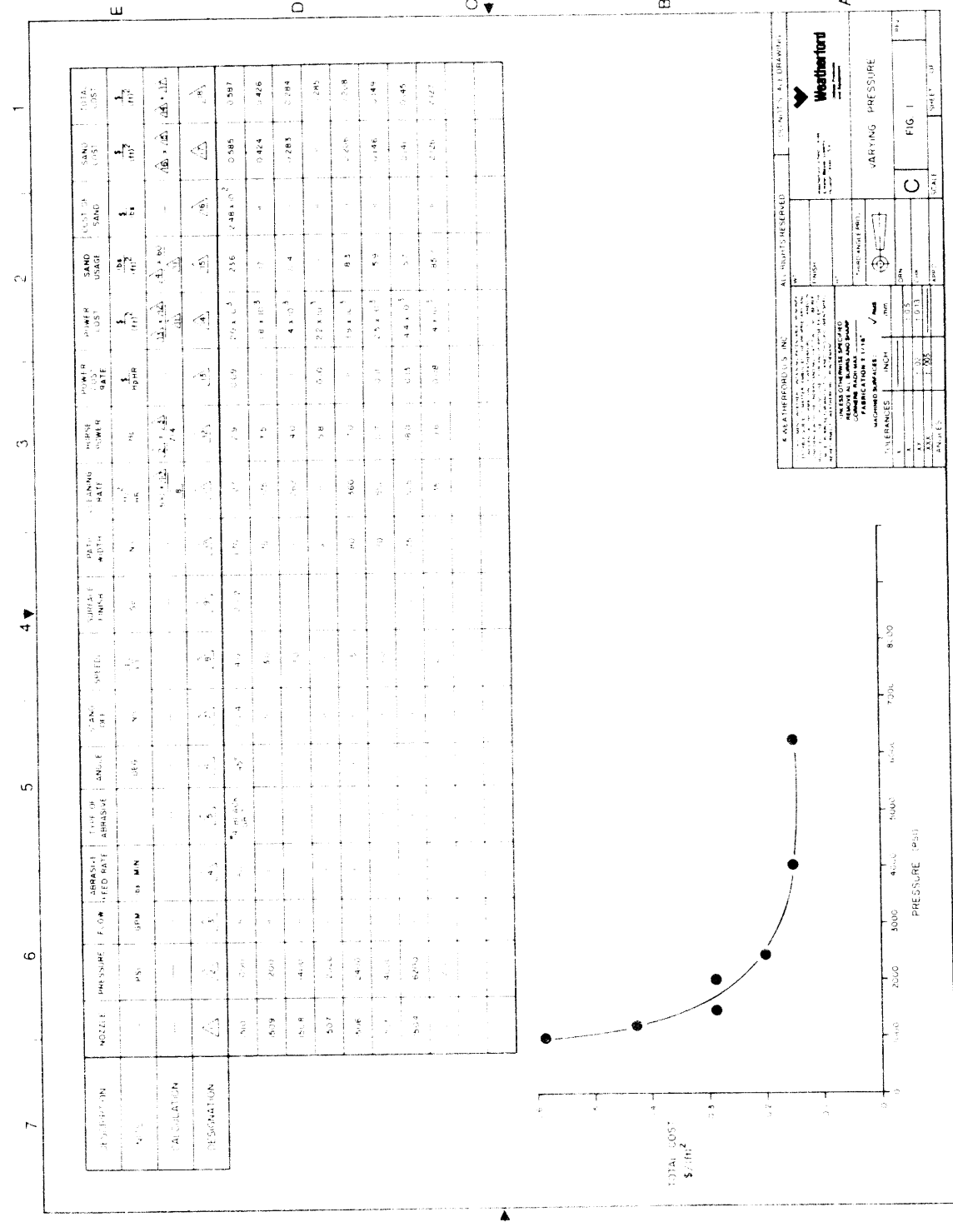


Figure 1. Cost per square foot cleaned versus pressure.



### Abrasive Feed Rate

The effect of abrasive feed rate between 9 lbs/min and 60 lbs/min on the cost per square foot (\$/ft<sup>2</sup>) was examined. The following conditions were maintained during these tests:

Water Jet Pressure	= 1,000 psi
Water Jet Flow	= 5 gpm
Stand-off Distance	= 3 inches
Type of Abrasive	= Black Grit Size BG-4 (20-40 Mesh)
Nozzle Incidence Angle	= 45°

The cost per square foot of surface cleaned was essentially constant as abrasive feed rate was increased from 9 lbs/min to 60 lbs/min.

The results of these tests are shown in Figure 3.

### Nozzle Stand-Off Distance

The effect of nozzle stand-off distance between two inches (2") and eight inches (8") on the cost per square foot (\$/ ft<sup>2</sup>) was examined. The following conditions were maintained during these tests:

Water Jet Pressure	= 1,000 psi
Water Jet Flow	= 5 gpm
Abrasive Feed Rate	= 50 lbs/min
Type of Abrasive	= Black Grit Size BG-4 (20-40 Mesh)
Nozzle Incidence Angle	= 45°

The cost per square foot of surface cleaned was essentially constant as nozzle standoff distance was increased from two inches (2") to eight (8") inches.

The results of these tests are shown in Figure 4.

### Discussion of Results

The data from the experimental tests is shown in Table 1 thru Table 4. The measured data is recorded in vertical columns 1 thru 7. The cost of sand used (Vertical Column 13) was taken as the current cost of bulk sandblast sand obtained from Clemtex, Inc. in Houston, Texas. The method of power cost was taken from Reference 4 (Figure 1). The method for determining the calculated values in Figure 1 thru 4 are shown in the horizontal row labeled "Calculation".

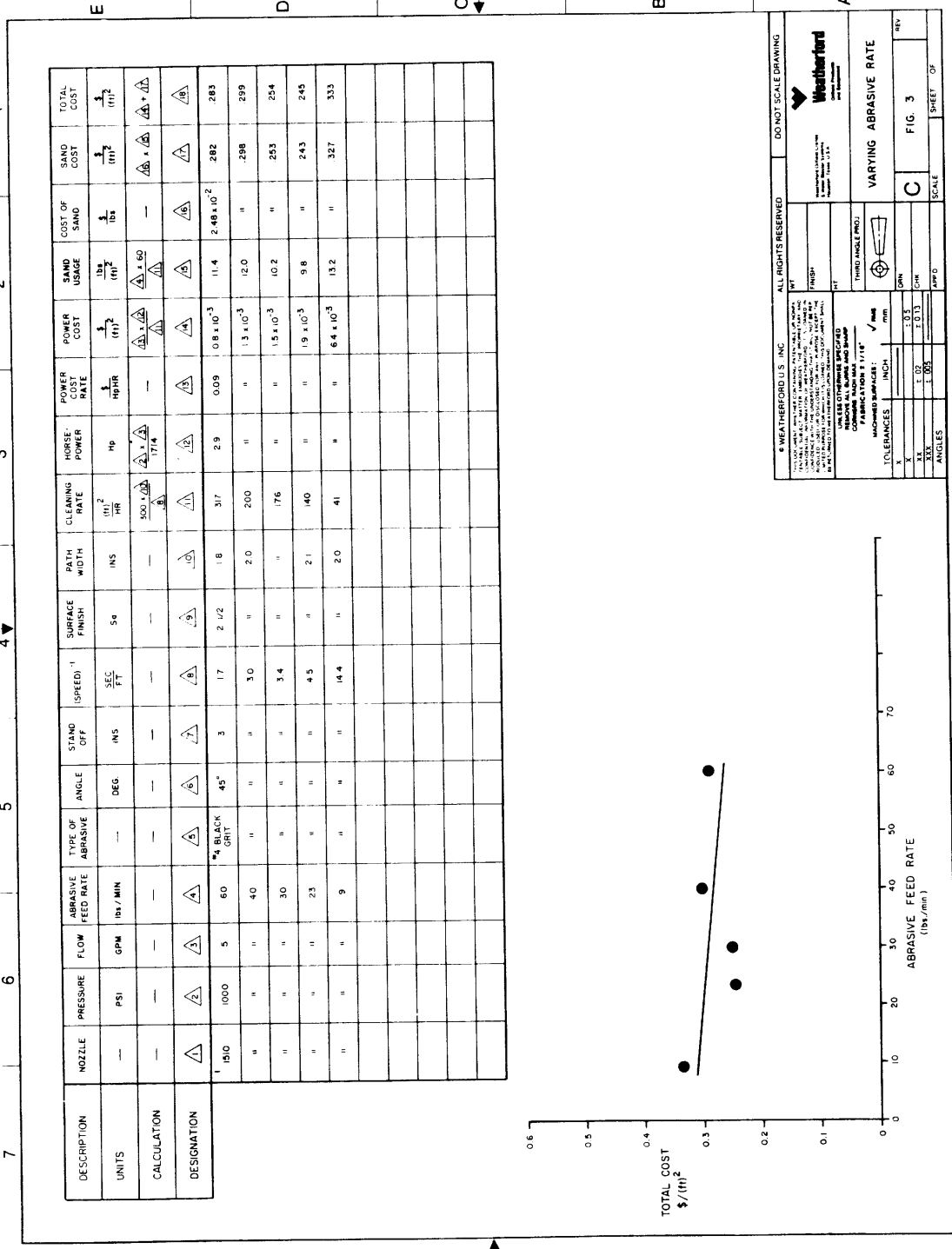


Figure 3. Total cost per square foot cleaned versus abrasive feed rate.

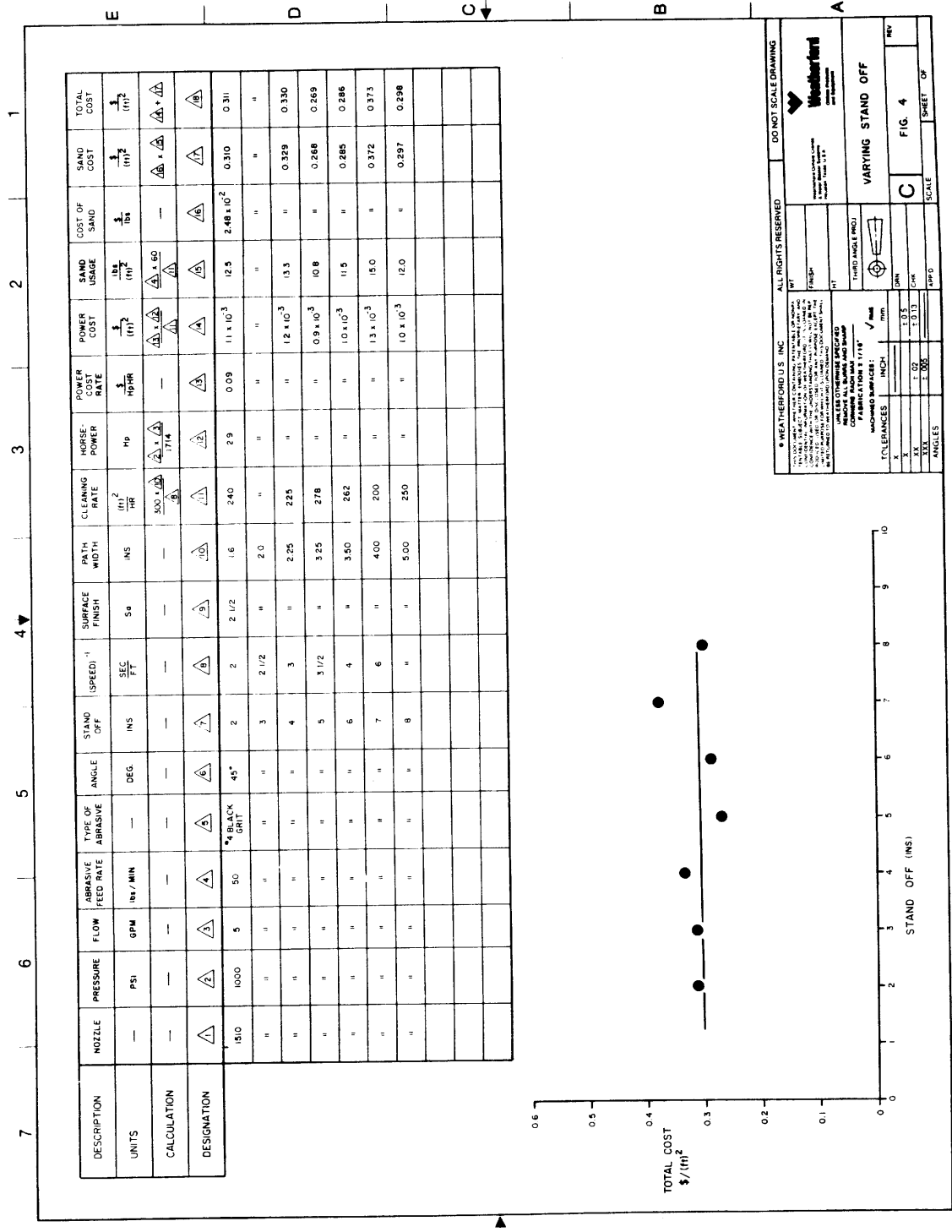


Figure 4. Total cost per square foot cleaned versus stand-off distance

The cost per square foot cleaned decreased as pressure was increased but at a decreasing rate until no further decrease in cost was noted with increased pressure. As water pressure is increased, the jet velocity is increased and in turn accelerates the abrasive particles to a higher velocity. The sheet metal sample had a contaminate layer of

finite thickness. It is assumed that at low particle velocity, several successive particle impacts were required to penetrate the contaminated layer. As the abrasive particle velocity was increased, fewer impacts were required to penetrate the contaminated layer until a point where individual impacts penetrated the contaminated layer and further increase in water pressure and particle velocity would not result in additional contaminant removal.

Cost per square foot cleaned decreased as water flow was increased but at a decreasing rate. It is assumed that at low water flow rate, some of the abrasive particles are not accelerated sufficiently. As water flow rate is increased, a greater portion of the abrasive is accelerated and increased the contaminant removal from the steel plate. Once all of the abrasive is adequately accelerated, no additional cleaning is achieved. Further increases in water flow, for a given abrasive flow, will not result in additional cleaning but will cause an increase in power cost.

Cost per square foot cleaned remained approximately constant as the abrasive flow rate was varied. This was true for the abrasive flow rates tested (9 lbs/min to 60 lbs/min). It is assumed that if the abrasive particles are accelerated to a velocity capable of removing the surface contaminant, this linear relationship between abrasive flow rate and cleaning cost will exist. It is further assumed that if abrasive flow rate is increased to a point where the water jet cannot accelerate the abrasive particles adequately (5), the cost per square foot cleaned will increase.

The cost per square foot cleaned remained approximately constant as stand-off distance was varied between two (2) inches and eight (8) inches. The sand nozzle used in these tests has a fan shaped jet. When the standoff distance is increased, the path width is increased. It is assumed that when the abrasive is accelerated to a velocity capable of removing the contaminant on the plate surface, the cleaning rate and cost will be proportional to the abrasive particle impact rate per unit area. Since the path width increased with increased stand-off distance, it was necessary to move the nozzle slower at increased stand-off to achieve constant particle impact rate. No tests were made at very large stand-off distances when it is assumed that particle velocity would be much lower, therefore, cleaning costs much higher.

## CONCLUSION

As was shown in Figure 2, the cost per square foot of wet abrasive blasting is 0.112\$/ft<sup>2</sup>. This compares with 0.178\$/ft<sup>2</sup> (1) for dry blasting showing the distinct cost advantage of wet abrasive blasting. One additional point to consider is that the sand consumption is reduced from 6.66 lbs/ft<sup>2</sup> for dry blasting to 4.28 lbs/ft<sup>2</sup> for wet blasting thus drastically impacting the associated cost of clean up after the job.

## REFERENCES

1. Clemtex Control Equipment & Supplies Clemtex commercial catalogue Clemtex, Inc. – Houston, Texas
- 2 Parts Manual Weatherford Water 2 Blaster System - Section 7 - Page 7. Printed January 1984 Weatherford Water Jetting Systems Houston, Texas

3. Barker, C. R.; Mazurkiewicz, M. and Anderson M. Evaluation of an Abrasive Cleaning System - Sixth International Symposium on Jet Cutting Technology April 6-8, 1982 BHRA Fluid Engineering, Cranfield, Bedford U.K.
4. Swan, S.P.D. "Economic Consideration in Water Jet Cleaning" The Second U.S. Water Jet Symposium, May 24-26, 1983, University of Missouri-Rolla, Rolla, Missouri
5. Hashish, M., "Experimental Studies of Cutting with Abrasive Jets," The Second U.S. Water Jet Symposium, May 24-26, 1983, University of Missouri-Rolla, Rolla, Missouri

## CLEANING THE TUBE SIDE OF HEAT EXCHANGERS

R. Paseman and L. Griffith  
Powerlance  
Houston, Texas

### ABSTRACT

There are many ways to clean shell and tube heat exchangers besides using high-pressure water. Some of the more popular methods are covered along with some myths associated with high-pressure water.

The authors represent the contracting industry who actually do the work and the accessory manufacturing business, and between them have 42 years of field experience.

Lee Griffith is Product Line Manager with Naylor Industrial Services, Inc. and has a Bachelor's degree in Chemical Engineering from Virginia Polytechnic Institute.

Richard Paseman is founder and President of American Powerlance Company.

### CLEANING THE TUBE SIDE OF HEAT EXCHANGES

It has only been since the late 1950's that heat exchangers have been cleaned with high pressure water. Prior to that time, they were cleaned by sand blasting, chemicals, rods, hand held drills, brushes on rods, bent sticks or whatever. Plant operators have even been known to burn exchangers.

In 1956 a man from Monsanto in St. Louis gave a talk to the Houston Coating Society in Houston, Texas on the benefits of using high-pressure water to remove contaminants from a surface before painting and between coats of paint. His conclusion that 750 psi. (52 bars) of water was better than steam cleaning or just flushing the surface was based on Monsanto's experience in repainting their own plants.

At about the same time, it was found that some of the early asphalt based mastics were not protecting steel surfaces as well as had been hoped when they were first applied. Removing mastic from 1/8 inch to 1/2 inch (0.003 to 0.012 meters) thick was a costly and time-consuming problem. High-pressure water was really the most practical way to remove the mastic. The best way to get rid of the mastic was to set fire to it, but that solution was frowned on.

When the plant people saw the advantages of using water to remove the mastic, they looked for other ways to utilize it too. And that is how high pressure water was introduced in the Gulf Coast area. However, it was not until the early 1960's that water blasting was accepted here and in Europe for cleaning heat exchangers.

Shell and tube heat exchangers are generally a cluster of tubes 3 to 45 feet (0.9 to 13.7 meters) long with the tubes being 0.5 to 2 inch (0.012 to 0.05 meters) in diameter. There can be 100 to several thousand tubes in a tube bundle, which is usually circular in shape. The diameter can be 1 to 10 feet (0.3 to 3.05 meters).

For our purposes here, we will lump reactors, re-boilers, and surface condensers as all being heat exchangers and they all have one thing in common. Sooner or later, they have to be cleaned. Like the radiator in your car, they need to be flushed and cleaned out.

It will depend on the service they are in how hard the tubes are to clean. Fresh water can build up solid calcium carbonate deposits that are harder than concrete which pose a problem to remove even when they are drilled. Salt and brackish water produce calcium sulfate. As plant operators run higher cycles on cooling towers and run their units at higher temperatures these water cooled exchangers are fouling faster than ever. Many plastics in chemical plant bundles can foul so bad the tubes are almost impossible to drill out. In fact, nylon, polyethylene and a few others cannot be drilled effectively.

Water is used in roughly 95% of the exchanger tube sides and around 5% in the shell side of exchangers in cooling water service. Continuous chemical treatment for scale control of cooling water used in exchangers is a big business. However, air pollutants and other contaminants can mix with the water as it cascades through the cooling tower to dilute its effect. Also, if the system is not constantly monitored, scale can form anyway.

Interestingly enough, a type of freshwater clam will attach itself to the inside of power plant surface condensers, and they will continue to grow there. Salt water deposits, whether marine growth or other foulant, can also restrict flow and heat exchange.

Because of the inconvenience of unbolting the exchanger heads, down time, and cost; various methods are used in cooling water service to prolong the time between shut downs in addition to the usual back flushing. For example, there is a process used in large power plant surface condensers that retards fouling by frequently running urethane or sponge balls through the tubes. Several hundred balls are introduced in the upstream side of the bundle and are recaptured in the downstream side. The system is so designed that all the tubes are cleaned by random selection and as the balls wear out, the equipment rejects them and pulls them out of service.

Another system used when water is run through the tubes utilizes magnets inside the channel head or on the inlet piping. The magnetic force reportedly keeps all the solids in suspension until they are dropped into the cooling tower basin rather than clinging to the tube walls. The solids then leave the system by the normal blow-down.

Another method is where a brush fits inside of the tube and is prevented from escaping by cages on each end of the tube. To clean the tube, the flow is reversed by valving, and the brush can be driven back and forth by changing the direction of the flow.

We understand that sometimes fouling can be reduced when static mixers are used inside the tubes. The static mixer is a flat piece of steel made into a spiral that is inserted at the inlet of each tube. Flow is forced to the periphery of the tube and because the velocity is increased, less fouling should occur. This is the same principle used in the design of spiral heat exchangers.

Equipment designers have attempted to reduce fouling by manufacturing equipment with very smooth surfaces. Consequently we have seen exchanger tubes manufactured of glass, polished alloys, and teflon. All surfaces still seem to foul occasionally; some surfaces foul as fast as with carbon steel. Other "solutions" by equipment designers have led to creations such as the scraped surface exchanger where a mechanical scraper is rotated inside a double pipe exchanger to continuously remove build up of foulant from the heat exchange surfaces. While this concept works on some products, it is certainly not universal.

For some very heavily fouled heat exchangers in heavy crude service or in certain polymer manufacturing areas such as butadiene, isoprene, nylon, and styrene, the heat exchangers are often "burned" to remove the contaminants. Originally these bundles were actually set on fire on a back corner of the plant. As metallurgies changed and environmental concerns arose, these bundles were sent to equipment fabricators who burned the bundles in a more controlled manner in their heat treating furnaces. This is still being done today in certain applications. The burning process does reduce the life of the exchangers, however, and now plant operators are looking at solvents and devices such as the Powerlance which can apply more energy directly on a pluggage.

Chemicals are the best method for getting tubes clean. They can be formulated to remove most fouling products and they have the added advantage of being able to clean tubes, piping, and vessels all at the same time with minimum manpower. The disadvantage is that they can't clean a plugged tube and disposing of the spent chemicals can be very expensive. It would not be unusual for chemical disposal to be the highest cost of the job.

Chemistry is added to hydroblast water, in certain instances, to enhance the cleaning capabilities of the high-pressure water. Detergents, soaps, and surfactants are mixed into water streams to aid in the removal of light hydrocarbon films. Chelants and sequestrants are used to remove light iron oxides and polyphosphates are used to passivate clean surfaces to retard oxidation. One important modification of the water, which is often overlooked, is to heat the water going to the pump. Especially when removing thick hydrocarbons, using hot water can make a substantial difference in time requirements. The use of hot water does sometimes preclude the use of manually operated lances due to safety considerations. This problem is alleviated by utilizing an automated lancing device such as the Powerlance.

Drilling out plugged tubes and using water to flush out the deposits has been used successfully for many years. Equipment is now available that will use high-pressure water up to 10,000 p.s.i. (690 bars) that helps the drilling process. Steel, brass or fiber brushes can also be used with drills or on the end of automated lancing equipment.

And blasting of tubes with sand, grit, or beads can also be effective to remove scale on the tube walls. One company in Europe has documented the improved flow characteristics inside tubes when they have been honed with glass beads!

Surface condensers can be cleaned by using air or water to blow a brush through the tubes. It is a fast and easy way to clean a lot of tubes in a short period of time and most light fouling is removed.

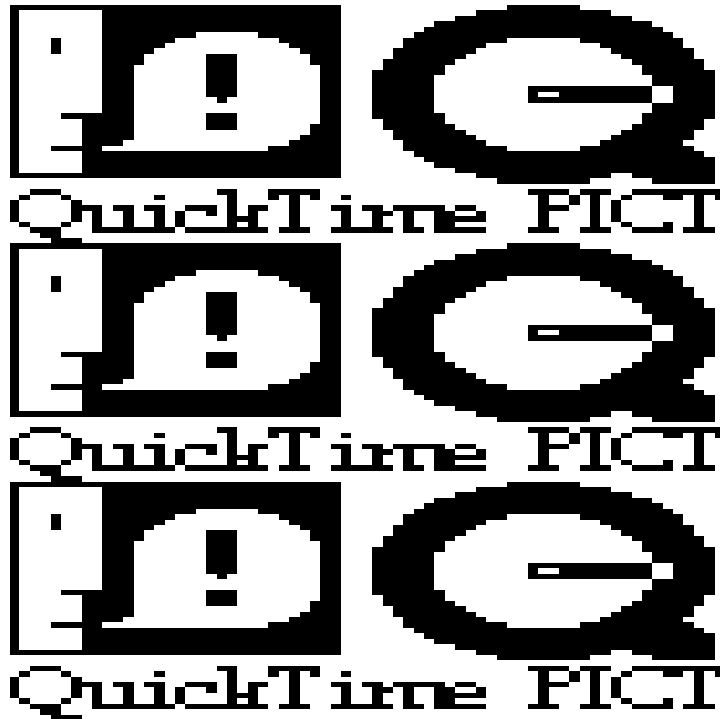
"Hydrosonics" is used to clean tubes in Australia and some plants in the United States. A plastic projectile is inserted into the tube and pushed through using a burst of water. It has been used very successfully for cleaning some styrene bundles. Styrene can be very sticky and will cling to whatever it comes in contact with. If using regular lances, the work goes better if a surfactant is added to the high-pressure water.

While all of the methods mentioned have been or are still being used, the most popular method used is high-pressure water. As you are all aware, water under pressure can be very effective in removing matter out or place.

Cleaning tubes poses special problems. Many times the work is carried out around the clock regardless of the weather. The bundles are not always in a convenient location, they can be vertical or horizontal and often need to be cleaned on an emergency basis. Twenty-four hour service is a necessary requirement not an advantage for the service contractor.

When water blasting started to become popular, 3,000 to 5,000 psi. (207 to 345 bars) was an acceptable pressure for cleaning. Using a walk lance, bundles were cleaned better and faster than previously. However, it soon became apparent that higher pressures were even a little better. Consequently, 10,000 psi. (690 bars) capacity pumps became and still are the requirement for contractors.

Because of room or access problems, flexible lances became and still are very popular for tube cleaning. The fact that they are highly inefficient was soon forgotten because they were more convenient. One man can flex lance while it takes a minimum of two to walk a rigid lance. Note drawing on pressure drop below.



To overcome the pressure drop on a Flex lance and increase the hitting power of the water, SuperWater or a similar polymer product is used to increase the viscosity of the water. The use of SuperWater does provide a better cleaning job and has meant the difference between being able and not being able to clean some exchanger tubes.

Because 70 to 80% of all tube bundles are cleaned with high pressure, water pumps and accessory equipment have improved. There are several manufacturers of water blasters here and abroad. Also, there are companies like Powerlance that just provide accessory equipment.

(If time permits, a 7 1/2 minute video tape on the Powerlance will be shown).

The pressure race is not over yet. Equipment is out working at 35,000 psi. (2,415 bars), and some folks are working on units that will work at higher pressures yet. It seems that at these higher pressures much of the cleaning being done is accomplished by setting up vibrations in the heat exchanger and foulant. Since they have different properties, they will vibrate at different frequencies which causes the scale to become detached from the tube surfaces. By reducing the strength of the bond between the tubes and the foulant, we can more easily remove the contamination.

The question of the right combination of volume and pressure is still up in the air. Every one has their own idea and everybody is right. For cleaning the tube side of exchangers, I was quite happy with the potential of 14 GPM (53 liters per minute) at 10,000 psi. (690 bars). As a contractor, I was not interested in line moleing or multi-gun operation where larger volumes are required. I never ran into a bundle I couldn't clean and usually was called in where others had failed.



Some Powerlance customers have 20,000 psi. units. Most have 20 gpm. (75 liters per minute) at 10,000 psi. (690 bars) and some have 10 gpm. (38 liters per minute) at 10,000 psi. (690 bars) unit. Most operate their Powerlance under 9,000 psi. (621 bars) as that will take care of 99% of the tube bundle cleaning. However, there are a few bundles that do require 12,000 to 13,000 psi. (828 to 897 bars) but those are the rare exceptions.

Cleaning the shell side of a bundle is a different matter. One contractor in the Gulf Coast area has a 1,500 H.P. pump. Using 240 gpm (905 liters per minute) at 7,000 psi. (483 bars) will clean about any bundle in the area. It is the odd one that takes 190 gpm (716 liters per minute) and 10,000 psi. (690 bars). In fact, that much force directed against the tube sheet will give acceptable cleaning to many tubes. It will not get through plugged tubes, though.



Nozzles are another area where there are differing opinions. The angle of attack and the amount of water per orifice is a matter of personal choice. We have made a variety of nozzles for our customers over the years. Our most popular is 13 GPM (49 liters per minute) at 10,000 psi. (690 bars) with one hole straight ahead and the others at 45 degrees facing forward. After that is the 24/45/90 or 24/45 degree, which means it has 24 orifices—12 with 45 degrees forward and 12 at 90 degrees. The 24/45 degrees means 24 holes at 45 degrees forward.

All forward jets in the nozzle produces better cleaning because all the hydraulic energy is directed against the fouling. U tube bundles are cleaned with all forward jet nozzles and the lance is adjusted so it stops before entering the "U" portion of the tube.

In-plant studies have shown that using the Powerlance rather than a flex lance is faster, safer, and better.



What size orifice is best for tube cleaning? Our experience indicates that it is better to have more smaller orifices than fewer larger ones. For example, our nozzles will permit a theoretical 1 GPM (3.78 liters per minute) per orifice at 10,000 psi. (690 bars). It is easier for us and our customers to size our nozzles to their pumps. Larger orifices do not seem to improve the cleaning result except on plugged latex tubes. On a flat surface the opposite is true. If the tube plug is exceptionally hard, then we recommend one large single orifice that will put a hole through most anything.

The Europeans have developed rotary nozzles that use the high pressure water flow to rotate a rotor on a fixed spindle. We have one, too, that operates on the same principle but with a few modifications. It has been very successful in some instances and in others has not been that much of an improvement over our regular nozzles. We can be more definitive next year on its use.

Does rotating the lance improve the cleaning ability? Some of our customers say yes and others don't think so. I would be inclined towards rotation but our sales and use of a rotation device does not indicate customer preference. The difference in cost between being rotational and non-rotational is about \$20.00 spread over three months, so cost is not a factor.

Is a multi-lance machine better than a single lance? We offer single, double, and triple lance. There, again, Powerlance customers prefer the single lance.

Is complete/total automation possible for cleaning heat exchangers? The answer is yes—but. The "but" only refers to cost—technology is there but the programs for indexing from one tube to the next and from one row to the other is where the real cost is. The program would not be cost effective unless the particular bundles are filled with a very dangerous substance and it was imperative that the operator be isolated from the cleaning area. If that was the case, then a TV system would be much cheaper. Or a

system could be designed that was operator assisted. If you opt for that solution, we are available to assist you. One group that we know of is currently working on a method whereby a heat exchanger can be hydro-blasted during operation. This system is not yet ready for commercialization but serves to show the range of development currently being looked at.

One question not addressed here is how clean is a cleaned tube? We have already said that the cleanest clean surface will be produced by chemicals. And most will agree that the right combination of volume and pressure will remove most if not all residue. But really, what is clean? The answer is—it's a process operators/engineers decision. His decision is based on time allotted-cost-and other factors the cleaning contractor is not always aware of. Recently a contractor cleaned a 340 tube bundle in an hour with his Powerlance. I would think that was little too fast but since he and his customer were happy, I guess I should be too.

If you want to know what the pressure drop is between the pump and the nozzle, refer to "Optimized Jet Cutting Power for Tube Cleaning", presented by John C. Wolgamott and Gerald P. Zink at the Second U.S. Water Jet Conference in May 24-26, 1983. Also refer to attachments at end of this paper.

"Chemical Cleaning from A to Z including Hydro Blasting Additives by Donald A. Alexander is an informative paper. For a copy, contact the National Petroleum Refiners Association for their paper MC42-1 presented at the N.P.R.A. conference held in New Orleans in February 1982. Mr. Alexander was with Chevron Oil in Richmond, Colorado until he retired last year.

"Industrial Chemical Cleaning" by James W. McCoy published by Chemical Publishing Co., in New York City in 1984 is another good source of general information.

Between the two of us, we have 42 years experience in water blasting and 15 years in chemical cleaning. We can assure you that we don't have complete answers to all your cleaning problems, but we have heard (conservatively) 95 to 98% of the questions. Cleaning heat exchanger tubes is not a science—it is an art, but we are still batting 99%. The man on the job is still the most important element in any cleaning operation.

Thank you for your attention, and hopefully we will hear the other (5 – 2%) of the questions.

PRES- SURE	VELCC- ITY	ORIFICE DIAMETER													
		1 64	1 32	3 64	1 16	5 64	3 32	7 64	1 8	9 64	5 32	11 64	3 16	7 32	1 4
PSI	FT/SEC.														
200	173	.102	.415	.932	1.66	2.58	3.72	5.07	6.62	8.37	10.3	12.5	14.9	20.2	26.38
400	244	.145	.586	1.32	2.34	3.64	5.25	7.15	9.34	11.8	14.6	17.6	21.0	28.6	37.31
600	299	.177	.718	1.61	2.86	4.46	6.42	8.76	11.45	14.5	17.9	21.6	25.7	35.0	45.70
800	345	.205	.829	1.86	3.30	5.15	7.42	10.1	13.21	16.7	20.6	24.9	29.7	40.4	52.77
1000	385	.228	.925	2.08	3.69	5.75	8.28	11.3	14.74	18.6	23.0	27.8	33.1	45.2	59.00
1200	422	.250	1.014	2.27	4.04	6.30	9.07	12.4	16.16	20.4	25.2	30.5	36.3	49.5	64.63
1400	456	.270	1.095	2.46	4.37	6.80	9.80	13.4	17.46	22.1	27.2	33.0	39.2	53.4	69.80
1600	488	.289	1.172	2.63	4.67	7.28	10.5	14.3	18.78	23.6	29.2	35.3	42.0	57.1	74.63
1800	519	.308	1.247	2.80	4.97	7.75	11.16	15.2	19.87	25.1	31.0	37.5	44.7	60.6	79.15
2000	546	.324	1.312	2.94	5.23	8.15	11.74	16.0	20.9	26.4	32.6	39.5	47.0	63.9	83.43
2200	572	.339	1.374	3.08	5.48	8.54	12.30	16.8	21.89	27.7	34.2	41.4	49.3	67.0	87.51
2400	598	.354	1.437	3.22	5.73	8.93	12.86	17.5	22.89	28.9	35.7	43.2	51.5	70.0	91.40
2600	623	.369	1.497	3.36	5.97	9.30	13.39	18.2	23.85	30.1	37.2	45.0	53.7	72.8	95.13
2800	645	.382	1.50	3.48	6.18	9.63	13.87	18.9	24.69	31.2	38.5	46.6	55.6	75.6	98.72
3000	670	.397	1.61	3.61	6.42	10.0	14.4	19.6	25.65	32.4	40.0	48.4	57.7	78.2	102.18
3200	691	.410	1.66	3.72	6.62	10.3	14.86	20.2	26.45	33.4	41.3	50.0	59.5	80.8	105.54
3400	711	.421	1.708	3.83	6.81	10.6	15.29	20.8	27.22	34.4	42.5	51.4	61.2	83.3	108.78
3600	731	.433	1.756	3.94	7.0	10.9	15.72	21.4	27.98	35.4	43.7	52.8	62.9	85.7	111.94
3800	751	.445	1.804	4.05	7.19	11.2	16.15	22.0	28.75	36.3	44.9	54.3	64.7	88.1	115.00
4000	771	.457	1.852	4.16	7.38	11.5	16.58	22.6	29.51	37.3	46.1	55.7	66.4	90.3	117.99
4200	791	.469	1.90	4.26	7.58	11.8	17.00	23.2	30.28	38.3	47.2	57.2	68.1	92.6	120.91
4400	803	.476	1.929	4.33	7.69	11.99	17.3	23.5	30.74	38.9	48.0	58.0	69.2	94.8	123.75
4600	827	.490	1.987	4.46	7.92	12.34	17.8	24.2	31.66	40.0	49.4	59.8	71.2	96.9	126.53
4800	843	.500	2.025	4.54	8.07	12.58	18.1	24.7	32.27	40.8	50.4	60.9	72.6	99.0	129.25
5000	860	.509	2.064	4.63	8.23	12.82	18.5	25.2	32.88	41.6	51.3	62.1	74.0	101.0	131.92

Multiply by 0.98 for Tapered Jets  
Multiply by 0.61 for Drilled Holes

PRES- SURE	VELOC- ITY	ORIFICE DIAMETER													
		1/64	1/32	3/64	1/16	5/64	3/32	7/64	1/8	9/64	5/32	11/64	3/16	7/32	1/4
PSI	FT/SEC.														
5200	879	.52	2.11	4.74	8.41	13.1	18.9	25.7	33.65	42.5	52.5	63.5	75.6	103.0	134.53
5400	896	.53	2.15	4.83	8.57	13.4	19.3	26.2	34.3	43.4	53.5	64.8	77.0	105.0	137.09
5600	913	.54	2.19	4.92	8.73	13.6	19.6	26.7	34.9	44.2	54.5	66.0	78.5	106.9	139.61
5800	929	.55	2.23	5.01	8.89	13.9	20.0	27.2	35.5	45.0	55.4	67.2	79.9	108.8	142.08
6000	945	.56	2.27	5.09	9.04	14.1	20.3	27.7	36.1	45.7	56.4	68.3	81.3	110.6	144.51
6200	960	.57	2.31	5.18	9.18	14.3	20.6	28.1	36.7	46.5	57.3	69.4	82.6	112.5	146.90
6400	976	.58	2.34	5.26	9.34	14.6	21.0	28.6	37.3	47.2	58.3	70.6	84.0	114.3	149.25
6600	991	.59	2.38	5.34	9.48	14.8	21.3	29.0	37.9	48.0	59.2	71.6	85.3	116.0	151.56
6800	1006	.60	2.41	5.42	9.62	15.0	21.6	29.5	38.5	48.7	60.1	72.7	86.5	117.8	153.85
7000	1020	.60	2.45	5.50	9.76	15.2	21.9	29.9	39.0	49.4	60.9	73.7	87.8	119.5	156.09
7200	1035	.61	2.48	5.58	9.90	15.4	22.3	30.3	39.6	50.1	61.8	74.8	89.0	121.2	158.30
7400	1049	.62	2.52	5.65	10.0	15.7	22.6	30.7	40.1	50.8	62.7	75.8	90.2	122.9	160.49
7600	1063	.63	2.55	5.73	10.2	15.9	22.9	31.1	40.6	51.4	63.5	76.8	91.5		
7800	1077	.64	2.58	5.81	10.3	16.1	23.2	31.5	41.2	52.1	64.3	77.8	92.7		
8000	1091	.65	2.62	5.88	10.4	16.3	23.5	32.0	41.7	52.8	65.2	78.9	94.9		
8200	1104	.65	2.65	5.95	10.6	16.5	23.7	32.3	42.2	53.4	65.9	79.8	95.0		
8400	1118	.66	2.68	6.03	10.7	16.7	24.0	32.7	42.7	54.1	66.8	80.8	96.2		
8600	1131	.67	2.71	6.10	10.8	16.9	24.3	33.1	43.2	54.7	67.6	81.8	97.3		
8800	1144	.68	2.74	6.17	10.9	17.1	24.6	33.5	43.7	55.4	68.3	82.7	98.4		
9000	1157	.68	2.78	6.24	11.1	17.3	24.9	33.9	44.2	56.0	69.1	83.6	99.5		
9200	1170	.69	2.81	6.31	11.2	17.5	25.2	34.3	44.7	56.6	69.9	84.6	100.6		
9400	1182	.70	2.84	6.37	11.3	17.6	25.4	34.6	45.2	57.2	70.6	85.4	101.7		
9600	1195	.71	2.87	6.44	11.4	17.8	25.7	35.0	45.7	57.8	71.4	86.4	103.		
9800	1207	.71	2.90	6.51	11.5	18.0	26.0	35.4	46.1	58.4	72.1	87.3	104.		
10000	1220	.72	2.93	6.58	11.7	18.2	26.2	35.7	46.6	59.0	72.8	88.2	105.		

Multiply by 0.98 for Tapered Jets  
Multiply by 0.61 for Drilled Holes

ATTACHMENT

PRESSURE DROP IN POUNDS PER SQUARE INCH  
PER 50 FEET (15.24 METERS) LENGTH

GPM	3/16 ID=0.187	1/4 ID=0.250	3/8 ID=0.375	1/2 ID=0.500	3/4 ID=0.750	1" ID=1.00
2	332	82	11	3		
4	1098	295	41	10	1	
6	2337	625	87	22	3	
8	4320	1064	148	36	5	1
10	6528	1608	223	55	8	2
12	9147	2253	313	77	11	3
14	12165	2997	416	103	14	4
16		3837	533	132	18	5
18		4771	662	164	23	6
20		5798	805	198	28	7
25		8760	1216	299	42	10
30		12275	1704	419	58	14
35			2266	559	77	19
40			2901	715	99	24
45			3607	889	123	31
50			4384	1080	150	37
55			5229	1288	178	44
60			6142	1514	210	52
65			7123	1755	244	61
70			8170	2013	279	69
75			9282	2287	318	77
80			10459	2576	359	88
85				2882	399	97
90				3204	445	110
95				3542	492	120
100				3993	541	133
110				4644	646	158
120				5419	758	187
130				6325	879	216
140				7256	1009	248
150				8243	1144	281
160				9288	1289	318
170				10390	1444	355
180					1506	396
190					1774	437
200					1948	480

# ROTARY WATERBLAST LANCING MACHINES

G. Zink and J. Wolgamott  
Stoneage,inc.  
Durango, Colorado

## ABSTRACT:

This paper will present an overview of a relatively new family of tools that utilize waterjets for cleaning. The basic design will be discussed covering: structural layout, motors, power transmission, positioning equipment, and specialized attachments. The benefits of using this equipment will be presented. These include: safety, speed, and superior capabilities. The safety aspects are: removal of operator from close proximity to the jets and hazardous materials, fewer operators, less physically demanding than hand lancing methods and the ability to operate remotely. The efficiency advantages are: fast lance transport, complete coverage with rotating jets, and balancing jets are not required so that all available power can be directed where needed. The superior capabilities are due to the machines' ability to handle large amounts of waterblast power and combine that with mechanical cutting.

Applications of these lancing machines will be described, including:

1. Cleaning of heat exchanger tube bundles.
2. Unplugging of cemented pipe.
3. Removal of catalyst from reactor vessels.

## INTRODUCTION

The technology of cleaning using high velocity waterjets has advanced steadily over the last several years. One of the recent innovations is the development of rotary swivels capable of reliable operation at high pressure and high speed rotation. Swivels are the basis for several waterblast tools: floor cleaners, two-and three-axis tank cleaning nozzles, rotary line moles, in situ pipe cleaning equipment, and the topic of this paper, rotary lancing machines. This equipment has many advantages over manual methods, primarily productivity and safety.

Rotary lancing machines (RLM's) are used for cleaning the inside of tubes, pipes and chambers that have long lengths, relatively small diameters and an access opening at the end. A nozzle with various angled jets on the end of a rotating rigid lance is fed into the object to be cleaned. They can be used in horizontal or vertical orientations. The rotation and linear movement of the nozzle is mechanically powered and controlled by an operator. The equipment is usually portable but has been used in fixed applications.

The safety benefits in using this type of equipment are substantial. The operators are further removed from contact with the high-pressure water and splash back from the cleaning operation. The nozzle is rigidly held by the machine, eliminating a misdirected or runaway jet. The machines are less physically demanding and require fewer personnel than manual methods. A vacuum line can be attached to a shroud around the lance and tube opening. This allows for almost complete containment and recovery of any hazardous materials. These features reduce the exposure risk and allow the use of better trained people.

RLM's apply more jet power to the removal of deposits than manual methods. The reaction thrust from the jets limits the power that can be handled manually or require that the jets

be balanced in the nozzle. With the lancing machine all of the jet power can be directed where it is most needed. In small diameter tube cleaning there is substantial pressure loss from flow through the lance. By eliminating the balancing jets less flow is required and higher nozzle pressure is available for more effective cutting. For example: when using a 1/4 in. schedule 80 pipe lance 20 ft in length (1.8 cm OD x .77 cm ID x 6.1 m), the line losses for 15 gpm (57 l/min) are about 600 psi (41 bar). This produces a significant reduction in the cutting ability of the forward jets.

Rotation of the jets offers significant advantages. Primarily this is due to the number of jets required to completely cover the surface. In non-rotary ID tube cleaning, a nozzle with several jets (10 to 20 is not unusual) are needed. For many rotary nozzle applications only two jets may be required. These jets will be larger in diameter to pass the same flow as several small jets. However, the larger jets will hit with more power for more effective cleaning. In the case of polishing, streaks can be eliminated rapidly.

Rotary lancing machine are very effective in the use of water. The machine is powered independently (not by water) and the jets are effectively positioned and moved. By eliminating balancing or pushing jets fewer jets are needed requiring less water consumption. The RLM's will remove the most deposit per gallon of water used, reducing the disposal quantities.

## EQUIPMENT DESIGN

There are several basic elements common to most rotary lancing machines. in general they are: structural frame, water swivel, motors and gearing, controls, lances, nozzles and support devices.

### Structural Frame

A rigid structural frame supports the moving lance, water swivel and rotation motor. Intermediate lance guides are often used to maintain the alignment of the lance during thrusting. The structural frame can be a tube with the swivel inside, welded or bolted channel sections, or a truss. The frame needs to be strong enough to withstand the reaction forces of the thrust and rotation, and to be able to transmit them along the length of the frame. The water swivel, rotation motor and gearing mount on the carriage. The lance attaches to the water swivel outlet.

Individual rod guides travel along the frame ahead of the carriage and provide intermediate support for the lance. The number of guides and their spacing is dependent on the stiffness of the lance and the anticipated thrust. A typical 22 ft (7 m) stroke machine has one stationary front guide and seven moveable guides spaced approximately 3 feet (1 m) apart. This is adequate for a 1/4 in. (1.28 cm OD) pipe lance and 150 lbs (670 N) thrust.

The frame also supports the drive mechanism for providing thrust. Typically this is a loop of chain between sprockets mounted at each end of the frame. One of the sprockets is driven while the other acts as an idler. The carriage is attached to one side of the chain and is driven back and forth between the sprockets. Other possible drive mechanisms are: screw drive, thrust cylinder, and rack with pinion drive.

For vertical cleaning or situations where the machine must be transported or maneuvered by hand the frame should be as light as possible. Aluminum is a good choice of material for this application.

## Motors and Gearing

An advantage of the lancing machine is its ability to apply more power to the cleaning task and require less effort by the operator. The powered thrust and rotary drive are key elements in achieving this. Machines without independent power sources extract power from the water, lowering jet pressure and reducing their cleaning ability.

The type of motor is determined by the situation in which the machine is to be used. Air motors are a common choice. The controls are simple, they have variable speed, rapid reverse, and can stall without damage. Electric motors are quiet but not a good choice for portable equipment because of the difficulty connecting to a power source. Hydraulic motors offer very positive output and should be considered when precise motion is required. They are light-weight and powerful, but require a hydraulic power source and two hose lines for each motor.

The size of motor and associated gear reduction depends on the task to be accomplished. A typical heat exchanger RLM might use a 1-1/2 hp (1.1 kw) air motor and gearbox to provide approximately 30 ft-lbs (41 N-m) of torque and up to 300 rpm. The same machine might use a 3000 rpm, 2 hp (1.5 kw) motor and 30 to 1 gearbox for the thrust drive. Those designed for heavy duty drilling would use more powerful motors and higher ratio gearboxes to provide more thrust and torque.

## Water Swivel

The rotary coupling or water swivel needs to be capable of reliable operation at high pressures and rotation rates. The swivel can be a side feed or end feed style.

The side feed swivel generally has a sturdy through shaft. One end of the shaft is driven while the other is the fluid output. Inline or offset motors can easily be coupled with the swivel drive shaft. The swivel or gearbox must have bearings capable of handling the thrust and side loads transmitted by the rotating lance.

An end feed style swivel usually offers less flow restriction than the side feed type. The rotation motor will have to be mounted offset however, and coupled to the output shaft or lance.

Water swivels are available in a variety of pressure and flow ratings. For operating pressures in excess of 30,000 psi (2000 bar) the flow rates are usually limited to less than 10 gpm (38 l/min). Some swivels rated for 10,000 psi (690 bar) operating pressures can pass 200 gpm (760 l/min) with less than 50 psi (35 bar) pressure drop. Flow restriction, package size, cost, seal life and ease of maintenance are all important considerations.

## Lances and Nozzles

The RLM can work with most common stiff lances. Pipe, tubing, carbon steel or stainless can be used. The size can be from 1/4 to over an inch (.6 - 2.5 cm) depending on the ID of the tube to be cleaned. The lance OD, surface finish and straightness are not critical.

Nozzle capacity is matched to the pump output and line losses. Conventional nozzle tips as well as special designs are used. Typically a nozzle for RLM use would have a few forward angled jets and a single carbide cutting edge. The combination of rotary mechanical cutting and waterblast erosion is a very effective means of unplugging and cleaning tubes.

## Support Fixtures

A variety of holding mechanisms can be employed to support the RLM and align it with the pipe or tube to be cleaned. They can be fixed, manually aligned, or even power controlled. The choice is determined by the need for mobility, volume of work, accessibility of the work station and hazards of the deposit.

The fixed mount is used when the items to be cleaned are easy to bring to the lancing machine or when discharge of materials must be carefully controlled. An example would be oil field tubulars. The RLM is solidly mounted and the plugged pipe is rolled into position on elevated rails. A clamp mechanism secures the pipe to the RLM to counteract the thrust forces of the rotating lance. For cleaning hazardous materials the RLM might be mounted inside of an enclosed chamber and operated remotely.

Several styles of manually operated positioners are used. For horizontal work a common style employs a simple box frame 4-5 feet (1.2 - 1.5 m) square with a horizontal crossbar. The RLM hooks onto the crossbar and can be slid from side to side manually or be raised and lowered by a hand crank. The positioner frame is attached to the heat exchanger tube sheet. A tripod and chain holds the rear of the RLM. Occasionally, the position or height of the box frame and tripod must be adjusted if the cleaning area is large or if the lance is very stiff.

For vertical cleaning applications the support system can be mounted to the tube sheet or be supported by scaffolding or other external means. Ease of setup, safety, and versatility are important to successful work in the plant environment.

A powered positioner performs the same functions as a manually operated system but by using motors they can be remotely controlled. Less labor will be required by a powered positioner. However, they are heavier and require more maintenance.

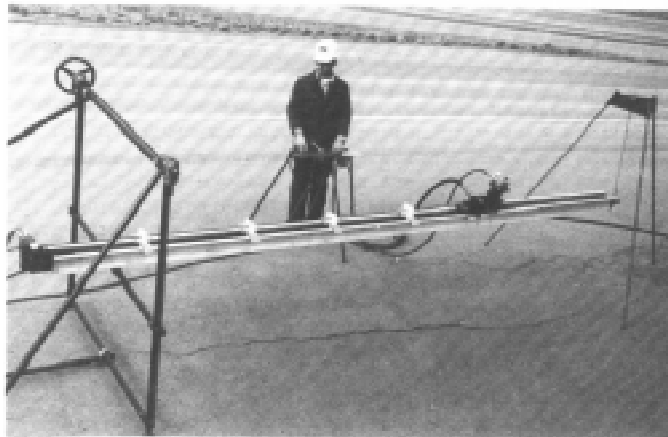


Fig 1. Typical Rotary Lancing Machine and Horizontal Positioner  
CASE HISTORY # 1: HEAT EXCHANGER CLEANING

The most common use of rotary lancing machines is the cleaning of shell and tube heat exchangers. These units typically consist of several hundred tubes in the 3/8 to 1 inch (1-2.5 cm) diameter range and 10 to 25 feet (3-7.6 m) in length. The RLM is effective in removing tough wall deposits and clearing completely plugged tubes.

The DuPont Company in LaPlace, Louisiana employed an RLM to clean heat exchangers in a chemical production unit<sup>1</sup>. The unit consisted of 1292 carbon steel tubes, 1 inch ID (2.5 cm), 8 ft long (2.4 m) and filled with deposits of a hard coke-like material. Manual waterblast methods required 100 to 200 hours for a 4-man crew. Even then as many as 20% of the tubes might remain plugged.

The first chance to try the RLM occurred during a 36 hour outage. A 2-man crew cleaned 1247 of the 1292 tubes within the allotted time and left little doubt that the other 35 tubes could have been cleaned if more time was available. The lance was rotated at 200 rpm with 18 gpm (68 l/min) of water at 10,000 psi (690 bar). The rotating jets of water removed virtually all of the baked-on material. A significant reduction in the time and cost to clean the tubes was realized.

#### CASE HISTORY # 2: REMOVING CEMENT FROM TUBULARS

It is not uncommon in the development of oil and gas wells to inadvertently plug several joints of pipe with cement. The rotary lancing machine offers a very effective and safe means of removing the cement so the tubulars can be used. The cleaning process is quite complete and no damage occurs to the pipe ID.

In February, 1986 StoneAge, Inc. undertook a typical pipe cleaning job. A load of 104 joints of 2-3/8 inch (6 cm OD) Hydrill tubing was delivered completely filled with cement. The tubing was unloaded onto a timber platform in line with a fixed rotary lancing machine. A quintuplex pump was used to provide 15 gpm (56 l) at 10,000 psi (690 bar). The nozzle head had two forward jets, a carbide cutting edge and rotated at 90 rpm. The procedure was to roll a joint of tubing across the timber, line it up with the RLM and clamp the end to the RLM frame. The nozzle was rotated and advanced toward the tube. Once the nozzle touched the cement plug, the operator activated the high pressure jets and started the cleaning the tube. With about 200 lbs (890 N) of thrust the nozzle advanced an average of 5 ft/min (1.5 m/min) while the cuttings washed back out the open tube end. Once through the joint the nozzle was retracted while still rotating and with full jet pressure. Any loose or remaining material was blown out the far end and the tube was scoured clean.

A one or two man crew spent a total of 36 manhours to complete the job. This included loading and unloading the pipe, and other setup operations. Twenty one hours of pump operating time was recorded. All of the tubing was completely cleaned and put back into service.

---

<sup>1</sup> Alan Briggs, "Rotary Hydroblasting Machine Minimizes Time and Labor to clean Heat Transfer Tubes", CHEMICAL PROCESSING, October 1984.



Fig 2 Example of Pipe Cleaning Machine

### CASE HISTORY #3: CATALYST REMOVAL FROM A REACTOR

Rotary lancing machines have been found effective in the removal of used catalyst from reactor vessels. The pea-sized catalyst pellets become fused together during use and this presents a problem in removal for reclamation.

A refinery on the Gulf Coast provided an opportunity to use this technique. The reactor vessel was approximately 20 ft (6.1 m) in diameter and 100 ft (30 m) tall. A very robust steel framed rotary lancing machine was mounted on top of the vessel. The RLM had a 10 ft (3 m) stroke and used a sectional lance with quick couplings. The procedure employed was to drill down through the catalyst, with a 3 in. (1.3 cm) diameter bit having forward angled jets and a carbide cutter. Once down through the material the bit was removed and a nozzle head with side jets was put on. The lancing machine then worked the rotating nozzle back up through the vessel cutting and washing the catalyst down to the bottom of the vessel where it flowed out. Approximately 100 gpm (380 l/min) at 8000 psi (550 bar) was provided by a combination of pumps.

This method proved superior to any previous attempts and has since become the standard removal procedure.

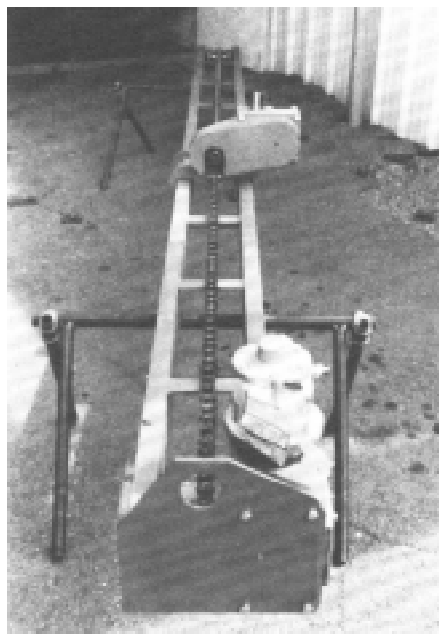


Fig 3 Heavy duty Rotary Lancing Machine for Catalyst Drilling

#### SUMMARY

The rotary lancing machine is a very effective tool for cleaning the inside of tubes, pipes and chambers. The combination of mechanical cutting and, waterblast erosion results in a safe and powerful technique. Less manpower, lower risk exposure and efficient water use all add up to a superior cleaning system.

# MATERIAL DYNAMIC RESPONSE DURING HYDROABRASIVE JET MACHINING {HAJM}

M. Mazurkiewicz and P. Karlic  
High Pressure Waterjet Laboratory  
University of Missouri-Rolla  
Rolla, Missouri

## ABSTRACT:

The technology of hydroabrasive jet cutting (HAJC) and machining (HAJM) is applicable in many types of industry for the purpose of metal machining. However at present practical application is limited to the operations of cutting, blasting, deburring and hole piercing. This technology becomes very important with the introduction of special requirements for safety or structural quality effected by the generation of excessive temperatures in the cutting zone.

The success of this technology depends upon the applicability of HAJM to a further type of machining operation - that of three-dimensional (non planar) controlled hydro-abrasive jet erosion (TDCHAJE). Hardware limits along with inaccurate process predictability have so far restricted the quality of results .

From the aspect of control, the prerequisite must be that the chosen control algorithm should have the dynamic properties of the controlled path - the series connection of the Hydroabrasive Jet Machine Tool (HAJMT) and the three dimensional erosion process (TDEP). A dynamically representative controlled-path model could be used in the design of automated manufacturing equipment - CNC HAJMT or specially tailored robots.

This paper consists of an analysis of the dynamic response of a TDCE controlled path . The subject has been examined from both the aspect of control systems as well as that of new technology. New criteria have been discussed and analyzed using two control variables - feed rate and nozzle stand-off distance, and allowing only these control variables to change during machining . The influences of disturbances have been estimated and the relative importance of these as well as that of different inputs and outputs have been examined. The representative transmittances for the controlled path have been selected and supported by the analysis of their responses under step inputs.

## NOMENCLATURE

A - workpiece/abrasive water jet flexibility factor  
 $A_g$  - geometrical accuracy factor  
 $A_d$  - dimensional accuracy factor  
 $A_k$  - abrasive particle kind  
B - thickness of work piece  
C - workpiece material constant  
C - ratio  
D - hole diameter  
 $D_c$  - crater diameter  
 $D_u$  - upper diameter of through hole

$D_L$  - lower diameter of through hole  
 $D_{A1...i}$  - technological disturbances of the HAJM process  
 $D_{M1...n}$  - technological disturbances of the HAJ Machine Tool System  
 $d_w$  - water nozzle diameter  
 $d_{aw}$  - abrasive-water mixture nozzle diameter  
 $E$  - hydroabrasive jet machining HAJM efficiency  
 $F(t)$  - generating line equation (function)  
 $F_C(t)$  - generating line of crater  
 $F_d(t)$  - generating line of deburred surface  
 $F_p(t)$  - equation of side surface generating line  
 $F_{kl...n}$  - equations of side kerf surface generating line at next cut  
 $F_o$  - initial generating line function  
 $f$  - feed rate (feed velocity)  
 $f_h$  - horizontal feed rate  
 $f_v$  - vertical feed rate  
 $f_o$  - initial feed rate  
 $G(s)$  - transmittance  
 $G_{MTi... (s)}$  - transmittances of Machine Tool System parts  
 $G_{A1... (s)}$  - transmittances of hydroabrasive iet machining process  
 $G_H(s)$  - transmittance of HAJM when output is depth of erosion  
 $G_D(s)$  - transmittance of HAJM when output is diameter of erosion  
 $G_{Hc}(s)$  - transmittance of hydroabrasive cyclic process  
 $G_N(s)$  - transmittance of HAJM when output is volume removal rate  
 $g$  - grainity of abrasive particles  
 $H$  - abrasive particle velocity distribution  
 $h$  depth of erosion  
 $h_c$  - crater depth (dead hole depth)  
 $h_{max}$  - maximum depth of erosion  
 $h_{min}$  - minimum depth of erosion  
 $h_o$  - initial depth of erosion  
 $I_{1...L}$  - control values (inputs of HAJM process)  
 $J$  - eroded surface texture factor  
 $K$  - gain factor  
 $K_{MT1...n}$  - gain factors of Machine Tool System parts  
 $K_{A1...n}$  - gain factors of HAJM process 2  
 $K_{hs}$  )  
 $K_{hf}$  )  
 $K_{ws}$  . . . . .) gain factors of HAJM  
 $K_{wf}$  )  
 $K_{NS}$  )  
 $K_{SF}$  )  
 $L$  – travel of feed  
 $l$  - length of erosion  
 $M$  - mass of impacting particle  
 $N$  - volume removal rate of eroded material  
 $n$  - constant

O - output signal  
 $O_{1...n}$  - outputs of HAJM process  
 p - pressure before water nozzle  
 $p_c$  - carrier fluid pressure  
 Q - flow  
 $Q_A$  abrasive mass flow  
 $Q_W$  - water mass flow  
 R roughness of eroded surfaces  
 $r_d$  - radius of deburred edge  
 $S_{1...2}$  - set values of controlled path  
 s - nozzle standoff distance  
 $s_c$  - critical nozzle standoff distance  
 T time constant  
 $T_A$  - HAJM cyclic process time constant  
 $T_h$  - standard hole piercing depth time constant  
 $T_{DU}$  - upper hole diameter time constant  
 $T_{DL}$  - lower hole diameter time constant  
 $T_D$  - standard hole piercing diameter time constant  
 $T_{H1...n}$  - hole piercing depth time constants  
 $T_{Ah}$  - HAJM cyclic process depth time constant  
 $T_{AW}$  HAJM cyclic process width time constant  
 $T_{AN}$  - HAJM cyclic process material removal rate time constant  
 t - time  
 U - volume of removed material  
 V - impacting velocity of particle  
 w - width of eroded surface  
 $W_u$  - upper kerf width  
 $W_L$  - lower kerf width  
   - nozzle axis angle (impingement angle)  
   - minimum flow stress of the target material  
   - energy efficiency of abrasive chamber system

## INTRODUCTION:

HAJM becomes very important in the machining of what are classically regarded as the "difficult to machine" materials (metals) and also where safety requirements or thermal restrictions apply.

Up to now the following types of metal machining operations use HAWJ where erosion is the metal-removing process:

- rough, one pass cutting (Figure 1a).
- rough, multi-pass cutting (Figure 1b).
- precision cutting.
- surface blasting (Figure 2a & 2b) of which deburring (Figure 3a & 3b) is a sub-operation.
- piercing of dead and thru'-holes (Figure 4a & 4b).

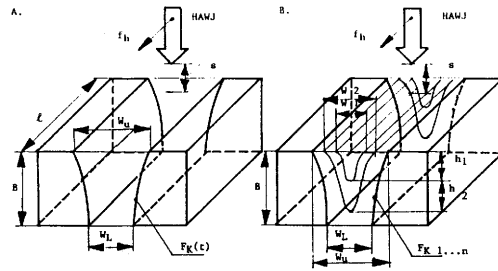


Figure 1. A – single-pass, rough kerf cutting with hydro-abrasive jet (HAJ).  
B – multi-pass, rough kerf cutting with hydro-abrasive jet (HAJ).

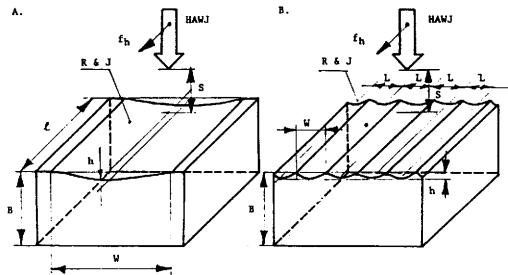


Figure 2. A - single-pass surface blasting with hydroabrasive jet (HAJ).  
B - multi-pass surface blasting with hydroabrasive jet (HaJ).

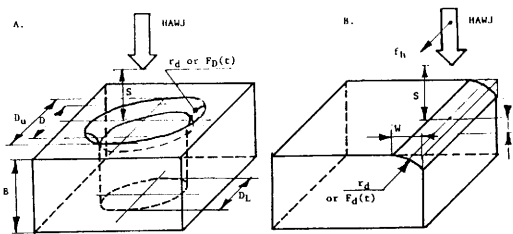


Figure 3. A - deburring of hole feather edge.  
B - deburring of 3-D part feather edge.

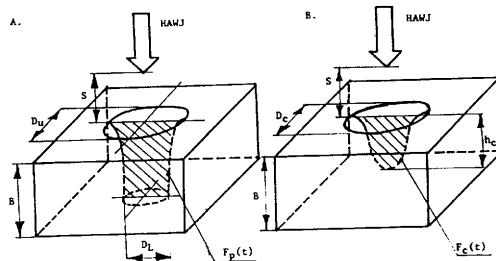


Figure 4. A – thru' hole piercing  
B – dead hole piercing.

Potential applications for HAJM are numerous (Figure 5). One of the more significant is that of three dimensional controlled erosion (TDCE) of the traditionally difficult to machine metals particularly those with surface burn restrictions and other thermal requirements. This is borne out during the machining of large forged titanium alloy parts, initially milled, with deep

slots and pockets and numerous corners. Successful use of TDCE by hydroabrasive jet (HAJ) depends ultimately on the quality of process control.

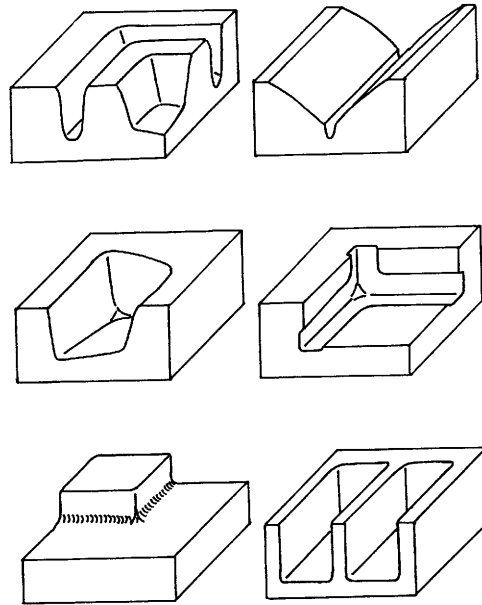


Figure 5. Examples of workpieces machined using three dimensional controlled erosion (TDCE).

#### Three Dimensional Controlled Hydroabrasive Jet Machining (TDCHAJM)

Accurate predictions of the machining parameters prior to the machining process and compensation for disturbances along with the use of new adaptive feedback control systems could lead to improved texture and surface finish, dimensional accuracy and all with significant cost savings.

The Authors propose the use of hydroabrasive jet technology for the controlled three dimensional erosion of metal. For this method of metal removal the machining operations must be carried out in two steps:

- first the effective removal of material maintaining restricted geometrical and dimensional accuracy ( $A_g$ ,  $A_D$ ) with the retention of mistakes generated on already eroded surfaces due to repeated traversing.
- second the removal of micro allowance maintaining constant machining parameters so that a defined surface quality factor (roughness R and texture J) can be achieved.

The successful design of a machine tool to achieve this requires the careful construction of models for the static and dynamic characteristics of the hydroabrasive jet erosion process.

Hydroabrasive jet erosion process models, described in the works of [13], [4], [5], predict only the depth of cut  $h$  or the kerf wall surface roughness  $R$  after the cutting operation. These models describe only the static characteristics of the erosion process and hence are useful only for the estimation of set values for the machining parameters. The fact that the "tool" in question is a stream of water and abrasives, flexible and with continually varying properties, consistency and shape, makes the machining operation difficult to define, since the tool itself also changes in time.

The erosion process is stochastic in nature and is greatly influenced by technological disturbances which are difficult to predict. Present models neglect the important changes brought about by factors such as the "washing-out" mechanism of the slurry, eroded metal particles and the effects they produce by recontacting the eroded surface and the change in abrasive water stream energy due to inconsistent levels of disintegration during mixing.

From the point of view of a control system the objective controlled path and the control system elements can be based on the:

- static characteristics relating gain factor changes and set values.
- dynamic characteristics for the description of transient responses caused by changes in inputs or disturbances.

Were it not for technological disturbances these models would suffice. This paper proposes dynamic models useful for the design of:

- controlled precision machine tools for three dimensional hydroabrasive controlled jet erosion (TDHACJE) for cutting, blasting, deburring, and hole piercing.
- semi-automated compensation control systems for technological disturbances (Adaptive Control System).
- semi-automated optimization control system for the on-line prediction of hydroabrasive jet erosion parameters.

#### CONTROLLED PATH:

In the case of high pressure hydroabrasive jet machining (HPHAJM) the controlled path consists of a series connection of two elements:

1. The erosion process involved in hydroabrasive jet action.
2. The hydroabrasive machine tool.

In general both of these control elements will experience technological disturbances  $D_{A_i}$  and  $D_{M_{1..n}}$  (Figure 6). The direct measurement or estimation of these disturbances is difficult and their prediction in real time practically impossible.

The dynamic responses of these elements will be very different to those of static or quasi-static representations especially in response to sudden changes. Although unable to predict these disturbances the control system will compensate for them in real time while accounting for each elements real time response characteristics. The set values  $S_{1..k}$  are input values to the control units. Control signals  $I_{1..L}$  are inputs to the hydroabrasive jet generated erosion process and at the output are output signals  $O_{1..m}$

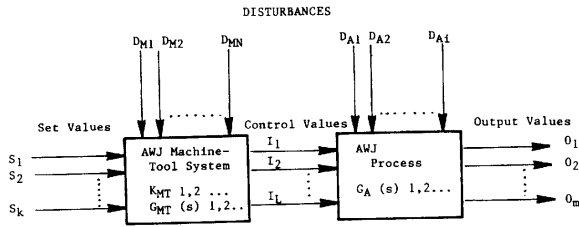


Fig. 6. Hydroabrasive jet machining (HAJM) controlled path.

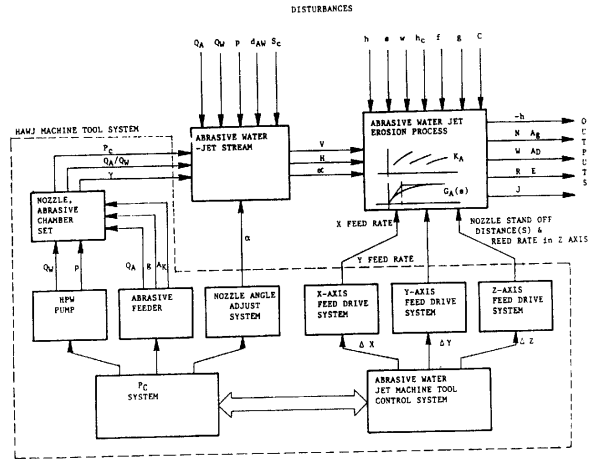


Figure 7. Signal distribution schematic for hydro-abrasive jet machining (HAJM).

The interconnection of static and dynamic responses to all signals shall govern the type of control algorithms and the selection of auxiliary equipment and the machining method and its characteristics.

A more detailed schematic of signal distribution is shown in (Figure 7) to illustrate the three dimensional controlled hydroabrasive jet erosion process.

## HYDROABRASIVE JET MACHINING (ERODING) PROCESS

### Outputs:

Of great importance in the analysis of the HAWJ process are changes in the output i.e. the transient response of the process. These may be quantities such as depth of erosion ( $h$ ), roughness of machined surfaces ( $R$ ), kerf width ( $w$ ) generated profile of the eroded surface ( $F$ ), geometrical and dimensional accuracy factors ( $A_e$ ,  $A_d$ ), volume of material removed ( $N$ ), machining efficiency ( $E$ ) etc.

In the case of the proposed three dimensional controlled hydroabrasive jet erosion, it is necessary to simultaneously maintain full control over multiple outputs. This requires the coupling of sets of output parameters for example geometrical and dimensional accuracies and the material removal and penetration rates.

Flexibility of control is possible with the use of different output parameters. For example power absorbed during the erosion process, flowrate of eroded material, flowrate of combined slurry and metal particles from the machining zone, acoustic emission factors, etc. Consideration should also be given to the use of output parameters such as the components of the reaction cutting forces, the dynamic properties of these forces during erosion and the dynamic properties of the metal-slurry stream.

In polishing, deburring and other finishing operations the volume of eroded material is of importance while in piercing and cutting it is the erosion depth ( $h$ ) or depth of penetration. For

three dimensional controlled erosion the important controlled factors are the depth of penetration, width of penetration and profile of eroded surfaces.

#### Control Values:

Theoretically there are many parameters which could be used as the control values. In practice though, state of the art limitations on high pressure jet equipment particularly high pressure pumps, abrasive feeder units and abrasive-water jet mixing chambers and nozzles allow only four parameters to be easily changed on-line during the hydro-abrasive jet operation:

1. Nozzle standoff distance (s) achieved by changing its position in the zaxis direction.
2. Feed rate (f) in all three xyz or more directions.
3. Feed direction (  $x, y, z$ ).
3. Nozzle axis angle (angle of impingement), ( ).

Between individual operations the following parameters can be changed and therefore used as control values:

1. Water nozzle pressure (p).
2. Type of nozzle.
3. Water nozzle diameter  $d_w$ .
4. Abrasive-water nozzle diameter,  $d_{aw}$ .
5. Type of abrasive material,  $A_k$ .
6. Grainity of abrasive particles (g).
7. Abrasive particle flowrate ( $Q_A$ )

#### Disturbances:

The analysis of disturbances can be split into two parts - the primary properties which the disturbances effect and which themselves effect other parameters and also the disturbances themselves. Disturbances effect the quality, static and dynamic properties of the hydroabrasive stream along with stream coherency, abrasive particle velocity distribution along and perpendicular to the stream axis [1], abrasive particle flowrate and stream pressure consistency and stream geometry.

Second are the disturbances to the erosion process, the factors which may initially lead to changes in the above and ultimately to transient behavior of output parameters.

1. Flexibility, which changes during machining operations, of the hydroabrasive stream along and perpendicular to the nozzle axis.
2. Workpiece geometry.
3. Eroded hole, kerf characteristics or other surface geometry.
4. Repeatability effect.
5. The covering of eroded surface by metal particle or abrasive particle water slurry.
6. Material properties such as hardness, crystalline structure and isotropy.
7. The control values themselves that may be interpreted as disturbances:
  - feed rate (f);
  - nozzle standoff distance (s);
  - nozzle axis angle (a).
8. Overall general effects created by the machine path plan itself

- reflections of the hydroabrasive stream resulting from continuity considerations with previously eroded surfaces;
- changes in the erosion conditions resulting from repeated tool path travel;
- the so-called entry stage effect and exit stage effect;
- the cyclic characteristics of deep erosion with the feed velocity perpendicular to the nozzle axis (Fig. 8).

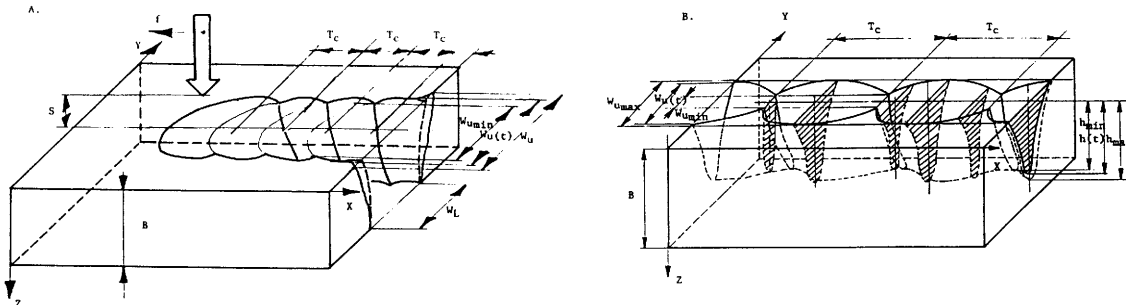


Figure 8. Effect of cyclic disturbances during thru (a) and dead (b) deep erosion (kerfing) with hydroabrasive jet (HAJ).

A true measure of control system quality and efficiency can only be obtained by the monitoring of output parameters and how clearly they "track" the set values input for the particular machining operation. The effect of disturbances is significant enough that the dynamic response of output parameters can be greatly influenced in real time making compensation difficult and prediction impossible. The important question to be posed is whether or not a method of using the control and set values to reduce any potential effect disturbances may have on output parameters, is possible, and to what extent.

#### Hydroabrasive Jet Machining Process Static Characteristics:

Abrasive jet machining is a process in which, material removal takes place due to erosive action of a stream of abrasive particles and high pressure water jet impacting at high velocity onto the workpiece surface. The theory of erosion phenomena is not fully understood and adequate data of its governing parameters are not available. Some of these parameters are interdependent and difficult to control. Volume of removed material is described by [6]

$$U = \frac{c f(\alpha) M V^n}{\sigma} \quad (1)$$

In the case of HAJM this model is many times more complicated because of hydrodynamic influences, abrasive particle velocity distribution and changes in stream coherency and geometry.

In [5] a simplified model for the computation of kerf depth is presented:

$$h = c \sqrt{\frac{Q_A v^2}{8\sigma f}} + \frac{2M(1-c) v^2}{\pi f \varepsilon d_j} \quad (2)$$

This can only be regarded as a simplified approach to HAWJ analysis. In order to obtain practical results the effects of distributions during the process must be accounted for. In the selection of the optimum control method the form and range of the gain coefficients are very important. We propose different Hydroabrasive jet Machining gain factors of the following form:

$$K_{hs} = \frac{dh}{ds} \quad (3)$$

$$K_{hf} = \frac{dh}{df} \quad (4)$$

for the output signal h (depth of erosion)

$$K_{ws} = \frac{dw}{ds} \quad (5)$$

$$K_{wf} = \frac{dw}{df} \quad (6)$$

for the output signal w (width of erosion, crater diameter)

$$K_{Ns} = \frac{dN}{ds} \quad (7)$$

$$K_{Nf} = \frac{dN}{df} \quad (8)$$

for the output signal N (volume removal rate).

Two inputs only are varied; nozzle standoff distance and feed velocity. If we restrict the analysis to a limited operating range in the neighborhood of our operating point then we can assume that the gain factors are constant. In truth these factors will change due to disturbances. Over a large range both gain factors and disturbances will change and the problem of dynamic response estimates becomes compounded.

#### Dynamic Characteristics of the Hydroabrasive Jet Machining Process (HAJM):

Knowledge of the transient or step responses of the process is necessary in the design of a control system. With this information the general dynamic properties of HAJM can be described and the effects of changes in the control values and disturbances or output can be evaluated. The step response method is used in this analysis of what is essentially a non-linear model. The important parameters whose responses are to be analyzed are depth of erosion (h), width of erosion (w) (or hole diameter D)) and volume removal rate (N). Responses are to step inputs in three control values - feed rate (f) in perpendicular and parallel direction to nozzle axis and nozzle standoff distance (s).

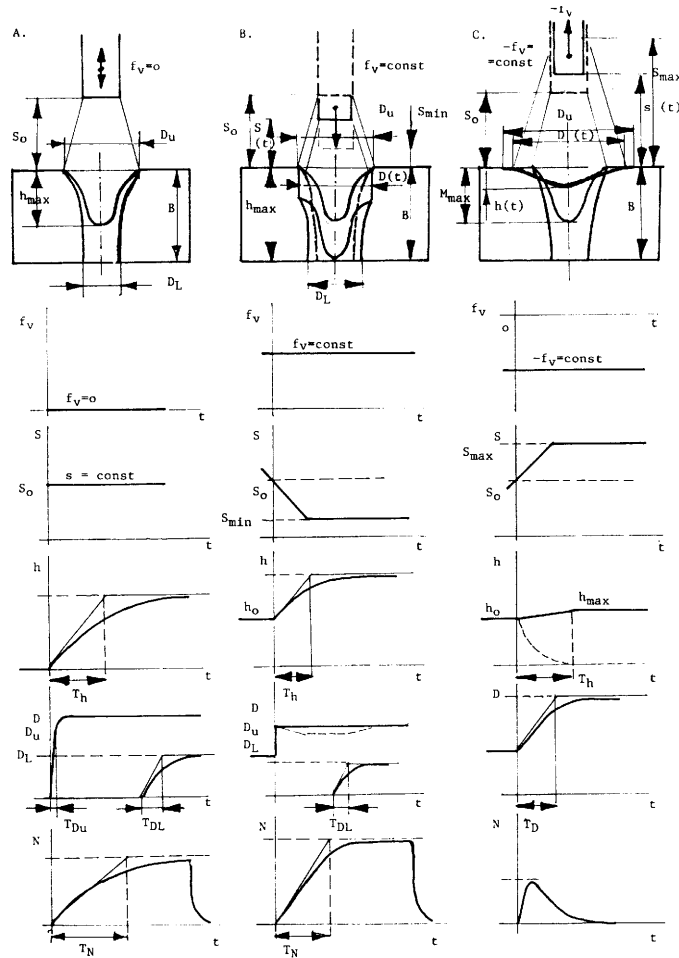


Figure 9. Transients during crater (hole) erosion

- (a) with  $s(t) = \text{constant}$  &  $f_v = 0$
- (b) with  $s(t) = \text{variable}$  &  $f_v = \text{constant}$
- (c) with  $s(t) = \text{variable}$  &  $-f_v = \text{constant}$

1. Figure 9(a) depicts the transient responses  $h(t)$ ,  $D(t)$ , and  $N(t)$  during crater erosion (dead and thru hole piercing) with constant nozzle standoff distance ( $s(t) = \text{constant}$  and  $f_v = 0$ ) For  $h(t)$ ,  $D(t)$  and  $N(t)$  first order inertia element transmittances are used.

$$G_h(s) = \frac{1}{1 + sT_h} \quad (9)$$

$$G_D(s) = \frac{1}{1 + sT_D} \quad (10)$$

$$G_N(s) = \frac{1}{1 + sT_N} \quad (11)$$

For the erosion of thru holes there are two time constants,  $T_u$  and  $T_L$  - the former to obtain the upper hole diameter  $D_u$  and the latter the lower hole diameter  $D_L$ .  $T_u$  is very short,

approximately zero. Time constant  $T_h$  (the attainment of depth  $h$ ) along with  $T_L$  depends on many technological factors of the machine tool and machining process, significantly on nozzle standoff distance ( $s$ ), pressure ( $p$ ), abrasive velocity ( $v$ ), ... etc.

So,

$$\begin{pmatrix} T_D, T_L, T_u \\ T_h \end{pmatrix} = f(p, s, B, C, h, g, \dots) \quad (12)$$

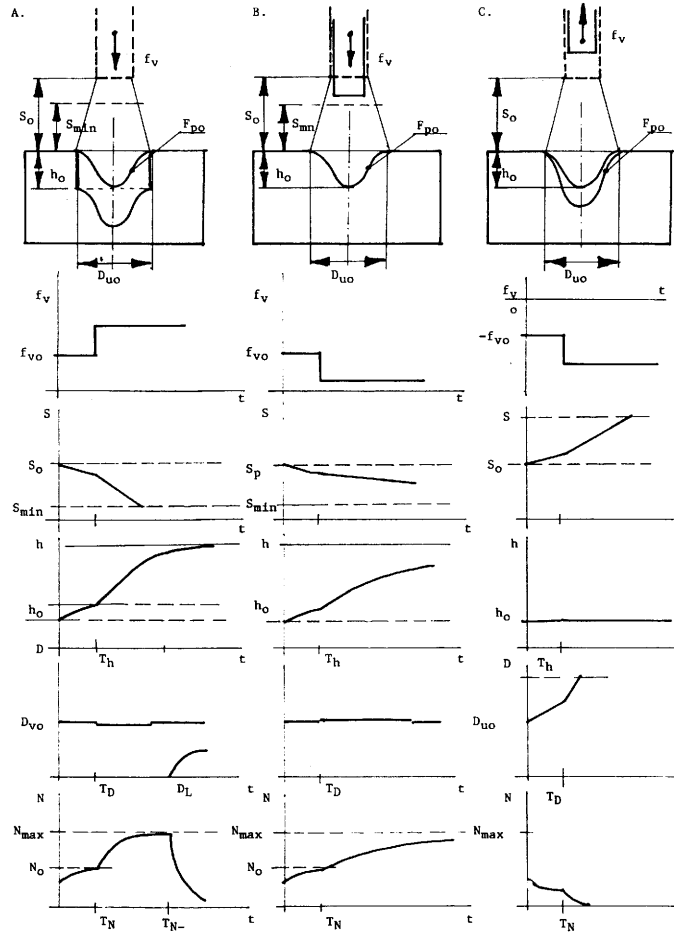


Figure 10. Transients during crater (hole) erosion

(a) with nozzle velocity step input

$$f_v(t) = f_{vo} + f_v$$

(b) with nozzle feed velocity step input

$$f_v(t) = f_{vo} - f_v$$

(c) with nozzle feed velocity step input

$$f_v(t) = -f_{vo} - f_v$$

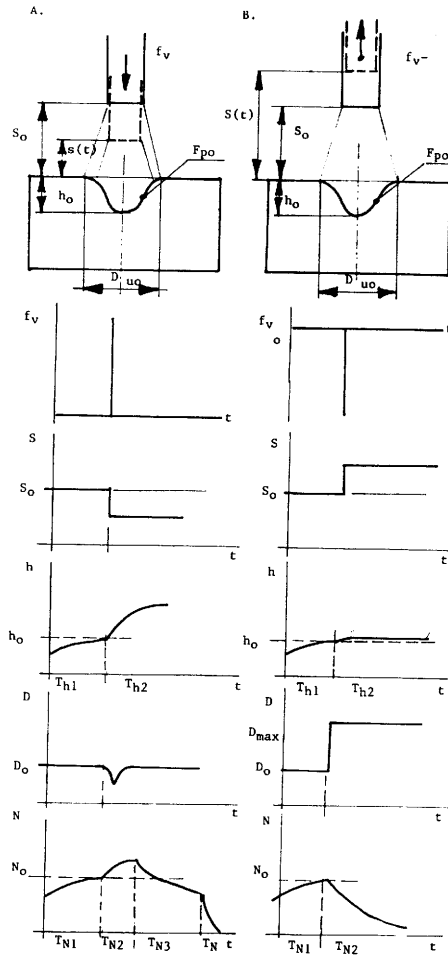


Figure 11. Transients during crater (hole) erosion

(a) with nozzle stand off distance step input  $s(t) = s_o -$

(b) with nozzle stand off distance step input  $s(t) = s_o +$

In reality the response  $N(t)$  is more complicated and it requires the use of a higher transmittance for accurate description.

2. Figure 9b depicts the responses  $h(t)$ ,  $D(t)$ ,  $N(t)$  during the erosion of a crater (hole piercing) with constant nozzle feed ( $f_v = \text{constant}$ ) and variable standoff distance ( $s(t)$  varies). The nozzle moves perpendicular to the eroded surface and standoff distance varies from  $S_o$  to  $S_{\min}$  or  $S_{\max}$ . To simplify the model the analysis begins when the upper crater diameter  $D_u$  is obtained, hence no delay time is involved.  $T_h$  is shorter as is  $T_u$  and  $N_{\max}$  is greater than in the case where  $F_v = 0$ .

Every parameter function could be described by equations similar to equations 9, 10, & 11. Only volume removed will vary as the equations are similar except for time constant values. For the case where the feed velocity direction changes sign dramatic increases in  $D_u$  and  $h$  are observed (Fig. 9c).

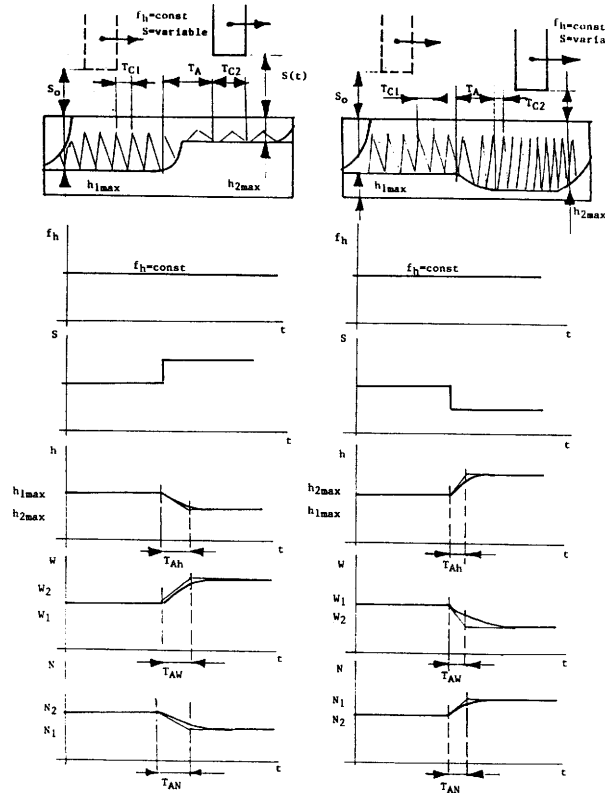


Figure 12. Transients of HAJM cyclic process with feed rate (velocity) step input  
 (a) for  $f_h(t) = f_{oh} + f$  &  $s(t) = \text{constant}$   
 (b) for  $f_h(t) = f_{oh} - f$  &  $s(t) = \text{constant}$

The important observations are that we are dealing with a non-linear model and the responses depend on the nozzle feed direction and the time constant values. Time constant  $T_h$  can vary over a large range.  
 for  $f_v$  positive direction  $T_h$  is shorter than in the case where  $F_v = 0$   
 for  $f_v$  negative direction  $T_h$  could equal zero  
 for  $s(t) < S_c$  and greater than zero for  $s(t) > S_c$  where  $S_c$  is the critical standoff distance.

Sudden upper hole diameter ( $D_u$ ) changes are observed when the nozzle standoff distance ( $s$ ) increases. For decreasing ( $s$ ) even though small increases and decreases in  $D_u$  occur (depends on feed rate) this diameter is essentially constant between  $S_0$  and  $S_{min}$ . The resulting  $D_L$  is greater than in the case of piercing with stationary nozzle (Fig.9a). The material removal rate for positive  $f_v$  is greater than the case of a stationary nozzle if  $f_{vc}$  (critical) is not exceeded. A constant volume removal rate is observed during the piercing of a cylinder hole. Generally with negative  $f_v$  the removal rate decreases if the time constant is larger than  $T_h$ .

3. Figures 10a, 10b, & 10c depict transient responses during crater erosion (piercing holes) for step inputs applied to the feed rate  $f_v$  (wide range).

$D(t)$  is constant in the case of changes in the feed velocity with positive sign. The time constants  $T_{h1...n}$  depend on the direction (sign) of feed. For  $f_v$  with a negative sign, depth of cut is almost independent but  $D_u$  changes in proportion to feed velocity (Fig. 10c).

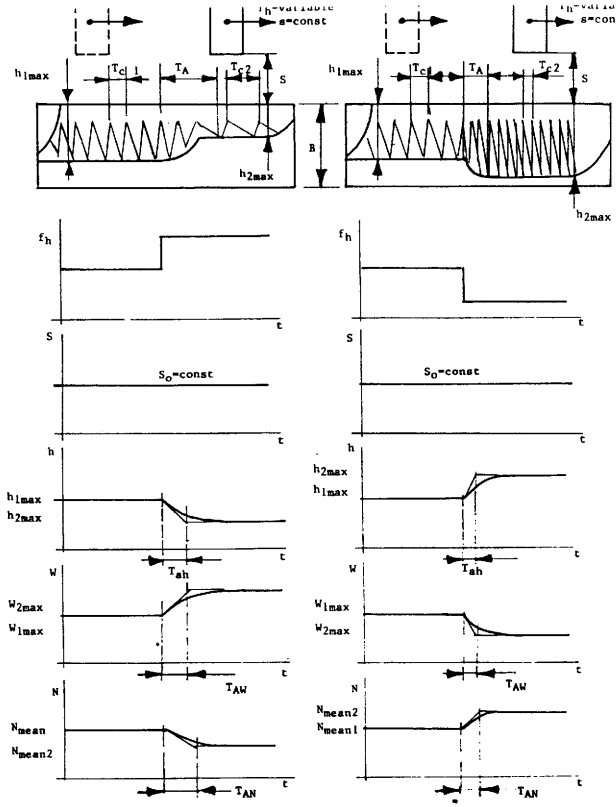


Figure 13. Transients of HAJM cyclic process with nozzle stand off distance step input  
 (a) for  $s(t) = s_0 - s$  &  $f_h(t) = \text{constant}$   
 (b) for  $s(t) = s_0 + s$  &  $f_h(t) = \text{constant}$

4. Figure 11a and 11b show responses when a step input is applied to nozzle standoff distance with feed velocity  $f_v = 0$ . This non-linear model gives transient responses  $h$ ,  $D$ ,  $N$ , which are strongly dependent upon the sign of the input.

5. Transient responses in HAJM during deep erosion are shown in Figure 12a and 12b for step inputs to feed rate with constant  $s$ . From [6] it is known that the character of the erosion process with HAJM is cyclic in nature (Fig. 8). Changes in feed velocity imply responsive changes in cyclic frequency, average and maximum depth of cut and erosion width. Dynamic representation is described with the following transmittance

$$G_{HC}(s) = \frac{1 - e^{-sT_A}}{s[1 + A(1 - e^{-sT_A})]} \quad (13)$$

where  $T_A$  is the cyclic process time constant

$$T_A = (f, h_o, p, s_o, f_o, c, \dots) \quad (14)$$

parameter A refers to the hydroabrasive jet flexibility.

6. Figure 13a and 13b show the transient responses for HAJM during deep erosion with  $f_h =$  constant in response to step inputs to nozzle standoff distance. The dynamic characteristics are modeled by equation 13. Differences lie only in time constant magnitudes, step input signs, etc.

7. During shallow erosion with HAJM the erosion process is not cyclic but constant and can be described by a first order inertia element. The time constant magnitude depends on many parameters of the abrasive water jet, especially flexibility.

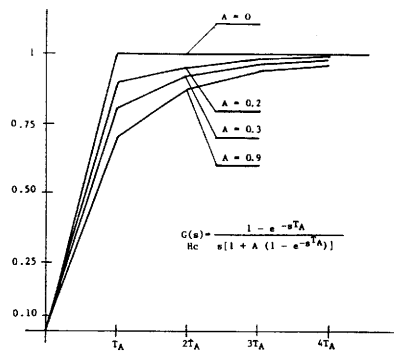


Figure 14. Transients of hydroabrasive jet erosion cyclic process transmittance

Figure 14 shows responses to step inputs to  $s$  for the transmittance described by equation 13 for different A factors. The width of erosion ( $w$ ) and the depth of erosion ( $h$ ) show the same characteristics in this case and also in the case when the step input is to feed rate.

## CONCLUSIONS

1. HAJM is a strongly non-linear process.
2. HAJE process gain factors can change sign and vary over a wide range [7].
3. Time constants depend strongly on many parameters and on disturbances.
4. It is possible to control depth of cut, width of cut and material removal rate using the control values of standoff distance and feed rate.
5. Important in the design of this control system will be the methods used to monitor all process outputs as well as the use of an automated compensation control system.
6. The design of a more satisfactory abrasive water jet nozzle could lead to the reduction of process non-linearity [2], [7].

## REFERENCES:

1. Galecki, G., Mazurkiewicz, M., 1987, "Hydroabrasive Cutting Head - Energy Transfer Efficiency"; paper for Fourth U.S. Water Jet Conference, pp 3.
2. Mazurkiewicz, M., Galecki, G., Olko, P., 1986, "Testing and Development of a Data Base for a High Pressure Hydro-abrasive Cutting System and its Improvements", Final Report for McCartney Manufacturing Company, Inc., Rolla, Missouri, p 54.

3. Hashish, M., 1986, "Aspect of Abrasive Waterjet Performance Optimization", Proceedings of the 8th International Symposium on Jet Cutting Technology, Paper 30, p 297308.
4. Tan, D.K.M., 1986, "A Model for the Surface Finish in Abrasive Waterjet Cutting", Proceedings of the 8th International Symposium on Jet Cutting Technology, Paper 31, pp 309-313.
5. Hashish, M., 1984, "On the Modeling of Abrasive Waterjet Cutting", Proceedings of the 7th International Symposium on Jet Cutting Technology, Paper E1, pp 249-265.
6. Verma, A.P., Lal, K.G., 1984, "An Experimental Study of Abrasive Jet Machining", Int. j. Mach. Tool. Des. Vol. 24, No. 1, pp 19-29.
7. Hashish, M., 1983, "Experimental Studies of Cutting with Abrasive Water Jets", Proceedings of the 2nd U.S. Water Jet Symposium, p 379, Rolla, Missouri.

# SURFACE FINISH CHARACTERIZATION IN MACHINING ADVANCED CERAMICS BY ABRASIVE WATERJET

D. C. Hunt, C. D. Burnham, and T. J. Kim  
Abrasive Waterjet Laboratory  
University of Rhode Island  
Kingston, Rhode Island

## ABSTRACT

An experimental study was conducted to determine the surface finish characteristics of sintered aluminum oxides by an abrasive waterjet system. A beam force transducer designed for this experiment was used to quantify the surface finish and the effectiveness of the abrasive waterjet cutting process using three different grades of alumina. It was found that the workpiece reactive force can be used as a major process parameter for determining and controlling the quality of the machined surface of advanced ceramics.

## INTRODUCTION

The emergence of advanced ceramics in various high technology applications has increased the need for the development of an efficient machining method applicable to ceramic materials such as, aluminum oxide, silicon nitride, and silicon carbide. The high pressure abrasive waterjet system which has recently been introduced in many industrial applications for cutting metallic materials can easily be adapted for machining difficult-to-machine materials. With the advent of robotics technology, an abrasive waterjet system coupled with a robot can be developed for use in precision material removal operations, especially for ceramic materials.

The mechanical methods of stock removal which are currently available for cutting and shaping ceramic components are cutting and grinding by diamond abrasive wheels. Several studies were conducted by Kim and Gielisse [1,2,3] with diamond abrasive wheels to determine the stock removal characteristics of ceramics in terms of the major processing parameters such as, removal force, grinding energy, interfacial temperature, and systems parameters. The results obtained were used for modeling an optimum system that could be used for this type of stock removal process as applied to ceramics. Even though this type of stock removal process can be optimized by controlling the above mentioned parameters, it is not considered to be the most efficient method for ceramic stock removal. Diamond abrasive wheels take longer machining time and the process is limited to two-dimensional machining applications.

Based on several preliminary investigations [6,9] on the machinability of advanced ceramics by an abrasive waterjet system, it was found that the material removal method by abrasive waterjet can effectively be applied for machining industrial ceramics. The abrasive water jet has a distinct advantage over traditional ceramic finishing methods simply because it reduces the number of critical processing parameters encountered during the ceramic grinding process such as interfacial temperature and tool wear.

The objective of this study is to determine the surface finish characteristics of ceramics machined by an abrasive waterjet system using one of the kinetic variables. A workpiece force sensor was developed to quantify the surface finish and to control the process variables to attain a desired surface finish. A study is currently underway to extend the present method for waterjet process optimization via an adaptive control method.

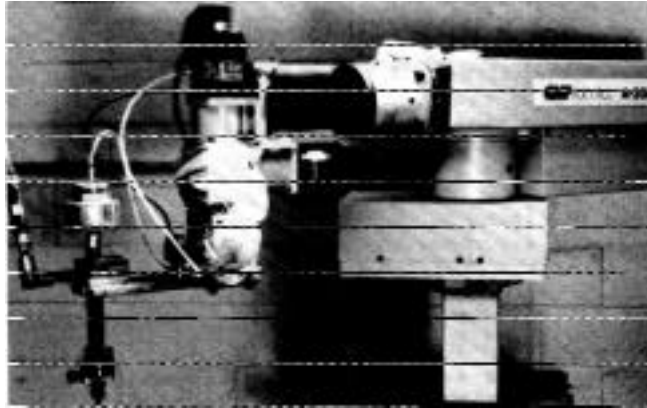


Fig. 1 Nozzle Assembly and Robot

#### EXPERIMENTAL APPARATUS AND PROCEDURE

The experimental setup used in this investigation is shown in Figure 1. The system consists of an IIX-6 series intensifier pump connected to a PASER nozzle assembly; both manufactured by Flow Systems Inc. The PASER assembly is manipulated by a CMF A - 200 robot with a KAREL controller. It has an AC servo drive system and a repeatability of  $\pm 0.0508$  mm, It moves in straight lines smoothly and at very slow speeds. The robot can be programmed by teaching points or by geometrically defining the motions off-line. For the cuts, the robot is programmed to move to a specified height above the workpiece and wait for a user command before turning on the PASER assembly. It then moves the jet stream into the workpiece at a pre-programmed rate until it reaches the end of the cut. At this time it turns off the water jet and moves back to its beginning point.

The ceramic workpieces are mounted on an aluminum beam force transducer, as shown in Figure 2, developed for this application at the Water Jet Laboratory of the University of Rhode Island [4,5].

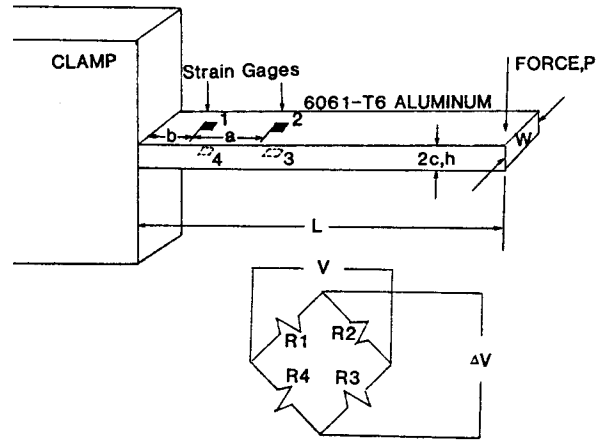


FIG. 2 Force Sensor Designed for Cutting Experiment

The output of the four active arm Wheatstone Bridge circuit is expressed in terms of the applied force P as

$$\frac{V}{V} = \frac{G_f ca}{2IE} (P)$$

where  $G_f$  is the gage factor for four identical strain gages used. Although a temperature gradient between gages could cause a slight change in output, the effect was minimized by using self-temperature compensating gages.

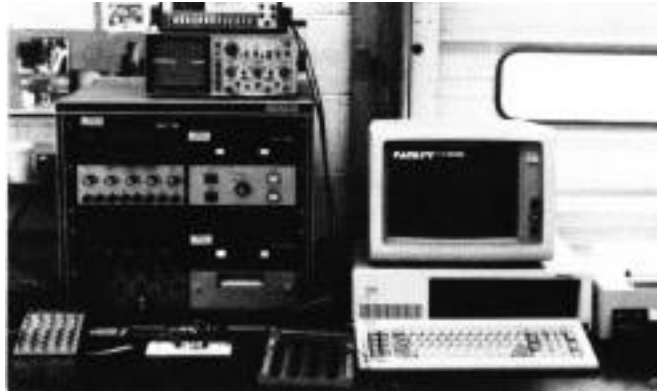


Figure. 3 Data Acquisition System

To measure the output from the beam transducer, both digital and analog recording devices were used as shown in Figure 3. A Vishay 20A multi-channel strain indicator was wired to the four strain gages. An analog signal from the strain indicator was connected to an op-amplifier with a gain of 200. This signal is then filtered to remove frequencies above 15 HZ and the final signal is fed into an A/D board in an IBM PC. A computer program was written in interpreted BASIC that would sample the force data at a frequency of 10 HZ for one second. That is, take 10 samples in one second. It then calculates the average for those ten samples and saves it in memory. After the cut was completed, the data was saved on a disk and analyzed using LOTUS 123.

The beam sensor was securely attached to a fixture that allowed the robot easy access to the workpiece for the cutting experiment. To maintain the accuracy and repeatability of the system, the calibration of the beam sensor was checked before each cutting experiment was conducted.

## SURFACE FINISH CHARACTERIZATION

### Workpieces and Abrasives:

Three grades of sintered alumina supplied by the Coors Porcelain Company were used to determine the surface finish characteristics by workpiece reactive force analysis. The workpieces with several different thicknesses, 6.4 mm (AD 85, AD 94), 9.5 mm (AD 99.5), 12.7 mm (AD 94), and 20.6 mm (AD 85) were selected for this experiment. In a previous study by Hunt and Kim [6], it was found that the mode of material removal and surface finish have a direct correlation with the mechanical properties of a material. It was also found that the level of a force associated with piercing or cutting can be used to determine the efficiency of the process. The three grades of alumina ceramics chosen for the present investigation have easily distinguishable mechanical properties as shown in Table 1.

Table 1

Properties	AD 85	AD 94	AD 99.5
Specific Gravity	3.42	3.62	3.84
Tensile Strength (MPa)	124	186	345
Young' s Modulus (MPa)	228x10 <sup>3</sup>	283x10 <sup>3</sup>	358x10 <sup>3</sup>
Bulk Modulus (MPa)	138x10 <sup>3</sup>	168x10 <sup>3</sup>	207x10 <sup>3</sup>
Hardness (Rockwell 45N)	75	78	81

The abrasives used in this work were #80 mesh H.P. Barton Garnet supplied by Barton Mines Corporation and #60 mesh A1203 supplied by the Norton Company. The H.P. Barton Garnet has a Mohs hardness scale of 9 and is a very sharp edged abrasive. Sharp edged abrasive grains are much more effective than round grain abrasives. The sharp edge acts as a micro-cutting tool, thereby increasing the probability of erosion failure initiation of the materials. The effect of physical and geometrical properties of the garnet abrasives on the mode of material removal was previously studied by several investigators including Hashish [7] and Shukla [8]. The efficiency of the waterjet process can be generally increased by a proper choice of abrasives. The result of a preliminary study by Kim and Posner [9] shows that a significantly improved rate of material removal can be achieved by use of hard abrasives such as Al<sub>2</sub>O<sub>3</sub> and SIC.

### Workpiece Reactive Force

A force sensor system developed for this study can provide a quantitative, near-real-time output of the measured force variable. It provides instant information of the cutting efficiency and the desired finish of the ceramic workpiece. Ultimately, the

system can be used in the development of a real time adaptive control routine for optimizing the waterjet machining process .

To minimize the effect of several process variables on the surface finish characterization, all variables were fixed except the traverse speed.

Abrasive Flow Rate: 0.55 Kg/min  
 Water Pressure at Pump: 262 MPa  
 Jewel Orifice: 0.46 mm  
 Nozzle Diameter: 1.57 mm  
 Nozzle/Workpiece Standoff: 1.5 mm

The effects of cutting speed, workpiece material type, and abrasives on the cutting force are examined. Figure 4 shows a typical output taken from a test run for a 12.7 mm thick piece of AD 85. The force begins near zero and climbs higher as the waterjet cuts deeper into the material . Finally , a steady state cutting force is achieved at about 9.25 N for the duration of the cut. At the end of the cut, the waterjet is simply turned off and the force returns to zero. Each data point represents an average value of ten samples per second.

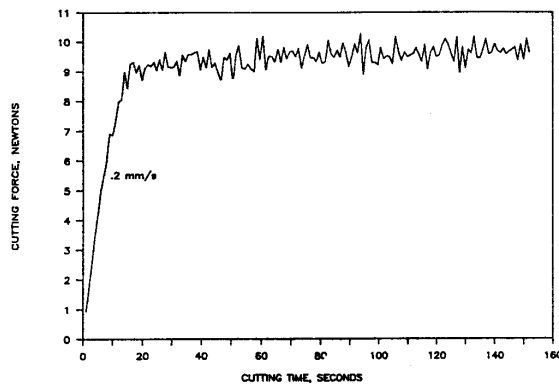


Figure 4 Cutting Force versus Cutting Time (AD 85 with Garnet )

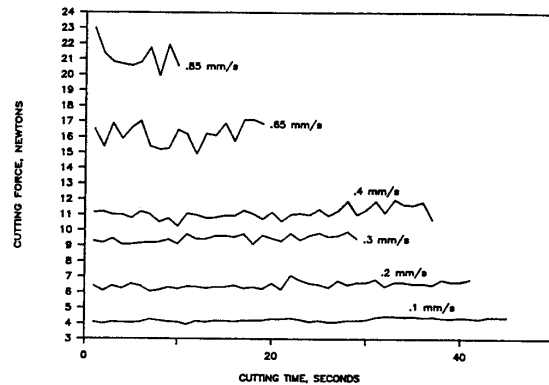


Figure 5 Cutting Force versus Cutting Speed (AD 99.5 with Garnet)

The fluctuation of the force level in time is mainly due to the unsteady cutting caused by the system such as;

- (a) water pressure oscillations,
- (b) cyclic nature of the cutting process,
- (c) oscillations of the transducer beam,
- (d) the accuracy and repeatability of the robot, and
- (e) electronic noise in the sensor circuit.

The A/D converter was set for a range of -10 to +10 volts and a 9.81 Newton force on the sensor presented about 1 volt to the A/D Converter. The total signal noise leading into the A/D board was 50mv. Using this information, the 50 mv noise signal creates an uncertainty of .52 Newtons. This means that a steady state signal measured at 2 Newtons

would have an error of plus or minus .26 Newtons. Read as 2.00 Newtons +.26. Figure 5 shows the measured force data associated with six different cutting speeds for a 9.5 mm thick AD 99.5 workpiece using garnet abrasive. The traverse speed of 0.85 mm/s is the maximum speed at which this high strength ceramic could be cut.

The average force at this speed is about 21.5 N. As the speed increases, the data point oscillations are more pronounced. The increase of the cutting speed results in an increase of the amplitude of the beam sensor oscillations. Figure 6 clearly shows the effectiveness of a harder abrasive (A1203) in machining the alumina.

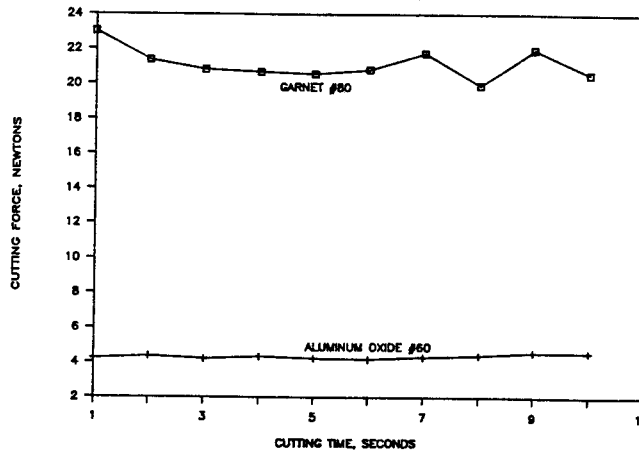


Figure 6 Cutting Force versus Abrasive Types (AD 99.5 with Garnet and  $Al_2O_3$  )



Figure. 7. (a) AD 99.5 (9.53mm) Cut with  $Al_2O_3$  at 0.85 mm/s  
 (b) AD 99.5 (9.53mm) Cut with Garnet at 0.85 mm/s

A 9.5 mm thick AD 99.5 ceramic was cut with alumina abrasive at the maximum speed attainable by garnet abrasive. The average force level decreased significantly from 21.5 N to 4.1 N. The corresponding quality of surface finish was markedly improved, as shown in Figure 7, from 270  $\mu$ inches of rms value for garnet to 130  $\mu$ inches for aluminum oxide.

The force level increases linearly as the cutting speed increases, as shown in Figure 8, for cutting 9.5 mm thick AD 99.5 with garnet abrasive. The same trend was also observed with the use of aluminum oxide abrasive. The scatter of each data point also increases as the cutting speed increases. The range of error at force levels of 6 Newtons is about +/- 0.25 N.

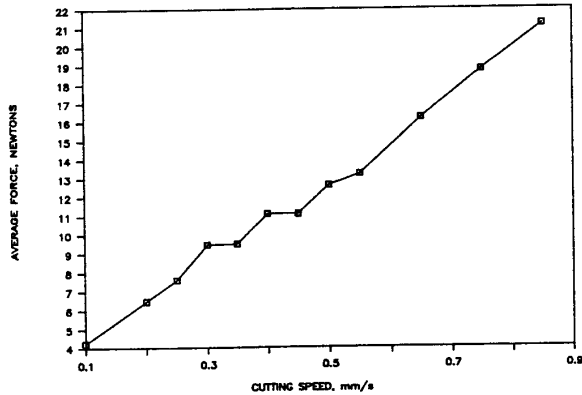


Figure 8 Cutting Force versus Cutting Speed (AD 99.5 with Garnet)

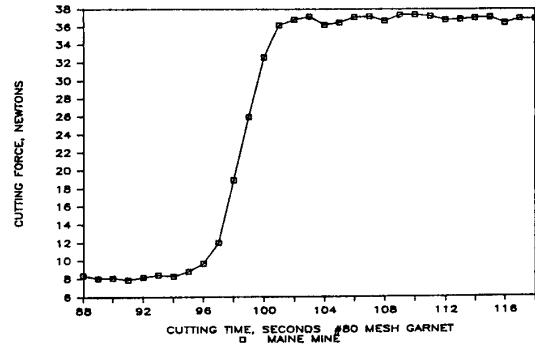


Figure 9 Effects of Clogged Abrasive Feed (4340 Steel with Garnet)

The surface finish of a workpiece is directly related to the cutting force. The higher the force, the rougher the finish. If an anomaly occurs in the system, it can easily be detected by the sudden changes of the cutting force. A good example of a system anomaly affecting the cutting force is shown in Figure 9. It shows the effects of a clogged abrasive tube on the cutting force of a 22mm thick piece of 4340 steel. In this particular case the abrasive hopper ran out of abrasive. This caused the force to go to a maximum of about 37 N. This is the same force that is encountered when this material is pierced at this pressure. This demonstrates that the efficiency of waterjet machining can be determined and controlled by the level of the force output which can be affected by other process variables, such as the abrasive flow rate, abrasive type, water pressure, etc.

### Analysis of Surface Quality

A typical characteristic of surface finish produced by the waterjet cutting process is the development of striation marks which transpire below an area of relatively smooth surface finish. These striation lines appear when the cutting efficiency decreases. This can happen in a number of ways. It could be that the cutting speed is too fast, the water pressure is too low, inappropriate abrasive flow rate or the material is too thick. A transition zone between the smooth upper surface and the rougher striated surface below can be seen in Figure 7, for AD 99.5 cut with garnet. If the parameters are properly controlled, an excellent surface quality can be achieved throughout the entire depth of the cut. This can be seen in Figure 7(a) where 9.53 mm thick of AD 99.5 was cut by A1203 obtaining a surface finish of about 130 micro inches.

The maximum cutting speed attainable for a 9.5 mm thick AD 99.5 ceramic was found to be 0.85 mm/sec for the garnet and 4.80 mm/sec for the aluminum oxide abrasive. These were determined by gradually increasing the cutting speed until the jet stream sprayed backwards at 90° or more in a “rooster tail” effect. Figure 10 clearly shows a visible trace of striation marks for AD 99.5 cut at the maximum speed for each abrasive.

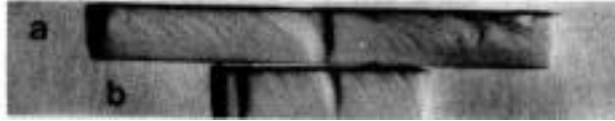


Figure. 10 (a) AD 99.5 (9.53mm) Cut with  $Al_2O_3$  at 4.8 mm/s  
 (b) AD 99.5 (9.53mm) Cut with Garnet at 0.85 mm/s

The surface finish left by the aluminum oxide and garnet was 300 and 270 micro inches, respectively. Much greater surface distortion seems to be present on the aluminum oxide cut, whereas the roughness values appear relatively similar. This is due to a spot error incurred during the surface roughness measurement around a speed of 4.2 mm/s using  $Al_2O_3$  abrasive as shown in Figure 11. The striation lines did occasionally become too large to be accurately recorded with the surface indicator.

It was generally observed that both higher force and greater speed tend to yield a rougher surface quality. Figure 11 shows the surface quality measured in micro inches (rms .) versus cutting speed in millimeters per second. The  $Al_2O_3$  abrasive can produce the same surface quality as the garnet abrasive at four times the cutting speed. One of the problems associated with using aluminum oxide abrasive is that the wear rate of the tungsten carbide nozzle is extremely high. The result of a nozzle wear study for  $Al_2O_3$  abrasive versus garnet abrasive is shown in Figure 12. The increase of nozzle diameter was measured in terms of the cutting time. A fairly linear variation between the nozzle diameter and the cutting time was observed. When using garnet as an abrasive, the normal life for a tungsten carbide nozzle is from 3 to 6 hours. Using  $Al_2O_3$ , the nozzle opened up over 1 mm in diameter in about 7 minutes. Therefore, the nozzle life using  $Al_2O_3$  is less than 1/32 the life of a nozzle using garnet.

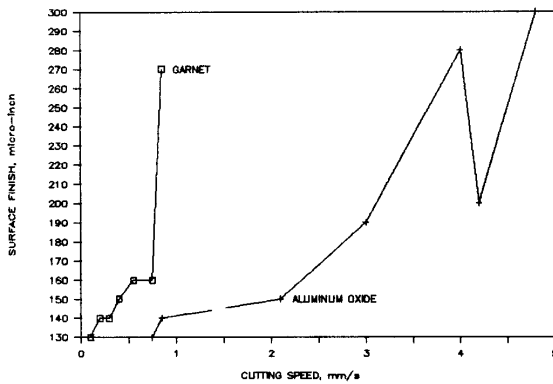


Figure 11 Surface Finish versus Cutting Speed (AD 99.5, 9.53mm Thick)

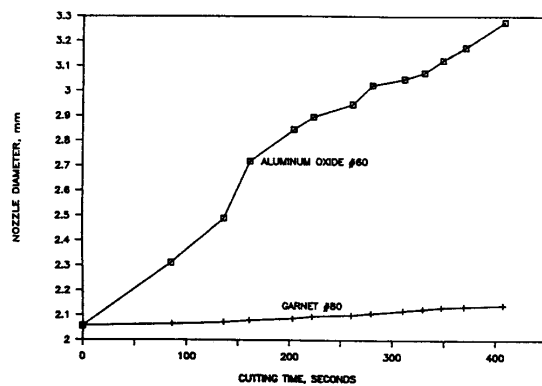


Fig. 12 Nozzle Wear versus time (WC Nozzle at 0.55 Kg/m)

As the traverse speed increases, the transition zone between the smooth and rough surface shifts upward. The cutting speed at which the transition zone shifts to the center of the workpiece can be interpolated from the speed versus surface roughness graph. For instance, with a speed of 0.75 mm/s and a roughness value of 160, the transition zone is

nearly at the center of the ceramic workpiece. By a slight increase of speed to 0.85 mm/s, the roughness value increases to 270 micro inch indicating a shift of the striation region to a halfway position. A drastic increase in surface roughness was observed with a seemingly small increase in cutting speed.

To quantify the quality of surface finish in terms of the force output, the surface roughness data shown in Figure 11 are expressed in terms of the cutting force as shown in Figure 13. The rms value of the surface finish increases gradually as the output force level increases. The trend for both abrasives is similar up to a force level (about 18 N) which corresponds approximately to a 170  $\mu$ -inch surface. A moderate deviation of two curves beyond this force level is mainly due to the nozzle wear for  $Al_2O_3$  abrasive. The nozzle diameter increased by approximately 28% at the last data point (34 N force) as compared to the last data point on the garnet curve. The wider jet stream through a worn nozzle tends to increase the kerf and decrease the cutting efficiency thus contributing to an increase of force level. It is interesting to note, from Figures 11 and 13, that a kinetic variable associated with the waterjet process is a suitable control parameter for surface finish characterization as compared to a kinematics variable such as traverse speed. Ultimately, the waterjet performance, measured in terms of surface finish  $S_f$ , can be expressed as

$$S_f = J_p F(f_w)$$

where  $J_p$  is a modified waterjet process parameter and  $f_w$  is the level of force output. The inverse of the above relation can be utilized in optimizing the process by an adaptive control method.

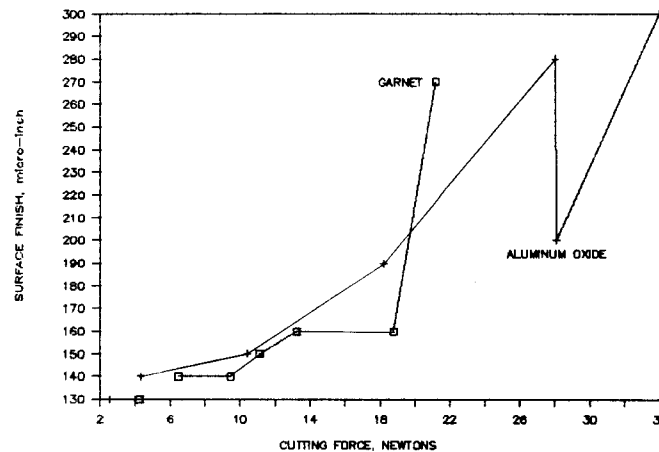


Figure 13 Surface Finish versus Cutting Force (AD 99.5, 9.53 M Thick)

#### REFERENCES

1. Kim, T.J. and Gielisse, P.J., "Energy for Grinding Aluminum Oxide," International Journal of Production Research, Vol. 17, No. 2, 1979, pp. 155-165.
2. Kim, T.J., Gielisse, P.J., and Short, J.F. "Wear of Diamond Particles for Grinding Ceramics" International Journal of Production, Vol. 22, No. 4, 1984, pp. 565-574.

3. Gielisse P.J., Choudry, A. and Kim, T.J., "Dynamics and Material Parameters in Brittle Fracture in Ceramics" Materials Science Research, Vol. 12, New York, Plenum Press, p. 285.
4. Field, G., "Workpiece Force Analysis of Waterjet Processes" Abrasive Waterjet Laboratory Report (85-1), University of Rhode Island, Kingston, RI, December 1985.
5. Hunt, D.C., "Development of an Adaptive Control System for Abrasive Waterjet Cutting," Abrasive Waterjet Laboratory Report (87-2), University of Rhode Island, Kingston, RI, March 1987.
6. Hunt, D.C. and Kim, T.J., "A Parametric Study of Waterjet Processes by Piercing," Proceedings of 8th International Symposium of Jet Cutting Technology , pp . 287-295, Durham, England, September 1986.
7. Hashish, M., "Experimental Studies of Cutting with Abrasive Water jet," Proceedings of the Second U.S. Waterjet Symposium, University of Missouri, Rolla, May 24, 1983.
8. Shukla, R.B., "Abrasive Jet Machining," Proceedings of TwentyThird Abrasive Engineering Society Conference' Chicago' Illinois' May 13, 1985, pp. 99-100.
9. Kim, T.J. , Sylvia, J.G., and Posner, L., "Piercing and Cutting of Ceramics by Abrasive Waterjet," International Symposium on Machining of Ceramic Materials and Components ' 1985 ASME Winter Annual Meeting, Proceedings PED-Vol. 17, December 1985, pp. 19-24.

# ABRASIVE WATERJET CUTTING OF METAL MATRIX COMPOSITES

K. F. Neusen, P. K. Rohatgi, C. Vaidyanathan, and D. Alberts  
University of Wisconsin-Milwaukee  
Milwaukee, Wisconsin

## ABSTRACT

An experimental investigation was conducted to determine the abrasive water jet cutting characteristics of metal matrix composites. A variety of composites including solidification processed aluminum-silicon carbide and magnesium-based composites were studied. The cut surfaces were examined under an optical and scanning electron microscope in order to illustrate the nature of the surfaces generated and to understand the mechanism of waterjet cutting of metal matrix composites. The effects of volume percentage of hard phase and its distribution on cutting performance were also determined.

In order to assess the effects of abrasive waterjet cutting parameters on cutting performance, a range of conditions was used to cut each material. Water pressure at the nozzle was varied from 172 to 310 MPa (25,000 to 45,000 psi). The jet traverse speed, which was controlled by a robotic positioner, was varied from approximately 12.7 to 254 mm/min (0.5 to 10.0 inch/min) so as to produce acceptable surface quality. Abrasive feed rates varied from 0.23 to 1.1 kg/min (0.5 to 2.5 lb/min).

## INTRODUCTION

Recent interest in metal matrix composites for use in applications where a high performance material is required stems from the very favorable properties of the materials as well as their low cost. Silicon carbide reinforced cast aluminum alloy and silicon carbide reinforced magnesium are examples of such composites and will be the subject of the present study. Compared to the unreinforced base metal, the composites exhibit higher strength, higher stiffness, improved wear and abrasion resistance, reduced thermal expansion coefficient and improved elevated temperature properties. When compared to other materials which can compete on the basis of high strength to weight ratios (e.g., titanium alloys and graphite epoxy composites), the metal matrix composites are generally much lower in cost. Although the list of favorable attributes for these new engineering materials is quite impressive, another factor which must be considered is machinability. When conventional machining methods such as milling or sawing are used, serious complications arise. The presence of the silicon carbide leads to very rapid tool wear. Consequently, even though the cast base metal is easily handled by conventional methods, machining the composite with these methods results in frequent and expensive tool changes, as well as excessive time required to complete the job.

Abrasive waterjet cutting seems to be a good choice for forming parts out of metal matrix composites. The abrasive particles entrained in the continuous high-velocity waterjet do the machining and there is no need to stop to replace a dull tool. The present study examines the cutting rates obtainable with abrasive waterjets for both silicon carbide-aluminum and silicon carbide-magnesium composites made by casting techniques

(8). In addition, since there are no previous reports of investigations of the micro-mechanics of abrasive waterjet cutting, the quality of the cut surface was assessed by measuring the surface roughness and examining the newly exposed surfaces using optical and scanning microscopy. These observations were made over a range of cutting speeds, nozzle pressures and abrasive flow rates.

The several advantages of all waterjet cutting systems apply to the case of abrasive waterjets applied to metal matrix composites. No heat affected zone is produced when parts are cut by waterjets. Airborne dust is virtually eliminated. The jet can pierce the stock and thereby enable cuts to be started away from the edges. A small diameter jet has inherent omni-directional cutting potential and this makes it a logical candidate for integration with a robotic system.

## PREVIOUS WORK

Abrasive waterjet cutting as a technology with commercial applications has a relatively short history. Although the abrasive jet concept has been known from some unpublished reports for at least a decade and possibly two decades, probably the first published reports to receive widespread attention were those presented at the International Symposium on Waterjet Cutting Technology held in 1982 at Guildford, England. M. Hashish presented two papers: one on steel cutting (1) and the other on concrete cutting (2), which established expected magnitudes of cutting parameters for cutting these two materials with abrasive waterjets. A paper by D. H. Saunders (3), outlining similar results for steel and rock, was presented at the same conference.

A summary article which outlined the principles of abrasive waterjet cutting and performance in a wide range of materials was published by Hashish in 1984 (4). The same author followed this article with a report of optimization criteria for selecting abrasive waterjet parameters and extensive data for cutting rates in aluminum, steel, concrete, stainless steel, and titanium (5).

A study of piercing performance of abrasive waterjets conducted at the University of Rhode Island was reported by Hunt et al. (6). The materials studied included aluminum, steel, super alloys and ceramics. The quality of cut surfaces produced by abrasive waterjets varies significantly with the choice of cutting parameters. A model for the prediction of surface finish was presented by Tan (7).

## EXPERIMENTAL SETUP

The experimental results for this study were obtained in the University of Wisconsin--Milwaukee Abrasive Waterjet Laboratory. The arrangement of equipment for the experiments was as shown in Figure 1.



Figure 1. Experimental setup, includes intensifier pump, robot, abrasive nozzle and catcher tank.

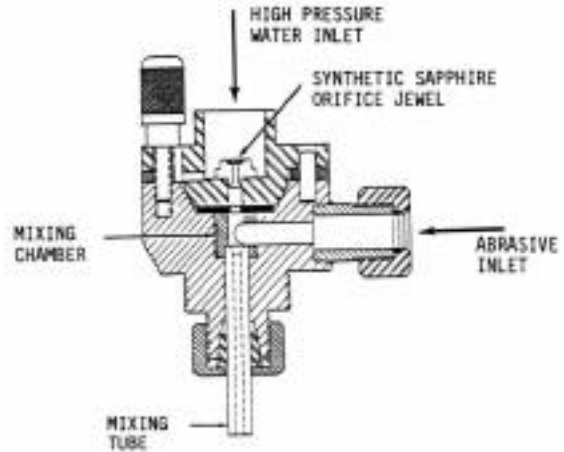


Figure 2. Schematic of abrasive nozzle assembly.

High pressure water to produce the waterjet was provided by a dual intensifier pump at pressures up to 379 MPa (55,000 psi). For this series of experiments, the high pressure water was admitted to a 0.330 mm (0.013 inch) sapphire nozzle to create the waterjet. After the waterjet is formed, it is directed into an induction chamber where abrasive particles are entrained and then on to a 1.19 mm (0.047 inch) tungsten carbide nozzle/mixing tube. A detailed schematic of the abrasive nozzle assembly is shown in Fig. 2.

Water velocities up to 750 mps (2500 fps) are produced at the sapphire nozzle exit. Abrasive particles are accelerated to an estimated 450 mps (1500 fps) in the tungsten carbide nozzle. The rate of abrasive feed is controlled by a calibrated restriction attached to a hopper. All of the present experiments were conducted using #80 mesh garnet as the abrasive.

A five axis, 6 kg robot was used to control the abrasive waterjet positioning. The robot's point to point velocity control also provided the required range of constant cutting speeds.

The cutting parameters that were systematically varied as independent variables in this study were:

- 1) cutting speed,
- 2) water pressure, and
- 3) abrasive mass flow rate.

Held constant in the study were:

- 1) stand off distance--2.54 mm,
- 2) abrasive material-garnet,
- 3) abrasive size--80 mesh, and
- 4) for all of the surface finish tests, the depth of cut was constant at 12.7 mm.

For each material tested, a nominal value was established for each of the three independent variables so as to produce a reasonable quality of cut. Then each of the independent variables was taken through a 5 point range.

The composition of the materials tested was as follows:

Designation	Matrix Material	Reinforcing Material and %
Base Aluminum	Aluminum 2014	None
Aluminum – 7%	Aluminum 2014	SiC, 7%
Aluminum – 11%	Aluminum 2014	SiC, 11%
Dural	Aluminum 357	SiC, 15%
Base Magnesium	Magnesium	None
Magnesium - 26.5%	Magnesium	SiC, 26.5%

Depth of cut tests were conducted, with cutting speed as the independent variable, for two materials-Aluminum 2014 and Dural.

Prior to using the garnet for cutting, some chemical analysis data and scanning microphotography were obtained for this mineral. The chemical compositions are given in the table below.

PERCENT OF ELEMENTS (Nominal Composition)

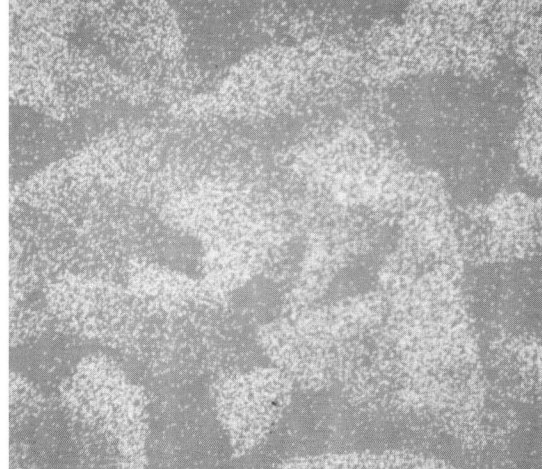
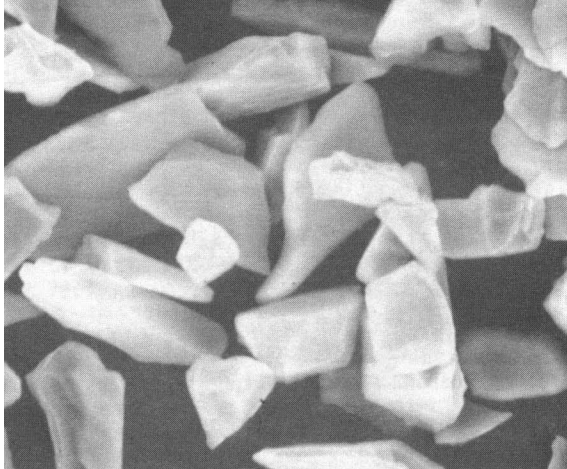
Location	Al	Si	Ca	Mn	Fe
Surface (from SEM)	13.8	43.2	4.0	3.6	35.4
Bulk (from Supplier)	19.3	19.9	0.0	3.0	57.8

The difference in the surface and bulk analysis could be due to surface segregation and absorption of species. Figure 3 shows the scanning microphotograph of garnet particles indicating the angular nature of the abrasive. The iron and silicon images show the concentrations of these elements in garnet.



Figure 3. Scanning microphotograph (100x) of #80 mesh garnet.  
(editors note in the scanning process it was not possible to achieve a high enough resolution to obtain legible images of 3(b) the iron image and 3(c) the silicon image)

The silicon carbide used to produce the composites was also examined separately. Figure 4 shows the scanning microphotograph and the silicon image of the SiC particles that were later dispersed in the Aluminum 2014 alloys. Since both garnet and SiC contain silicon, the presence of iron makes it possible to distinguish between the two types of particles. In addition, the garnet particles appear bright white due to differences in charging characteristics.



a) scanning microphotograph 1000x

Silicon image, 1000 x

Figure 4. SEM of #400 mesh silicon carbide.

### SURFACE ROUGHNESS RESULTS

Irregularities in the surface texture of a cut material that result from inherent actions of the production process are known as surface roughness. The measurement of the roughness is routinely accomplished using a moving stylus type instrument. In the present experiments, the arithmetic average values of the roughness were obtained at several locations on each cut surface. Figure 5 shows typical cut surfaces generated by the abrasive waterjet. The surface roughness results are plotted in Figs. 6 through 10 with the highest and lowest values indicated.

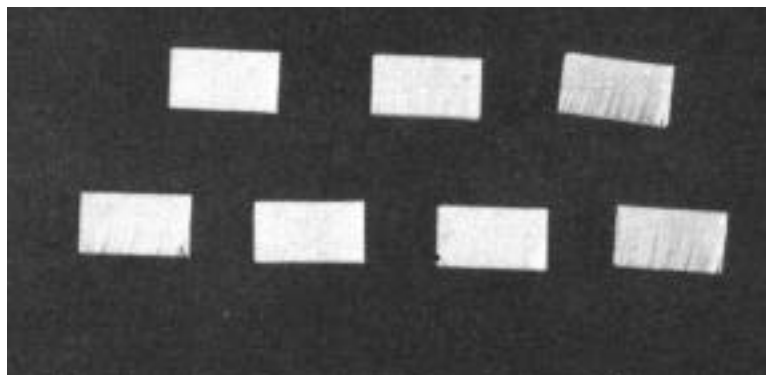


Figure 5. Microphotograph of waterjet cut surfaces showing increasing roughness (striations) where jet leaves the cut material at high cutting speeds.

The data seem to indicate clear trends that the surface roughness increases with an increase in cutting speed and decreases with an increase in abrasive flow. There is no clear trend for the surface roughness data when the water pressure and the percentage of silicon carbide are varied.

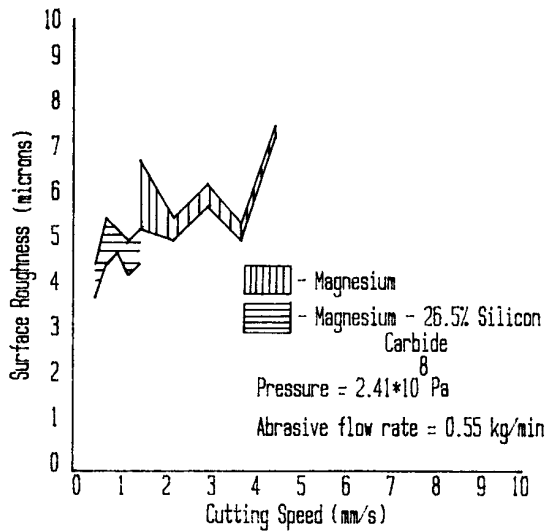


Figure 6. Effect of cutting speed on surface roughness for magnesium and magnesium-26.5% SiC.

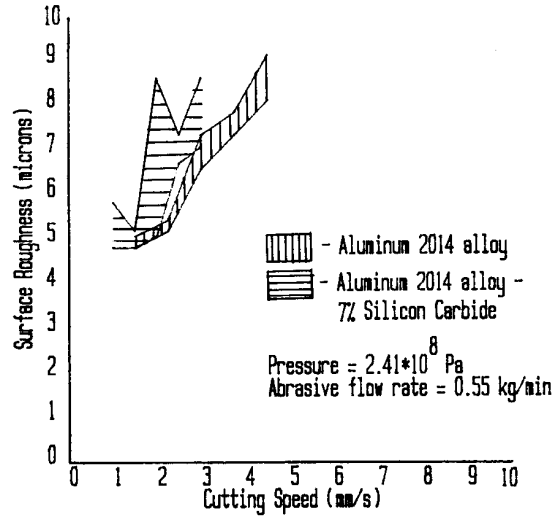


Figure 7. Effect of cutting speed on surface roughness for Aluminum 2014 & Aluminum 2014 – 7% SiC

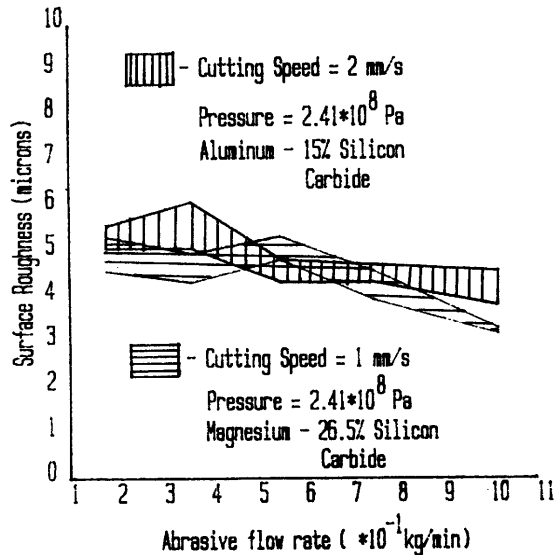
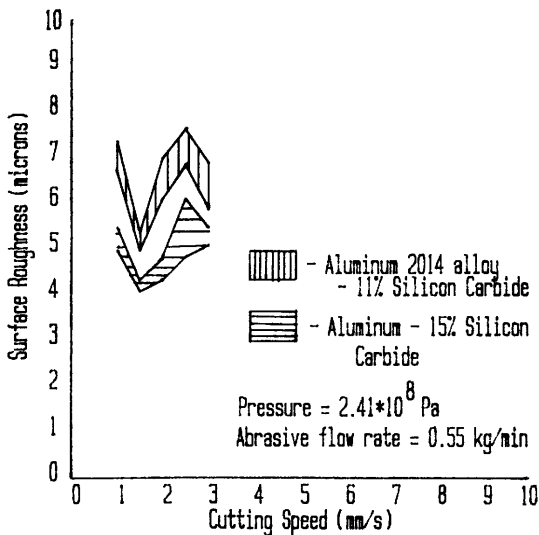


Figure 8. Effect of cutting speed on surface roughness for Aluminum 2014 – 11% SiC and Aluminum 357 – 15% SiC.

Figure 9. Effect of abrasive flow rate on surface roughness for magnesium – 26.5% SiC and Aluminum 357 – 15% SiC.

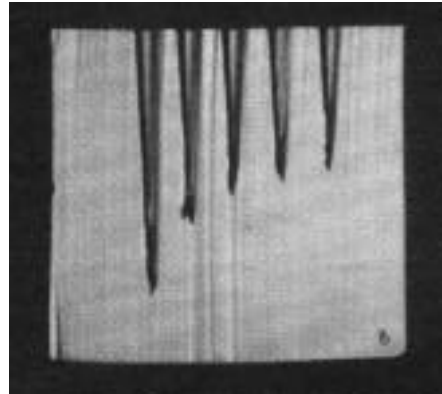
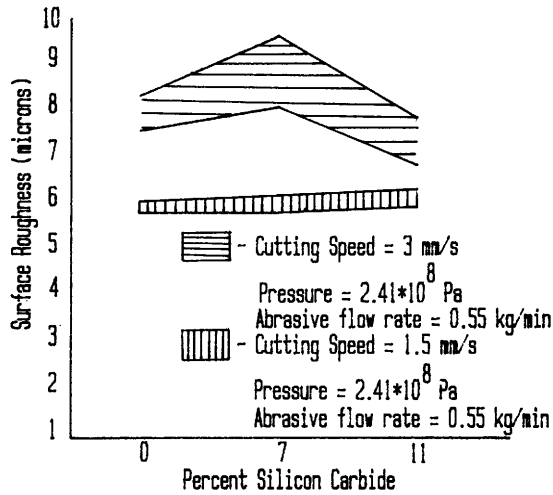


Figure 10. Effect of percent SiC on surface Roughness for Aluminum 2014 and Aluminum 2014 composites.

Figure 11. Microphotograph of depth of cut sample using Dural composite.

### DEPTH OF CUT RESULTS

When the abrasive waterjet was applied to very thick pieces of stock, for a given cutting speed a maximum depth of cut is achieved. This depth of cut is exhibited as a region of constant depth in the groove produced in the stock. Figure 11 shows a macro photograph of a sample obtained to measure depth of cut versus cutting speed. The depth of cut data obtained for Aluminum 2014 and Dural composite are plotted in Fig. 12. Predictably, the depth of cut increases as the cutting speed decreases. There does not appear to be a significant difference in the performance of these two materials. Dural has only ISX SiC in its composition. With continued increases in the SiC content, the depth of cut for the composite should be reduced to values less than those for the alloy.

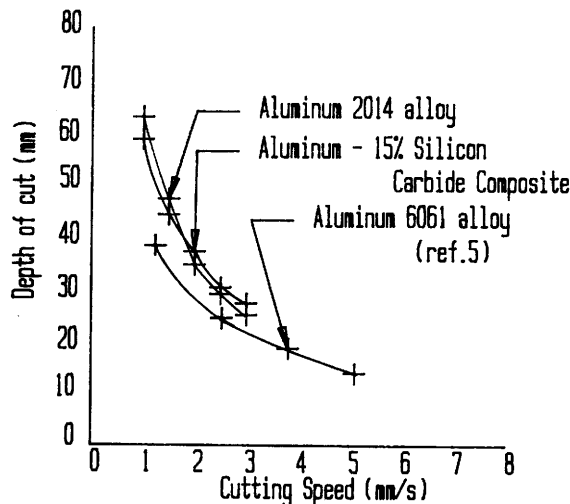


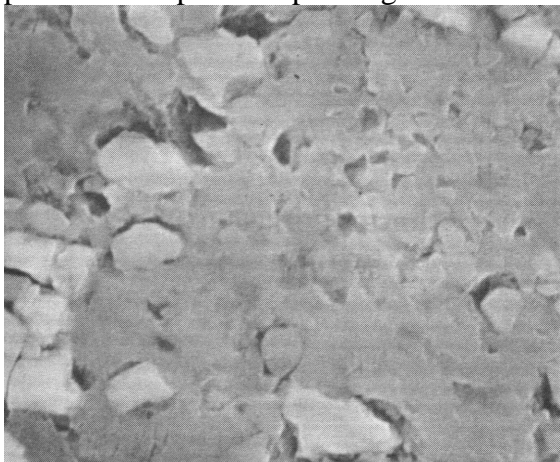
Figure 12. Effect of cutting speed on depth of cut for aluminum alloys and composite.

The depth of cut results obtained by Hashish (5) for aluminum alloy at similar conditions are also shown in Fig. 12 for comparison. His data were obtained using Aluminum 6061-T6 rather than 2014, but the magnitudes of the cutting depths are similar.

### SCANNING ELECTRON MICROSCOPY RESULTS

Scanning electron microscopy was performed on a waterjet cut surface, a diamond wheel cut surface and an as-cast surface of the aluminum-SiC composite. The purpose of this study was to determine the change in character of the surface and the percent distribution of elements on the various surfaces. There was a marked difference between the elemental analysis of the waterjet cut specimen and that of the diamond cut specimen of the same composite. It was noticed that the iron percentage on the waterjet cut surface increased. This suggests the presence of garnet. SEM examination confirmed that individual garnet particles were indeed lodged on the waterjet cut surface. The silicon image of the waterjet cut surface shows that there is reduction in the degree of concentration of silicon corresponding to SiC particles as compared to the as-cast material as well as the diamond wheel cut material. This could be due to smearing of aluminum matrix over the silicon carbide particles present in the matrix.

The scanning microphotography in Figs. 13 through 16 show that single garnet particles have plowed wear tracks in the composite in an abrasive wear mode. The garnet particles themselves are lodged at the end of the track, apparently after their kinetic energy is reduced below the level needed to permit further movement of the particles. It is likely that there is some fragmentation of the individual garnet particles during the process of impact and plowing.

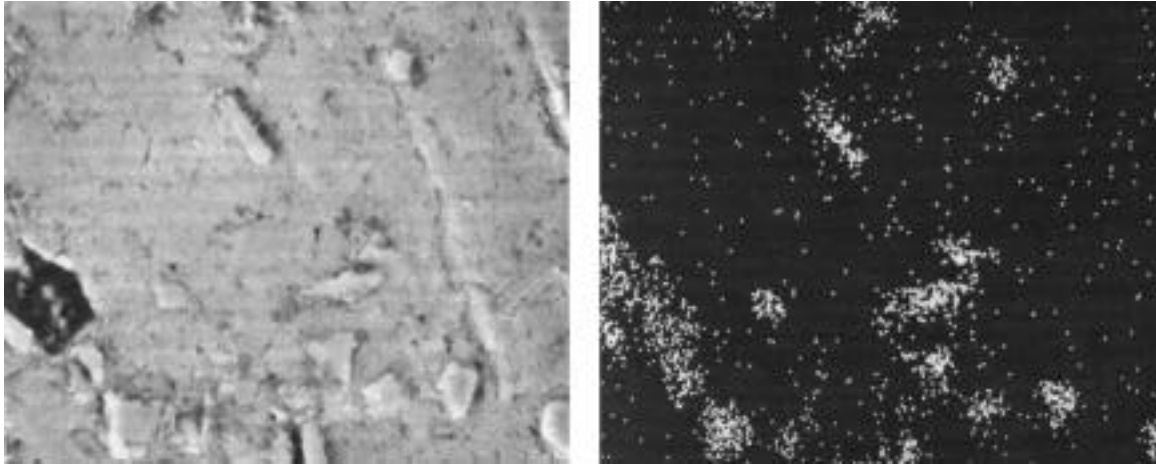


a. Scanning microphotograph, 3000x



b. silicon image 3000x

Figure. 13. SEM of as-cast Dural composite.



a. Scanning microphotograph, 1000x      b. Silicon image, 1000x  
 Figure. 14. SEM of diamond wheel cut Dural composite

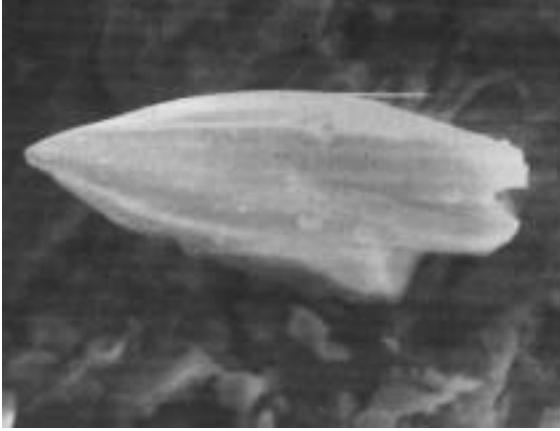
The width of the abrasive wear track appears to be uniform corresponding to the width of the profile of the particle doing the plowing. The depth of the wear track appears to vary across the width apparently corresponding to the profile of the abrading particle.

#### OPTICAL MICROSCOPIC OBSERVATIONS OF WATERJET CUT SURFACES OF AL 2014 AND AL 357-15% SiC COMPOSITE

The waterjet cut edge of Aluminum 2014 alloy and Aluminum 357 alloy-15% SiC composite were analyzed under an optical microscope to study the micromechanism of cutting. The waterjet cut edges were mounted carefully in a bakelite mount. High pressures were used during mounting so as to obtain good packing of the bakelite. The mounted samples were then polished and etched before the metallographic examination.

The waterjet cut surface of the non-composite matrix 2014 alloy shows a non-planar surface. There does not appear to be a direct correlation between the microscopic structure consisting of the dendrites and interdendritic  $\text{CuAl}_2$  phase, and the path of the waterjet cut surface. There appears to be small particles of aluminum near the waterjet cut surface.

The metallographic examination of the cut edges of the composite showed that the silicon carbide was also cut by the abrasive waterjet, almost to the same depth as aluminum (Fig. 17). There were some instances where broken SiC particles were found near the waterjet cut surface. However, by and large, the presence of embedded silicon carbide particles at the surface indicates good bonding between silicon carbide and the matrix; otherwise all silicon carbide particles would have been dislodged.



a. Scanning microphotograph, 1000x

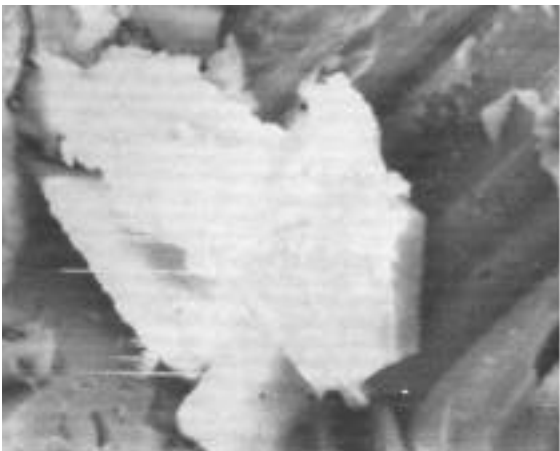


b. Iron image, 1000x



c. Silicon image, 1000x.

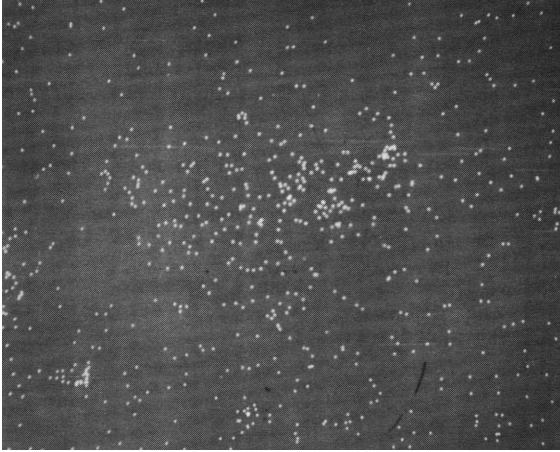
Figure 15. SEM caption of abrasive waterjet cut Dural composite showing garnet particle imbedded in surface.



a. Scanning microphotograph, 1000x

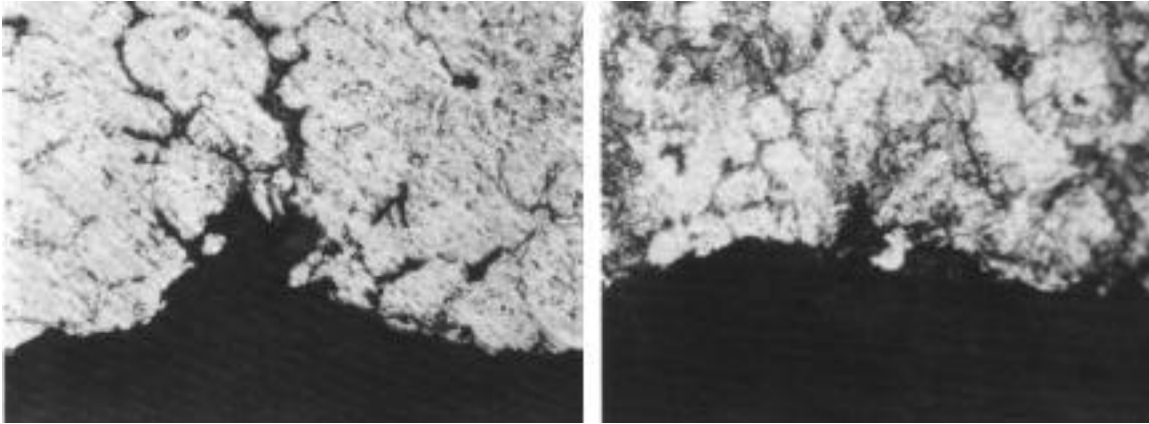


b. Iron image 1000x



c. Silicon image 1000x

Figure 16. SEM of abrasive waterjet cut Dural composite showing garnet particle lodged at the end of a track plowed by the particle.



a. Aluminum 2014, 240x

b. Dural, 240x

Figure 17. Optical microscopic photo of waterjet cut Aluminum 2014 and Dural composite showing broken SiC particles near cut surface of composite.

## CONCLUSIONS

- 1) The silicon on the abrasive waterjet cut surface of the Aluminum 2014 composites is not concentrated in distribution as in the as-cast or the diamond cut surfaces. This is probably due to smearing of the matrix aluminum over the cut surface. The iron content of the waterjet cut surfaces, as reflected by SEM, shows an increase over the as-cast and diamond cut surfaces due to the presence of garnet particles and smearing of aluminum.
- 2) Optical microscopic examination shows that the surfaces of 2014 alloy and 2014 - SiC composite are quite rough. The cutting profile does not seem to follow any particular microscopic feature. The silicon carbide particles remain attached to the abrasive waterjet cut surface suggesting good bonding and scanning examination shows that individual garnet particles plow tracks on the surface of the composite,

and get lodged at the end of wear tracks. Abrasive wear by individual garnet particles therefore appears to be one of the micromechanisms of material removal.

- 3) On increasing the abrasive flow rate, the surface roughness deviation is decreased; the cut surface becomes smoother as the abrasive rate increases. Surface roughness increases with an increase in cutting speed.
- 4) The depth of cut obtainable for both the composite and the non-composite samples decreased as the cutting speed increased.

#### ACKNOWLEDGEMENTS

We gratefully acknowledge the support of the General Motors Corporation, BOC Division, for part of this research work. We thank Mr. Michael Maclaurin of the SEM lab, UWM, for giving us many hours of his time. We also extend our gratitude to Norton Company for the silicon carbide, Dural for the aluminum- silicon carbide composite, Flow Systems, Inc., for the Abrasive Waterjet Cutting Machine and DOW Chemicals for the magnesium-silicon carbide composite.

#### REFERENCES

- 1) Hashish, M., "Steel Cutting with Abrasive Waterjets," Proceedings of 6th International Symposium on Jet Cutting Technology, BHRA Fluids Engineering, Cranfield, Bedford, England, 1982, pp. 465-87.
- 2) Hashish, M., "The Application of Abrasive Jets to Concrete Cutting," Proceedings of 6th International Symposium on Jet Cutting Technology, BHRA Fluids Engineering, Cranfield, Bedford, England, 1982, pp. 447-63.
- 3) Saunders, D. H., "A Safe Method of Cutting Steel and Rock," Proceedings of 6th International Symposium on Jet Cutting Technology, BHRA Fluids Engineering, Cranfield, Bedford, England, 1982, pp. 503-518.
- 4) Hashish, M., "Cutting with Abrasive Waterjets," Mechanical Engineering, Vol. 106, No. 3, March, 1984.
- 5) Hashish, M., Aspects of Abrasive Waterjet Performance Optimization," Proceedings of 8th International Symposium on Jet Cutting Technology, BHRA Fluids Engineering' Cranfield' Bedford, England, 1986, pp. 297-308.
- 6) Hunt, D. C., Kim, T. J., and Sylvia, J. G., MA Parametric Study of Abrasive Waterjet Processes by Piercing Experiment," Proceedings of 8th International Symposium on Jet Cutting Technology, BHRA Fluids Engineering, Cranfield, Bedford, England, 1986, pp. 287-296.
- 7) Tan, D. K. M., "A Model for the Surface Finish in Abrasive Waterjet Cutting," Proceedings of 8th International Symposium on Jet Cutting Technology, BHRA Fluids Engineering, Cranfield, Bedford, England, 1986, pp. 309-313.
- 8) Rohatgi, P. K., Asthana, R., and Das, S., "Solidification Structures and Properties of Cast Metal-Ceramic Particle Composites," IMR 1986, Vol. 31, No. 3, pp. 115-139.